Petrogenesis of the Cortlandt Complex

A Dissertation presented

by

John Francis Bender

to

The Graduate School

in partial fulfillment of the requirements

for the degree of

Doctor of Philosophy

in

Earth and Space Sciences

State University of New York

at

Stony Brook

December, 1980

STATE UNIVERSITY OF NEW YORK

AT STONY BROOK

THE GRADUATE SCHOOL

JOHN FRANCIS BENDER

We, the dissertation committee for the above candidate for the Ph.D. degree, hereby recommend acceptance of the dissertation.

Oct 28 1980
Date

Gilbert N. Hanson
G. N. Hanson
Professor of Geochemistry

Nov. 3 1980
Date

A. E. Bence
A. E. Bence, Advisor
Professor of Geochemistry

Dec. 10, 1980
Date

James J. Papike
James J. Papike
Professor of Geochemistry

Dec. 10, 1980
Date

James W. Granath
James W. Granath
Assistant Professor of Geophysics

Nov. 13, 1980
Date

Nicholas M Ratcliffe
Nicholas M. Ratcliffe
U. S. Geological Survey, Reston, Va.

The dissertation is accepted by the Graduate School.

Dean, Graduate School

DECEMBER, 1980

Abstract of the Dissertation

Petrogenesis of the Cortlandt Complex

by

John Francis Bender

Doctor of Philosophy

in

Earth and Space Sciences

State University of New York at Stony Brook

December, 1980

Geochemistry of the mafic (gabbro, norite, diorite) and ultramafic (cortlandtite, clinopyroxenite, amphibole-pyroxenite) plutonic rocks of the Cortlandt, Stony Point, and Rosetown complexes show that the parental composition of these sequentially intruded plutons is alkalic. Major (Mg#) and trace (Ni, Sc, Cr, REE) element abundances of samples from the amphibole-pyroxenite suite are very similar to those of proposed primary alkali basalts derived from upper mantle peridotite.

Quantitative chemical modelling reveals that the major and trace element abundances of most Cortlandt region basic rocks can be related by fractional crystallization to a parental composition having similar chemistry to the amphibole-pyroxenites. Cortlandite

and clinopyroxenite are cumulus rock types consisting of olivine, clinopyroxene, orthopyroxene ± kaersutite and generally contain less than 20% trapped, interstitial melt. Samples of the diorite and gabbroic plutons of the Cortlandt complex are related to the parental composition by differentiation involving primarily kaersutite and plagioclase. Accumulation of these phases is responsible for formation of cumulus rocks such as hornblendite and kaersutite-rich diorite. The percentage of interstitial liquid in these rocks varies from 0% (adcumulate) to 50%. Samples of the norite pluton are related to one another through fractional crystallization of plagioclase (predominant), orthopyroxene, clinopyroxene, and amphibole. Several samples of this body have chemical characteristics that are consistent with an adcumulate origin.

Strontium isotopic data, in conjunction with major and trace element modelling data, indicate that the varied and distinct $^{87}Sr/^{86}Sr)_i$ ratios of the Cortlandt region samples from different plutons, reflect varying degrees of contamination rather than source heterogeneity. Sr isotopic data of the diorites, kaersutite gabbro, and norite plutons of the Cortlandt complex, indicate that contamination by crustal rocks

occurred before emplacement. This proposed first-stage contamination event did not strongly affect the major and trace element chemistry of the parent magma(s). However, for the norite parent magma, this event had a strong effect on the major (Al_2O_3, CaO, SiO_2, K_2O) and trace (REE) element chemistry. Diorites of the Cortlandt complex experienced extensive interaction with the pelitic country rock at the emplacement site. The geochemistry of differentiated samples from the gabbro, diorite, and norite plutons of the Cortlandt complex indicates that these bodies may have mixed with aqueous fluid before solidification, causing enrichment of Rb, Ba, LREE, K_2O, Na_2O, and SiO_2 in the late-stage liquids. This second stage mixing event, however, did not affect the Sr isotopic systematics.

The Cortlandt region granodiorites are characterized by low REE abundances and unusually high Zr/Nb ratios. The granodiorites appear to be related to the basic rocks of the Cortlandt region by liquid immiscibility.

Trace element abundances of an emery xenolith within the Cortlandt clinopyroxenite pluton indicate that this former pelitic rock lost SiO_2, K_2O, and Na_2O to the alkalic basic melt not by partial melting, but instead by metasomatism.

TABLE OF CONTENTS

LIST OF FIGURES

LIST OF TABLES

ACKNOWLEDGMENTS

I wish to express thanks to Ted Bence and Gil Hanson for their advice, encouragement, and supervision of this project, and also for their interest in my personal and scientific development. In addition, thanks are due to Nick Ratcliffe for allowing me to work with his unpublished data and also for his assistance in the field.

I am also grateful to two of my fellow graduate students, Charlie Langmuir and Bob Vocke, not only for their help in the mass spectrometry lab, but also for numerous discussions, some of which aided in solving scientific problems and others which added zest and zaniness to daily life.

I would also like to thank all members of the Earth and Space Sciences Department for providing an excellent environment for professional growth.

Thanks are also in order to Fred Allen who helped write a computer program essential to this work, to Shirley King for the typing of this manuscript, and to Lois Koh for the drafting of many figures.

Finally, special thanks and gratitude are due to my wife, Kathy, for her assistance in the preparation of this thesis as well as for her constant encouragement and inspiration.

INTRODUCTION

For almost one hundred years the basic plutonic rocks of the Cortlandt complex have been the focus of geological investigations (Dana, 1881; Williams, 1884, 1886, 1887; Kemp, 1888; Rogers, 1911; Bowen, 1922, 1928; Balk, 1927, 1937; Butler, 1936; Shand, 1942; Steenland and Wollard, 1952; Friedman, 1952, 1954, 1956; Barker, 1964; Ratcliffe, 1968; Dallmeyer, 1975). The concensus of these studies has been that the diverse rock types of the Cortlandt complex are products of magmatic fractionation and various degrees of crustal contamination. In fact, the presence of numerous emery bearing xenoliths throughout the Cortlandt complex, led Bowen (1922, 1928) to believe that the group of hypersthene-labordorite gabbros known as norites are products of an assimilation process between gabbro and aluminous-rich sediments.

Recent remapping of the Cortlandt complex (Ratcliffe, unpublished data) indicates that Shand's (Shand, 1942) assumption that the Cortlandt mafic rocks formed by differentiation <u>in situ</u> from a single norite parent is not correct. Instead, Ratcliffe's field investigations reveal that there exists at least six discrete, sequentially intruded plutons in the main

portion of the Cortlandt complex alone.

The presence of these varied and distinct plutons within such a small geographic area presents an excellent opportunity to evaluate the petrogenetic evolution of the Cortlandt magmas. The purpose of this study is to analyze major element bulk chemistry, trace element abundances, phase chemistry, and strontium isotopic compositions in order to determine the influence of the following factors upon the petrogenesis of the Cortlandt complex:

1. the source mineralogy and chemistry of the parental magma(s);
2. the role of mineral fractionation and crystal accumulation in the development of the observed rock types; and
3. the nature and extent of crustal contamination within each of the plutons.

In addition, this study provides implications in three different areas of emphasis:

1. the similarity between the Cortlandt complex and similar igneous suites;
2. the effects of amphibole fractionation on major and trace element abundances;

3. quantitative modelling of magmatic processes through trace element data; and
4. large scale liquid immiscibility.

More specifically, this study not only delimits the origin of the Cortlandt complex but also gives insight into the origin of many similar igneous suites. Primarily, the isotopic and chemical affinities of the Cortlandt rocks are very similar to those alkaline ultramafic basic magmas of Archean greenstone belts (Arth and Hanson, 1975; Schultz et al., 1979; Hanson, 1980) and also to those modern alkali basalt suites present on both ocean islands and continents (Zielenski and Frey, 1970; Kay and Gast, 1973; Sun and Hanson, 1975, 1976).

In addition, because amphibole fractionation has played such an important role in the derivation of the Cortlandt suite, its immediate and long term effects on the major and trace element abundances of a basic melt have been thoroughly evaluated.

Also, a major emphasis of this investigation is to combine the Cortlandt high precision trace element data with presently available distribution coefficients to quantitatively model the magmatic processes of the Cortlandt suite of rocks. The trace elements used for

mathematical modelling are the rare earths, Rb, Sr, Ba, transitions metals, Zr and Nb.

Finally, this study presents strong evidence that the granodiorite-diorite rocks of the Cortlandt region have chemical characteristics indicating that large-scale liquid immiscibility played a major role in their petrogenesis.

GEOLOGIC BACKGROUND

The Cortlandt complex (Fig. 1) is an oval-shaped igneous body (∿ 40 square kilometers) that crops out along the eastern margin of the Hudson River approximately 56 kilometers north of New York City. Directly across from the Cortlandt complex, on the western side of the Hudson River, are two smaller mafic intrusions: the Rosetown complex (∿ 1.5 square kilometers) (Fig. 2 and Fig. 4), and the Stony Point complex (∿ 0.8 square kilometers) (Fig. 3). These bodies are presumed to be extensions of the Cortlandt complex and contain chemically and mineralogically similar rock types. Lithologic units of the three complexes include: norite, diorite, hornblendite, pyroxenite, granodiorite, and cortlandtite.

The Cortlandt and the Stony Point complexes were emplaced into regionally metamorphosed Cambrian-Ordovician schists and marbles of the Manhattan Prong (Fig. 1). Rosetown magmas intruded into the Grenville age gneisses of the Hudson Highlands (Fig. 1). The lower Paleozoic country rocks, regionally metamorphosed during the Taconic orogeny, have a metamorphic gradient that increases from west (chlorite) to east (sillimanite).

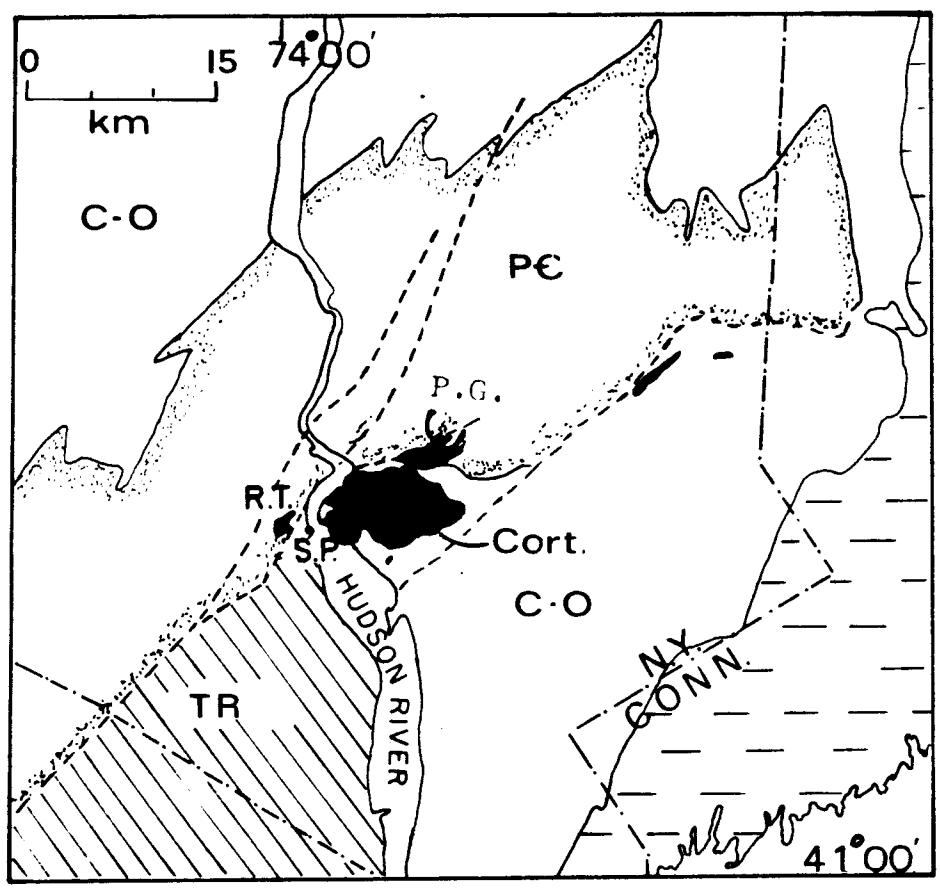

Fig. 1. Simplified geologic map of southern New York modified after Mose et al., 1976, showing location of Cortlandt (Cort.), Stony Point (S.P.), and Rosetown (R.T.) complexes, plus Peekskill granodiorite (P.G.). Cambrian-Ordovician (C-O); Precambrian (P-Є); Triassic (TR).

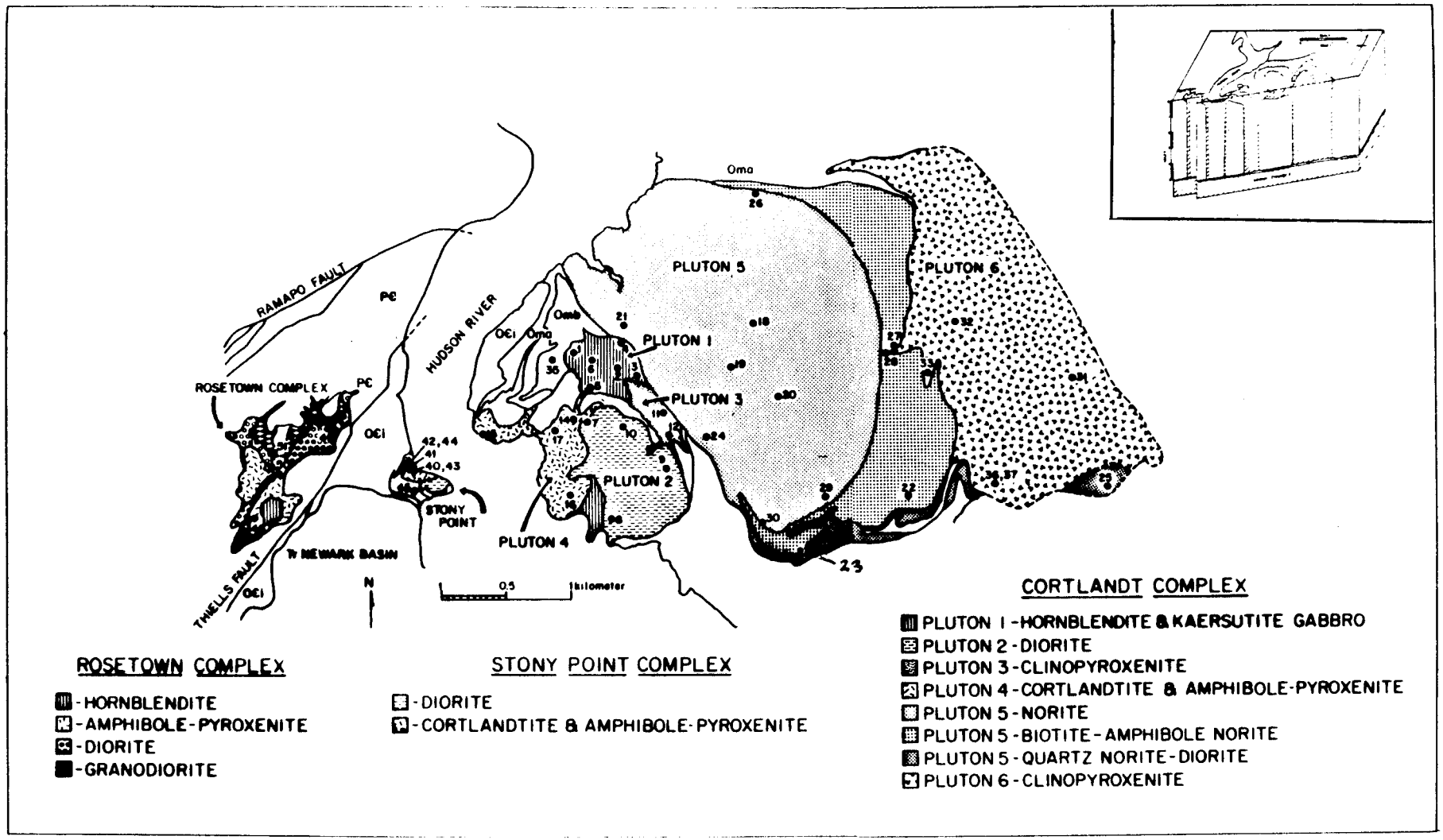

Fig. 2. Geologic and sample location map of the Cortlandt, Stony Point, and Rosetown complexes. Figure is simplified from geologic map compiled by Ratcliffe (unpublished data). Inset shows the proposed conduits of Steenland and Woolard, 1952.

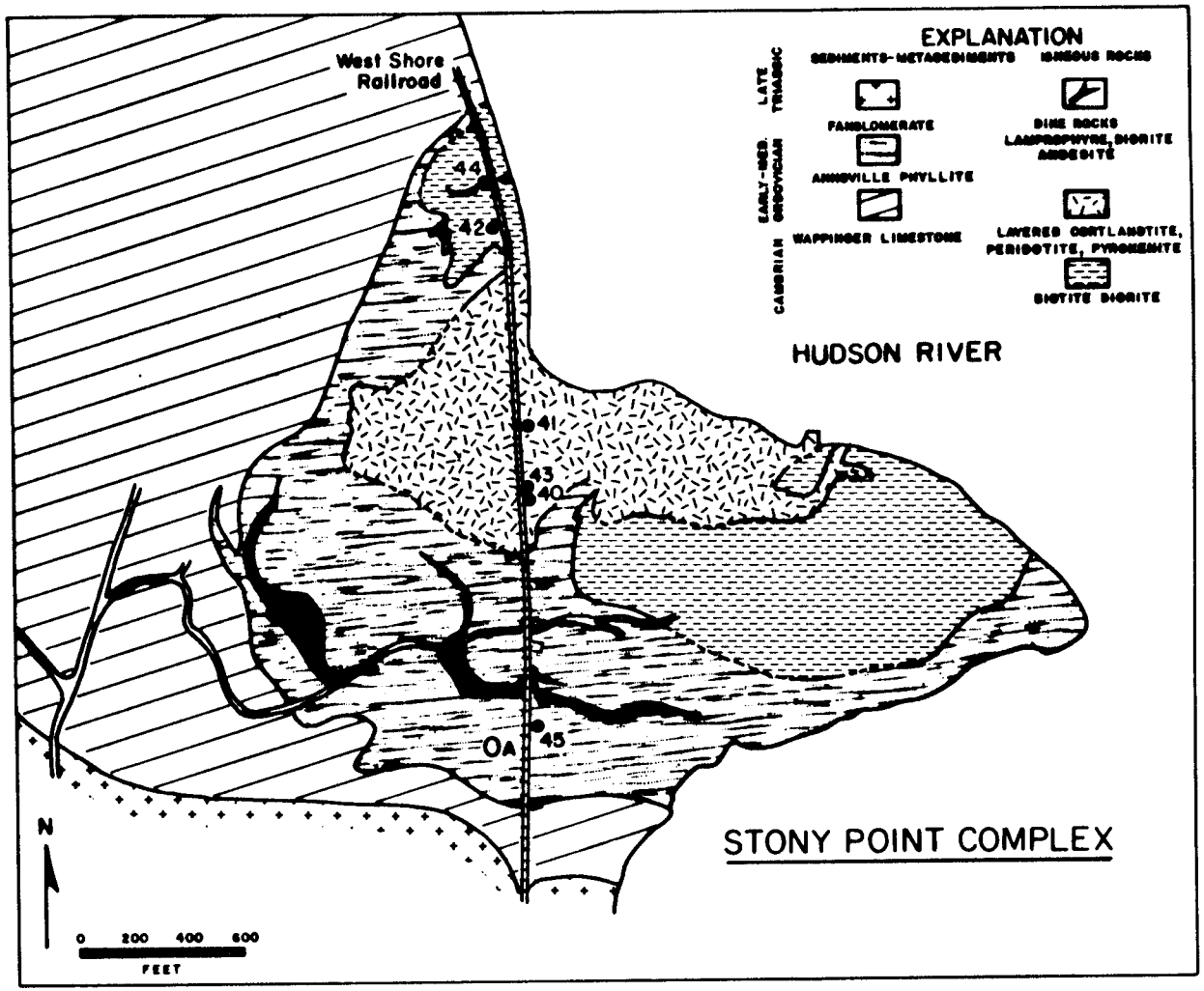

Fig. 3. Geologic and sample location map of the Stony Point complex. Figure modified from N.M. Ratciffe (1968).

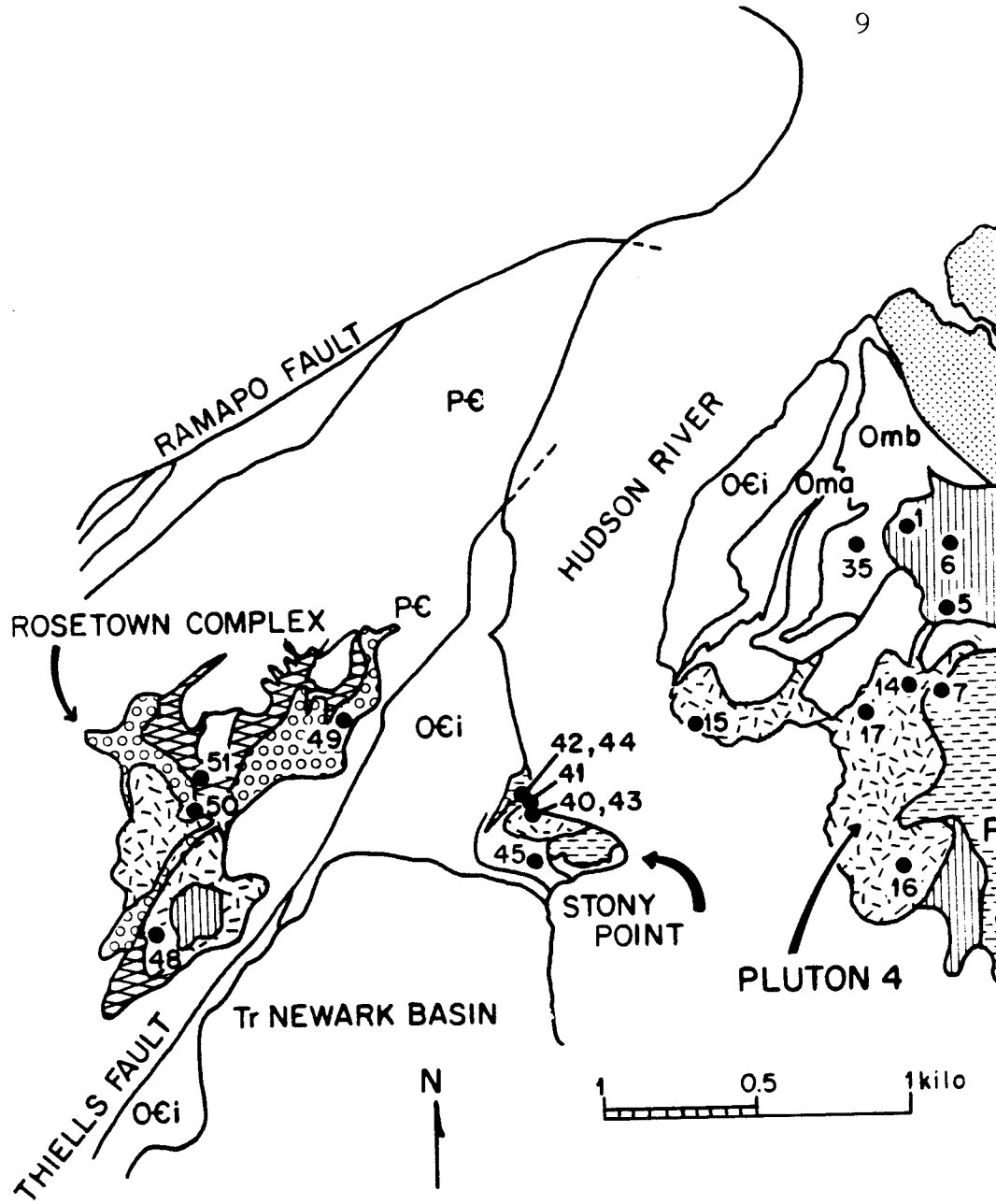

ROSETOWN COMPLEX

- HORNBLENDITE
- AMPHIBOLE-PYROXENITE
- DIORITE
- GRANODIORITE

Fig. 4. Geologic and sample location map of the Rosetown complex. Figure is simplified from geologic map compiled by Ratcliffe (unpublished data).

From the distribution of the regional metamorphic zonation and pelitic xenolith fabrics, Ratcliffe (1979, personal communication) concludes that the Cortlandt plutons were intruded during or near the maximum P-T conditions of the Taconic event. While the Cortlandt complex experienced slight folding during the Acadian orogeny (Ratcliffe, personal communication), its chemistry, mineralogy, and igneous textures appear to be unaltered. K-Ar (Long and Kulp, 1962) and $^{40}Ar/^{39}Ar$ (Dallmeyer, 1975) ages for biotites and amphiboles from the Cortlandt and Rosetown complexes range between 420 and 450 million years.

Early mapping of the Cortlandt complex (Rogers, 1911; Balk, 1927, 1937; Shand, 1942) revealed that the internal flow structures of the Cortlandt rock types define roughly concentric patterns. From this information, Balk (1937) concluded that the complex was a single funnel-shaped intrusion which contains three smaller interior funnels. Stony Point and Rosetown were considered to be coeval with the larger Cortlandt body. Shand (1942) concurred with the single funnel hypothesis of Balk and concluded that the parental magma for the entire complex was noritic, and that differentiation, crystal accumulation, and assimilation of crustal rocks led to the production of the diverse

rock types. A geophysical study of the Cortlandt area (Steenland and Woollard, 1952) shows no evidence of a feeder pipe in the central region of the complex as postulated by Balk and Shand. The gravity data suggest that there are four distinct feeder pipes located along an east-west line from the eastern edge of the Cortlandt complex to the Rosetown exposure (Fig. 2). The inferred width of these pipes varies from 0.3 kilometers in diameter at Rosetown and Stony Point to as large as 3.9 kilometers at the eastern margin of the complex.

Cortlandt Complex

Recent mapping of the Cortlandt, Stony Point, and Rosetown complexes (Fig. 2) by Ratcliffe (1968, 1971, personal communication) reveals that these bodies are composite (Fig. 2) and were not formed by differentiation of a single parental magma. Ratcliffe has mapped six sequentially intruded, contemporaneous plutons within the Cortlandt complex. From oldest to youngest these are: (1) hornblendite to amphibole gabbro; (2) diorite; (3) clinopyroxenite; (4) cortlandtite and amphibole-pyroxenite; (5) norite; and (6) clinopyroxenite.

Rocks from the hornblendite pluton (pluton 1) are amphibole (kaersutite)-rich gabbros that have a well-

developed flow structure defining a northwest trending funnel-shaped body. Differentiated rocks within this pluton also contain orthopyroxene, biotite, and quartz. Diorites of pluton 2, which are separated from pluton 1 by a screen of pelitic country rock, are composed of plagioclase, biotite, quartz, orthopyroxene, and kaersutite. Minor amounts of almandine garnet are also found in these peraluminous diorites. Clinopyroxenite of pluton 3 has a cumulus textural relationship involving clinopyroxene, orthopyroxene, olivine, opaques, and kaersutite suggesting formation by crystal accumulation. Coarse amphibole pyroxenite and amphibole peridotite (cortlandtite) of pluton 4 is characterized by poikilitic kaersutite amphibole enclosing euhedral olivine, orthopyroxene, and clinopyroxene grains. Norite (pluton 5), the largest of the Cortlandt plutons, cuts plutons 1 and 3 along a northwest trending intrusive contact. The norite pluton is considered by Ratcliffe (personal communication) to be a thin, spoon-shaped sill originating from an eastern conduit. The central region of the norite pluton consists of well-layered norite containing abundant inclusions of Inwood marble and Manhattan schist. Xenoliths of Manhattan schist, which have been altered extensively due to interaction with

the noritic magma, range in size from centimeters to hundreds of meters in thickness. Rhythmically layered norite, the dominant lithology, consists of plagioclase, orthopyroxene, clinopyroxene, biotite, and opaques. Amphibole is generally lacking in the norites except near the center of pluton 5 which is marked by a region of norite containing poikilitic kaersutite. Zones within and along the margins of the norite pluton contain K-feldspar and quartz and the composition is more monzodioritic rather than noritic. Pyroxenite of pluton 6 crosscuts flow layering of the norite pluton. Mineralogy and cumulate textures duplicate those found within the clinopyroxenite of pluton 3.

The Peekskill granodiorite-quartz monzonite intrusion is located at the northern margin of the norite body (Fig. 1). This steep-walled, elongated pluton cuts across the faulted boundary of the Reading and Manhattan Prongs and is separated from the main portion of the Cortlandt complex by a thin (0.5 km) screen of Manhattan schist. Geologic relationships (Mose et al., 1976) show that the Peekskill pluton postdates the mafic plutons of the Cortlandt complex. However, controversy exists as to whether the Peekskill granodiorite is temporally and genetically related to the intrusions of the Cortlandt mafic complex. Mose and

others (1976) obtained a 371 ± 14 m.y. Rb-Sr whole rock isochron age for the Peekskill pluton and they conclude that the age and field relationships suggest that the Peekskill pluton is post-tectonic and much later than the intrusion of the Cortlandt complex. However, Armstrong (unpublished data) found that, although the isotopic data for the Peekskill pluton plot very close to his Cortlandt isochron (∿ 420 m.y.), two samples with high Rb/Sr ratios do not. These two samples control the isochron because of their low Sr concentrations. In addition, resetting during the Acadian orogeny may be responsible for the younger ages of these two samples.

Stony Point Complex

At Stony Point, diorite and cortlandtite plutons are mineralogically similar to plutons 2 and 4 of the Cortlandt complex (Figs. 2 and 3). However, the diorite at Stony Point contains considerably more almandine garnet (∿ 3 volume %) than diorites on the eastern side of the Hudson River (∿ 0.1 volume %). Numerous diorite, cortlandtite, and lamprophyric dikes crosscut the diorite and cortlandtite plutons at Stony Point. Ratcliffe (personal communication) suggests that the main Cortlandt intrusion and the plutons at Stony Point are continuous beneath the Hudson River. However, strontium isotopic

data obtained as part of this study indicate that the diorite and cortlandtite rocks of the Stony Point and Cortlandt complexes may not be physically or genetically related.

Rosetown Complex

The Rosetown complex consists of three intrusive sequences that are elongate parallel to the nearby Ramapo fault system (Figs. 2 and 4). The oldest intrusive center contains concentrically zoned hornblendite, cortlandtite, and amphibole diorite (Ratcliffe, 1971). These closely resemble the rocks from plutons 1, 2, and 4 of the Cortlandt complex. A north-northeast trending amphibole-biotite diorite pluton cuts the oldest intrusive center. This body contains xenoliths of lower Paleozoic sedimentary rocks similar to those contained by the Cortlandt complex. The youngest sequence is a granodiorite which crops out near the northern and southern ends of the Rosetown body. This granodiorite, which closely resembles the Peekskill granodiorite, contains numerous mafic cognate xenoliths near its contact with the kaersutite-bearing diorite pluton.

ANALYTICAL METHOD AND UNCERTAINTY

Samples were collected from the three Cortlandt region complexes as mapped by N. M. Ratcliffe on the basis of their location within a pluton, mineralogical composition, and lack of alteration. From these samples, which were representative of the individual plutonic areas, approximately 200 polished thin sections were prepared in order to determine petrographic features and modal percentages of the various rock types. Mineral chemistries were determined through use of an automated, four spectrometer, ARL-EMX-SM electron microprobe. All analyses were reduced by the method of Bence and Albee (1968) with a correction matrix modified from one reported by Albee and Ray (1970). All pyroxene analyses were reduced by the procedure of Papike et al. (1974). On the basis of certain crystal chemical constraints, this method estimates the ferric iron content and the percentage of other than quadrilateral components. Reported amphibole analyses were reduced by a similar procedure; however, the complex nature of the amphibole crystal chemistry limits the constraints on estimating the amount of ferric iron. Therefore, the tabulated amphibole analyses reported are mean Fe^{3+} values of the allowable ferric iron abundances according to the Papike et al. (1974) calculation scheme.

Whole rock samples were prepared for use by splitting 5-10 kilograms of fresh rock to 30 grams and grinding to -80 mesh size. Major element analyses were obtained through microprobe examination at Stony Brook, through x-ray fluorescence analysis by A. J. Erlank at Cape Town, and through gravimetric and atomic absorption analysis by N. H. Suhr and J. B. Bodkin at the Pennsylvania State University.

At Stony Brook, approximately 400 mg of the -80 mesh powders were fused in air without flux on an iridium strip furnace (Nicholls, 1974) and were analyzed by the electron microprobe. Homogenous glasses were obtained by this method for most samples with SiO_2 contents less than 55 wt.%. Samples with higher silica contents could not be successfully fused to crystal free glasses and were, therefore, analyzed through x-ray fluorescence. Each Stony Brook major element analysis (10 elements) represents an average of six or more spots using a 35 micrometer beam. All analyses were calibrated using the U.S.G.S. standard rocks BCR-1 and BHVO-1 (Flanagan, 1973; Ayuso et al., 1976; Mazzullo and Bence, 1976). Internal precision depends on the abundance of the element but is generally $\sim 5\%$.

Ferrous iron, total iron as Fe_2O_3, P_2O_5 and $H_2O^{\pm}$

were determined for several samples at the Pennsylvania State University Mineral Sciences Laboratory.

Twenty-six samples were analyzed for major (13 elements) and trace (Rb, Sr, Ba, transition metals, Y, Nb, and Zr) elements by x-ray fluorescence at the University of Cape Town. These analyses were obtained on a Phillips PW 1220 2KW semi-automatic x-ray spectrometer. Collection methods and precision for these data are reported by Willis et al. (1971) and Erlank and Kable (1976).

Rare-earth elements (REE) and Ba analyses were obtained by isotope dilution techniques on the Stony Brook fully automated, 12-inch radius, 90^{o} sector, NBS design, mass spectrometer. The chemical technique for REE is that of Arth (written communication, 1973) and Hanson (1976). Chemical dissolution of samples was performed with a lithium metaborate flux following the procedures developed by Hänny and reported by Vocke (1980). Rb and Sr were also analyzed by isotope dilution using a 6-inch, 60^{o} sector, NBS designed, mass spectrometer. The analytical precision for each REE is better than 2%, except for Gd and La, for which it is better than 5%. Leedey chondrite values (Masuda et al., 1973) divided by 1.2 are used for normalizing purposes in this study.

Rb and Sr values have uncertainties of less than 1% of the amount present, while the analytical precision for Ba is better than 3%. Replicate analyses of Rb, Sr, and Ba by isotope dilution and XRF analysis yield similar values which attest to the precision of both methods.

$^{87}Sr/^{86}Sr$ ratios were measured on the 6-inch mass spectrometer using a digital readout and the chemical procedures of Hanson et al. (1971). Nine runs of standard SRM 987 yielded a value of 0.71010 with a standard deviation of $\pm$ 0.0001(2σ). The standard deviation of the mean for these data is $\pm$0.00004(2σ). Four replicate analyses, as well as the nine runs on the strontium standard, suggest that the uncertainty of any one analysis is approximately $\pm$ 0.0001(2σ).

ANALYTICAL RESULTS

PETROGRAPHY AND MINERAL CHEMISTRY

Brief petrographic descriptions and mineral chemistries for each of the major rock types found both within and associated with the Cortlandt, Stony Point and Rosetown complexes are presented in this section. Detailed petrographic descriptions of individual samples are contained in Appendix 1. The rock names used are those originally assigned by Williams (1884, 1886, 1887), Rodgers (1911), and Shand (1942) and are retained for the purposes of this study. The rock units discussed are those found within individual plutons and include: 1. hornblendite-kaersutite gabbro; 2. diorite; 3. clinopyroxenite; 4. cortlandtite and amphibole-pyroxenite; 5. norite; and 6. granodiorite. Data are also presented for two mafic dikes crosscutting the Stony Point plutons. The petrology and mineralogy of samples from the Salt Hill emery mine (Barker, 1964) conclude this section.

Hornblendite-Kaersutite Gabbro: Cortlandt Complex-Pluton 1

The hornblendite-kaersutite gabbroic pluton is the oldest of the Cortlandt plutons (Ratcliffe, unpublished data). It is characterized by strong preferred

orientation of primary prismatic amphibole which appears to be a consequence of flow. The rocks are medium to coarse grained with amphibole crystals often attaining lengths of several centimeters. In general, samples from this pluton consist of high titanium ($\sim$ 3.6 wt.%), high alumina ($\sim$ 14 wt.%) amphibole, plagioclase (An_{80-34}), and biotite (Fe/(Fe + Mg) 0.29-0.36). According to the classification of Papike et al. (1974) these titaniferous amphiboles are magnesio-kaersutites and pargasites. Accessory phases include: ilmenite, magnetite, rutile, pyrite, pyrrhotite, apatite, and sphene. The amount of kaersutite determines classification as hornblendites (>70% kaersutite) or kaersutite gabbros (< 70% kaersutite). A small region of this pluton (sample #3) is characterized by a rock which contains iron-rich orthopyroxene, interstitial quartz, and K-feldspar in addition to amphibole ($\sim$ 15%), plagioclase, and biotite. Amphibole-norite will be the future reference for this rock unit contained within pluton 1.

In thin section, the amphiboles are dark reddish-brown to yellow-brown in color and frequently exhibit lamellae of ilmenite and rutile parallel to the c-direction (Fig. 5). These exsolved lamellae appear to be products of a breakdown (oxidation) reaction, probably

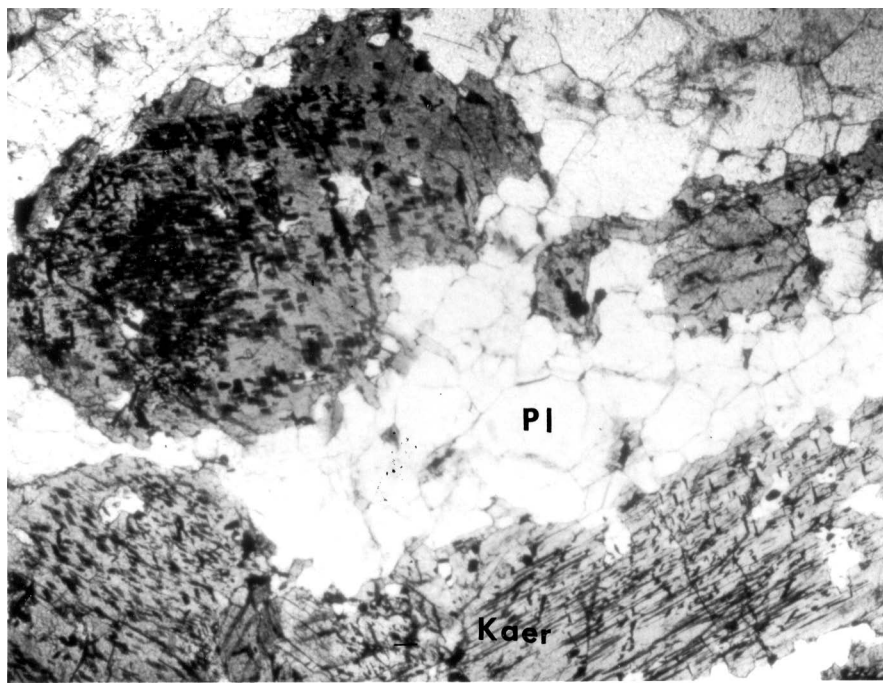

Fig. 5. Photomicrograph of kaersutite (Kaer) exhibiting lamellae of ilmenite and rutile. Plagioclase (Pl) coexists with the kaersutite crystals in this hornblendite sample 4. Length of field is 3.5 mm. Uncrossed nicols.

the result of local reheating of these rocks by the intrusion of the nearby norite pluton. The cumulate amphibole grains within the hornblendite samples are unzoned and frequently appear to have been broken, then fused with other large kaersutite crystals. Often, plates of biotite occur at the sutures between the joined amphibole grains (Fig. 6). Biotite grains and rutile and ilmenite inclusions in these rocks may be observed in coexisting kaersutite grains. In general, biotite is a minor constituent of the hornblendites (< 3 volume %), usually comprising less than 15% of the kaersutite gabbros.

Plagioclase, the second most abundant phase within these rocks, usually exhibits a subhedral to euhedral morphology and varies in modal proportion from approximately 5% (hornblendite) to 55% (kaersutite-gabbro). The most calcic plagioclases (An_{80}) are associated with the cumulate hornblendites and display both normal and reverse zonation. With the gradational change from hornblendite through gabbro, plagioclase compositions within the rocks becomes both increasingly more sodic ($\sim An_{50}$) and less idiomorphic. Appendix 2 contains selected amphibole, biotite, plagioclase, and orthopyroxene analyses for rocks of pluton 1. Plotted on

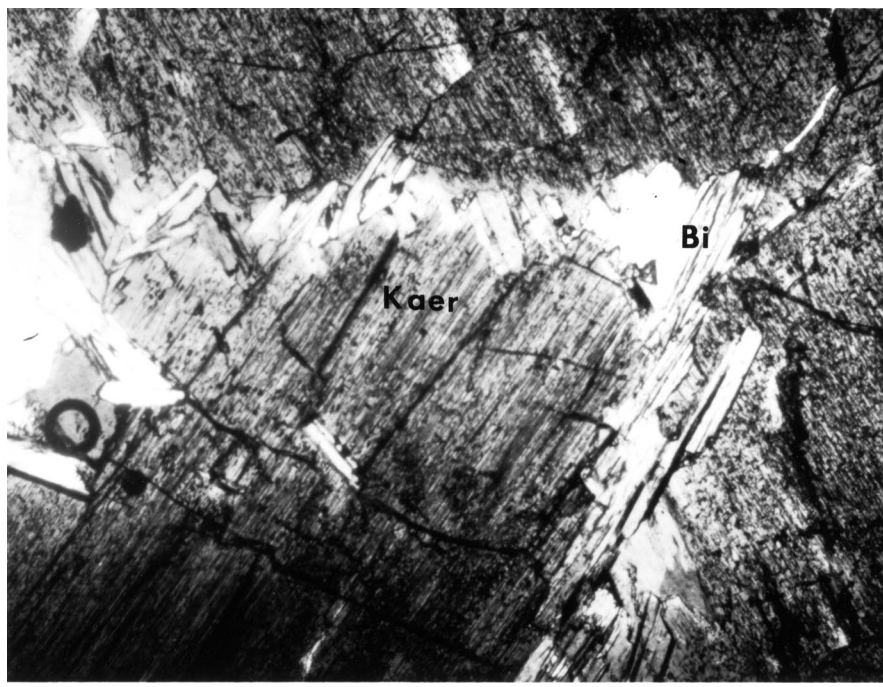

Fig. 6. Photomicrograph of broken and sutured kaersutite (Kaer) crystals with biotite (Bi) grains along breaks. Hornblendite sample 1. Length of field is 3.5 mm. Uncrossed nicols.

Figs. 7 and 8 are the quadrilateral relationships of the pyroxene and amphiboles analyzed from the hornblendite-kaersutite gabbro body.

Diorite: Cortlandt, Stony Point, and Rosetown Complexes

Cortlandt Complex-Pluton 2

Samples from pluton 2 of the Cortlandt complex are medium to coarse grained and consist of equal proportions of euhedral kaersutite (0.25-0.75 mm) and fresh plagioclase (0.5-3.0 mm) with subordinate amounts of biotite and orthopyroxene. Generally, the plagioclase laths are randomly oriented and tightly packed together with the prismatic amphibole grains indicative of a cumulate texture. Accessory phases include magnetite, ilmenite, pyrite, pyrrhotite, and apatite. Almandine garnet crystals are infrequently present in these rocks. Mineral compositions (Appendix 3) and textures of rocks from this pluton are closely related to those of the nearby hornblendite-kaersutite gabbros of pluton 1. The high anorthite content (An_{77}-An_{51}) of the plagioclase in samples from this body result in classification of these rocks as gabbroic rather than dioritic. Orthopyroxene, when present, exists as small (0.5-1.5 mm), euhedral to subhedral, sometimes rounded grains. These grains are pleochroic from pink to pale yellow and are occasionally altered to fibrous brown amphibole along

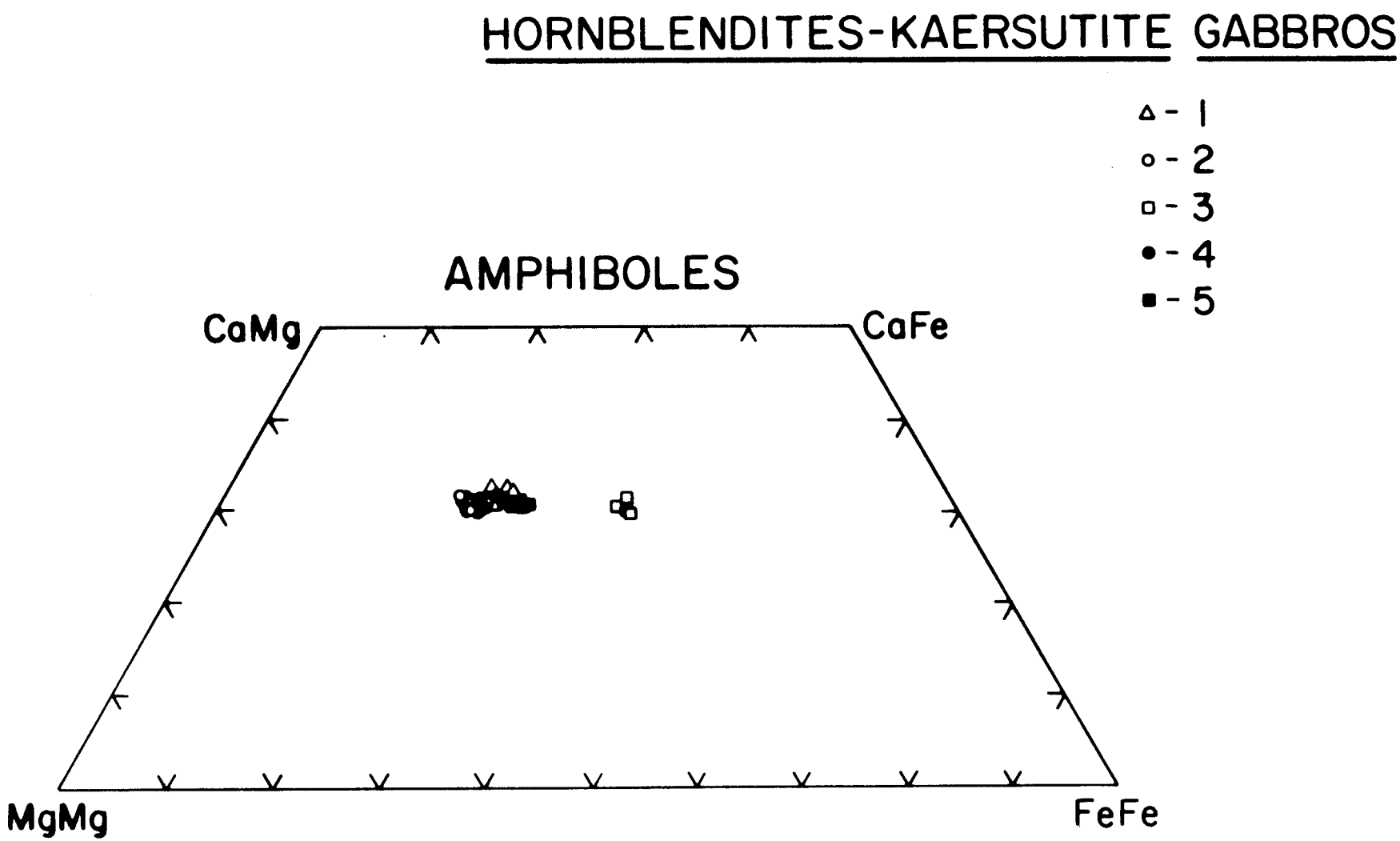

Fig. 7. Quadrilateral relationships of amphiboles analyzed from the hornblendite kaersutite gabbro of the Cortlandt complex from pluton 1. Selected amphibole analyses from each sample (see Fig. 2 for sample location) are represented by the designated symbol.

▫ 3

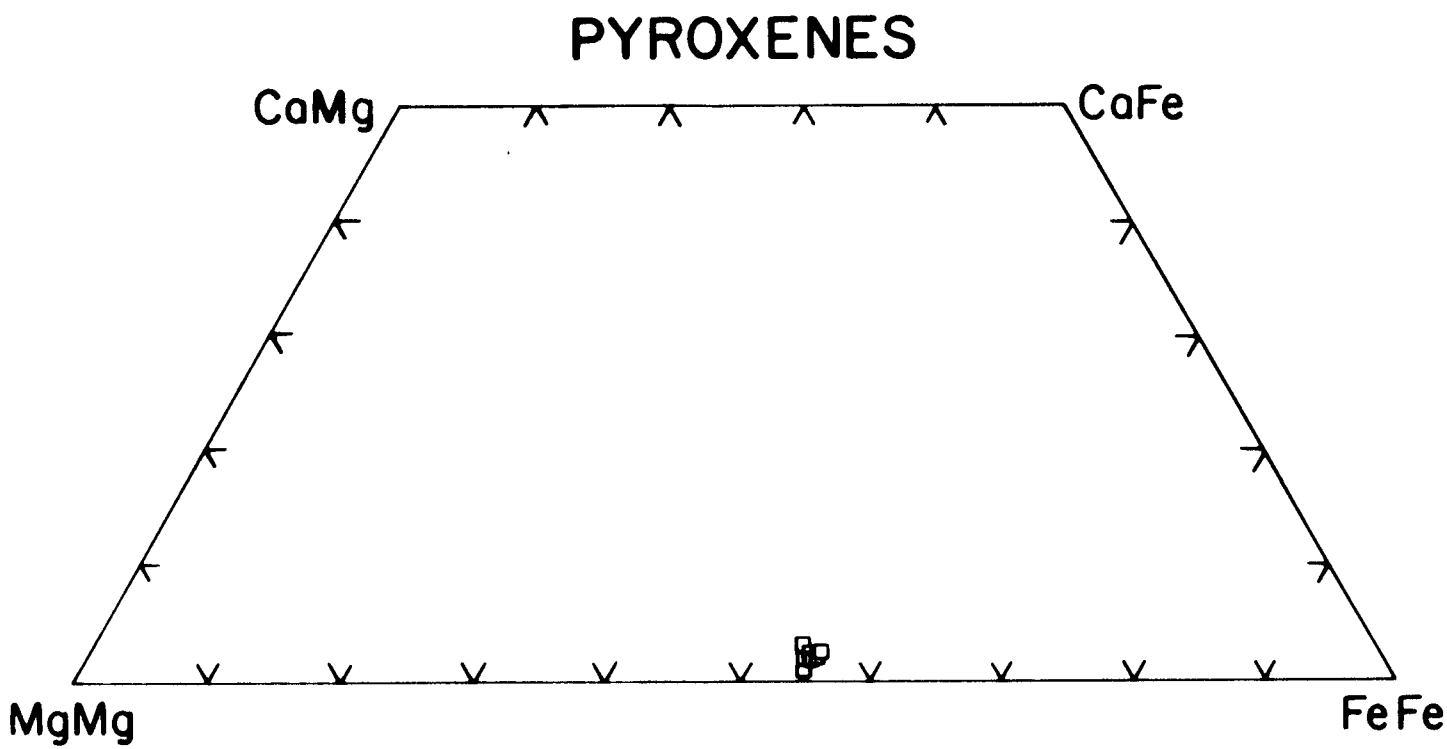

Fig. 8. Quadrilateral relationships of pyroxenes analyzed from the hornblendite kaersutite gabbro of the Cortlandt complex from pluton 1. Selected pyroxene analyses from sample 3 (see Fig. 2 for sample location) are represented by the designated symbol.

fractures. Amphibole compositions (Appendix 3, Fig. 9) show greater overall chemical variation than the amphiboles of pluton 1. In fact, some amphiboles (sample #8) have much lower titanium and calcium abundances than kaersutites from other parts of pluton 2. The lower TiO_2 content apparently prevented the exsolution of ilmenite and rutile lamellae in these hornblendes.

Phase chemical analyses of amphibole, plagioclase biotite, and orthopyroxene for the Cortlandt diorite are contained in Appendix 3. Amphibole and pyroxene compositions for this same pluton are illustrated in Figs. 9 and 10.

Stony Point Complex

While the diorites of the Cortlandt complex have a distinctly basic character, the diorites immediately across the Hudson River at Stony Point do not have this same affinity. The dioritic material exposed at Stony Point lacks both amphibole and orthopyroxene and consists almost entirely (70%) of sodic plagioclase (An_{20}) and an iron-rich biotite ($Fe/(Fe + Mg) \approx 0.69$) (Appendix 3). Plagioclase crystals in this coarse-grained rock are quite large (0.4-1.0 cm) and display well-developed crystal faces. Unlike the plagioclase in pluton 2, many of the plagioclase laths at Stony

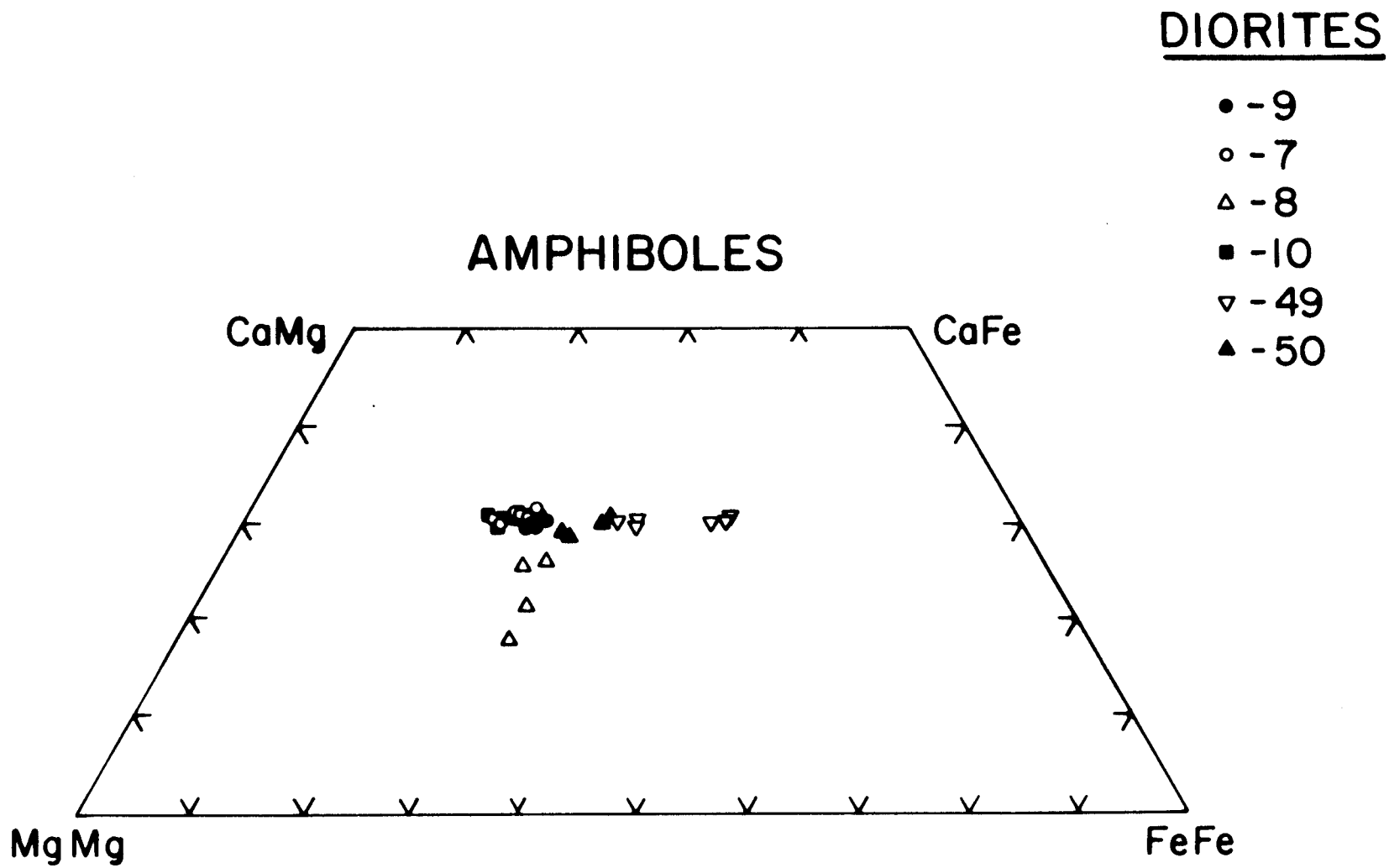

Fig. 9. Quadrilateral relationships of amphiboles analyzed from the diorites of the Cortlandt (pluton 2), Stony Point, and Rosetown complexes. Selected amphibole analyses from each sample (see Fig. 2 for sample location) are represented by the designated symbol.

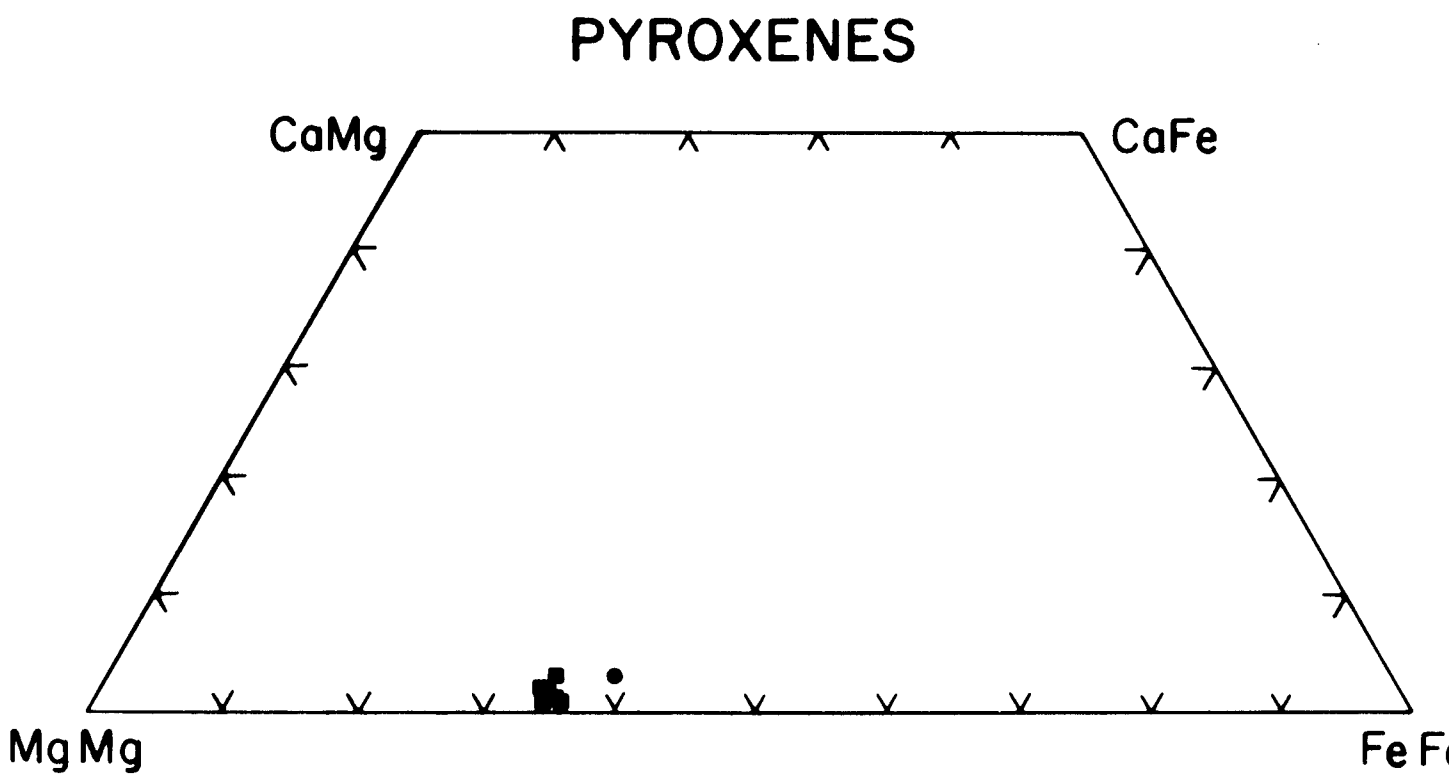

Fig. 10. Quadrilateral relationships of pyroxenes analyzed from the diorites of the Cortlandt (pluton 2), Stony Point, and Rosetown complexes. Selected pyroxene analyses from each sample (see Fig. 2 for sample location) are represented by the designated symbol.

Point are partially sericitized. Some crystals also show oscillatory zoning. Anhedral plates (1-7 mm) of green-brown biotite are evenly distributed throughout these rocks and are partially rimmed by magnetite and ilmenite. Zircon, epidote, and apatite are minor additional phases. Constituting approximately 2 volume percent of the Stony Point diorite are euhedral (0.5-5.0 mm) almandine garnets (Appendix 3) that sometimes occur as inclusions within plagioclase crystals. These garnet grains lack signs of alteration (i.e., biotite replacement) (Fig. 11) or physical transport, and, thus, appear to have crystallized from the dioritic magma rather than country rock relics. Occasional garnet-rich layers (1-3 cm) are present throughout the Stony Point diorite and suggest that garnet may have been an important fractionating phase in this pluton.

Rosetown Complex

Diorites at the Rosetown complex are intermediate to the basic variety of the Cortlandt complex and the more felsic type at Stony Point. At Rosetown, diorite samples lack orthopyroxene but contain substantial amounts of kaersutite and biotite coexisting with an intermediate plagioclase (An_{24-36}) (Appendix 3). Samples from this pluton are coarse to medium grained and

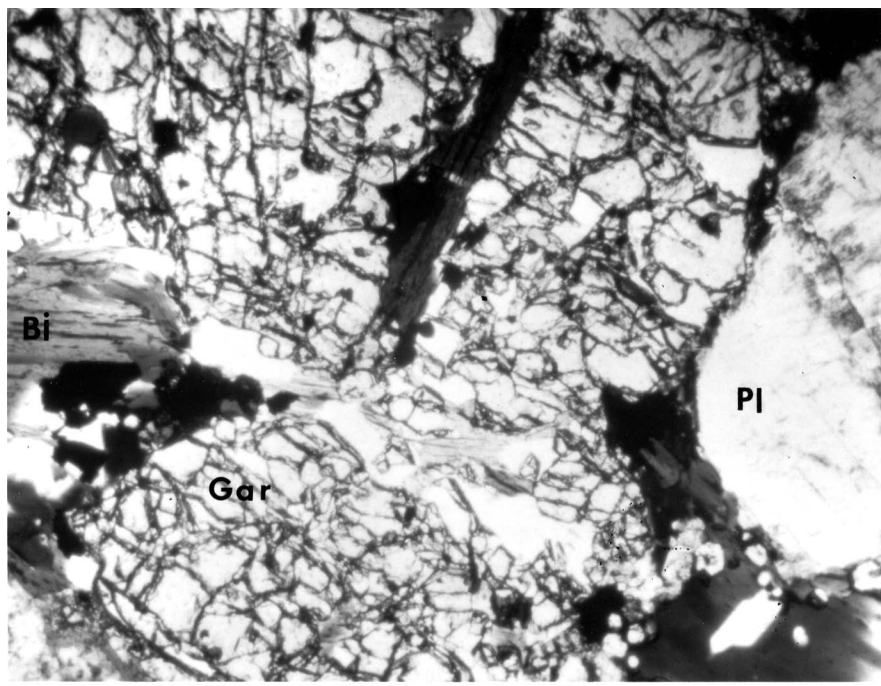

Fig. 11. Photomicrograph of almandine garnet (Gar), biotite (Bi) and plagioclase (Pl) in diorite sample 42. Length of field is 3.5 mm. Uncrossed nicols.

are composed of equal amounts of felsic and mafic minerals. Euhedral kaersutite is the most abundant ($\sim$30%) mafic phase and frequently is partially replaced with red-brown biotite. Kaersutite (Appendix 3, Fig. 9) lacks evidence of rutile and ilmenite exsolution. Plagioclase grains display euhedral to subhedral morphologies and generally are cloudy in thin section due to sericitization. Often, plagioclase laths are strongly normally zoned ($\sim An_{36-15}$) (Appendix 3). Biotite (Appendix 3) comprises approximately 15-20% of the rock by volume and occurs as flakes and small plates; it is often associated with amphibole. Quartz and K-feldspar are interstitial. Accessory phases include: sphene, apatite, epidote, ilmenite, magnetite, pyrite, and pyrrhotite.

Clinopyroxenite: Cortlandt Complex--Plutons 3 and 6

Black colored clinopyroxenites from these two widely separated plutons (Fig. 2) show remarkable similarity in texture, modal mineralogy, and phase chemistry (Appendix 4). In general, the rocks from these two bodies are medium grained hypidiomorphic to allotrimorphic-granular and rich in clinopyroxene ($\sim$60 volume %; $Wo_{\sim 43-51}$, $En_{\sim 42-48}$, $Fs_{\sim 5-12}$). Modal proportions of orthopyroxene (10-35%; $Wo_{\sim 1-3}$, $En_{\sim 69-83}$, $Fs_{\sim 15-30}$) and olivine (0-35%; Fo_{79}-Fo_{75}) vary in these

ultramafic rocks depending upon sample locality but, most often, these phases are found to coexist with kaersutite (< 5%) and opaques (magnetite, ilmenite, pyrite, and pyrrhotite). Plagioclase and biotite, when present, form irregular interstitial grains. Clinopyroxene and orthopyroxene grains in these rocks display hypidiomorphic outlines and an extremely variable grain size (0.5 mm-1.0 cm). Typically, clinopyroxene grains in these rocks are twinned, simple or repeated on (100) and are often slightly pleochroic from pale yellow to pink, reflecting high titania contents ($\sim$ 1 wt.%) (Appendix 4). Both orthopyroxene and clinopyroxene in these rocks display well-developed Schiller structure (Fig. 12) with larger grains having fine (< 3 microns) exsolution lamellae of pyroxene. A characteristic feature of clinopyroxenes of pluton 3 is the presence of large (3-6 mm) euhedral orthopyroxene crystals that are bent and twisted (Fig. 13). Olivine occurs as colorless, round, anhedral grains (1-9 mm) that are commonly cut by a network of fractures. The olivine grains are unzoned and usually show only minor serpenterization (< 5%) along these breaks. Smaller ($\sim$ 1 mm) unfractured olivine grains are frequently enclosed within orthopyroxene and clinopyroxene grains and have identical compositions to the larger external

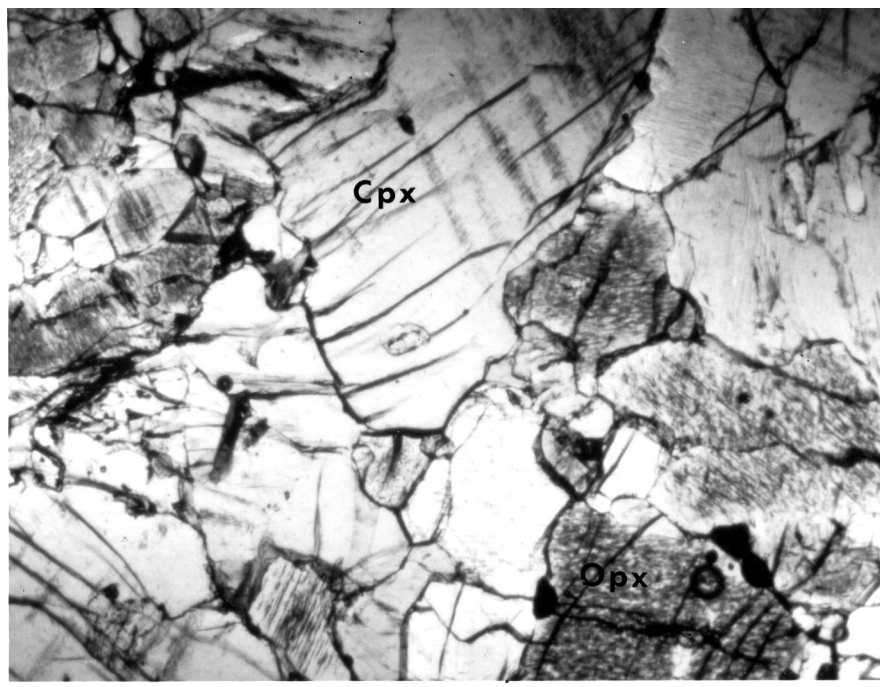

Fig. 12. Photomicrograph of clinopyroxenite (sample 31) exhibiting cumulate textures of clinopyroxene (Cpx) and orthopyroxene (Opx). Also, well-developed Schiller structure. Length of field is 3.5 mm. Uncrossed nicols.

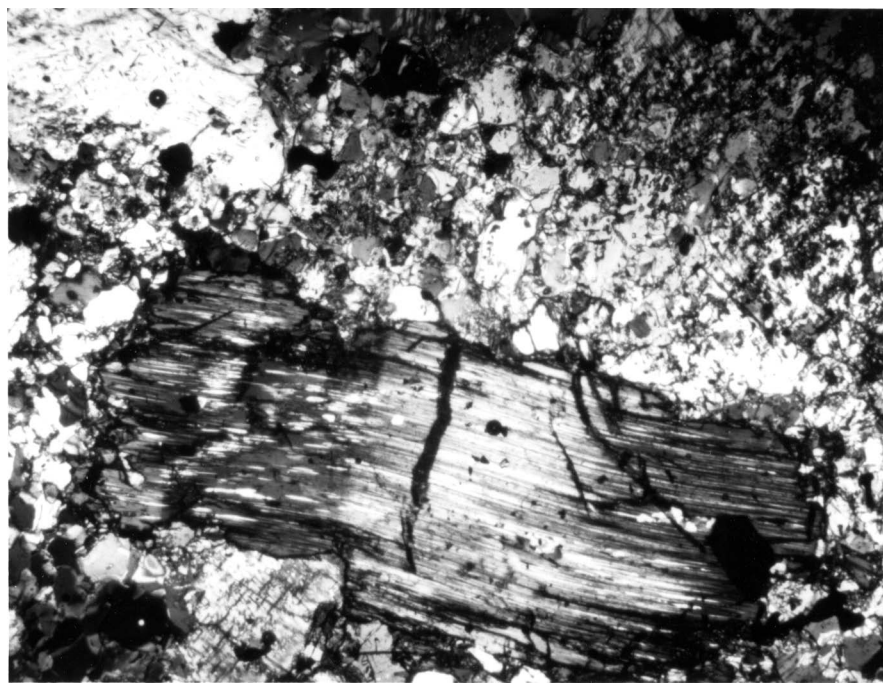

Fig. 13. Photomicrograph of clinopyroxenite sample 12 showing deformed orthopyroxene crystal. Length of field is 3.5 mm. Crossed nicols.

olivines. Red-brown kaersutite ($\sim$ 5%) is found interstitially, with a vein-like appearance between the other mafic phases and commonly has fine-grained ($\sim$ 0.5 mm) opaques (ilmenite, magnetite, and iron sulfides) associated with it. Red-brown magnesium-rich biotite (Appendix 4), like amphibole, is usually found along grain boundaries but also forms larger ($\sim$ 1 mm) plates at the juncture of pyroxene and olivine grains. Very small, rare spinel (Appendix 4) grains are found in one sample from pluton 6 and these occur enclosed within pyroxene. Plagioclase is generally a minor ($<$ 1 volume %) interstitial phase and displays a variable composition (An_{95-58}) (Appendix 4). Compositions of coexisting olivine, clinopyroxene, and orthopyroxene in these clinopyroxenite samples (Appendix 4) are consistent with the equilibrium Fe^{2+}-Mg partitioning data of Grover and Orville (1969) suggesting that these mafic phases crystallized together. The textures and the general lack of a significant felsic component in these samples indicate a cumulate origin and minor amounts of trapped intercumulus liquid. Clinopyroxenite, pyroxene, and amphibole compositions in molar Ca-Mg-Fe are illustrated on Figs. 14 and 15.

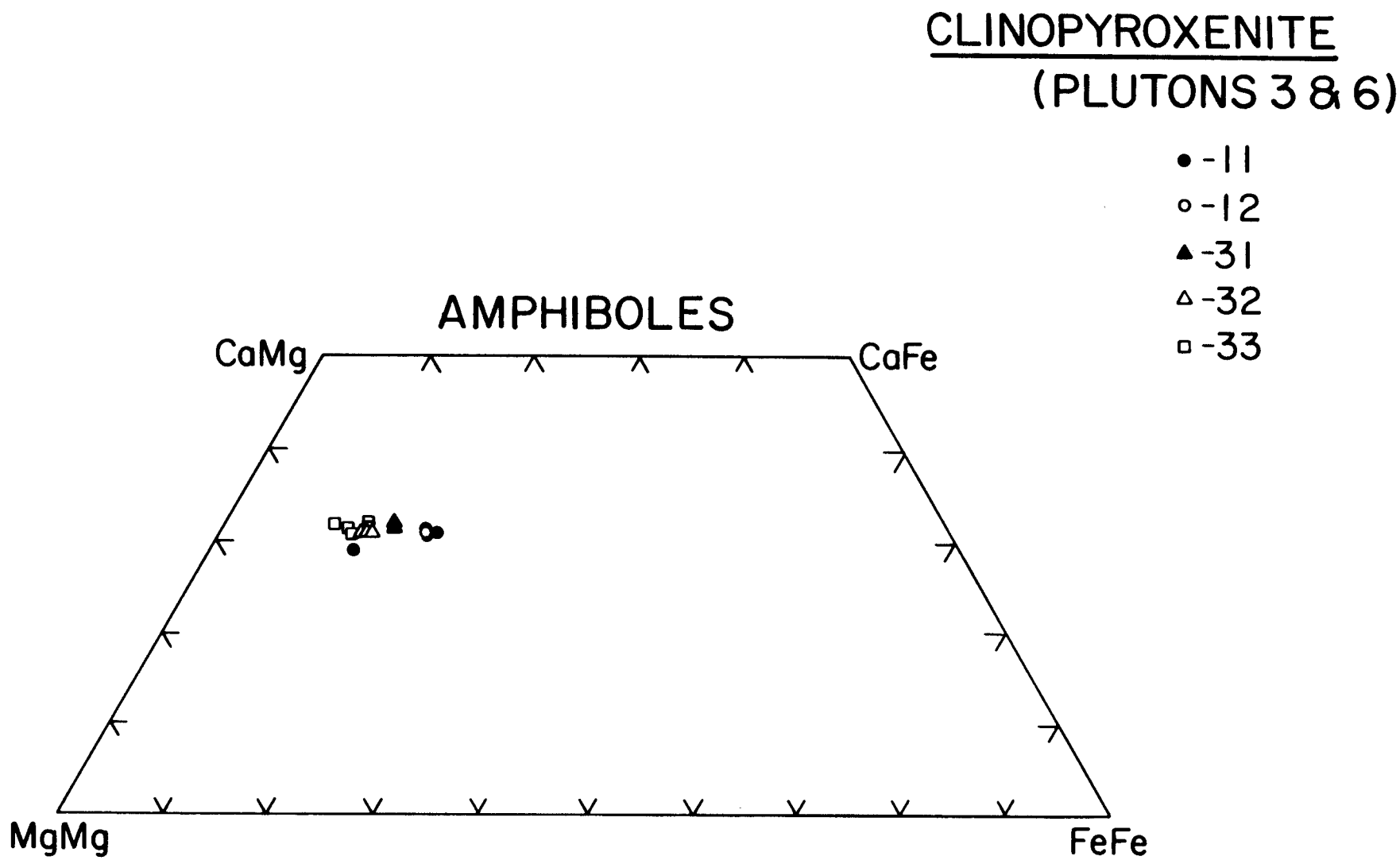

Fig. 14. Quadrilateral relationships of amphiboles analyzed from the clinopyroxenites of the Cortlandt complex (plutons 3 and 6). Selected amphibole analyses from each sample (see Fig. 2 for sample location) are represented by the designated symbol.

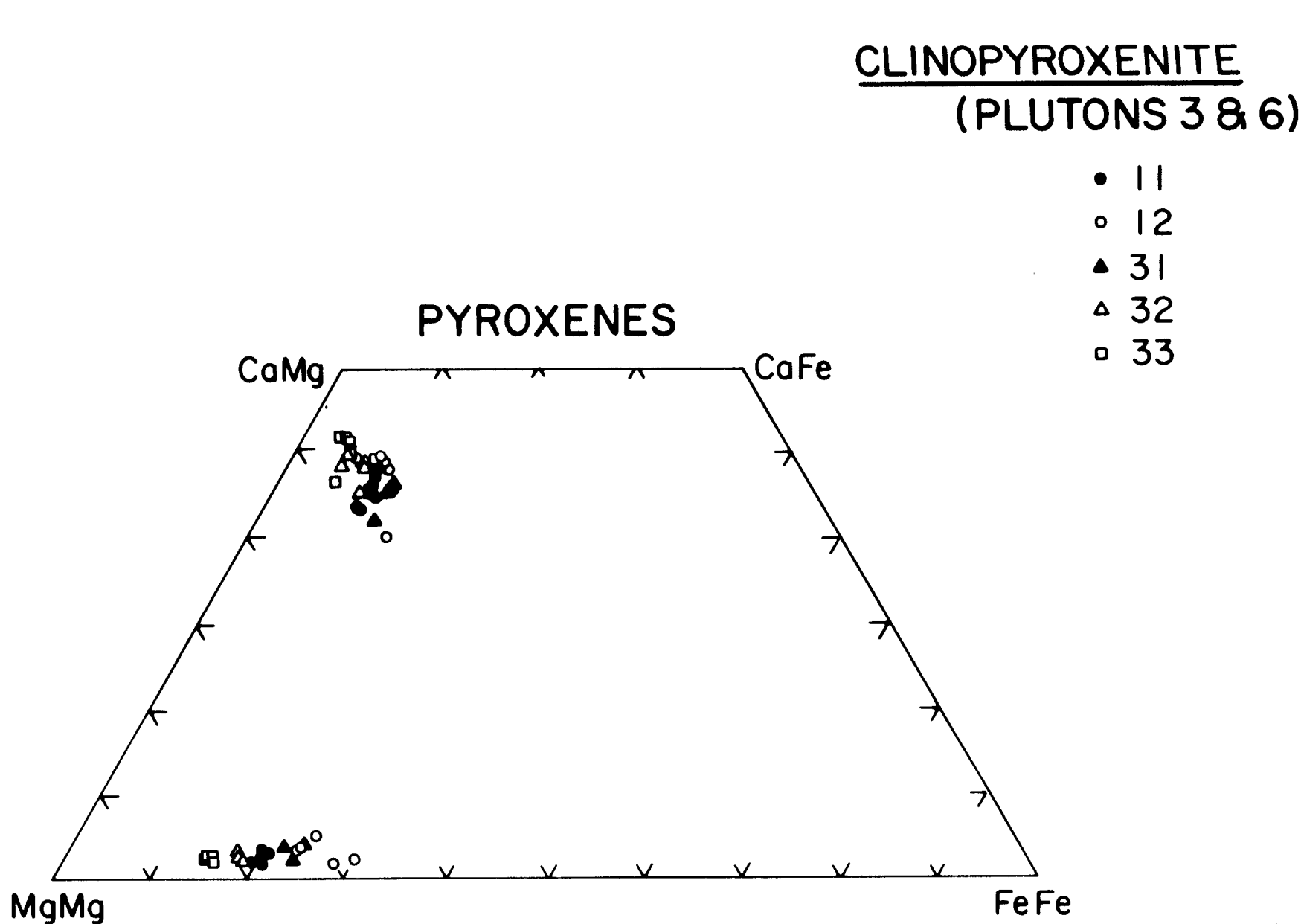

Fig. 15. Quadrilateral relationships of pyroxenes analyzed from the clinopyroxenites of the Cortlandt complex (plutons 3 and 6). Selected pyroxene analyses from each sample (see Fig. 2 for sample location) are represented by the designated symbol.

Cortlandtite and Amphibole Pyroxenite: Cortlandt--Pluton 4, Stony Point and Rosetown Complexes

Cortlandtite and amphibole pyroxenite rocks occur within pluton 4 of the Cortlandt complex and at the Stony Point and Rosetown complexes (Figs. 2 and 4). Cortlandtite, which consists of olivine, clinopyroxene, orthopyroxene, and amphibole, resembles both the texture and phase chemistry of the olivine-bearing clinopyroxenites of plutons 3 and 6. However, cortlandtites contain greater abundances of olivine (25-50%) and kaersutitic amphibole (10-30%). Generally, the amphibole is characterized by a poikilitic texture. Cortlandtite within these plutons grades into a rock type referred to as amphibole-pyroxenite, which lacks olivine and orthopyroxene. Clinopyroxene, kaersutite, biotite, and plagioclase are the major constituents of the amphibole-pyroxenites. Discussion of the petrography and phase chemistry of cortlandtite will be treated first, followed by a similar discussion of amphibole-pyroxenite.

Cortlandtite:

Cortlandtite is a black-colored, medium-grained rock which occurs within the Cortlandt and Stony Point complexes, but is apparently not exposed at Rosetown. The olivine (Fo_{80}-Fo_{75}) in this amphibole peridotite is

usually rounded, but sometimes exhibits a distinct crystal outline. Large ($\sim$ 5 mm) olivine grains are not uncommon but the olivine present is usually more diminutive (0.25-1 mm). In thin section, the olivine grains are colorless and usually crosscut by numerous fractures. Serpentine frequently fills these cracks and creates a vein-like network that extends away from the olivine grains and either collects or interjects along clinopyroxene grain boundaries. Often, magnetite, rather than serpentine, is located along the olivine fractures (Fig. 16). Alteration of olivine is never severe and normally comprises less than 10%. Olivines (Appendix 5) from the cortlandtite show limited ranges in composition (Fo_{80}-Fo_{76}) and large and small olivine grains are very similar in phase chemistry. Interlocked with olivine in these cortlandtite samples are subhedral to anhedral crystals of clinopyroxene. These clinopyroxenes are frequently twinned and have variable grain size (0.5-8 mm). In general, the clinopyroxene grains are larger than the associated olivine. Clinopyroxenes ($Wo_{\sim 43\text{-}49}$, $En_{\sim 43\text{-}50}$, $Fs_{\sim 5\text{-}10}$) are usually unzoned but, unlike olivine, there is considerable variation in chemical composition from large to small grains. Most often, the smaller anhedral pyroxenes have the lower Mg/(Mg + Fe) ratios within each rock. Overall,

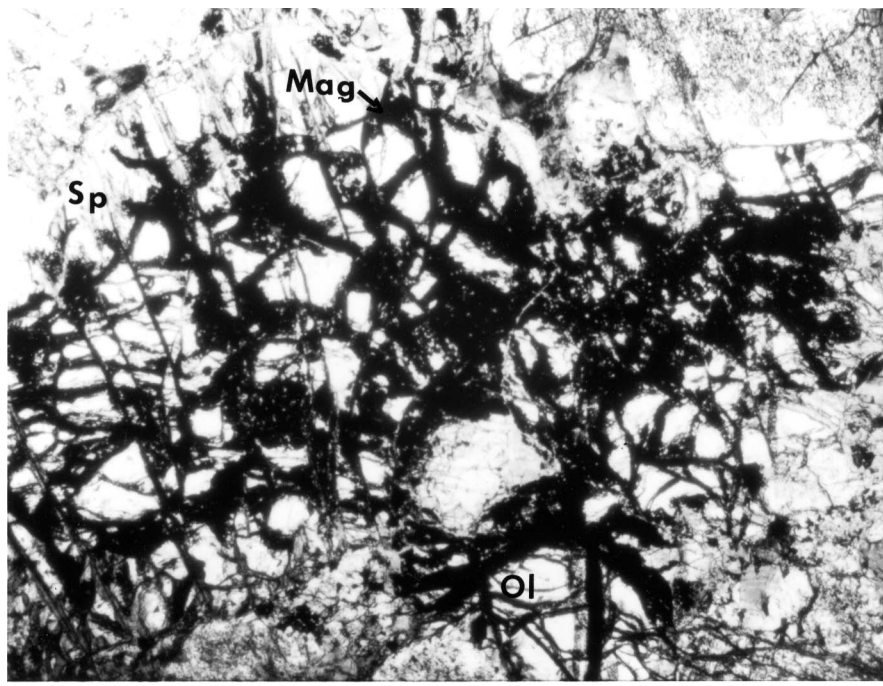

Fig. 16. Photomicrograph of highly fractured olivine (Ol) grain from cortlandtite sample 14. Magnetite (Mag) fills internal cracks with serpentine (Sp) found along margins. Length of field is 3.5 mm. Uncrossed nicols.

the phase chemistries of clinopyroxenes in the cortlandtite samples are very similar (Appendix 5, Fig. 18). Also, the orthopyroxene compositions in these samples overlap (Appendix 5, Fig. 18). Orthopyroxene ($Wo_{\sim 1-3}$, $En_{\sim 78-84}$, $Fs_{\sim 15-20}$) in cortlandtite usually comprises less than 5% of the rock; its abundance becomes high ($\sim$ 15%) only when the modal proportions of olivine is near 50%. Kaersutite in cortlandtite varies from approximately 2% to 20%. As it increases in abundances, the texture of the kaersutite changes from interstitial to poikilitic (Figs. 19, 20, and 21). Kaersutite crystals enclosing pyroxene and olivine sometimes attain sizes of 1-2 cm. This poikilitic texture has been interpreted as in situ crystallization of intercumulus or trapped liquid (Wager and Brown, 1968). The amphibole in each sample, whether appearing in a vein-like network or a poikilitic fashion, shows strong pleochroism from reddish-brown to yellow, and a variable chemistry (Appendix 5, Fig. 17). Magnetite, ilmenite, pyrite, and pyrrhotite are the common accessory phases of this rock; however, the cortlandtite from Stony Point contains a small portion ($< 1\%$) of sodic phlogopite (Appendix 5) within its serpentine network.

Amphibole-Pyroxenite:

This rock type occurs at all three complexes and

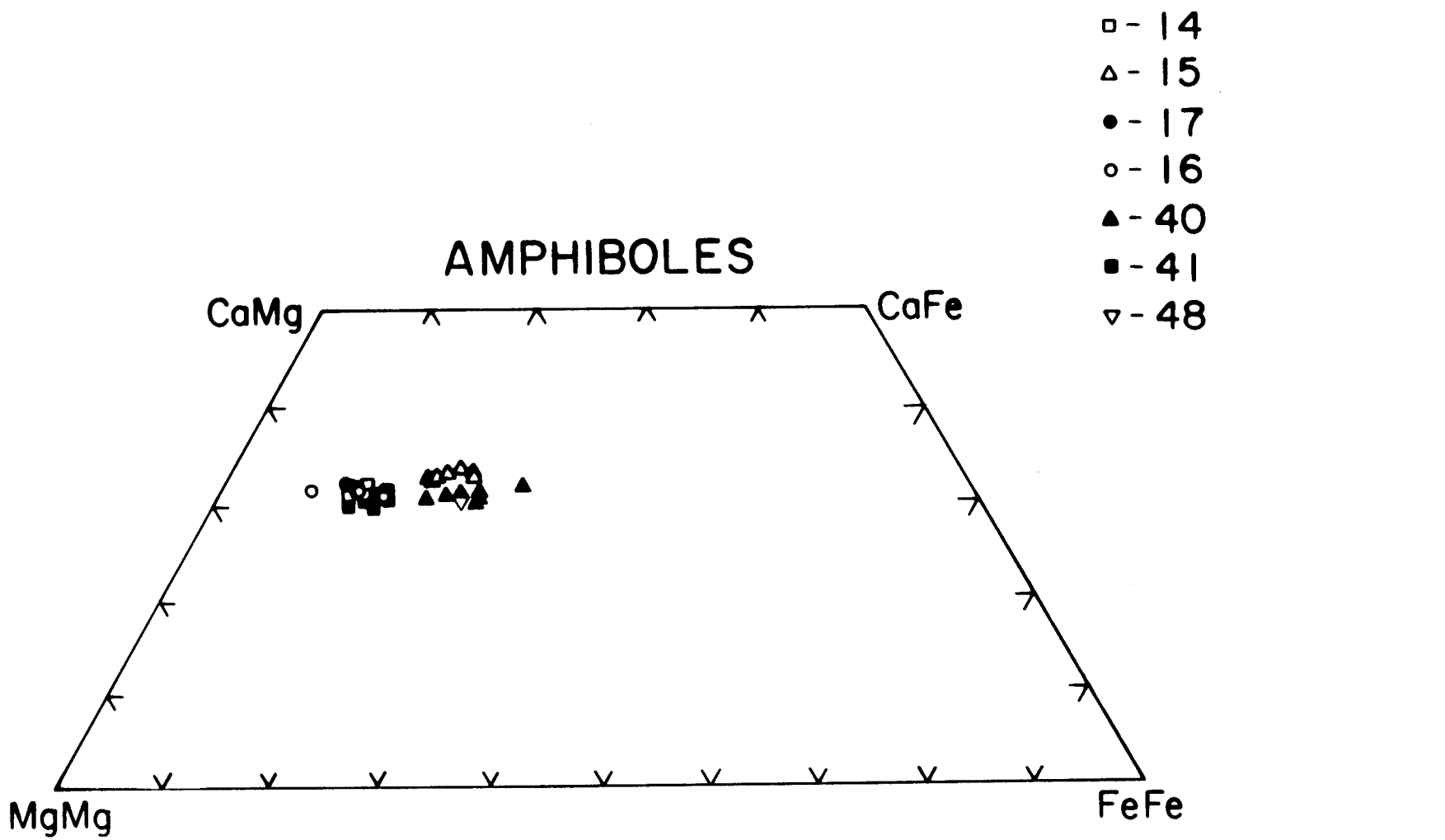

Fig. 17. Quadrilateral relationships of the amphiboles analyzed from the cortlandtites and amphibole-pyroxenites of the Cortlandt (pluton 4), Stony Point, and Rosetown complexes. Selected amphibole analyses from each sample (see Fig. 2 for sample location) are represented by the designated symbols.

CORTLANDTITE & AMPHIBOLE-PYROXENITE

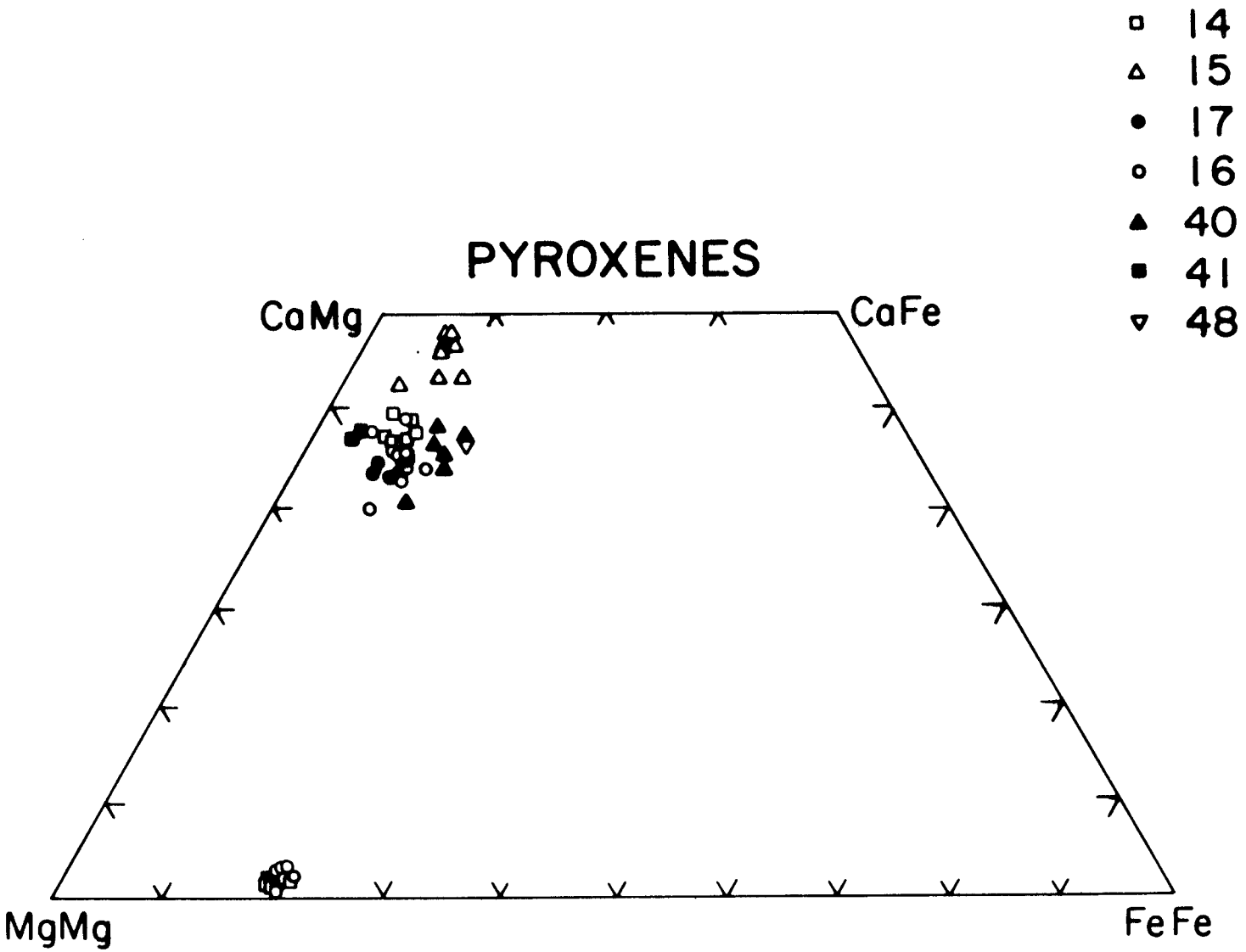

Fig. 18. Quadrilateral relationships of the pyroxenes analyzed from the cortlandtites and amphibole-pyroxenites of the Cortlandt (pluton 4), Stony Point, and Rosetown complexes. Selected pyroxene analyses from each sample (see Fig. 2 for sample location) are represented by the designated symbol.

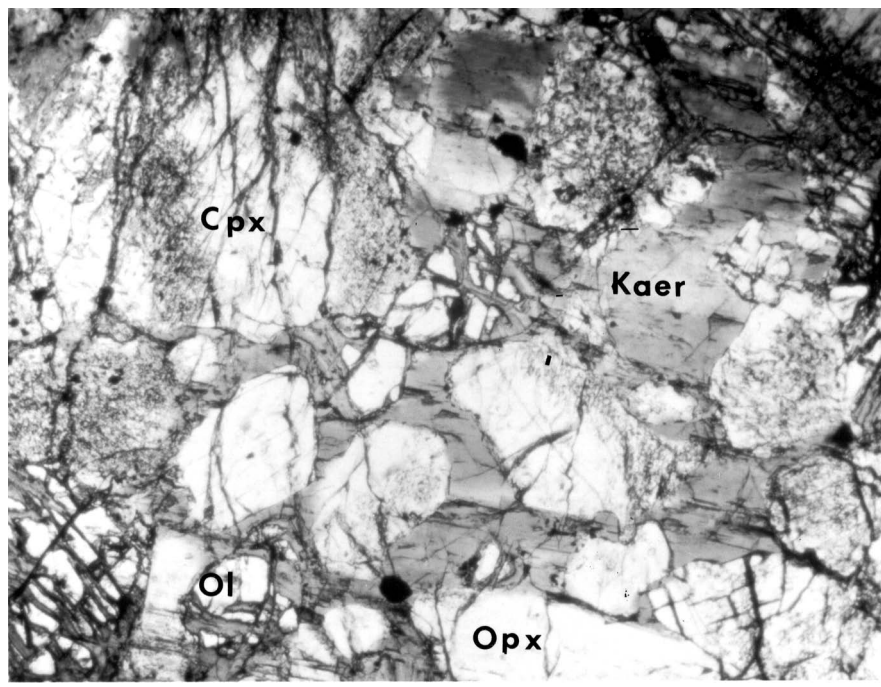

Fig. 19. Cortlandtite sample 14 showing interstitial kaersutite (Kaer) between grains of clinopyroxene (Cpx), orthopyroxene (Opx), and olivine (01). Length of field is 3.5 mm. Uncrossed nicols.

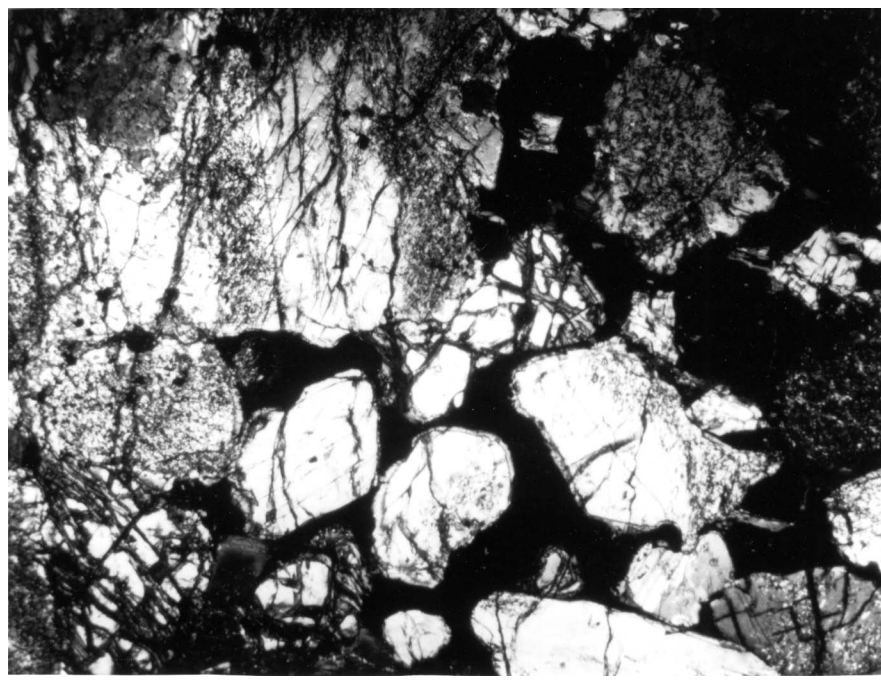

Fig. 20. Crossed nicols of 15A showing that kaersutite is optically continuous.

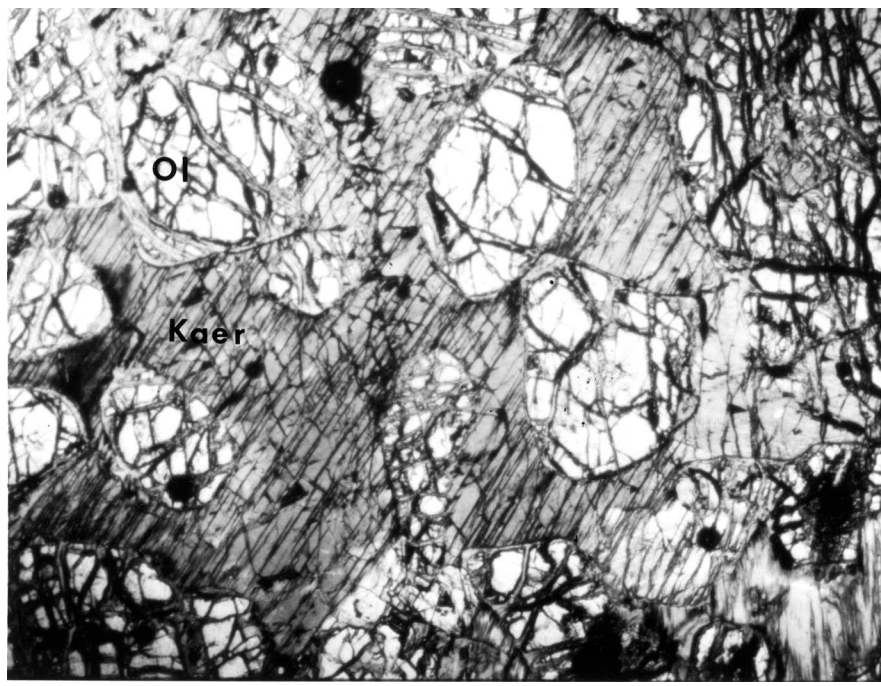

Fig. 20. Crossed nicols of 15A showing that kaersutite is optically continuous.

is comprised of kaersutite (50% or greater) and clinopyroxene (30-40%) with subordinate amounts of plagioclase, biotite, apatite, ilmenite, magnetite, pyrite, and pyrrhotite. The amphibole in these medium to coarse grained, black-colored rocks has both a prismatic and poikilitic habit and ranges in size from 0.1 to 2.0 cm. Euhedral amphibole crystals are normally zoned and chemical compositions for both the poikilitic and prismatic amphibole in the same sample can be identical (Appendix 5, Fig. 17). Shand (1942) believes that the poikilitic amphibole in both the amphibole-pyroxenites and cortlandtites was produced by deuteric alteration. However, Williams (1886) concludes that the amphibole poikicrysts simply represent a portion of the residual magma trapped within these rocks. The presence of prismatic and poikilitic kaersutite with similar chemical compositions found within the same thin section supports this conclusion. In addition, coexisting phases such as plagioclase and clinopyroxene lack substantial alteration indicating that large volumes of late-stage magmatic fluid did not pass through these rocks. In thin section, clinopyroxene is clear to faintly green colored and ranges in size from 2.5 to 3.0 mm with euhedral to subhedral outlines. Clinopyroxenes ($Wo_{\sim 43-57}$, $En_{\sim 36-50}$, $Fs_{\sim 3-14}$) are normally zoned and show greater chemical

variations than clinopyroxenes of the cortlandtite samples (Appendix 5, Fig. 18). As was noted earlier, orthopyroxene does not occur within the amphibole-pyroxenite samples. The common interstitial phases with the amphibole-pyroxenites are plagioclase (An_{50-30}), biotite, opaques, and apatite. Amphibole-pyroxenite near the carbonaceous contact (sample 15) contains approximately 3% calcite (Fig. 22), possibly the result of a carbonate assimilation reaction. This calcite-bearing amphibole-pyroxenite is characterized by unusual clinopyroxene phase chemistry (high Al_2O_3 and Fe_2O_3) (Fig. 18, Appendix 5).

Norite: Cortlandt Complex--Pluton 5

Norite is a gabbroic rock type in which orthopyroxene rather than clinopyroxene is the predominant pyroxene, and, by this definition, most of the rocks within pluton 5 of the Cortlandt complex can be classified as norites. However, clinopyroxene is never subordinate to orthopyroxene in any part of the noritic body, and in several norite samples, the abundance of clinopyroxene almost equals orthopyroxene. In addition to variations in the orthoclinopyroxene ratio, the quantity of amphibole, biotite, quartz, and K feldspar can differ from one noritic sample to the next, resulting

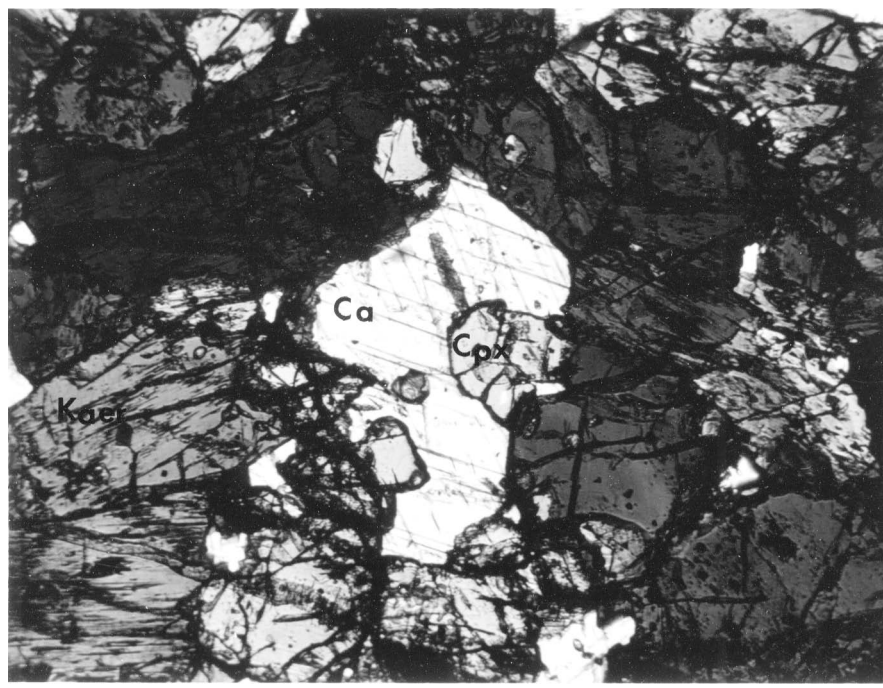

Fig. 22. Photomicrograph of interstitial calcite (Ca) enclosed by kaersutite (Kaer) and a minor amount of clinopyroxene (Cpx) in amphibole-pyroxenite sample 15. Length of field is 2.5 mm. Uncrossed nicols.

in what appears to be several noritic species. The most recent attempt to map the aereal distribution of mineralogically different rock types within the norite pluton has been by Ratcliffe (personal communication) who identifies four distinct textural and compositional units present in pluton 5. These are: 1. amphibole-free norite; 2. biotite-amphibole norite; 3. kaersutite norite; and 4. feldspathic quartz norite. In general, these four separate groups of norites exist within pluton 5 on a large scale; however, samples of one noritic species can exist within the map area of another group. Discussion of the petrography and phase chemistry of noritic samples will follow Ratcliffe's map units and classification scheme. However, because of the similarity of the textures, mineral abundances, and phase chemistries, discussion of the amphibole-free norites and the biotite-amphibole norites will be combined.

Amphibole-Free Norite and Biotite-Amphibole Norite:

Samples from the largest zone of pluton 5 consist of both coarse- and fine-grained, well-layered norite which frequently displays strong flow orientation of its plagioclase and orthopyroxene crystals. These norites are easy to distinguish in the field because of their pink-colored plagioclase and euhedral black pyroxene

crystals. The pink coloration of the plagioclase, which was noted and discussed in some detail by Williams (1887) and Rogers (1911), is due to the presence of extremely small hematite plates. Most samples of these norites consist of plagioclase (50-60%), orthopyroxene (20-25%), clinopyroxene (5-10%) and biotite (5-10%). Amphibole, when present, is interstitial and usually constitutes less than 5 volume percent of these rocks. Generally, the plagioclase grains are euhedral to subhedral in shape and range in size from 0.5 to 6.0 mm. Frequently, large and small plagioclase laths in thin section show excellent parallel alignment with each other and with coexisting pyroxene grains (Fig. 23). Plagioclase twin lamellae are often bent or show evidence of being broken by strain, indicative of flow and possible filter pressing processes. Plagioclase usually lacks any appreciable sericitization and, while the range of feldspar composition is from An_{73-38}, most samples contain plagioclase with anorthite contents of 40 to 50% (Appendix 6). These samples exhibit both normal and reverse zoning profiles.

Orthopyroxene (Wo_{1-4}, En_{47-66}, Fs_{32-49}), the key mineral of the entire norite group, occurs as stout euhedral to subhedral grains that are usually small (0.25-0.50 mm). In coarse-grained samples, orthopyroxene crystals can attain dimensions as great as 4 mm;

Fig. 23. Photomicrograph of aligned plagioclase and pyroxene grains in norite sample 22. Length of field is 3.5 mm. Crossed nicols.

the small orthopyroxene grains usually predominate and often cluster together to form large (1-2 mm) aggregates. Orthopyroxene (Appendix 6, Fig. 25) is pleochroic (pale pink to green) and frequently contains ilmenite inclusions (Schiller structure) that are seldom opaque but usually reddish in color. The larger orthopyroxene crystals contain fine exsolution lamellae of clinopyroxene and inclusions of both plagioclase and clinopyroxene. Clinopyroxene (Wo_{31-48}, En_{34-43}, Fs_{11-26}) closely resembles the co-existing orthopyroxene. In thin section, the clinopyroxene, like orthopyroxene, is reddish-brown in color due to ilmenite inclusions, and it displays a slight pleochroism from pale green to pink. The pleochroic nature of the clinopyroxenes is most likely the cause of the under-estimation of the amount of clinopyroxene in these rocks by earlier investigators (Williams, 1884, 1886; Rogers, 1911; Shand, 1942). Chemical compositions of these clinopyroxenes are remarkably similar (Appendix 6, Fig. 25). Dark brown to yellow biotite comprises less than 10% of these rocks by volume and shows limited Mg/(Mg + Fe) values (Appendix 6). Phase chemistry of the green colored amphibole present in these samples is listed in Appendix 6 and plotted on Fig. 24.

Modal abundance of opaques in this suite varies

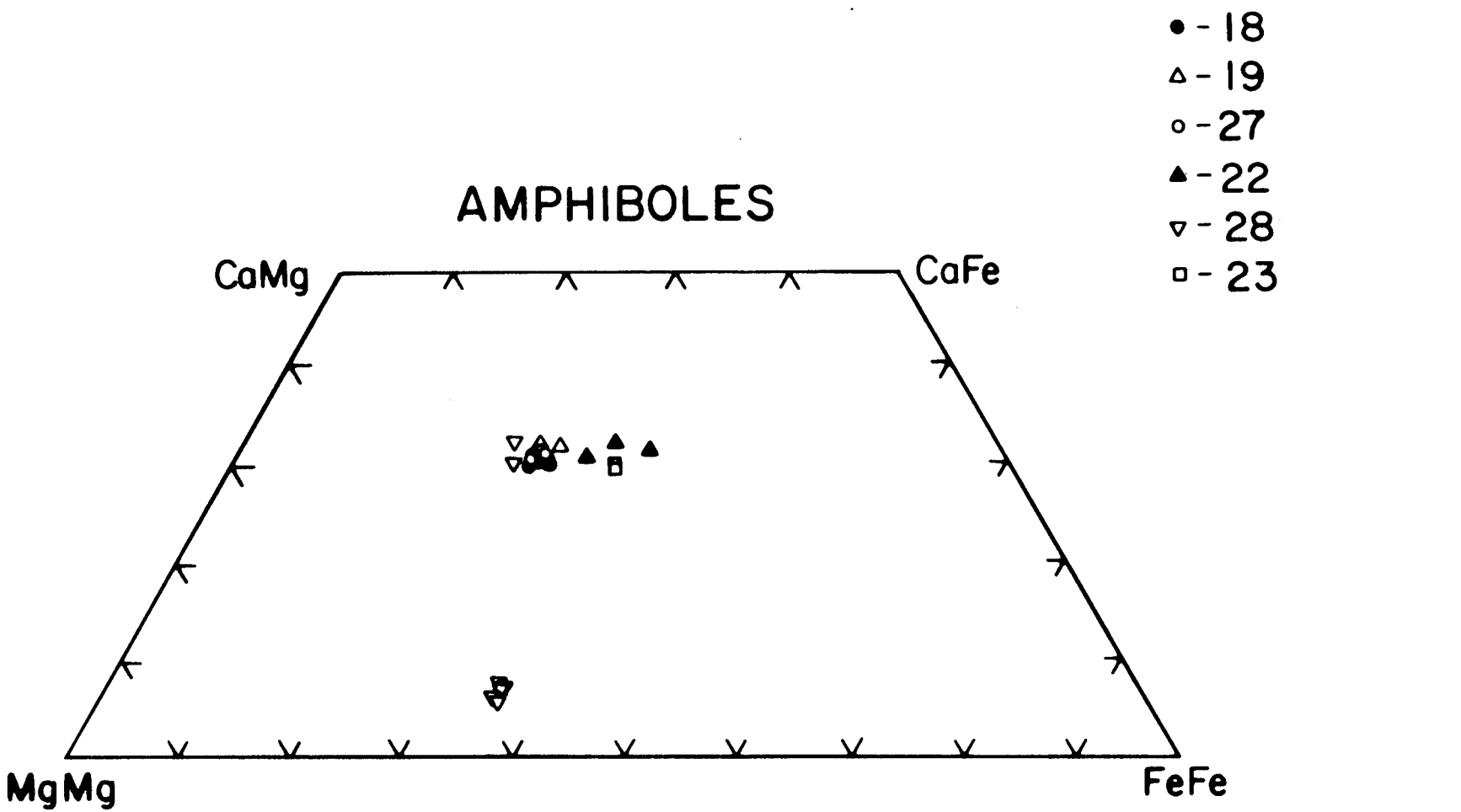

Fig. 24. Quadrilateral relationships of amphiboles from norite of the Cortlandt complex (pluton 5). Selected amphibole analyses from each sample (see Fig. 2 for sample location) are represented by the designated symbols.

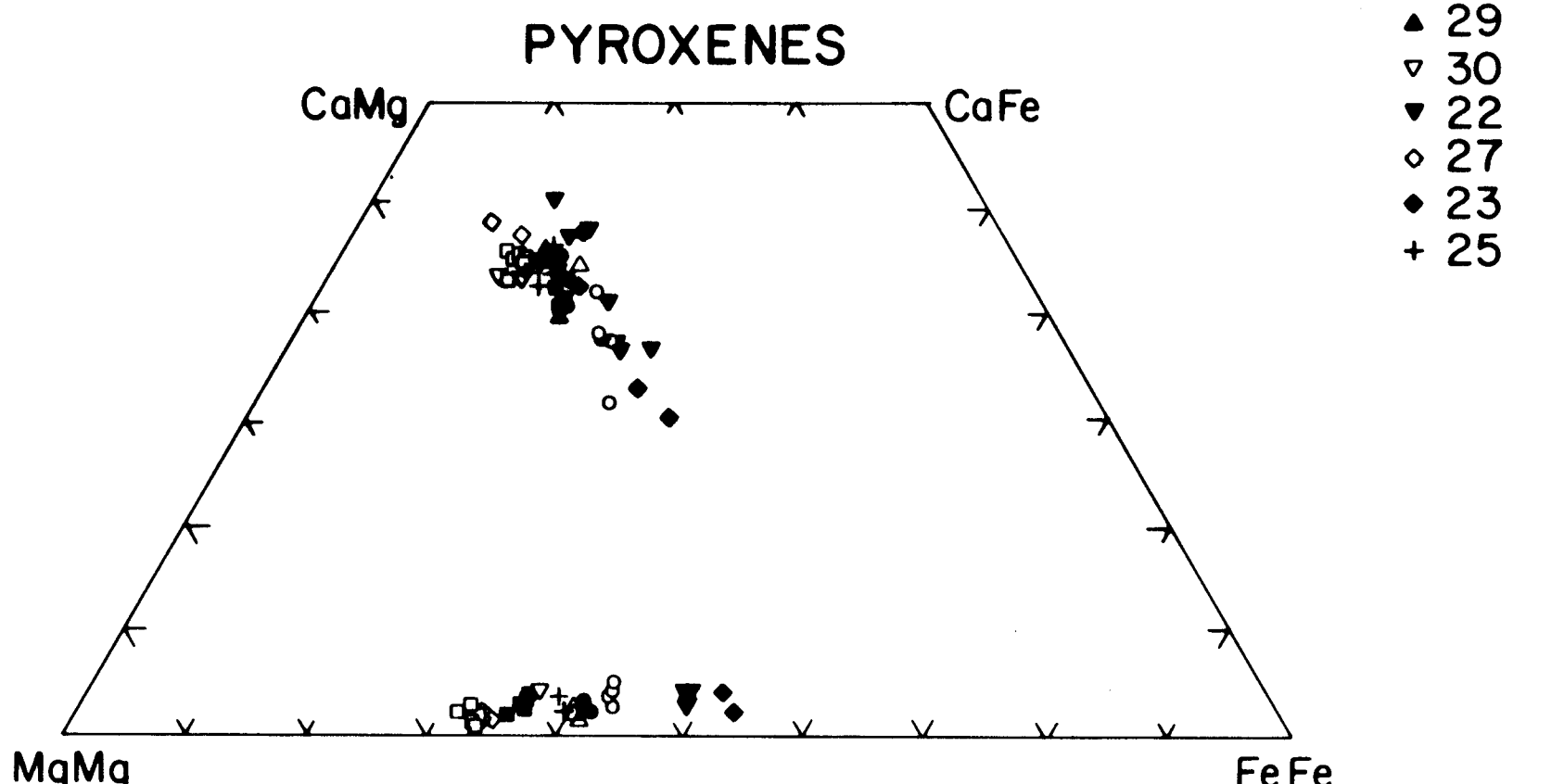

Fig. 25. Quadrilateral relationships of pyroxenes from norite of the Cortlandt complex (pluton 5). Selected pyroxene analyses from each sample (see Fig. 2 for sample location) are represented by the designated symbol.

from 2% to 5%, with ilmenite and iron-sulfides predominant. Magnetite is present, though subordinate. Euhedral apatite is an accessory phase.

Kaersutite Norite:

This unusual norite from near the geometric center of pluton 5 contains approximately 40% poikilitic kaersutite (Fig. 26) in addition to plagioclase (30%), orthopyroxene (25%), and clinopyroxene (5%). Large (0.2-1 mm) brown to yellow amphibole poikicrysts enclose plagioclase (An_{74}), orthopyroxene ($Wo_{\sim 2}$, $En_{\sim 66}$, $Fs_{\sim 32}$), clinopyroxene ($Wo_{\sim 46}$, $En_{\sim 40}$, $Fs_{\sim 14}$), apatite and opaque grains. The composition of kaersutite (Appendix 6, Fig. 24) is very similar to that of the kaersutitic amphiboles found in pluton 1 (Appendix 2, Fig. 7). Plagioclase (Appendix 6) is very fresh and has anorthite contents ($\sim$70) considerably higher than most other noritic plagioclase. In thin section, the plagioclase, orthopyroxene, and clinopyroxene closely resemble in size, coloration, and texture, those within the amphibole-free norite group. Biotite grains are rare.

Feldspathic Quartz Norite:

This norite group is part of the norite-monzodiorite border facies that rims the southern portion of plutons 5 and 6 (Fig. 2). This unit generally consists

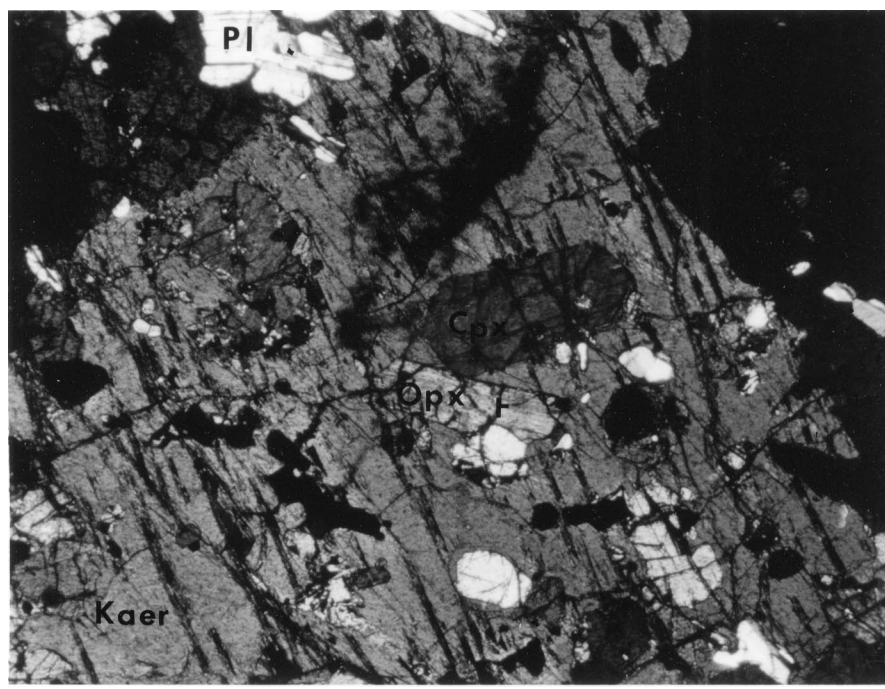

Fig. 26. Photomicrograph of poikilitic kaersutite (Kaer) grain enclosing orthopyroxene (Opx), clinopyroxene (Cpx), and plagioclase (Pl) crystals in kaersutite-norite sample 18. Length of field is 3.5 mm. Crossed nicols.

of plagioclase (∿50%), K-feldspar (∿15%), orthopyroxene (∿15%), clinopyroxene (∿5%), amphibole (∿10%), biotite (∿5%), and minor amounts of quartz (∿3%). Plagioclase grains are unaltered and have anorthite contents that range from 53 to 37% (Appendix 6). Many of the plagioclase laths (0.5-5.0 mm) frequently display strong oscillatory zoning profiles in thin section, and are well oriented. Plagioclase occasionally exhibits a myrmekitic texture when it is contiguous with the interstitial K feldspar. Orthopyroxene ($Wo_{\sim 3}$, $En_{\sim 36-37}$, $Fs_{\sim 53}$) crystals are small (∿0.2 mm) and generally aligned with the larger plagioclase grains. Coexisting clinopyroxene ($Wo_{\sim 30-42}$, $En_{\sim 36-37}$, $Fs_{\sim 21-35}$) has larger grain size (∿2 mm). These feldspathic quartz norites contain the most iron-rich pyroxenes of any of the norites (Appendix 6, Fig. 25). Amphibole is green to yellow in color and often has a poikilitic habit enclosing orthopyroxene and plagioclase grains. Mineral compositions for this amphibole are listed in Appendix 6 and plotted on Fig. 24. Ilmenite, the principal opaque mineral, is usually surrounded by biotite or amphibole rims.

Granodiorite: Cortlandt Complex, Rosetown Complex, and Peekskill Pluton

Samples of granodioritic composition from a dike crosscutting the Cortlandt norite, from the Rosetown complex

and from the Peekskill pluton have similar modal mineralogies and phase chemistries. Plagioclase (∿60%), quartz (∿30%), and K-feldspar (5-10%) are the main constituents with subordinate amounts of biotite, muscovite, and chlorite. Samples from the Rosetown and Peekskill plutonic bodies are medium-grained, white-colored rocks, while samples obtained from the Cortlandt dike are light grey in color and have a porphyritic texture (Fig. 27). In the porphyritic dike (sample 24), the large (0.5-2 mm), extremely fresh, plagioclase phenocrysts are normally zoned (An_{26-12}), sometimes in an oscillatory manner (Appendix 7). These euhedral feldspars are surrounded by a fine-grained (∿0.1 mm) interlocked assemblage of quartz, plagioclase, and K-feldspar. Brown to yellow colored biotite occurs as single grains randomly distributed throughout the groundmass, and in multi-grained aggregates that sometimes attain 1 mm size dimensions. Biotite in either morphology has similar chemistry (Appendix 7). Rare muscovite and epidote grains also occur with biotite in the groundmass of this felsic dike. This felsic dike rock is a rhyodacite, the extrusive equivalent of the coarser-grained granodiorite samples. However, throughout the text this dike rock will be referred to as a granodiorite dike on the basis of its chemical composition. Granodiorite samples from both the

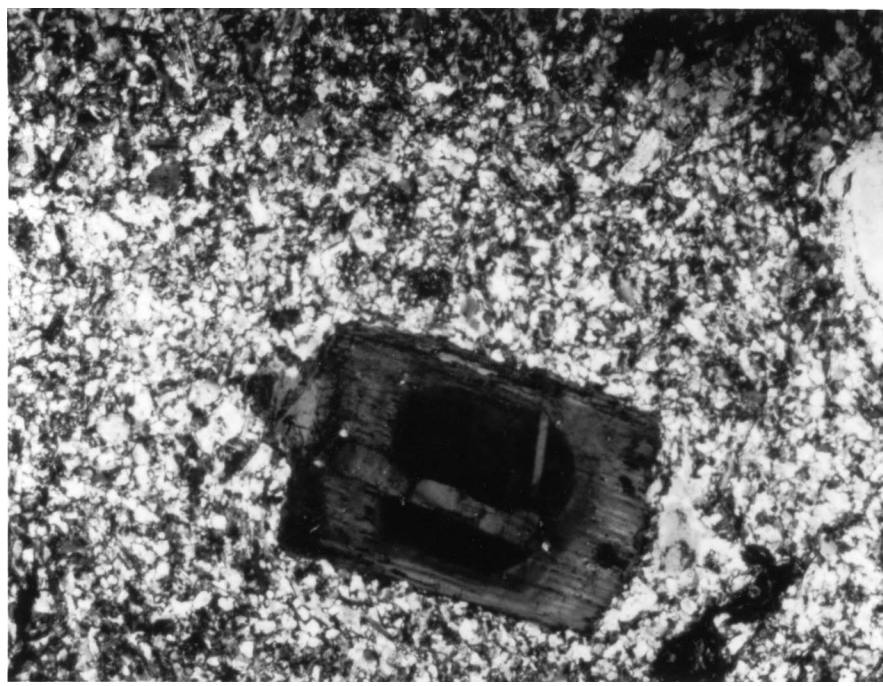

Fig. 27. Photomicrograph of porphyritic texture of sample 24 a rhyodacite. Strongly zoned plagioclase phenocryst is featured in field of view. Length of field is 3.5 mm. Crossed nicols.

Peekskill and Rosetown localities are very similar in texture and mineral composition. Rocks from these two areas lack any extensive alteration and are composed of euhedral to subhedral plagioclase laths (0.5-2.0 mm) with anhedral quartz (∿1 mm) and K-feldspar (0.25-1.0 mm) grains. Plagioclase laths are normally zoned (An_{27-6}) and occasionally display oscillatory extinction and myrmekitic texture. K-feldspars are perthitic and frequently exhibit grid twinning. Biotite, muscovite, and chlorite plates are interstitial and randomly distributed throughout the rock along with rare epidote grains.

Mafic Dike: Stony Point Complex

Samples were collected from the mafic-lamprophyric (spessertite) dikes that crosscut the cortlandtite-amphibole pyroxenite and diorite plutons at Stony Point (Fig. 3). The dikes consist of kaersutite (20-40%), biotite (∿30%), plagioclase (20-40%), and opaques (25%) with accessory apatite, epidote, sphene, and calcite. Samples from the 10 cm wide dike which cuts the cortlandtite-amphibole-pyroxenite show fine-grained, allotriomorphic-granular textures with grain sizes less than 0.1 mm. The anhedral plagioclase grains in this sample show a limited range in composition (An_{34-28}) as does the coexisting magnesium biotite and kaersutite (Appendix 8, Fig. 28).

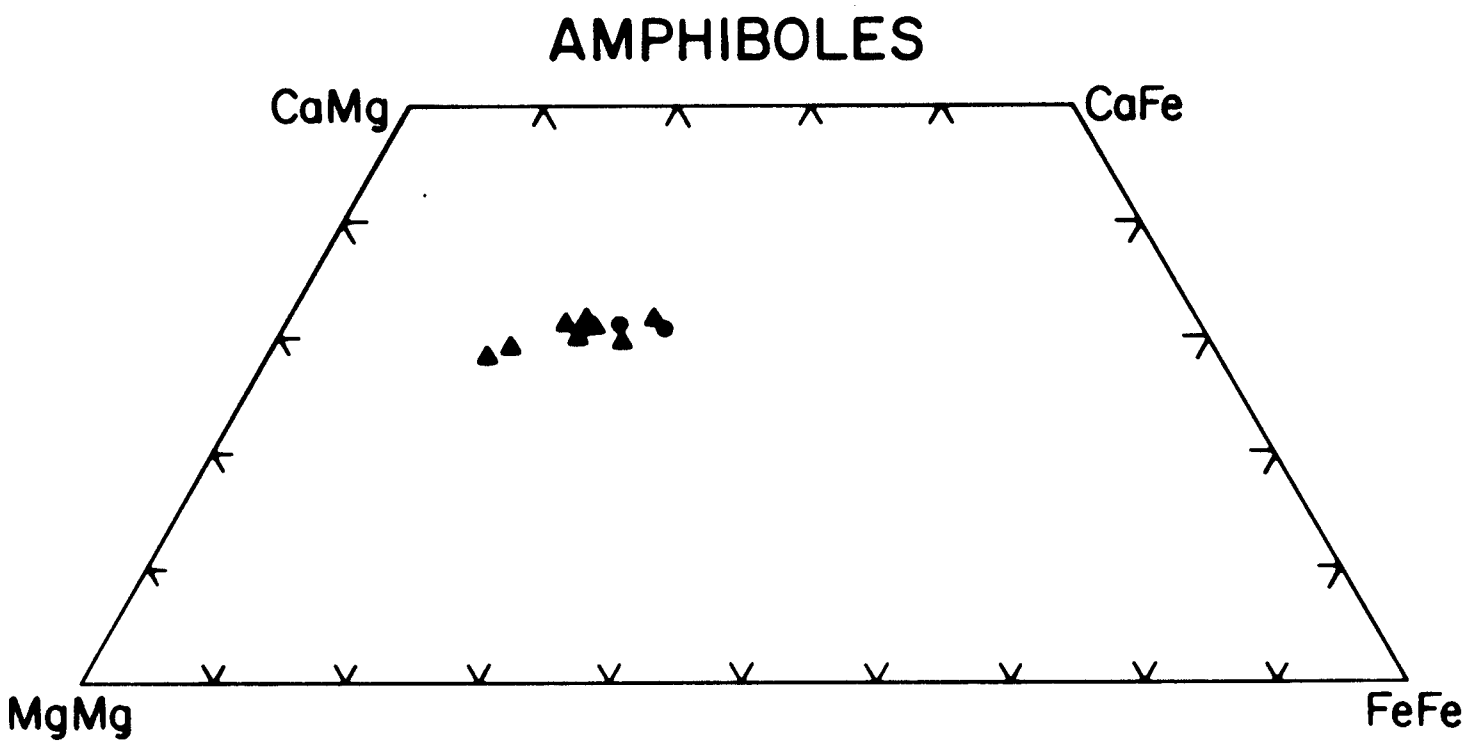

Fig. 28. Quadrilateral relationships of amphibole from the mafic dike rocks of the Stony Point complex. Selected amphibole analyses from each sample (see Figs. 2 and 3 for sample location) are represented by the designated symbols.

The sample from the 30-cm-wide dike which crosscuts the almandine-bearing diorite is medium-grained and contains euhedral kaersutite crystals as large as 1.5 mm. These amphibole grains are strongly zoned from core to rim (Appendix 8, Fig. 28) and display ilmenite exsolution lamellae. While amphibole displays a large variation in chemical composition, coexisting biotite grains have limited Mg/Mg + Fe values (Appendix 8). Plagioclase is found interstitially and is sodic (An_{26-19}) in composition (Appendix 8).

Salt Hill Emery and Related Quartz-Feldspathic Dikes: Cortlandt Complex

Samples from the Salt Hill emery mine located at the sountern portion of pluton 6 (Fig. 2) have been the subject of numerous investigations since Williams (1886) first described the locality (Rogers, 1911; Shand, 1942; Friedman, 1952, 1956; Barker, 1964; Caporuscio and Morse, 1978). The rock at this locality is black colored and very dense. It consists of sillimanite, green spinel (pleonaste), corundum, cordierite, almandine garnet, staurolite, biotite, white mica, sapphirine, and opaques (ilmenite and magnetite). Kyanite, andalusite, quartz, plagioclase, and orthopyroxene are also present in minor amounts. Proportions of minerals vary greatly in thin

section. Generally, bladed sillimanite, opaques, biotite, and white mica are ubiquitous throughout the emery body. When present, sapphirine occurs as large blue-green tabular crystals that are strongly pleochroic.

Estimates of the intensive thermodynamic parameters of P, T, and fO_2 for the Salt Hill emery during formation were recently determined by Caporuscio and Morse (1978). They postulated that these emery xenoliths originated at temperatures in excess of 800°C and at relatively high oxygen fugacities (between HM and QFM). Pressure estimates were less constrained but generally believed to be between the Al_2SiO_5-triple point and 9.5 kb. Mineral analyses for spinel, garnet, biotite, sapphirine, and plagioclase of the Salt Hill emery are listed in Appendix 9.

Numerous quartz-rich dikes or veins that vary in width from approximately 0.5 cm to 0.5 meters (Fig. 29) occur throughout the Salt Hill emery deposit. These felsic dikes consist of quartz (∿85%), plagioclase (∿10%), almandine garnet (∿5%), with minor amounts of interstitial muscovite and chlorite. Garnet occurs as small (∿0.1 mm), round, slightly pink, crystals oriented in a chain-like fashion between larger (1-2 mm) anhedral quartz grains (Fig. 30). These garnets (Appendix 9) are similar in chemical composition to the almandine garnets in the

Fig. 29. Photograph of Salt Hill emery containing numerous quartz-feldspathic veins.

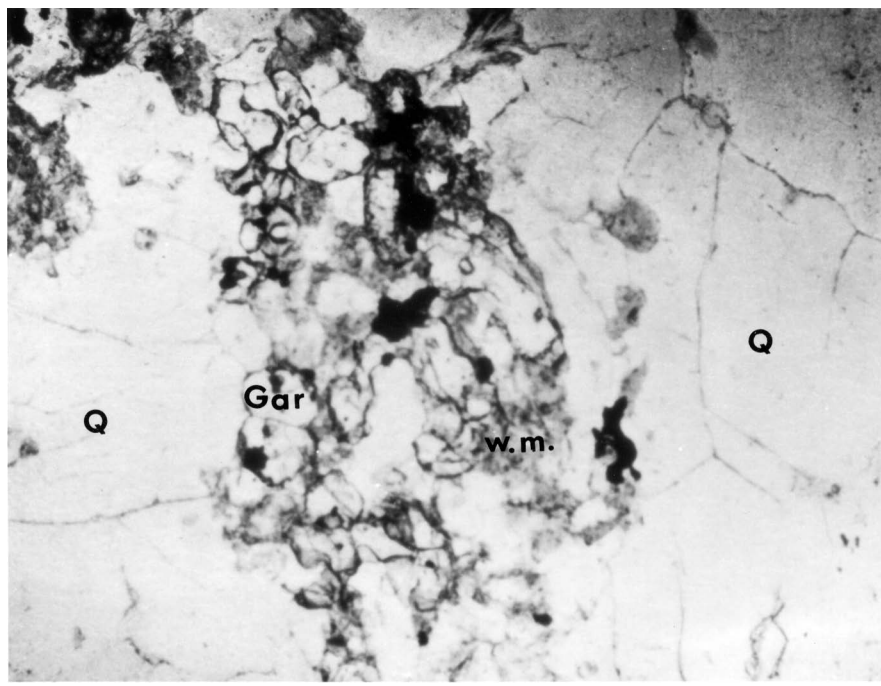

Fig. 30. Photomicrograph of almandine garnet (Gar) in Salt Hill quartz-feldspathic vein, sample 36. In addition to garnet, quartz (Q), white mica (W.M.), and opaques are within the field of view. Length of field is 3.5 mm. Uncrossed nicols.

nearby emery (Appendix 9). Plagioclase is unaltered and generally found in fine-grained aggregates at quartz triple junctions. Plagioclase mineral compositions (Appendix 9) are variable (An_{80-33}) throughout the sample.

Summary

The mafic rocks of the Cortlandt, Stony Point, and Rosetown complexes are relatively unaltered with extremely similar mineralogies, chemistries, and petrographic features. In general, these basic rocks are medium to coarse-grained and have hypidiomorphic-granular to panidiomorphic-granular textures. Well-developed igneous lamination and cumulate textures in several of the Cortlandt region mafic rocks indicate that crystal accumulation processes played an important role in the petrogenesis of these rocks. Olivine, clinopyroxene, and orthopyroxene are the principal cumulate phases of cortlandtite and clinopyroxenite while kaersutite and plagioclase are the cumulus minerals of the hornblendites and the amphibole-rich diorites. One of the outstanding features of the Cortlandt region suite is the presence of kaersutite in each of the different basic plutons. It occurs in both prismatic and poikilitic morphologies, sometimes with both forms coexisting within

the same sample. The poikilitic nature of the kaersutite in the cortlandtite, clinopyroxenites, and norites suggests that the interstitial melt of these cumulus rocks was nearly identical in composition to that of the titanium-rich kaersutite. The presence of kaersutite and biotite suggests an alkali affinity for the basic rocks of the Cortlandt suite; however, modal orthopyroxene and quartz in several of these same basic rocks also indicates a tholeiitic affinity. These contrasting characteristics (hybridization) are unusual. A search of the literature found the coexistence of kaersutite and orthopyroxene in two other basic plutonic complexes. The first occurrence was noted by Nockolds (1941) in the Garabal Hill-Glen Fyne complex of Scotland where gabbros are associated with peridotites, pyroxenites, and hornblendites. The second occurrence is in the basic plutons of the Peninsular Range batholith of southern California where kaersutite gabbros coexist with norite, peridotite, and anorthosite (Walawender, 1976; Walawender et al., 1979; Walawender and Smith, 1980). At both localities the postulated parental magma for the suite of mafic rocks was a high-alumina (calc-alkali series) basalt that experienced various degrees of localized contamination with pelitic schist. However, the basic rocks of these two complexes contain substantially less potassium (<1 wt.%) and

titanium ($\sim$ 1 wt.%) than the mafic rocks of the Cortlandt suite. The hybrid characteristics of the Cortlandt region suite may reflect source region chemistry, magma generation processes, and/or crustal contamination.

ANALYTICAL RESULTS

MAJOR ELEMENT ANALYSES

Thirty-eight major element analyses of rocks from the Cortlandt, Stony Point, and Rosetown complexes are listed in Table 1. Sample locations and descriptions are contained in Fig. 2 and Appendix 1. An AFM plot (Fig. 31) shows the relative iron-enrichment trend of the Cortlandt region suite. This plot indicates that the Cortlandt suite is very similar to the calc-alkaline series defined by Irvine and Baragar (1971). Clinopyroxenite (samples 11, 12, and 31) and olivine-rich cortlandtite samples (14, 16, 41) are tightly clustered near the iron-magnesium boundary of the AFM diagram, consistent with a cumulate (olivine-pyroxene) origin. Hornblendite (1, 2, 5) and diorite (7, 8, 9, 10) samples plot much closer to the iron (F) apex of the AFM diagram due to their high proportion of cumulate kaersutite and opaques while noncumulus (differentiated) rock types (amphibole-pyroxenite, diorite, gabbro, and norite) are more widely scattered, generally parallel to the A-M boundary. Granodiorite samples (24, 34, 51) plot extremely close to the A-apex because of their low iron and magnesium abundances and high alkalis.

Table 1.

Major Element Analyses

	1			2		3		4	5	6	7		8		9
	a	b	c	a	b	a	b	b	b	b	a	b	a	b	b
SiO_2	42.8	43.2	40.6	39.1	40.3	56.9	55.4	46.8	39.5	52.0	40.8	41.8	46.9	47.5	43.9
TiO_2	3.59	3.74	3.94	3.55	3.61	1.20	1.25	2.76	3.91	2.09	3.64	3.52	2.55	2.83	3.49
Al_2O_3	17.1	17.5	14.3	17.4	18.1	18.4	19.2	19.4	19.6	15.0	20.6	21.3	18.2	18.7	20.6
Fe_2O_3	3.08	---	---	3.83	---	1.50	1.35	---	---	---	5.30	---	4.62	4.09	---
FeO	9.12	---	---	9.62	---	5.37	5.46	---	---	---	7.92	---	7.32	7.64	---
FeO*	---	12.3	14.9	---	13.4	---	7.22	8.20	14.7	9.78	---	11.9	---	11.9	12.3
Fe_2O_3**	---	---	---	---	---	---	7.43	---	---	---	---	---	---	12.6	---
MnO	0.16	0.14	0.26	0.13	0.12	0.13	0.13	0.09	0.13	0.06	0.14	0.18	0.13	0.12	0.12
MgO	7.86	8.35	11.1	9.14	9.31	2.29	2.47	7.56	7.82	7.12	6.22	6.13	4.39	4.55	5.58
CaO	9.60	9.99	10.9	11.0	11.5	5.30	5.56	9.89	10.3	7.44	10.8	11.1	8.25	8.42	9.88
Na_2O	1.94	2.25	1.40	1.58	2.04	3.35	3.41	2.65	1.94	3.11	1.94	2.41	1.97	2.19	2.86
K_2O	1.86	1.76	1.72	1.22	1.30	3.58	3.63	1.81	2.10	2.33	0.63	0.66	1.54	1.46	1.11
Cr_2O_3	---	0.01	0.04	---	0.02	---	0.01	0.02	---	---	---	0.03	---	0.00	0.01
P_2O_5	0.12	---	---	0.02	0.08	0.46	0.45	0.15	---	---	0.06	0.10	1.47	1.44	0.07
S	0.03	---	---	0.65	---	0.03	---	---	---	---	0.29	---	0.19	---	---
L.O.F.[z]	2.17	---	---	1.92	---	0.98	---	---	---	---	1.61	---	1.95	---	---
H_2O^+	0.07	---	---	0.06	---	0.09	0.27	---	---	---	0.15	---	0.07	---	---
H_2O^-	---	---	---	---	---	---	0.17	---	---	---	---	---	---	---	---
Σ	99.4	99.2	99.3	99.3	99.7	99.6	99.2	99.2	100.0	98.9	100.0	99.1	99.6	99.0	99.8
Mg#	0.61			0.63		0.43	0.45				0.58		0.52	0.52	

a *X-ray fluorescence.*

b *Electron microprobe plus wet chemical.*

c *Fused kaersutite mineral separate (electron microprobe).*

* *Total iron.*

** *Total iron as* Fe_2O_3.

z *Loss on fusion.*

Table 1 (cont.).

Major Element Analyses

	10	11		12	14		15		16	18		19		20	
	b	a	b	b	a	b	a	b	b	a	b	a	b	a	b
SiO_2	41.5	49.0	49.5	49.6	45.5	47.2	37.4	40.0	47.7	42.4	43.9	46.0	---	53.5	53.2
TiO_2	3.71	0.76	0.76	0.90	0.67	0.66	2.40	2.57	0.72	2.99	2.90	2.93	---	1.50	1.41
Al_2O_3	18.6	4.59	4.68	4.78	3.86	4.13	13.8	15.0	4.04	14.3	14.7	17.2	---	17.3	17.8
Fe_2O_3	---	1.40	1.83	---	3.73	---	3.95	3.85	---	3.57	---	3.87	4.00	2.04	---
FeO	---	9.47	9.22	---	7.40	---	6.37	6.69	---	11.4	---	9.39	8.89	6.71	---
FeO*	13.9	---	10.8	10.4	---	11.1	---	10.3	11.4	---	14.2	---	---	---	8.03
Fe_2O_3*	---	---	12.1	---	---	---	---	11.3	---	---	---	---	13.9	---	---
MnO	0.14	0.19	0.18	0.18	0.16	0.16	0.12	0.12	0.16	0.20	0.23	0.22	---	0.16	0.14
MgO	7.67	18.4	18.7	15.9	20.8	22.2	10.4	11.2	21.1	10.2	10.6	7.33	---	4.83	4.69
CaO	9.89	13.8	14.1	16.3	13.0	13.7	15.6	16.6	13.9	9.98	10.3	9.48	---	6.56	6.63
Na_2O	2.10	0.43	0.38	0.52	0.41	0.49	1.61	2.16	0.55	1.34	1.50	1.92	---	3.02	3.33
K_2O	1.05	0.18	0.16	0.10	0.14	0.13	1.88	1.96	0.10	0.63	0.65	0.33	---	3.05	3.15
Cr_2O_3	0.01	---	0.10	0.09	---	0.14	---	0.02	0.08	---	0.06	---	---	---	0.02
P_2O_5	---	0.03	0.08	---	0.02	---	0.12	0.19	---	0.74	---	0.94	0.92	0.54	---
S	---	0.23	---	---	0.34	---	0.26	---	---	0.42	---	0.05	---	<0.005	---
L.O.F	---	1.40	---	---	3.22	---	4.90	---	---	1.03	---	1.17	---	0.815	---
H_2O^+	---	0.06	---	---	0.20	---	0.08	---	---	0.07	---	0.13	---	0.10	---
H_2O^-	---	---	---	---	---	---	---	---	---	---	---	---	---	---	---
Σ	98.6	99.9	99.5	98.8	99.4	99.8	98.9	100.1	99.6	99.4	99.0	100.9		100.1	98.4
Mg#		0.78	0.78		0.83		0.74	0.75		0.61		0.58		0.56	

a *X-ray fluorescence.*

b *Electron microprobe plus wet chemical.*

* *Total iron.*

** *Total iron as* Fe_2O_3.

Σ *Loss on fusion.*

Table 1 (cont.)

Major Element Analyses

	21		22	23		24	25	31		34	35	36	37	40	
	a	b	b	a	b	a	b	a	b	a	a	d	d	a	b
SiO_2	53.1	53.0	52.9	54.5	54.0	71.9	50.0	49.1	49.8	71.2	63.3	90.5	29.2	45.8	46.4
TiO_2	1.77	1.68	1.80	1.69	1.70	0.15	1.68	0.93	0.90	0.05	0.66	0.38	3.10	2.14	2.18
Al_2O_3	18.3	19.0	18.8	17.6	18.0	15.7	16.6	5.17	4.89	16.6	16.5	3.62	30.4	11.6	11.8
Fe_2O_3	2.02	---	---	1.96	1.63	0.37	---	1.49	---	0.21	1.47	0.82	18.6	3.20	3.07
FeO	6.22	---	---	6.26	6.49	0.78	---	11.1	---	0.24	3.41	1.80	7.35	7.43	7.57
FeO*	---	7.77	8.31	---	7.84	---	9.37	---	12.4	---	---	---	---	---	10.5
Fe_2O_3**	---	---	---	---	8.86	---	---	---	---	---	---	---	---	---	11.5
MnO	0.14	0.11	0.08	0.13	0.14	0.02	0.19	0.23	0.26	0.01	0.05	0.14	0.18	0.16	0.18
MgO	4.18	4.10	3.30	3.21	3.17	0.53	7.59	19.6	20.8	0.14	3.96	0.73	3.58	10.9	11.4
CaO	7.08	7.22	6.16	5.57	5.69	2.00	8.95	10.9	11.2	1.50	1.26	1.11	4.12	12.5	12.9
Na_2O	3.58	3.76	3.22	3.18	3.35	5.83	2.58	0.28	0.15	5.99	2.00	0.25	1.11	1.74	2.25
K_2O	2.37	2.42	3.72	3.69	3.80	2.01	1.85	0.01	0.00	2.72	4.89	0.10	1.13	1.04	1.01
Cr_2O_3	---	0.00	0.00	---	0.01	---	0.01	---	0.14	---	---	---	---	---	0.07
P_2O_5	0.50	---	0.59	0.52	0.50	0.05	---	0.02	---	0.04	0.08	< 0.01	0.12	0.25	0.29
S	< 0.005	---	---	< 0.005	---	< 0.005	---	0.59	---	< 0.005	< 0.005	---	---	0.35	---
L.O.F.[z]	0.65	---	---	1.06	---	0.53	---	0.70	---	0.59	2.22	---	---	2.51	---
H_2O^+	0.04	---	---	0.06	---	0.04	---	0.06	---	0.10	0.17	0.35	0.39	0.20	0.55
H_2O^-	---	---	---	---	---	---	---	---	---	---	---	0.04	0.04	---	0.48
Σ	99.9	99.0	98.4	99.5	98.2	100.0	98.9	100.2	100.5	99.4	100.0	99.9	99.3	99.7	100.0
Mg#	0.55			0.48	0.47	0.55		0.76		0.51	0.67	0.42	0.46	0.72	0.73

a *X-ray fluorescence.*

b *Electron microprobe plus wet chemical.*

d *Determined at the Pennsylvania State University Laboratories.*

* *Total iron.*

** *Total iron as* Fe_2O_3.

z *Loss on fusion.*

Table 1 (cont.)

Major Element Analyses

	41	42		43		44		45		48		49		50
	a	a	b	a	b	a	b	a	b	a	b	a	b	b
SiO_2	39.2	52.9	53.5	48.7	51.2	47.5	46.1	59.3		45.4	46.2	52.1	49.4	53.1
TiO_2	0.83	1.15	1.17	1.95	1.89	2.10	2.35	0.96		2.36	2.51	1.93	2.18	1.64
Al_2O_3	4.95	20.4	20.9	15.5	16.2	15.2	14.7	18.8		10.5	10.5	17.0	18.3	14.9
Fe_2O_3	4.93	2.26	1.61	3.10	2.63	2.92	2.09	1.75		3.68	3.40	3.18	2.48	---
FeO	11.2	6.22	6.62	6.48	6.89	7.53	8.09	4.39		7.73	7.90	6.72	7.11	---
FeO*	---	---	8.21	---	8.82	---	11.2	---		---	11.1	---	10.7	~~14.9~~ 10.3
Fe_2O_3**	---	--- *	8.98	---	10.3	---	11.1	---		---	12.2	---	10.4	---
MnO	0.21	0.07	0.07	0.14	0.08	0.16	0.11	0.06		0.17	0.17	0.14	0.12	~~0.26~~ 0.29
MgO	25.9	1.69	1.71	6.88	7.05	7.18	8.56	2.70		10.4	11.2	3.00	3.36	~~11.1~~ 5.35
CaO	4.47	3.89	3.78	7.98	7.82	8.80	9.45	0.64		13.2	13.8	6.00	6.67	~~10.9~~ 6.89
Na_2O	0.62	5.20	4.62	3.16	3.59	2.92	3.04	1.32		1.92	2.15	4.29	4.76	~~1.40~~ 3.68
K_2O	0.48	2.97	2.99	2.00	2.00	2.46	2.35	6.83		1.05	1.04	2.16	2.14	~~1.72~~ 2.62
Cr_2O_3	---	---	0.01	---	0.00	---	0.05	---		---	0.00	---	0.00	~~0.04~~ 0.01
P_2O_5	0.19	0.81	0.79	0.41	0.43	0.57	0.58	0.12		0.44	0.49	0.65	0.62	---
S	0.42	0.02	---	0.63	---	0.12	---	0.03		0.28	---	0.08	---	---
L.O.F.[z]	6.46	1.24	---	2.63	---	1.73	---	2.52		1.79	---	1.67	---	---
H_2O^+	0.18	0.09	---	0.10	---	0.07	0.50	0.07		0.08	---	0.13	---	---
H_2O^-	---	---	---	---	---	---	0.14	---		---	---	---	---	---
Σ	100.0	99.9	97.8	99.7	99.1	99.2	99.2	99.5		99.1	99.1	99.1	98.2	99.3
Mg#	0.80	0.33	0.32	0.65	0.65	0.63	0.65	0.52		0.71	0.72	0.44	0.46	

a *X-ray fluorescence.*

b *Electron microprobe plus wet chemical.*

* *Total iron.*

** *Total iron vs* Fe_2O_3.

z *Loss on fusion.*

Table 1 (cont.)

Major Element Analyses

	51	BCR-1
	a	
SiO_2	71.7	
TiO_2	0.16	
Al_2O_3	15.5	
Fe_2O_3	0.66	
FeO	0.53	
FeO*	---	
Fe_2O_3*	---	
MnO	0.02	
MgO	0.31	
CaO	1.70	
Na_2O	5.24	
K_2O	3.29	
Cr_2O_3	---	
P_2O_5	0.03	
S	< 0.005	
L.O.F.	0.76	
H_2O^+	0.03	
H_2O^-	---	
Σ	99.9	
Mg#	0.51	

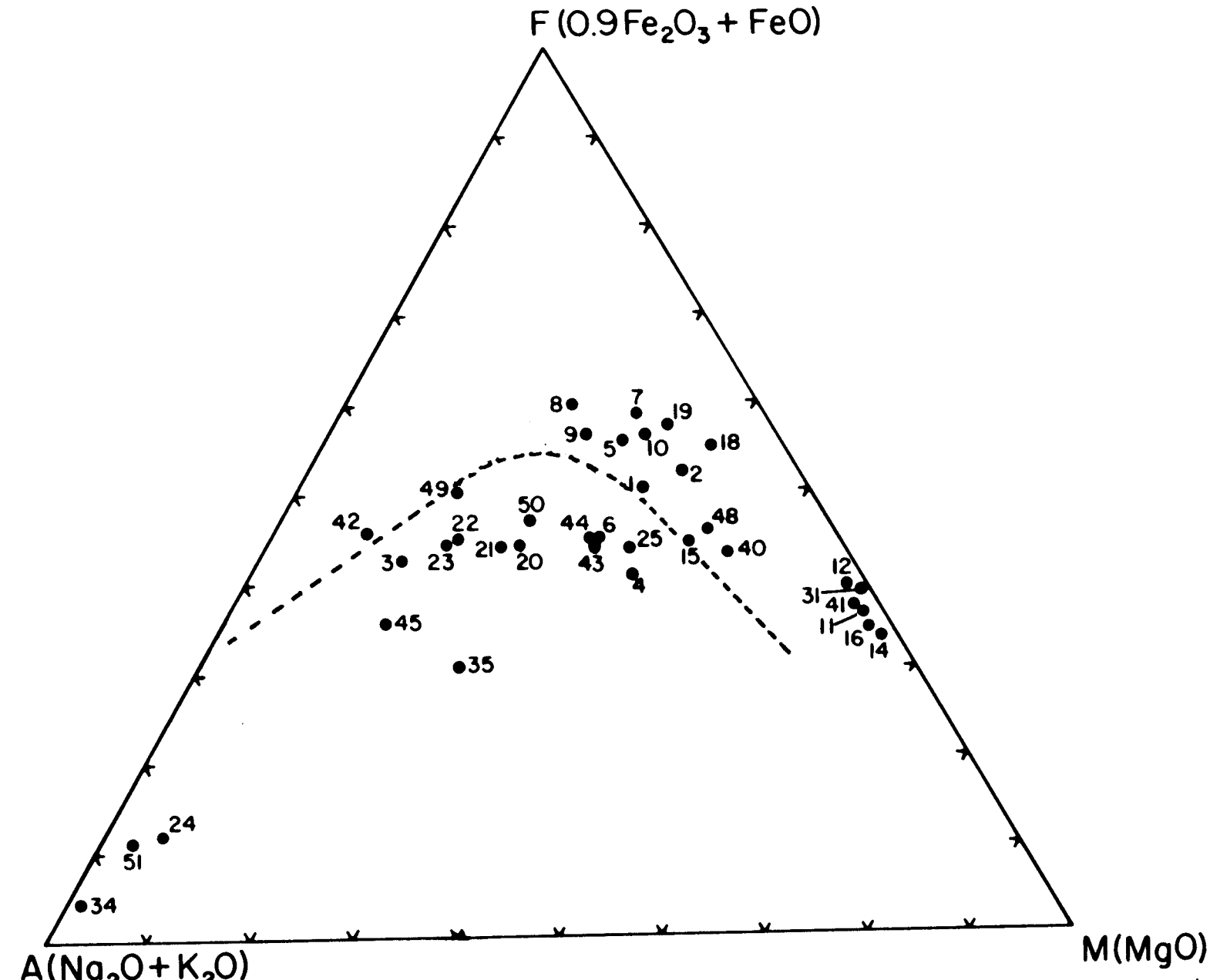

Fig. 31. AFM diagram showing samples of the Cortlandt, Stony Point, and Rosetown complexes. Dashed line after Irvine and Barager (1971) separating tholeiitic (above) and calc-alkaline (below).

Plotting of the C.I.P.W. norms (Table 2) of the Cortlandt region samples on the normative basalt triangles (Fig. 32) of Yoder and Tilley (1962) magnifies these major element differences. The chemistry of the mafic igneous rocks ranges from silica undersaturated (nepheline normative) to silica oversaturated (quartz normative), implying that these mafic rocks have both alkalic and tholeiitic affinities, further supporting the hybrid character determined from the petrographic data. Samples that are nepheline normative and hence plot on the alkali-basalt triangle, generally contain modal amphibole in quantities greater than 50 volume percent. Cortlandtite, clinopyroxenite, and amphibole-pyroxenite samples generally contain a much higher proportion of normative diopside than do the diorite, hornblendite, and kaersutite gabbro or norite samples. Norite samples (19, 20, 21, 23) are tightly grouped near the hypersthene apex reflecting their high modal orthopyroxene/clinopyroxene ratio.

A kaersutite gabbro sample (3) and two diorite samples (8, 42) are corundum normative, indicating that these basic rocks have undergone extensive amphibole fractionation (Cawthorn and Brown, 1976; Cawthorn et al., 1976) or have experienced pelitic country rock contamination (Bowen, 1928; Green and Ringwood, 1968). In

Table 2.

C.I.P.W. Norms in Weight Percent for Analyzed Samples of Table

	1	2	3	4	5	6	7	8	9	10	11	12	14	15	16	18	19	20	21
Ab	12.2	2.03	28.8	15.0	---	26.3	15.2	17.1	12.7	6.95	3.72	4.40	3.64	---	4.65	11.6	16.3	25.7	30.6
An	33.2	38.0	23.7	35.7	38.5	26.1	46.5	32.2	40.2	38.3	10.2	10.41	8.63	26.6	8.26	31.8	37.6	24.8	26.9
Or	11.2	7.45	21.5	10.7	---	13.8	3.78	9.40	6.56	6.20	1.06	0.59	0.83	---	0.59	3.78	2.01	18.1	14.1
Ol	16.7	18.2	---	17.6	27.2	12.6	12.4	---	20.2	25.3	14.0	14.0	21.7	27.7	33.6	15.2	---	---	---
Fa	5.43	5.29	---	6.75	14.7	6.00	2.95	---	11.6	13.4	3.77	4.66	3.69	2.91	9.9	5.58	---	---	---
Fo	11.3	12.9	---	10.8	12.5	6.63	9.47	---	8.58	11.9	10.3	9.35	18.0	14.6	23.7	9.57	---	---	---
Di	11.8	14.9	---	10.8	6.91	13.8	6.19	---	7.39	8.93	47.4	56.9	46.3	17.2	48.8	11.3	2.84	3.68	4.16
Hy	---	---	12.8	---	---	8.27	---	17.0	---	---	19.7	10.7	11.6	---	2.29	13.5	26.6	18.8	15.6
Ne	2.48	6.42	---	4.01	8.89	---	0.86	---	6.21	5.86	---	---	---	7.88	---	---	---	---	---
Q	---	---	7.13	---	---	---	---	7.12	---	---	---	---	---	---	---	---	1.27	1.69	1.07
Leu	---	---	---	---	9.73	---	---	---	---	---	---	---	---	9.31	---	---	---	---	---
Cor	---	---	0.49	---	---	---	---	1.87	---	---	---	---	---	---	---	---	---	---	---
Ap	0.28	0.05	1.07	---	---	---	0.14	3.50	---	---	0.07	---	0.05	0.28	---	1.74	2.18	1.25	1.18
Il	6.97	6.99	2.32	5.24	7.43	3.97	7.07	4.98	6.63	7.05	1.48	1.71	1.33	4.86	1.37	5.79	5.58	2.89	3.38
Mt	4.57	5.97	2.22	---	---	---	7.84	6.89	---	---	2.06	---	5.64	6.10	---	5.29	5.63	2.99	2.94
Sp	---	0.01	---	0.03	---	---	0.01	0.01	0.01	0.01	0.15	0.13	0.19	0.28	0.12	0.04	0.01	0.01	0.01
Hm	---	---	---	---	---	---	---	---	---	---	---	---	---	---	---	---	---	---	---

Table 2 (cont.)

	22	23	24	25	31	34	35	36	37	40	41	42	43	44	45	48	49	50	51
Ab	27.3	27.4	49.6	21.8	2.45	51.4	17.4	2.12	9.39	15.2	5.67	45.4	27.8	22.4	11.5	13.6	37.4	31.1	44.8
An	26.0	23.2	9.65	28.3	12.9	7.28	5.88	5.44	19.7	21.5	10.0	14.3	23.2	21.6	2.49	17.4	21.7	16.3	8.34
Or	22.0	22.2	11.9	10.9	0.06	16.3	29.6	0.59	6.68	6.32	3.01	18.0	12.2	15.0	41.7	6.38	13.1	15.5	18.9
Ol	8.24	---	---	15.8	11.0	---	---	---	---	14.6	49.7	3.67	8.50	13.9	---	12.0	---	13.7	---
Fa	5.15	---	---	7.33	3.19	---	---	---	---	3.48	10.4	2.46	2.46	4.66	---	2.91	---	7.96	---
Fo	3.09	---	---	8.51	7.85	---	---	---	---	11.1	39.3	1.21	6.04	9.24	---	9.10	---	5.77	---
Di	3.85	1.15	---	13.2	33.4	---	---	---	---	32.5	9.95	---	12.1	15.7	---	37.61	3.83	14.9	---
Hy	7.65	15.0	2.24	5.54	35.8	0.55	14.3	4.08	8.92	0.15	11.5	7.50	6.72	---	12.3	---	12.8	4.02	0.99
Ne	---	---	---	---	---	---	---	---	---	---	---	---	---	1.61	---	1.70	---	---	---
Q	---	3.72	25.1	---	---	22.8	23.3	84.2	4.59	---	---	---	---	---	18.7	---	1.31	---	25.1
Leu	---	---	---	---	---	---	---	---	---	---	---	---	---	---	---	---	---	---	---
Cor	---	---	0.48	---	---	1.17	5.95	1.11	20.2	---	---	3.54	---	---	8.61	---	---	---	0.38
Ap	---	1.23	0.12	---	0.02	0.09	0.19	0.02	0.28	0.63	0.46	1.95	1.00	1.37	0.28	1.07	1.53	---	0.07
Il	3.42	3.27	0.28	3.19	1.77	0.09	1.27	0.72	5.89	4.20	1.69	2.24	3.84	4.10	1.88	4.62	3.76	3.11	0.30
Mt	---	2.89	0.54	---	2.17	0.30	2.17	1.19	15.3	4.80	7.70	3.36	4.67	4.35	2.61	5.51	4.73	---	---
Sp	---	---	---	0.01	0.21	---	0.01	---	---	0.06	0.04	---	0.06	0.04	0.01	0.03	0.01	0.01	---
Hm	---	---	---	---	---	---	---	---	8.05	---	---	---	---	---	---	---	---	---	---

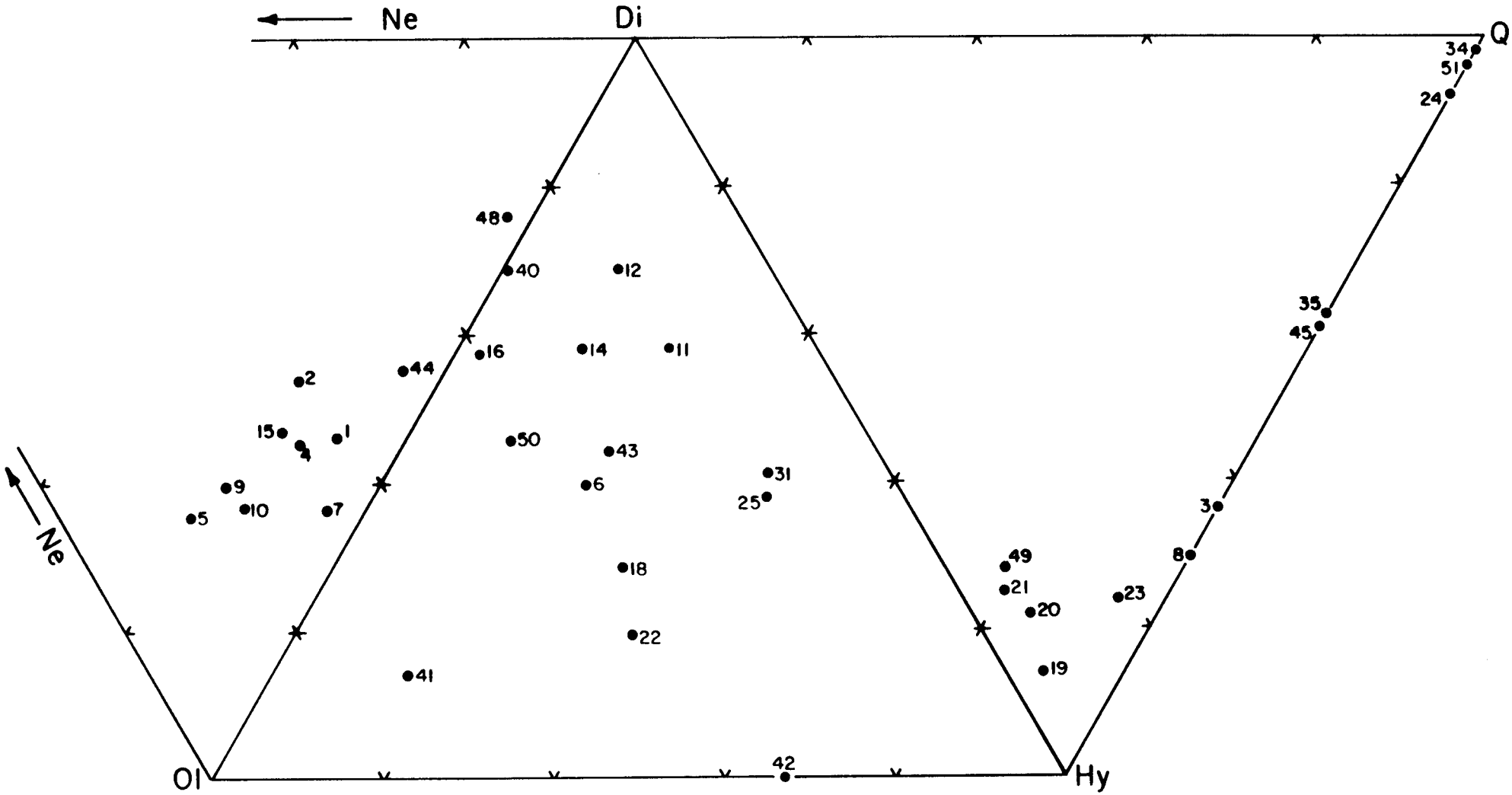

Fig. 32. Ne-Di-Ol-Hy-Q normative diagram for samples of the Cortlandt, Stony Point, and Rosetown complexes.

general, rocks that are corundum normative also contain almandine garnet as a minor constituent. The diorite samples (8, 42) do contain almandine garnet crystals. Later discussion determines whether almandine garnet of these Cortlandt region diorites crystallized from a basic melt or are remnants of incomplete assimilation of a garnet-bearing pelitic schist.

Oxide variation diagrams show a smooth decrease of MgO, FeO, and CaO with increasing SiO_2 for the Cortlandt region basic suite, with the exception of the ferromagnesium cumulate rocks (cortlandtite and clinopyroxenite). CaO and TiO_2 show a positive correlation with $Mg/(Mg + Fe^{2+})$, while Al_2O_3 and K_2O are negatively correlated. Throughout the entire suite, titania concentrations vary from less than 1% to almost 4%. The low TiO_2 abundances can be correlated to rocks dominated by plagioclase, olivine, and pyroxene, while high titania corresponds to rocks with high modal percentages of kaersutite and ilmenite. In general, rocks of the diorite, hornblendite-kaersutite gabbro, and norite plutons are characterized by high potassium (1.5-3.8 wt.%) abundances, indicative of an alkalic affinity. Figure 33, a binary oxide plot of Al_2O_3 against MgO, shows the aluminous nature of the Cortlandt basic rocks as well as

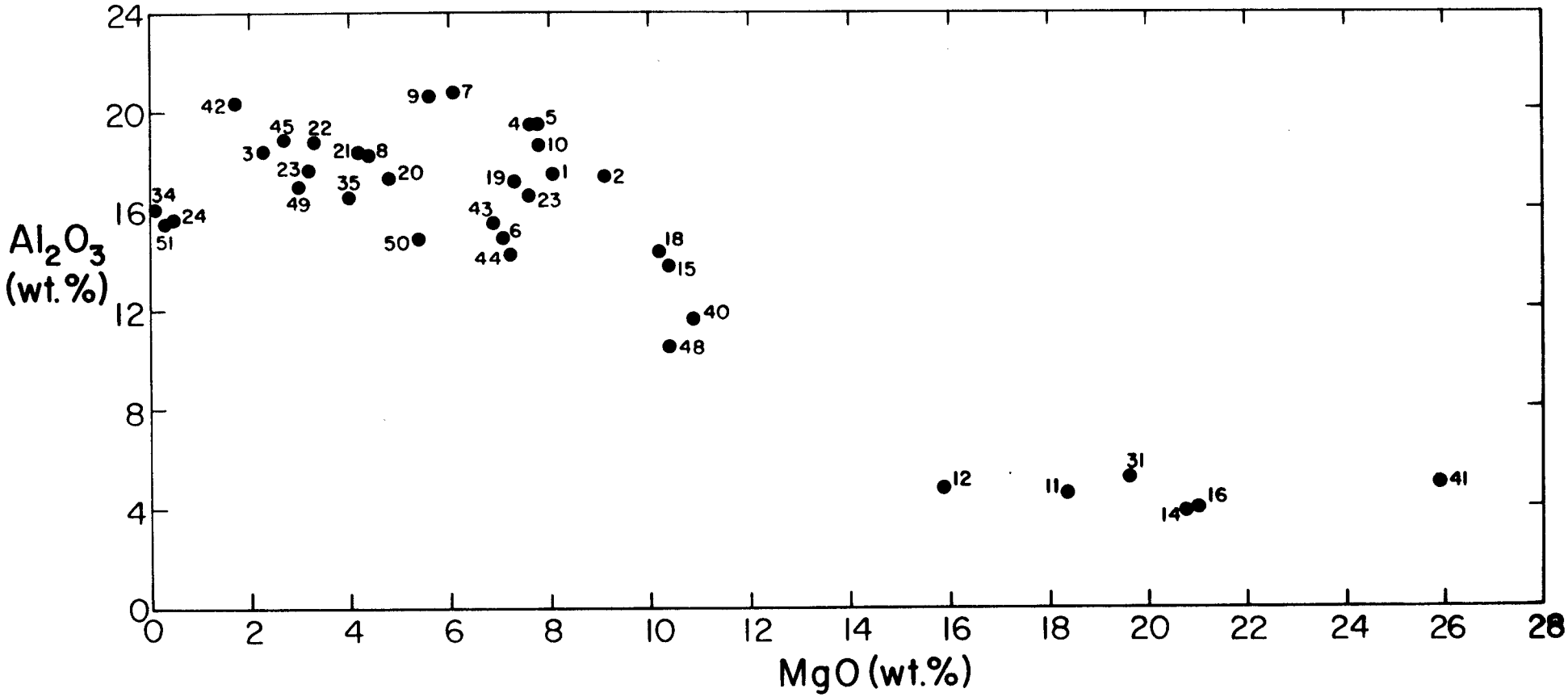

Fig. 33. Al_2O_3 vs MgO plot of samples from the Cortlandt, Stony Point, and Rosetown complexes.

the effects of plagioclase and ferromagnesian (pyroxene, olivine, and amphibole) fractionation or accumulation. This diagram shows a distinct negative correlation of alumina and magnesia, with the abundance of Al_2O_3 varying by a factor of five (4-20 wt.%) and MgO by more than an order of magnitude (0.3-26 wt.%) for the basic samples. Figure 33 also shows that hornblendite and amphibole-rich diorite samples have appreciably higher alumina contents for a given MgO value, indicating a substantial proportion of cumulus plagioclase and kaersutite within these rocks. The general trend of the data in this plot is consistent with crystal fractionation processes. Samples with high MgO (low Al_2O_3) represent ferromagnesian (olivine, pyroxene, and amphibole) cumulates while those with high Al_2O_3 (low MgO) are the resultant differentiates. From these data and from calculated fractionated trends, a possible parental composition(s) for the Cortlandt basic suite should have Al_2O_3 and MgO abundances of approximately 13 and 11 wt.%, respectively. The amphibole-pyroxenite samples (15, 40, 48) have the required Al_2O_3 ($\sim$13 wt.%) and MgO ($\sim$11 wt.%) characteristics, suggesting that this rock type is a possible parental composition for the Cortlandt basic suite.

ANALYTICAL RESULTS

TRACE ELEMENT ANALYSES

Twenty-five samples have been analyzed for rare earth elements (REE), Rb, Sr, Ba, Nb, Zr, Y, and a complete set of first series transition metals (Table 3). Strontium varies from 1608 ppm in the Stony Point diorite (sample 42) to less than 100 ppm in several cortlandtite and clinopyroxenite samples, with a majority of values in the range 500 to 700 ppm. Rb abundances vary from less than 1 ppm in a clinopyroxenite (31) to a high of 117 ppm in a quartz-norite (23). Barium ranges from 4 ppm to 2600 ppm. This large variation in Sr, Rb, and Ba abundances of the Cortlandt suite can be attributed to the effects of fractional crystallization involving the minerals plagioclase, kaersutite, olivine, clinopyroxene, and orthopyroxene. Low abundances of Sr (<100 ppm), Rb (<4 ppm) and Ba (<60 ppm) in rocks such as the Cortlandt region peridotites (cortlandtite and clinopyroxenites) indicate sole accumulation of ferromagnesian phases with small amounts of trapped interstitial liquid. Diorite (7), hornblendite (2), and norite (18, 19) samples with high Sr (>600 ppm) at relatively low Rb (<8 ppm) levels are indicative of plagioclase accumulation because the partition coefficient for

Table 3.

Trace Element Analyses in ppm.

	1			2		3		4	5	6	7		8		9
	a	b	c	a	b	a	b	b	b	b	a	b	a	b	b
Rb	41	44.2		8.3	8.44	76	76.2				3.7	4.20	45	45.0	16.1
Sr	475	522		581	584	592	585				731	724	675	667	720
Ba	525	628		365	506	1122	1181				218	253	722	728	458
Rare Earth Elements															
La		23.4	13.4		9.26		43.2	19.5				7.22		34.3	12.0
Ce		65.0	44.8		31.7		88.8	48.4				19.8		81.3	32.3
Nd		48.6	43.3		30.7		41.5	35.2				16.9		45.4	26.2
Sm		12.0	12.1		8.90		7.53	8.36				4.70		9.16	7.43
Eu		3.03	3.08		2.46		2.34	2.38				1.72		2.24	2.23
Gd		11.1	11.9		8.69		5.96	7.36				4.72		7.30	7.06
Dy		9.48	11.0		7.43		4.34	6.12				4.49		5.50	6.20
Er		4.68	5.32		3.58		2.33	3.04				2.32		2.65	3.08
Yb		3.64	4.15		2.69		2.10	2.29				1.86		2.10	2.27
Transition Metals															
Sc	51			52		13					31		16		
V	449			557		85					304		287		
Cr	21			41		12					31		35		
Co	55			85		15					52		43		
Ni	38			16		< 4.0					31		33		
Cu	26			30		10					31		31		
Zn	95			31		88					113		115		
Nb	24			11		25					13		14		
Zr	97			61		274					43		125		
Y	43			34		22					24		27		

a *X-ray fluorescence.*

b *Isotope dilution.*

c *Kaersutite mineral separate (isotope dilution).*

Table 3 (cont.)

Trace Element Analyses in ppm.

	10	11		12	14		15		16	18		19		20	
	b	a	b	b	a	b	a	b	b	a	b	a	b	a	b
Rb		4.0	4.78		2.0	3.06	15	16.5		5.2		2.3	2.76	49	
Sr		67	69.3		80	89.0	456	456		718		927	914	720	
Ba		65	59.4		36	43.3	338	412		304		249		1469	
Rare Earth Elements															
La			6.02			3.82		21.5			23.6		25.0		47.8
Ce			18.5			11.4		47.4			59.0		52.9		91.2
Nd			15.8			10.1		26.9			38.0		29.2		44.7
Sm			4.38			2.88		5.79			7.89		5.35		8.24
Eu			1.13			0.856		1.69			2.16		1.89		2.53
Gd			4.14			2.72		5.06			6.42		4.20		6.46
Dy			3.70			2.41		4.32			4.63		3.00		5.03
Er			1.78			1.15		2.19			2.17		1.41		2.55
Yb			1.42			0.880		1.82			1.63		1.14		2.19
Transition Metals															
Sc		53			44		24			31		19		22	
V		223			186		239			396		299		156	
Cr		651			767		29			183		73		84	
Co		98			119		47			76		37		34	
Ni		358			643		68			98		27		37	
Cu		62			111		46			88		43		21	
Zn		79			70		96			126		95		103	
Nb		< 1.8			2.4		28			13		15		19	
Zr		51			32		150			62		33		136	
Y		19			13		23			24		17		25	

a *X-ray fluorescence.*

b *Isotope dilution.*

Table 3 (cont.)

Trace Element Analyses in ppm.

	21		22	23		24	25	31		34	35	36	37	40	
	a	b	b	a	b	a	b	a	b	a	a	b	b	a	b
Rb	43		80.1	113	117	67		< 1.1		80	142			16	16.4
Sr	730		696	636	659	405		50		474	134			375	379
Ba	1165		1456	1152	1261	539		3.7		515	879			235	257
Rare Earth Elements															
La		39.5	47.7		67.6	5.77***			2.89	8.80***		4.89***	58.1***		16.1
Ce		78.5	89.5		138	11.6			10.8	17.1		6.95	107		38.8
Nd		37.9	44.5		62.3	5.33			12.0	7.57		3.16	47.3		26.1
Sm		7.08	8.14		11.0	1.08			3.64	1.49		1.00			6.29
Eu		2.47	2.50		2.42	0.327			1.00	0.454		0.390	2.10		1.92
Gd		5.52	6.27		8.16	0.804			3.72	1.06		1.81			5.77
Dy		4.34	4.26		6.64	0.701			3.19	0.941		2.82	2.98		5.28
Er		2.14	1.47		3.40	0.383			1.62	0.520		1.75	1.16		2.59
Yb		1.80	2.04		2.96	0.366			1.32	0.511		1.66	1.04		2.07
Transition Metals															
Sc	18			16		3.3		54		2.0	13			41	
V	164			146		13		279		3.6	80			268	
Cr	45			16		7.7		932		8.6	81			292	
Co	31			27		< 2.7		113		< 3.0	13			68	
Ni	54			7		4		507		4.8	24			196	
Cu	23			20		6.9		242		< 2.1	20			61	
Zn	83			104		28		86		15	68			77	
Nb	15			36		< 1.3		< 1.8		< 1.3	11			16	
Zr	118			380		75		40		95	257			108	
Y	22			32		3.9		17		4.9	11			26	

a *X-ray fluorescence.*

b *Isotope dilution.*

*** *Rare earth elements determined by isotope dilution at Stony Brook.*

Table 3 (cont.)

Trace Element Analyses in ppm.

	41	42		43		44		45		48		49		50
	a	a	b	a	b	a	b	a	b	a	b	a	b	b
Rb	8.4	69	69.1	40	27.8	59		176	177	13	12.8	46		
Sr	201	1639	1608	664	476	706		104	111	442	451	1219		
Ba	136	2620	2641	627	664	1042		1165	1332	295	330	953		
Rare Earth Elements														
La	14.2***		36.2		36.4		50.9		40.9		22.9		42.2	32.8
Ce	28.5		78.6		77.0		102		88.1		56.6		85.8	72.6
Nd	14.2		42.7		36.7		47.4		38.4		38.1		42.1	35.8
Sm	2.84		7.34		7.00		8.58		7.43		8.67		8.04	6.54
Eu	0.795		3.37		2.08		2.28		1.48		2.58		2.44	2.00
Gd	2.68		4.55		6.15		6.40		6.38		7.46		6.17	5.01
Dy	2.11		1.99		4.66		5.16		5.98		6.69		5.03	4.32
Er	1.02		0.569		2.41		2.51		3.83		3.25		2.33	2.13
Yb	0.844		0.386		2.05		2.12		3.76		2.61		1.82	1.86
Transition Metals														
Sc	15	3.5		25		29		17		49		9.6		
V	96	16		193		228		86		307		98		
Cr	198	13		235		212		81		104		25		
Co	161	12		43		42		17		59		23		
Ni	1163	4.3		82		88		25		100		28		
Cu	201	15		38		40		18		87		62		
Zn	115	176		99		109		99		78		103		
Nb	10	49		35		32		21		23		53		
Zr	67	725		222		271		322		138		199		
Y	12	11		25		25		31		31		24		

a *X-ray fluorescence.*

b *Isotope dilution.*

*** *Rare earth elements determined by isotope dilution at Stony Brook.*

Table 3 (cont.)

Trace Element Analyses in ppm.

	51		BCR-1
	a	b	b
Rb	47	47.4	
Sr	613	605	
Ba	1179	1184	672
Rare Earth Elements			
La		9.35	25.4
Ce		17.5	53.3
Nd		7.57	28.6
Sm		1.39	6.54
Eu		0.500	1.93
Gd		1.06	6.27
Dy		0.847	6.37
Er		0.434	3.68
Yb		0.412	3.32
Transition Metals			
Sc	1.9		
V	8.0		
Cr	3.8		
Co	< 3.0		
Ni	13		
Cu	2.6		
Zn	27		
Nb	1.4		
Zr	92		
Y	4.3		

a *X-ray fluorescence.*

b *Isotope dilution.*

Table 3. Rare Earth Normalizing Values.

La	0.315
Ce	0.813
Nd	0.597
Sm	0.192
Eu	0.0722
Gd	0.259
Dy	0.325
Er	0.213
Yb	0.208

Sr between plagioclase and basaltic melt is greater than 1 (Philpotts and Schnetzler, 1970). The plagioclase partition data also indicate that the parental magma of these rock types probably contained approximately 500 ppm Sr. Mafic samples such as those of several norites and diorites with high Ba, Rb, and K abundances and high Rb/Sr ratios represent differentiates containing little or no cumulate minerals produced by fractional crystallization and dominated by the removal of plagioclase. The K/Ba ratios of the Cortlandt region basic samples averages approximately 22 and shows smaller variation than the K/Rb ratios (Fig. 34). The highest K/Rb ratios (1000-1200) occur in rocks (2, 7, 18, 19) that consist predominantly of cumulate kaersutite and plagioclase.

Zirconium abundances of the Cortlandt basic suite range from 32 ppm (cortlandtite) to 725 ppm (Stony Point diorite) with a majority of the values varying from 100 to 200 ppm. Zirconium, because it is excluded from the liquidus phases in basaltic suites (Saunders and Tarney, 1979), can be used as an indicator of extent of differentiation as well as a means of estimating the amount of trapped interstitial liquid in the cumulate rock types.

To illustrate the range of trace element variation due to crystal fractionation processes, Ni and Rb have

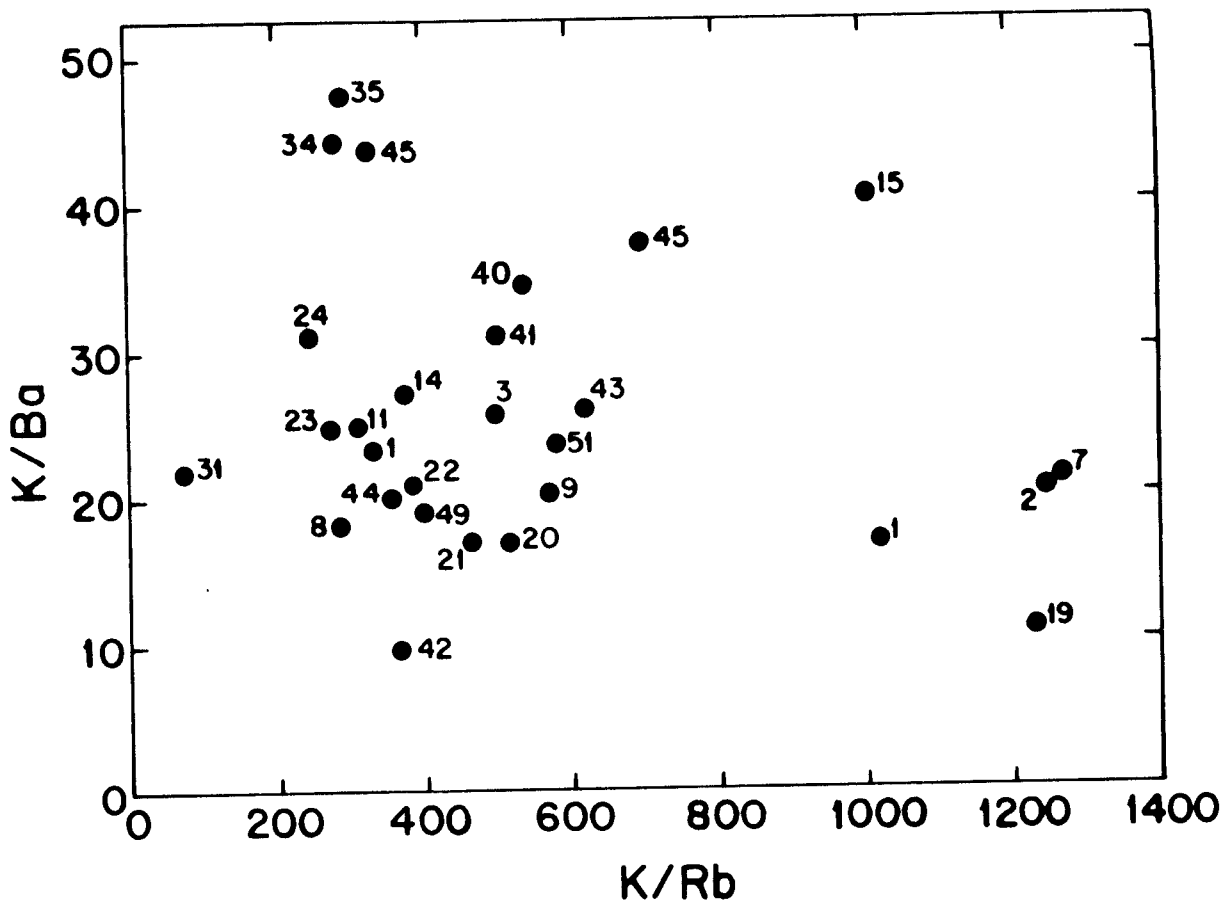

Fig. 34. K/Ba vs K/Rb plot for samples of the Cortlandt, Rosetown, and Stony Point complexes.

been plotted against MgO (Figs. 35 and 36). MgO shows a strong positive correlation with Ni and a negative correlation with Rb. Rb and Ni concentrations vary by two orders of magnitude reflecting the accumulation of olivine and pyroxene in the peridotitic rock types (Ni 358-1300 ppm; Rb 1-8 ppm) and extensive crystal fractionation involving plagioclase and ferromagnesium phases in the differentiated rocks (Ni 5-30 ppm; Rb 60-117 ppm). As in Fig. 34, samples 2, 7, 18, and 19, rocks which contain a substantial proportion of cumulate plagioclase, plot significantly below the main Rb-MgO trend.

It should be noted that the average K/Ba, K/Rb, Rb/Sr ($\sim$0.04), and Zr/Nb ($\sim$7) ratios of the Cortlandt region basic rocks are more typical of those of alkali basalts than those of tholeiitic basalts (Hanson, 1977).

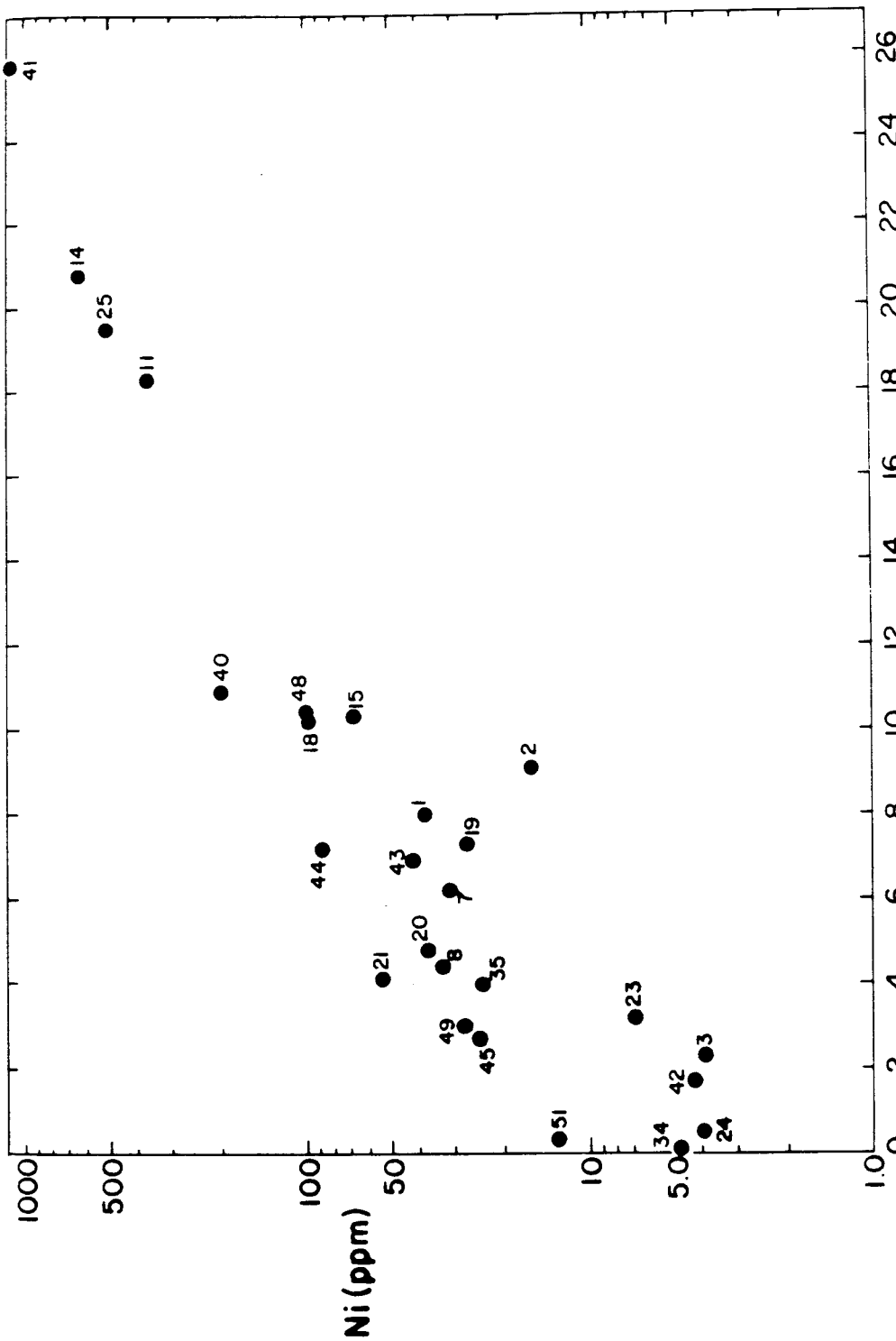

Fig. 35. Ni vs MgO plot for samples of the Cortlandt, Stony Point, and Rosetown complexes.

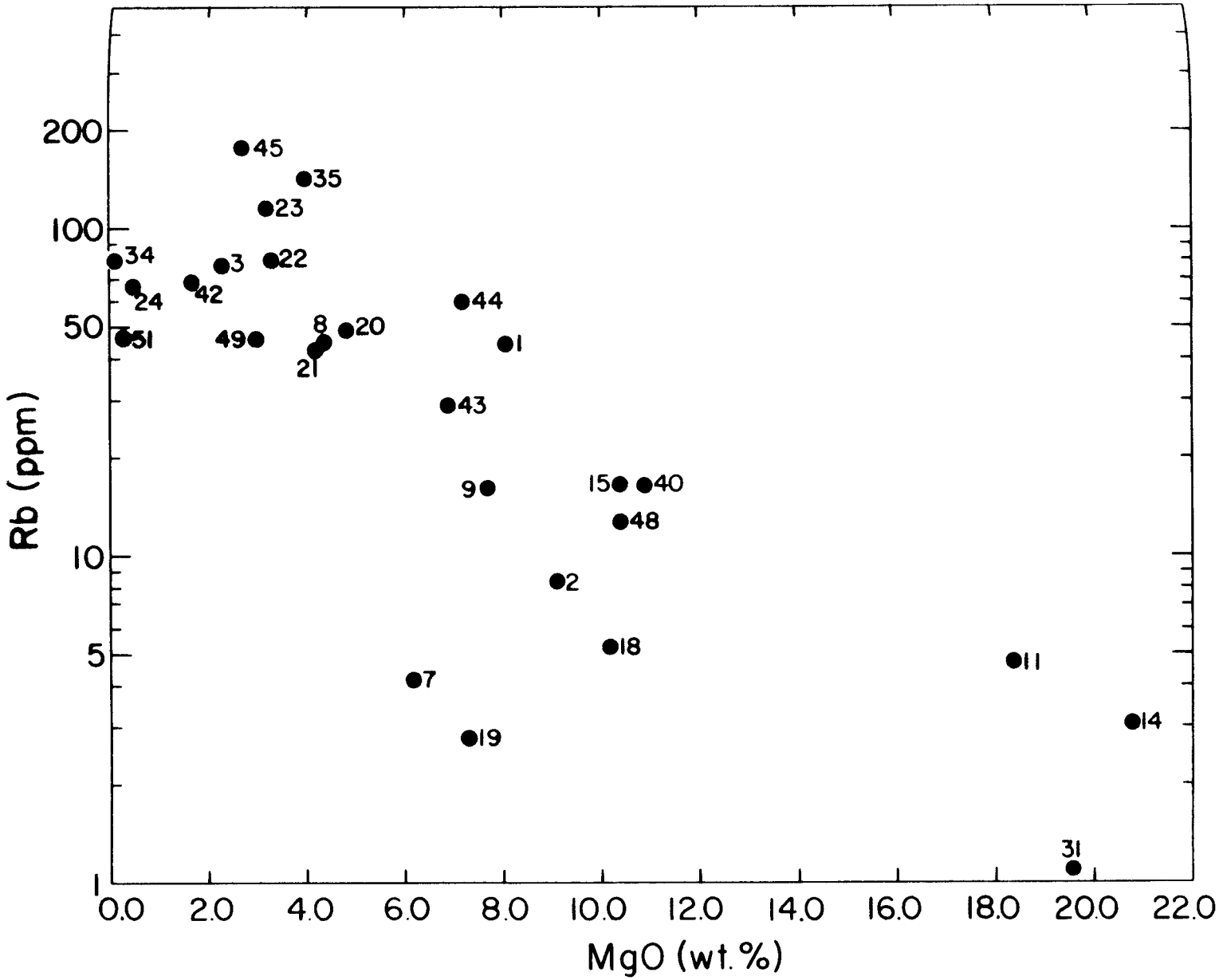

Fig. 36. Rb vs MgO plot for samples of the Cortlandt, Stony Point, and Rosetown complexes.

ANALYTICAL RESULTS

RUBIDIUM-STRONTIUM ISOTOPIC ANALYSIS

$^{87}Sr/^{86}Sr$ ratios for seventeen of the Cortlandt igneous rocks and one sample of pelitic country rock are given in Table 4. Rb/Sr data for these eighteen samples are plotted on a strontium evolution diagram in Fig. 37. The $^{87}Rb/^{86}Sr$ values of the igneous suite have a restricted range (0.0087-0.3764) and, because of scatter, the collective data on this plot do not define an isochron. Yet, data points from an individual pluton such as the three data points from the norite body do lie very close to a line with an age of 440 m.y., an age that is supported by the geological field relationships. A line parallel to that of the norite line can also be drawn through rocks of the hornblendite kaersutite-gabbroic body (pluton 1) of the Cortlandt complex while a line through samples from the Cortlandt complex diorites (pluton 2) has a substantially steeper slope ($\sim$900 m.y.). The diorite slope extrapolates very close to the pelitic country rock data point which has a high Rb/Sr and $^{87}Sr/^{86}Sr$ ratio, defining a potential mixing line. Sample 14 (cortlandtite) and sample 15 (amphibole-pyroxenite) from pluton 4 of the Cortlandt complex also lack any correlation of $^{87}Sr/^{86}Sr$ and Rb/Sr to a 440 m.y.

Table 4. Strontium Isotopic Data.

Sample	$^{87}Sr/^{86}Sr$	$^{87}Rb/^{86}Sr$	$(^{87}Sr/^{86}Sr)_i$ [c]
1	0.70821	0.2447	0.70668
2	0.70707	0.0418	0.70681
3	0.70926	0.3764	0.70690
7	0.70618	0.0168	0.70607
8	0.70945	0.1950	0.70823
9	0.70850	0.0646	0.70810
11	0.70739	0.1993	0.70614
14	0.70551	0.0994	0.70489
15	0.70681	0.1046	0.70615
19	0.70653	0.0087	0.70648
22	0.70853	0.3326	0.70645
23	0.70968	0.5131	0.70646
40	0.70506	0.1250	0.70428
42	0.70535	0.1242	0.70457
43	0.70527	0.1688	0.70421
45	0.75968	4.608	0.73080
48	0.70530	0.0820	0.70479
51	0.70647	0.2264	0.70505

c: based on a 440 m.y. old age.

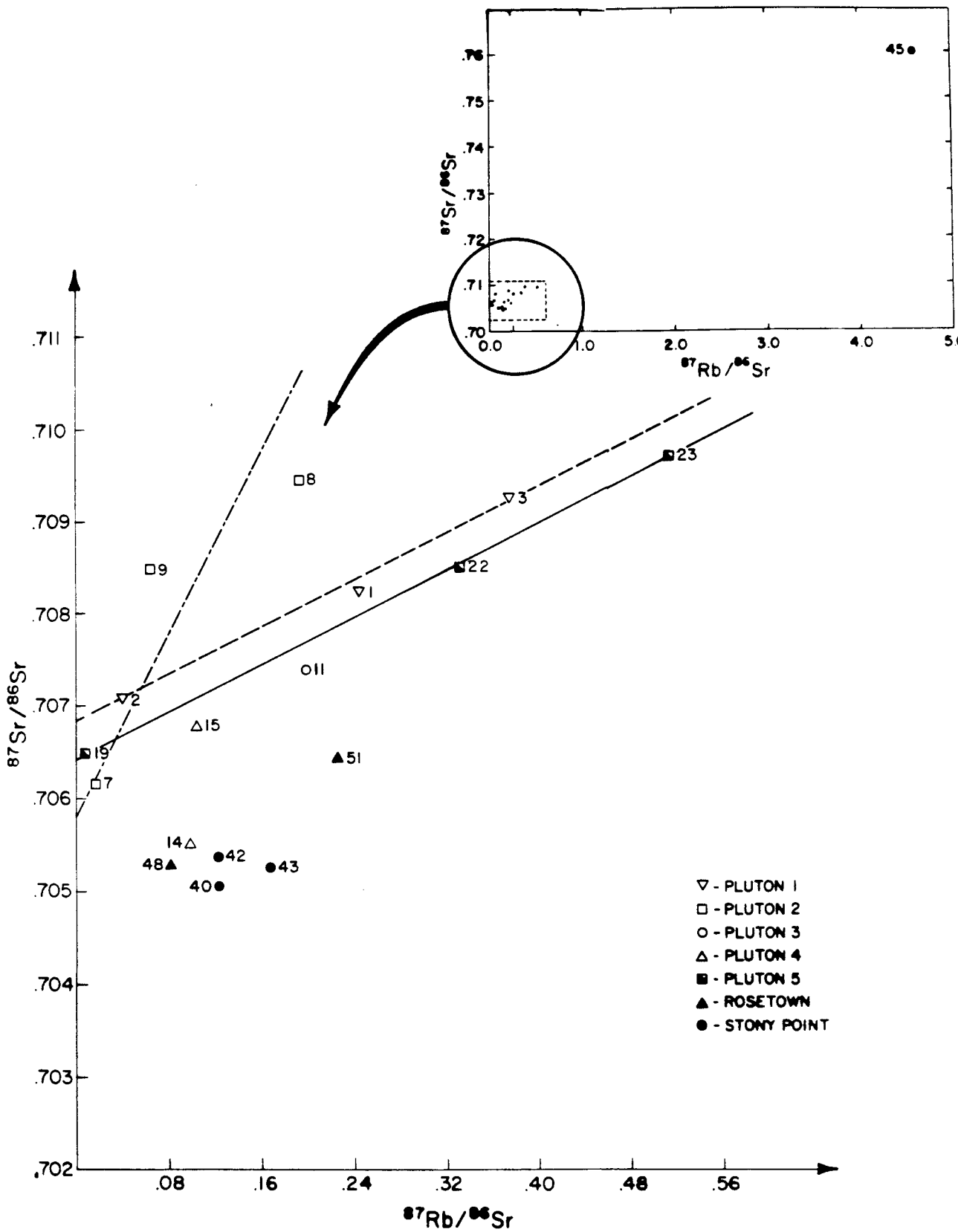

Fig. 37. $^{87}Sr/^{86}Sr$ vs $^{87}Rb/^{86}Sr$ plot for samples listed in Table 4.

age. The strontium isotopic data indicate that each pluton from the Cortlandt, Stony Point, and Rosetown complexes is isotopically distinct. Strontium initials ($^{87}Sr/^{86}Sr]_i$), based on a 440 m.y. age have been calculated (Table 4) and are displayed on Fig. 38, a plot of $^{87}Sr/^{86}Sr)_i$ against Rb/Sr. The wide diversity of $^{87}Sr/^{86}Sr$ initial ratios (0.70421-0.70823) for these samples suggests source heterogeneity and/or contamination of an initial parent with a low $^{87}Sr/^{86}Sr)_i$ ($\sim$0.704) by older crustal material. From Fig. 30 and Table 4 it is apparent that samples from the Cortlandt complex have considerably higher $^{87}Sr/^{86}Sr)_i$ values than do the samples from the Stony Point and Rosetown complexes on the western side of the Hudson River.

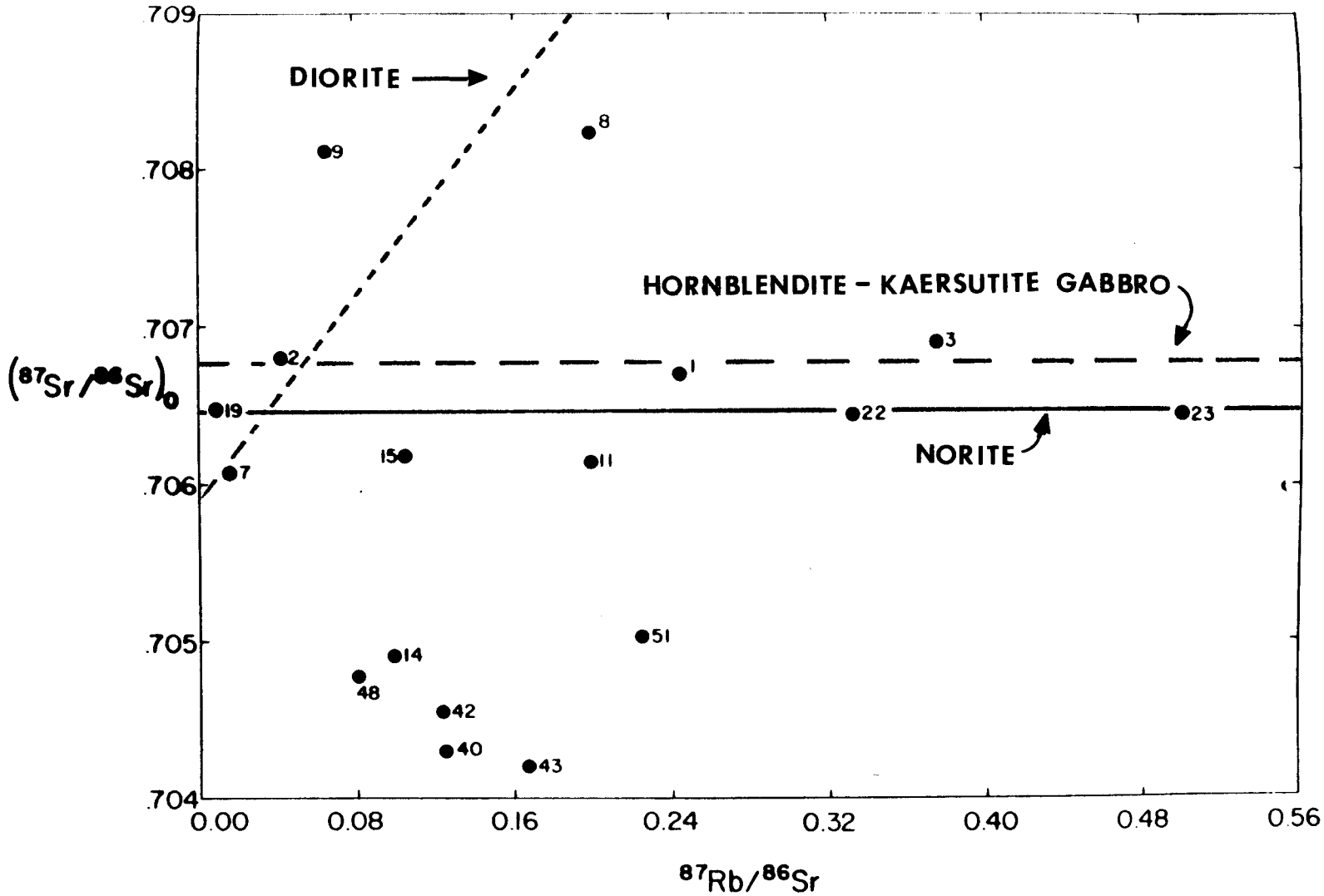

Fig. 38. $^{87}Sr/^{86}Sr)_i$ vs $^{87}Rb/^{86}Sr$ plot for samples listed in Table 4. Lines relate samples from the same pluton.

ANALYTICAL RESULTS

RARE EARTH ELEMENT DATA AND PETROCHEMICAL CHARACTERISTICS

The rare earth element (REE) data for this study is presented separately because of the usefulness of the REE in determining relationships among igneous rock suites. The REE analyses, together with other major and trace element data, should clearly show the geochemical variations among the Cortlandt region rock types, as well as the processes that may have caused these variations. Samples from the cortlandtite and amphibole-pyroxenite suite will be discussed first, since the major and trace element characteristics of the amphibole-pyroxenites indicate that they are possible parental compositions of the other basic rock types.

Cortlandtite and Amphibole-Pyroxenite

REE patterns for two cortlandtites (14, 41) and three amphibole-pyroxenites (15, 40, 48) are illustrated on Fig. 39. All samples have fractionated REE patterns with $(La/Yb)_n$ ratios ranging from 2.9 to 11.0. The two cortlandtite samples, 41 from Stony Point and 14 from the Cortlandt complex, have middle (MREE) and heavy (HREE) REE abundances that are approximately 50% less than those of the amphibole-pyroxenite samples (15, 40, 48).

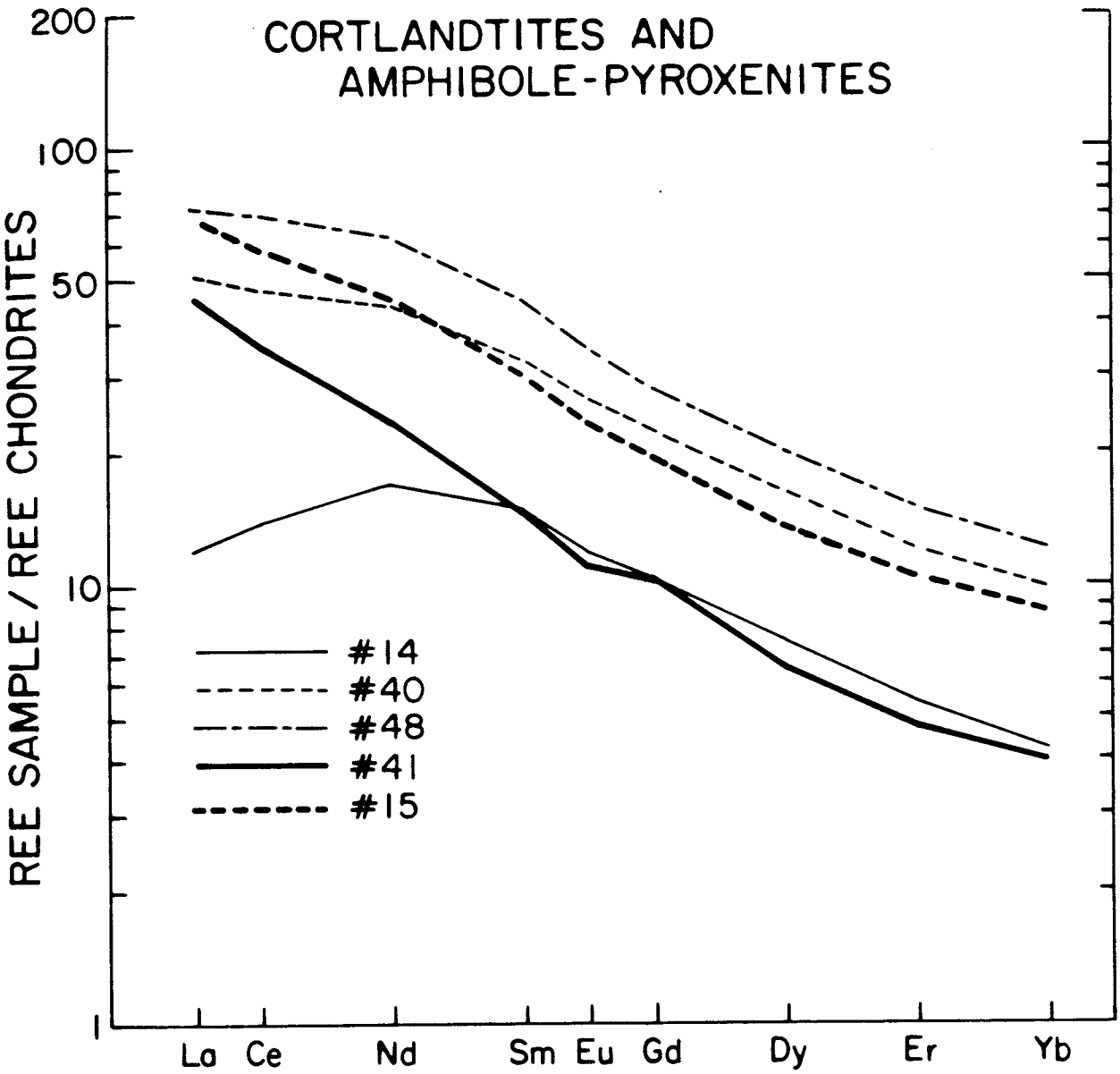

Fig. 39. Chondrite-normalized rare-earth patterns for cortlandtite and amphibole-pyroxenites of the Cortlandt, Stony Point and Rosetown complexes.

However, cortlandtite sample 14, unlike cortlandtite sample 41, has a greater downward concavity in its light rare earth (LREE) pattern (Fig. 39). The extreme downward concavity of the REE pattern of cortlandtite sample 14, plus its low Rb (3.1 ppm), Sr (89 ppm), Ba (43 ppm), Zr (32 ppm), Nb (2.4 ppm) abundances and its high Mg/(Mg + Fe^{2+}) (Mg# 0.83), Ni (739 ppm), Sc (44 ppm), and Cr (767 ppm) values indicate that it is a rock which contains large percentages of cumulate olivine and clinopyroxene and minor amounts of trapped intercumulus liquid. This conclusion is in agreement with the petrographic data. The relative REE abundances in the parent melt from which the cumulate minerals (olivine, clinopyroxene, orthopyroxene) of sample 14 crystallized were probably similar to those of the three fractionated amphibole-pyroxenite samples (15, 40, 48). Cortlandtite sample 41 from Stony Point also appears to have had a cumulate origin (Ni 1312 ppm; Mg# 0.80). It lacks the LREE concavity because it contains more trapped intercumulus melt than sample 14. Entrapment of a greater amount of liquid ($\sim$50%) also explains the higher incompatible element (Rb 8.4 ppm; Sr 201 ppm; Zr 67 ppm; Nb 10 ppm) abundances of sample 41 compared to those of sample 14. This conclusion is consistent with the petrography (Figs. 19 and 21). Sample 14 contains only a small proportion

(~15%) of interstitial kaersutite while sample 41 contains a large enough proportion of kaersutite that it has a poikilitic texture. Kaersutite, as was mentioned earlier, is believed to closely approximate the major element chemistry of the parental melt; hence, any trapped intercumulus liquid in these rocks crystallized as kaersutite.

The fractionated REE patterns and trace element ratios (Rb/Sr, Zr/Nb, etc.) of the three amphibole-pyroxenite samples from the cortlandtite plutons are similar to those of alkali basalts which originate from the mantle and have garnet as a residual phase (Kay and Gast, 1973; Sun and Hanson, 1975; Hanson, 1977; Frey et al., 1978). The Mg numbers (0.71-0.72) and Ni abundances (100-196 ppm) of amphibole-pyroxenite samples 40 and 48 suggest that these rocks could represent primary (relatively undifferentiated) basaltic melts from upper mantle peridotite (Green, 1970, 1971; Sun and Hanson, 1975; Frey et al., 1978), and could be the parental magma for other basic rock types of the area. Sample 15 is not considered to be representative of a primary basaltic magma, even though it has REE abundances and a Mg number similar to those of samples 40 and 48. Rather, sample 15 seems to have assimilated substantial carbonate country

rock at the emplacement site which considerably changed its calcium (15.6 wt.%) and silica (37.5 wt.%) abundances (Table 1).

Clinopyroxenites

REE patterns (Fig. 40) for the clinopyroxenite samples from the western (11) and eastern (31) portions of the Cortlandt complex are similar and are characterized by a strong downward curvature of the LREE, negative Eu anomalies, and linear fractionated REE for Gd through Yb. Sample 31 from pluton 6 has slightly lower REE abundances and a greater downward concavity of its LREE than sample 11. The REE patterns and the high Sc (53 and 54 ppm), Ni (358 and 507 ppm), and Cr (651 and 932 ppm) abundances, plus the low incompatible element values, indicate that these clinopyroxenites, like cortlandtite sample 14, are ferromagnesian (clinopyroxene, orthopyroxene, and olivine) cumulates. Also, like the cumulus cortlandtite sample 14, only a small proportion of melt appears to have been trapped in the cumulate pile of these two clinopyroxenites.

Hornblendite-Kaersutite Gabbros

The REE patterns for four rock samples and one kaersutite mineral separate from pluton 1 of the Cortlandt

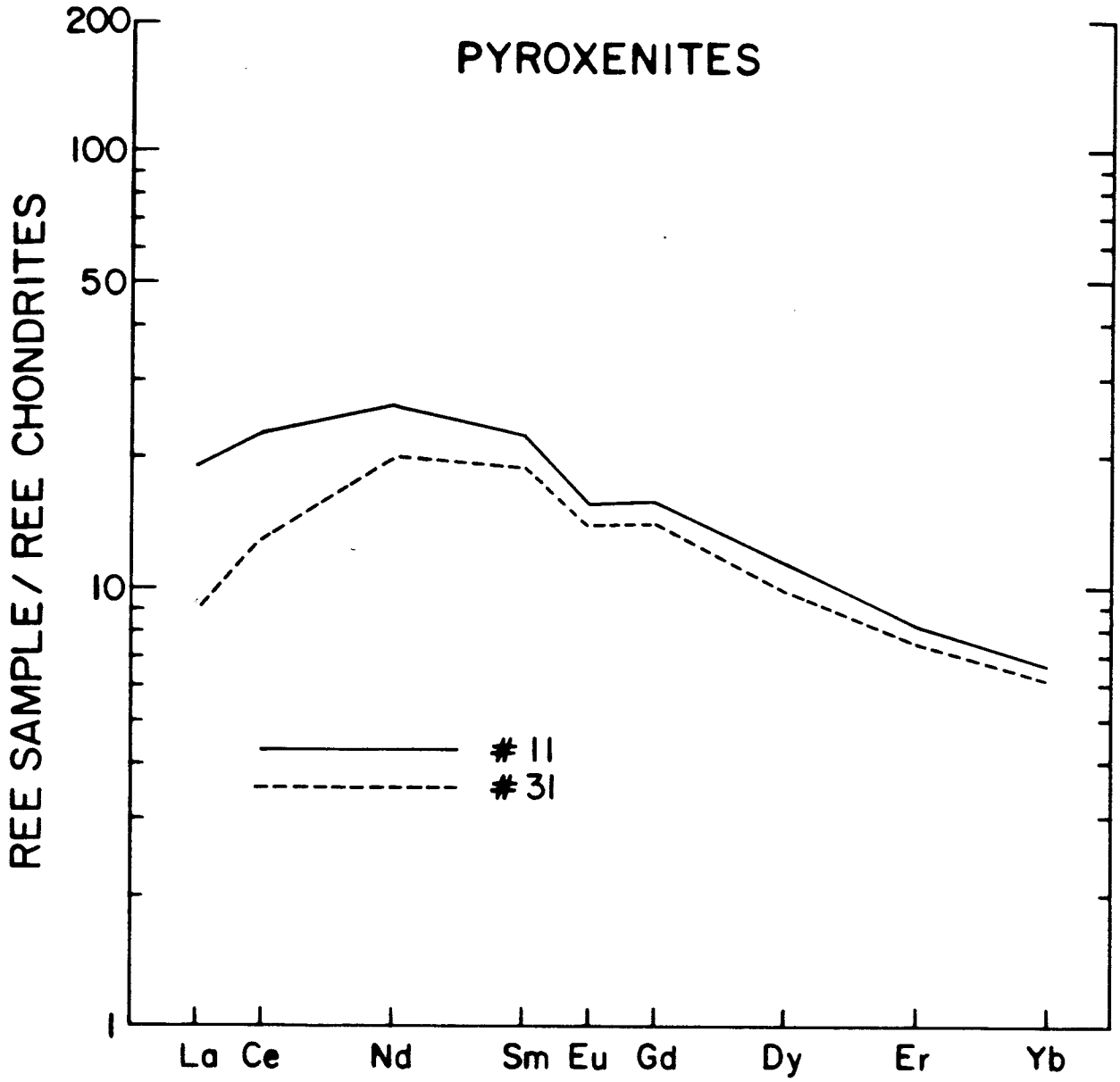

Fig. 40. Chondrite-normalized rare-earth patterns for two clinopyroxenites of the Cortlandt complex.

complex are shown in Fig. 41. The three hornblendite whole rock patterns (1, 2, 4) are characterized by a strong concave down curvature in the LREE and negative Eu anomalies very similar to those of the kaersutite mineral separate (#1 kaer) reflecting the large proportion (70-80%) of cumulate kaersutitic amphibole in these rocks. The low Rb/Sr ratios (0.01) of hornblendite sample 2 indicates that plagioclase is also a cumulate phase. Petrographic data also support this conclusion that amphibole and plagioclase are both cumulus minerals within many of the samples of pluton 1. The overall differences in the REE abundances of these three hornblendites (1, 2, 4) indicate possible variation in the amount of plagioclase, the other major mineral constituent in these rocks, trapped intercumulus liquid, and the abundance of trace mineral phases such as sphene. REE and major elements (Table 1) were determined on a kaersutite mineral separate to aid in the evaluation of partitioning between kaersutite and basaltic melt which was useful in quantitative modelling.

A kaersutitic gabbro, sample 3, has a highly fractionated REE pattern ($(La/Yb)_n \approx 14$) and probably represents a derivative liquid. The high Rb (76 ppm), Ba (1181 ppm), K_2O (3.58 wt.%) and SiO_2 (56.9 wt.%)

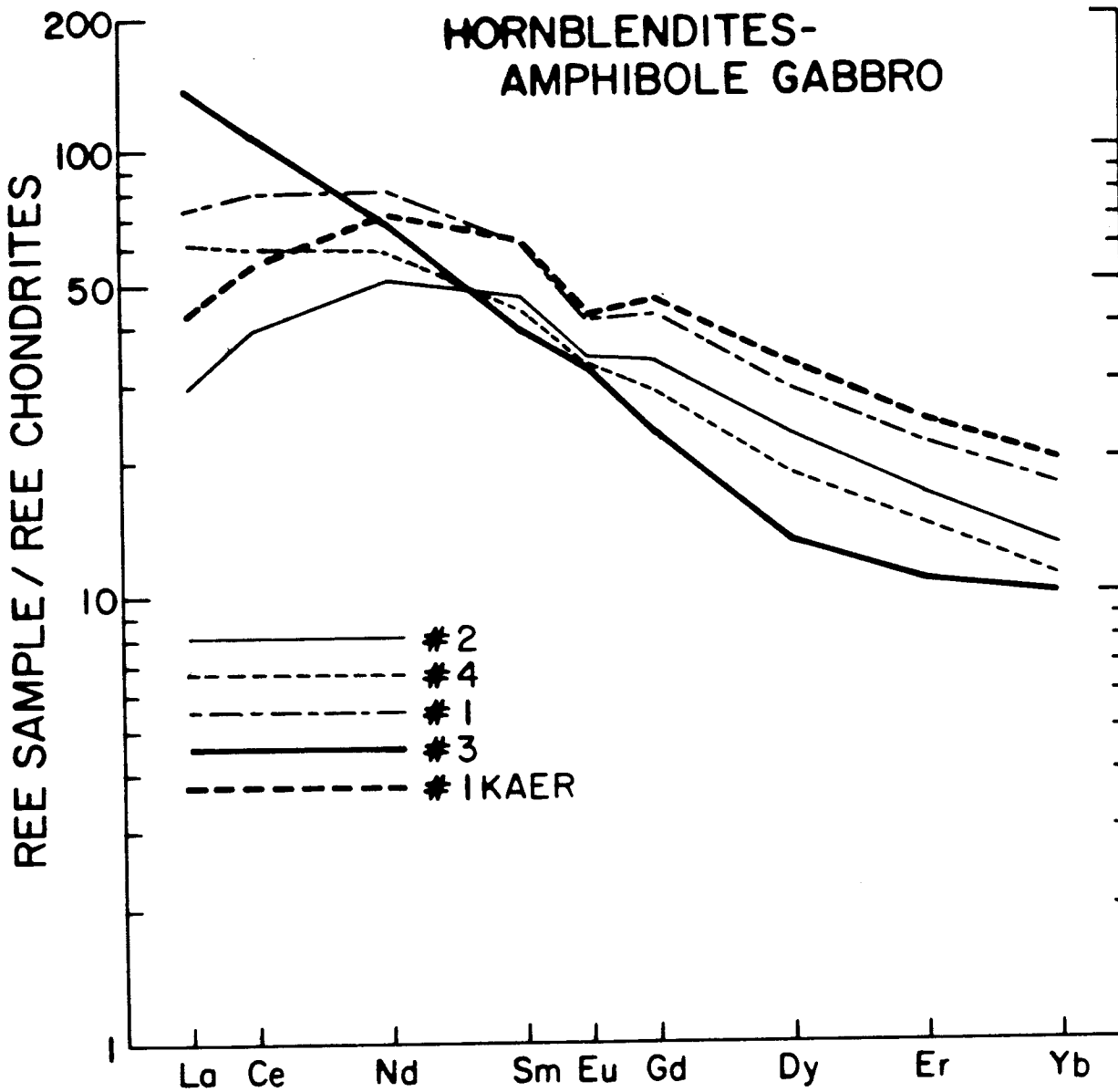

Fig. 41. Chondrite-normalized rare earth patterns for hornblendites and kaersutite gabbros of the Cortlandt complex. Also illustrated is the REE pattern of a kaersutite mineral separate (1 KAER) from hornblendite sample 1.

values of sample 3 suggest that this kaersutite gabbro is a late-stage differentiated liquid from the same magma that produced the cumulus hornblendite rocks.

Diorites

The REE patterns for six diorite samples from the Cortlandt, Stony Point, and Rosetown complexes are illustrated on Fig. 42. Two of the diorite samples from pluton 2 of the Cortlandt complex (7, 9) have REE patterns that are slightly concave downward in the LREE, indicating possible accumulation of kaersutite. The low silica (41.8 and 43.9 wt.%) and high Mg numbers (0.58) of these two samples (Table 1) are consistent with accumulation of amphibole. The low Rb/Sr ratios of samples 7 and 9 (0.005 and 0.022) and the lack of appreciable negative Eu anomalies suggest that plagioclase is also a cumulate phase in these diorites. The third diorite sample (8) analyzed from pluton 2, has a more highly fractionated REE pattern ($(La/Yb)_n \approx 11$), higher silica (47.5 wt.%), and lower Mg number (0.52) (Table 1), indicating that it consists principally of differentiated melt. Diorite sample 8, like the kaersutite gabbro sample 3 from pluton 1, is corundum normative (1.87%) (Table 2), possibly due to the addition of pelitic material.

The REE pattern (Fig. 42) for the Stony Point

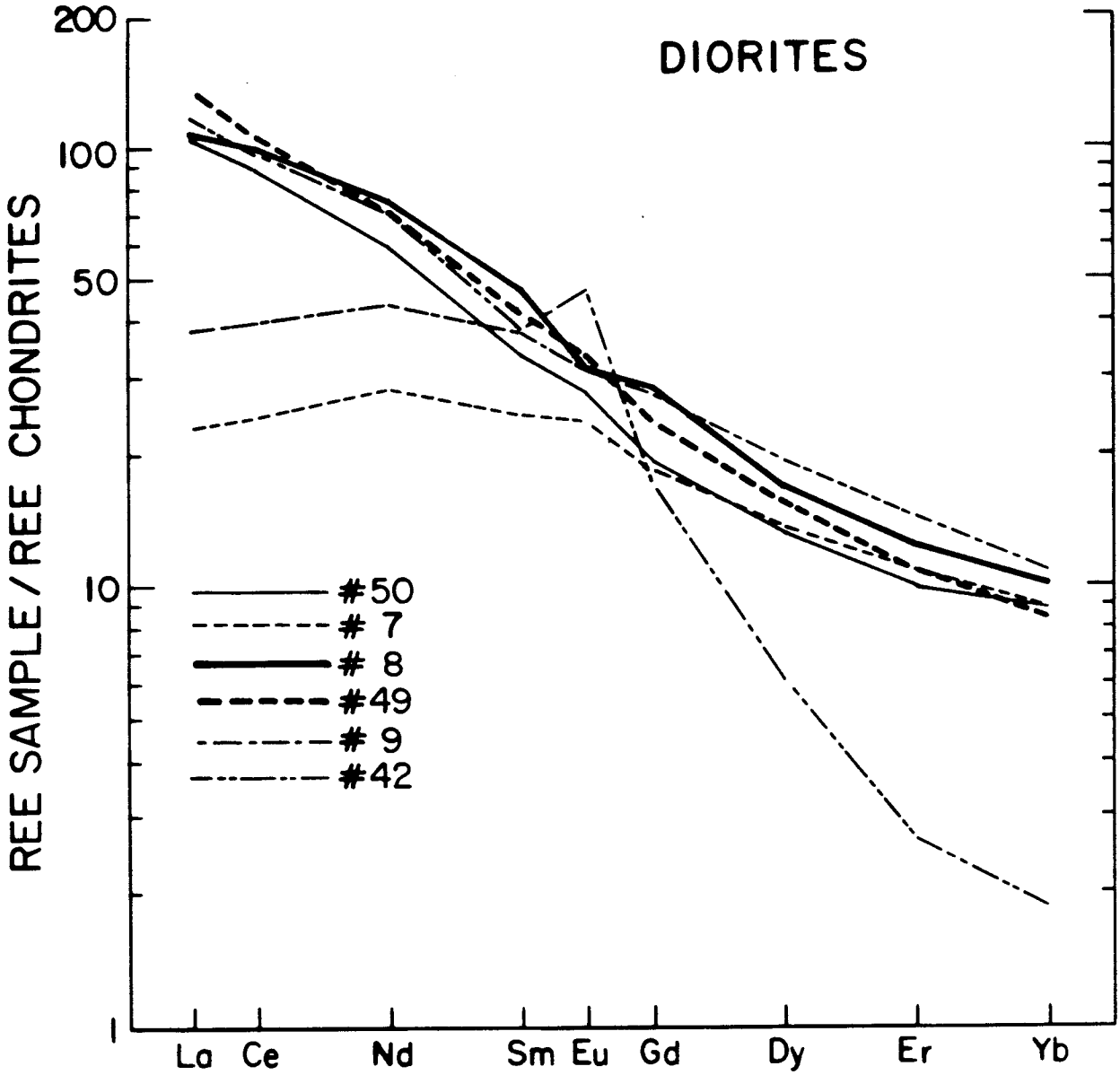

Fig. 42. Chondrite-normalized rare-earth patterns for diorites of the Cortlandt, Stony Point, and Rosetown complexes.

diorite sample (42) is characterized by a large positive Eu anomaly and very low heavy rare earth element (HREE) abundances ($(La/Yb)_n \approx 66$). This diorite, like sample 8, contains almandine garnet (~ 3 modal %) and is corundum normative (3.54%). The high Al_2O_3 (20.4 wt.%), Na_2O (5.20 wt.%), and Na_2O/K_2O ratio (1.75), and the Ba (2641 ppm) and Sr (1639 ppm) contents of this diorite are very similar to those of the Archean syenodiorites studied by Arth and Hanson (1973). The high Al_2O_3, Sr abundances, as well as the large positive Eu anomaly, suggest that this diorite sample may contain a substantial proportion of cumulate plagioclase. It is believed that crystallization and subsequent fractionation of garnet from the diorite melt is responsible for the low HREE abundances of sample 42.

The Rosetown complex diorites (49, 50) have fractionated REE patterns ($(La/Yb)_n \approx 13$). However, unlike the derivative liquids represented by samples 8 and 42, these two diorites from Rosetown are not corundum normative (Table 2). Sample 50 is a diorite inclusion removed from a nearby granodiorite body (Fig. 4) while sample 49 is from the diorite pluton at Rosetown. The REE data and major element compositions suggest that samples 49 and 50 may be related by amphibole and plagioclase fractionation.

Norites

The alkalic nature of six norite samples from the Cortlandt pluton 5 is further demonstrated by their strongly fractionated REE patterns ($(La/Yb)_n \approx 14$) (Fig. 43). These norites include kaersutite norite (18), biotite amphibole norite (19, 20, 21, 22), and a quartz norite (23) with a very high alkali content ($K_2O \approx 3.80$ wt.%; $Na_2O \approx 3.35$ wt.%). Unlike the differentiated samples from the Cortlandt hornblendite and diorite plutons, the norite samples, though high in alumina (~ 18 wt.%), have higher SiO_2/Al_2O_3 ratios (~ 3.0) and, therefore, are not corundum normative (Table 2). The REE patterns of these samples are subparallel and REE abundances vary by almost a factor of three. Pronounced Eu anomalies are present only in norite samples 23 (negative anomaly) and 19 (positive anomaly). These correlations, plus the similarity of trace element ratios (Rb/Sr, K/Rb, Ba/Sr) suggest that these six norite samples may be related to each other by fractional crystallization involving various amounts of plagioclase, amphibole, orthopyroxene, clinopyroxene, and biotite.

Granodiorites

Three granodiorite samples collected from Rosetown (#51), Peekskill (#34), and a rhyodacite dike crosscutting the norite pluton of the Cortlandt complex (#24), have

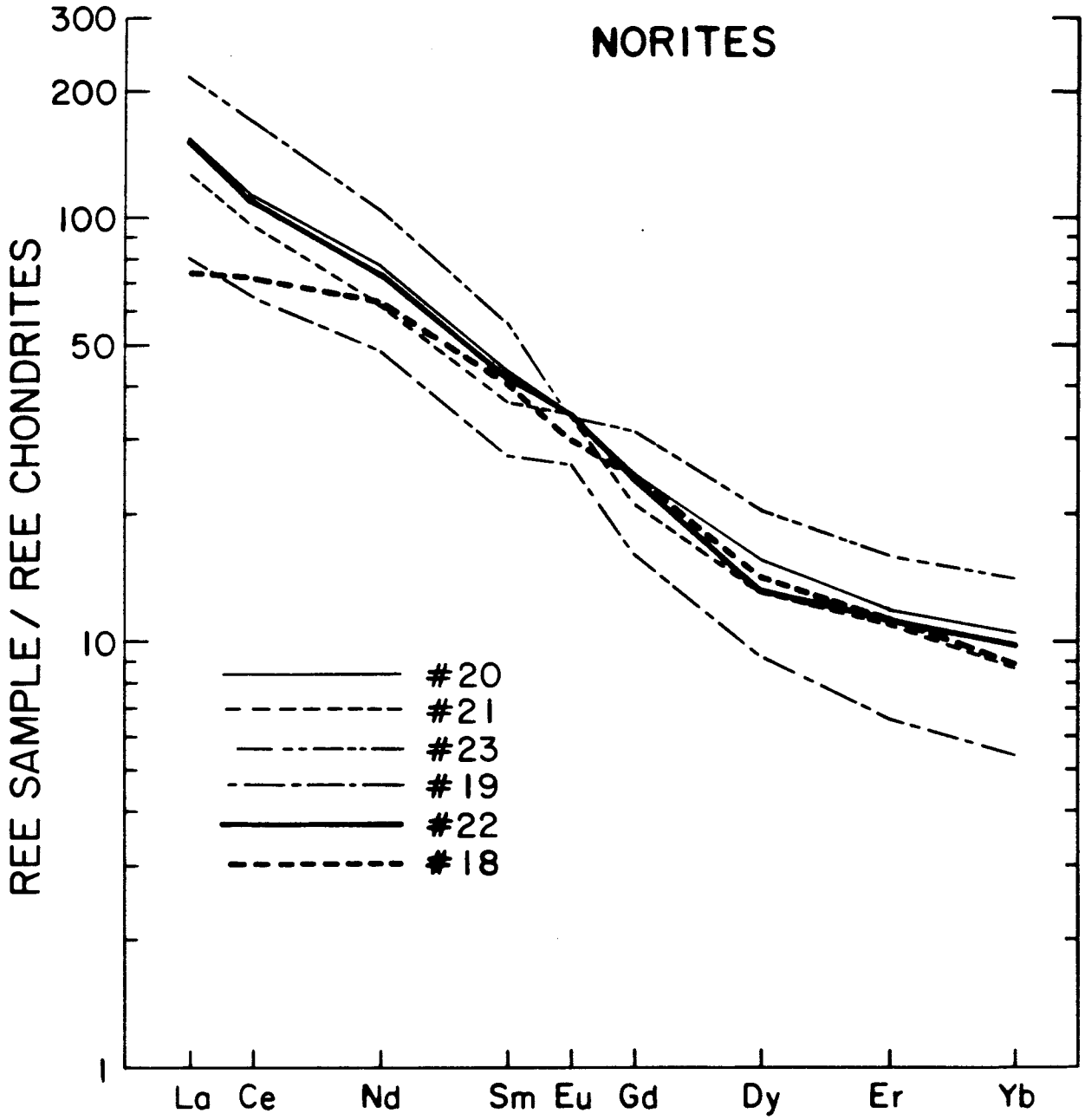

Fig. 43. Chondrite-normalized rare-earth patterns for norites of the Cortlandt complex.

subparallel REE patterns which are approximately linear from La to Er ($(La/Er)_N \approx 13$) and then flatten out between Er and Yb (Fig. 44). All three samples have slight positive Eu anomalies. REE abundances are unusually low for granitic rocks which generally have La and Yb concentrations that are 100x and 10x those of chondrites, respectively. Low REE abundances preclude the possibility that the granodiorites are related to the basic rocks of the Cortlandt region by any fractional crystallization process. The low P_2O_5 ($\sim$218 ppm), Zr ($\sim$95 ppm), and Nb ($\sim$ 1.4 ppm) concentrations and the low Rb/Sr ($\sim$0.169) ratios of these granodiorites also suggest that they cannot be partial melts of graywacke or any other crustal material. Their textures and chemistries indicate that they are not feldspar-quartz cumulates. The low abundance of high-field strength elements (REE, P, Cr, Nb, Zr, Ni, and Y) are consistent with an origin involving liquid immiscibility.

Mafic Dike Rocks

The REE patterns for two mafic dikes which cross cut the cortlandtite (43) and diorite (44) plutons at Stony Point (Fig. 3) are illustrated on Fig. 45. Like their major and trace element abundances (Tables 1, 3), the REE values of these two dike rocks are similar. The REE patterns are fractionated ($(La/Yb_n \approx 13$) and are

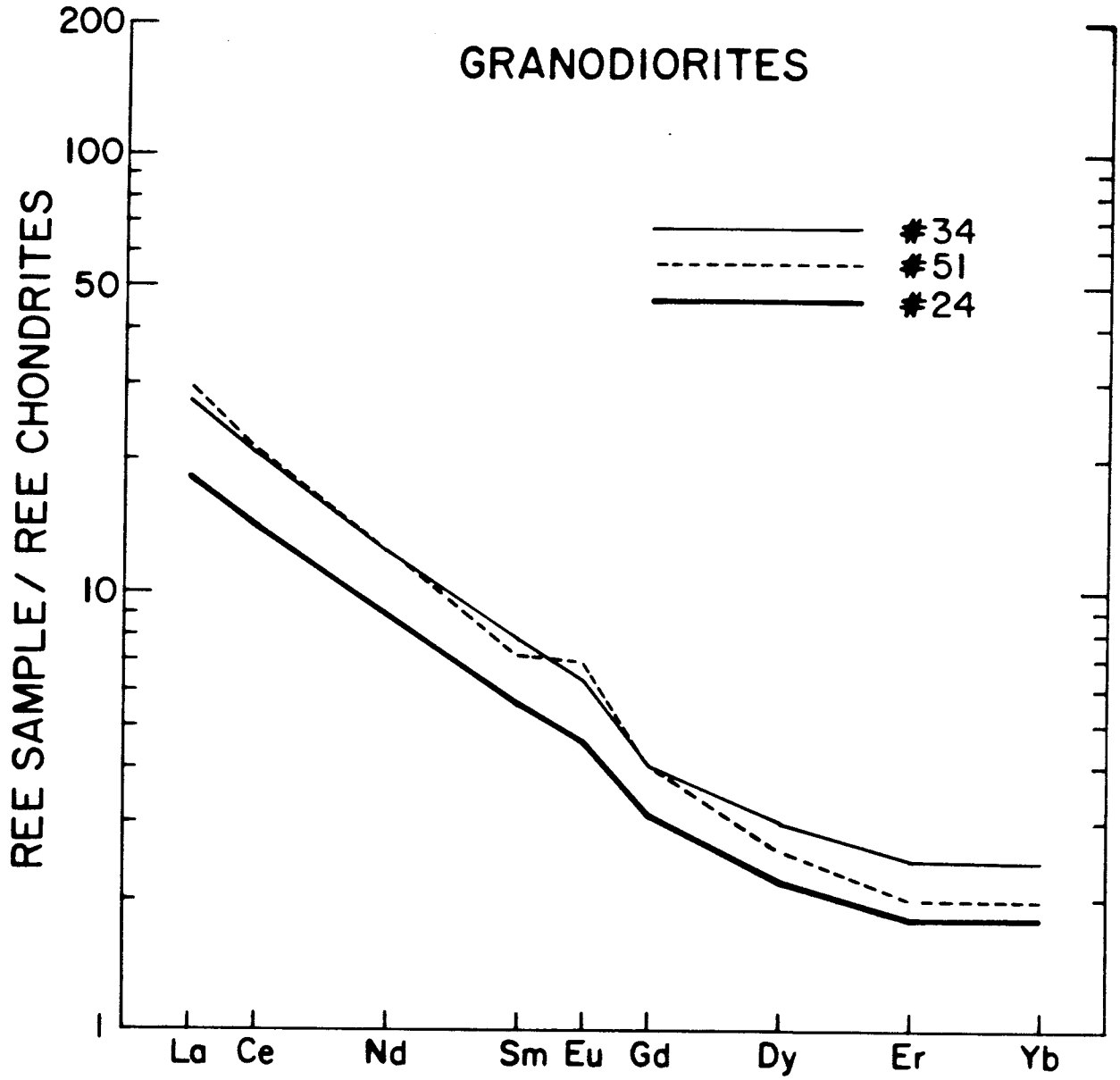

Fig. 44. Chondrite-normalized rare-earth patterns for granodiorites of the Peekskill pluton and the Cortlandt and Rosetown complexes.

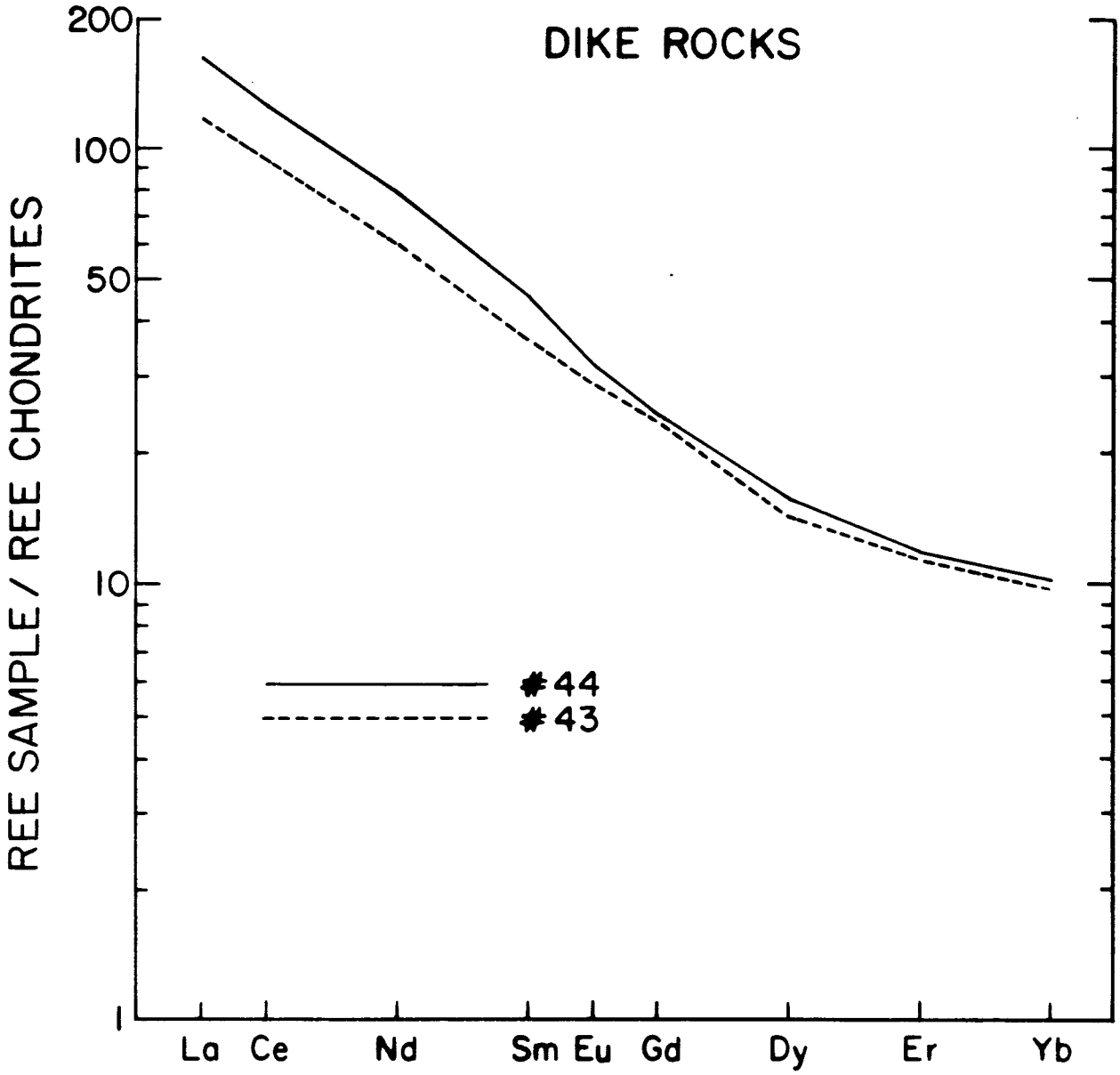

Fig. 45. Chondrite-normalized rare-earth patterns for two mafic (lamprophyric) dikes of the Stony Point complex.

nearly identical in the MREE and HREE. However, sample 44 has 30% greater abundances of the LREE. These mafic dike rocks have very similar major and trace element and phase chemistries to the amphibole-pyroxenites of Rosetown (48) and Stony Point (4), suggesting generation from the same source.

Salt Hill Emery, Related Felsic Dikes, and Country Rock Pelitic Schist

The REE patterns for emery (37), a siliceous dike (36) crosscutting the emery, and a sample of pelitic country rock (45) are illustrated on Fig. 46. The pelitic schist (45) has a fractionated REE pattern ($(La/Yb)_n \approx 7$), a negative Eu anomaly, and a flat HREE pattern that is very similar to that of North American composite shale (Haskin et al., 1968). This aluminous (19.4 wt.%) schist has high concentrations of Rb (177 ppm), Ba (1332 ppm), and K_2O (7.05 wt.%) (Tables 1, 3).

The Salt Hill emery (37) has a REE pattern (Fig. 46) parallel to that of the pelitic schist in LREE and MREE abundances. However, while the pelitic material has flat HREE at 18x chondritic, the HREE abundances of the emery are fractionated with Yb values almost a factor of four lower than those of the pelite. The fractionated REE pattern and high LREE abundances of the emery sample (37) cannot be a consequence of its formation through partial melting of the pelitic schist. If anatexis of the pelitic

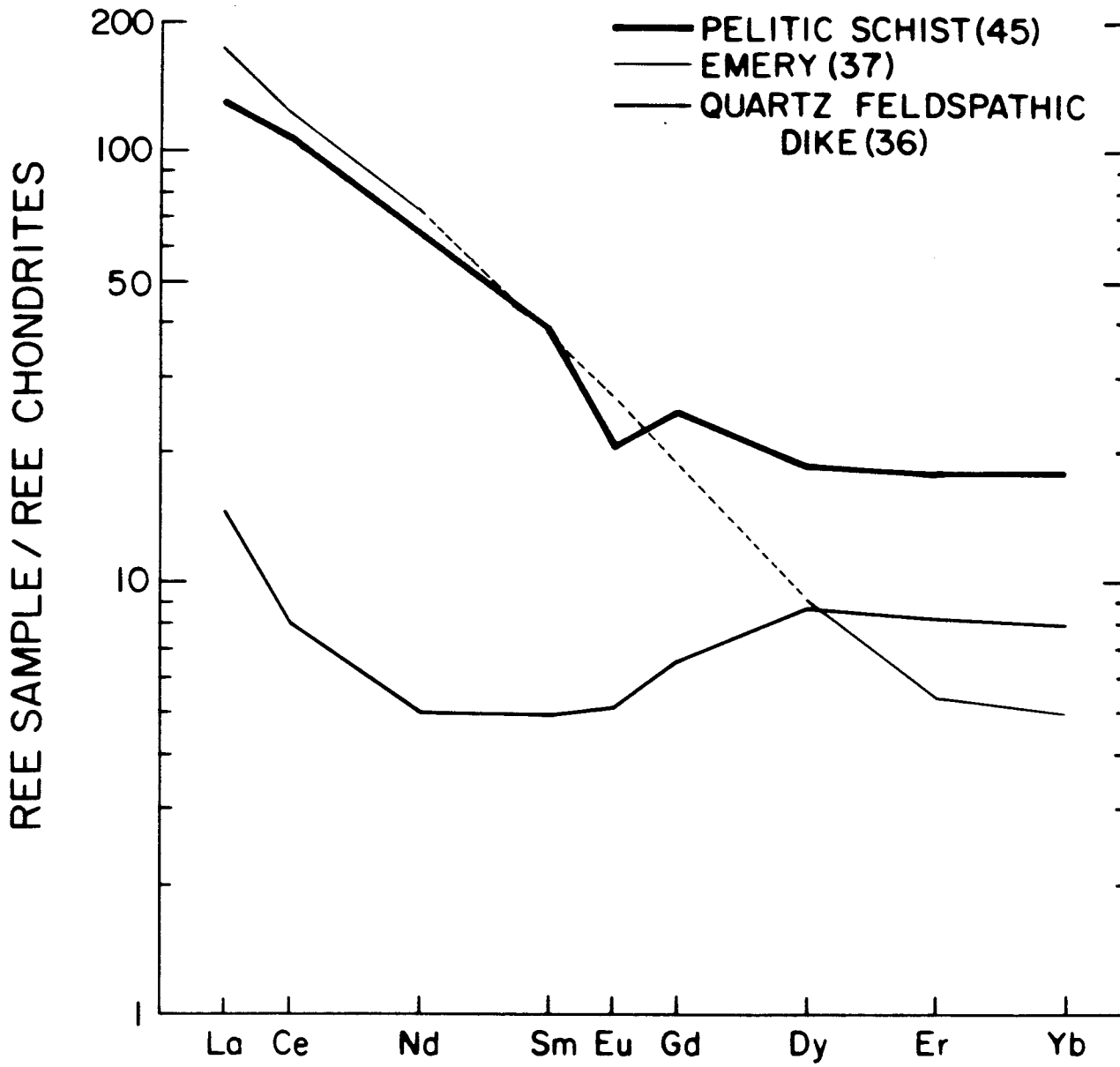

Fig. 46. Chondrite-normalized rare-earth patterns for the Salt Hill Emery, quartz-feldspathic dike and pelitic schist.

schist was responsible for producing the silica- and alkali-deficient emery, then the LREE and MREE abundances of the emery would be greatly depleted, not slightly enriched as they seem to be.

A quartz-feldspathic dike rock (36) found cutting the emery at the Salt Hill location (Fig. 2) has a REE pattern with a strongly concave upward shape in the LREE and MREE. The HREE are flat at 8x chondrites. It is believed that sample 36 may have crystallized from an aqueous fluid that originated from the former pelitic xenolith (emery sample 37).

DISCUSSION

The aim of this investigation is to assess the following factors and their role in the petrogenesis of the Cortlandt complex:

1. the source mineralogy and chemistry of the parental magma(s);
2. the role of mineral fractionation and crystal accumulation in the development of the observed rock types; and
3. the nature and extent of crustal contamination within each of the Cortlandt region plutons.

The petrographic, geochemical, and isotopic data presented indicate that the ultra-basic and basic rocks of the Cortlandt suite have strong alkalic affinities. However, the presence of modal orthopyroxene throughout the series, plus the occurrence of quartz in the more differentiated mafic samples, demonstrates the atypical nature of the Cortlandt region basic suite. Observed petrographic and chemical variations within rocks of the peridotite (clinopyroxenite and cortlandtite) plutons reveal that differentiation of a mildly alkalic liquid and subsequent accumulation of the liquidus minerals, olivine, clinopyroxene, and orthopyroxene, is responsible for their formation. Amphibole-pyroxenite, which occurs with cortlandtite in the same body, because of its geochemistry, is considered to be a possible parent composition

not only of the cortlandtite and clinopyroxenites but also of the gabbros, diorites, and norites. The implication and further assessment of amphibole-pyroxenites as a parental composition will be discussed in detail in another section. Crystal accumulation processes have also played an important role in the petrogenesis of rocks from the hornblendite-kaersutite gabbro and diorite plutons of the Cortlandt complex. These bodies (plutons 1 and 2) contain cumulate rocks predominantly composed of kaersutite and plagioclase indicating that these two minerals are very important in the fractional crystallization history of the diorite and gabbroic magmas. Within the norite pluton, petrographic and geochemical data show that plagioclase, orthopyroxene, and clinopyroxene, as well as lesser amounts of kaersutite and biotite, have been involved in the petrogenesis of this body. Mineralogical data such as the ubiquitous nature of kaersutite throughout the Cortlandt basic rock types, geochemical similarities of all the basic rocks, plus the proximity of the diverse rock types, suggest that the Cortlandt region plutons may be related to a common magma. Thus, the observed chemical variations in these plutons would represent different magma chambers (conduits) that have experienced various

degrees of differentiation.

The large variations in $^{87}Sr/^{86}Sr)_i$ ratios of the Cortlandt basic rocks would, at first glance, seem to preclude the hypothesis that the suite of samples is related to a common alkalic parent. However, any magma passing through the continental crust is susceptible to isotopic modification (contamination) as a result of interaction with crustal material on route to its level of emplacement. Possible interaction processes between magma and its surroundings upon ascent include: (1) assimilation; (2) wall-rock reaction, and (3) isotopic exchange. Any one or a combination of these methods could provide a means of changing not only $^{87}Sr/^{86}Sr$ ratios of a magma but also, to some extent, its major and trace element chemistry. Hence, it is believed that the varied and distinct $^{87}Sr/^{86}Sr)_i$ ratios of the Cortlandt samples from different plutons could reflect varying degrees of contamination rather than source heterogeneity. Thus, one parental composition may be responsible for the production of the Cortlandt suite.

Through quantitative trace element modelling of the Cortlandt region chemical data, the general hypothesis of a common parent magma, isotopically modified by crustal contamination will be evaluated. The ability of this type of modelling to test, interpret, and set

limits on various magmatic processes has proven successful in many other investigations (see Allegre and Minster, 1978, and Hanson, 1978, for reviews). However, an essential part of these modelling calculations is the selection of proper mineral-melt partition coefficients and correct identification of a parental composition. Discussion of crystal fractionation modelling techniques, procedures, and methods used to select both proper partition coefficients and a parental melt follow.

TRACE ELEMENT MODELLING EQUATION AND MINERAL-MELT PARTITION COEFFICIENT

Recent studies (Bryan et al., 1969; Wright and Doherty, 1970; Zielinski and Frey, 1970; Zielinski, 1975; Sun and Hanson, 1976; Arth et al., 1978) have been moderately successful in the quantitative modelling of fractional crystallization and its effects upon major and trace element chemistries of both volcanic and plutonic rock suites. These investigations have used trace element mineral-melt distribution coefficients (Kd's) with mineral and bulk compositional relationships to predict the trace element abundances in different rock types. Equations governing trace element behavior during fractional crystallization are based on the Rayleigh (1896) distillation process. This equation, describing trace-element behavior during fractional crystallization (Neuman et al., 1954; Greenland, 1970) may be expressed as: $C_L/C_0 = F^{(D-1)}$, where F is the fraction of melt remaining, C_0 is the concentration of a particular trace element in the original melt, C_L is the concentration of the same element in the residual liquid, and D is the bulk mineral-melt distribution coefficient for the crystalline phases removed from the melt. D can be expressed as

$$D = \sum_{\alpha}^{n} x_{\alpha} K_d^{\alpha/L},$$

where $K_d^{\alpha/L}$ is the mineral-melt elemental distribution coefficient for each fractionating phase and is defined as the weight fraction of a trace element in a particular phase divided by the weight fraction of the same element in the coexisting liquid. X_{α} represents the weight fraction of α in the precipitating phases. For any element, as D approaches zero, $C_L/C_0 \approx 1/F$, so that the concentration of that element is enriched inversely proportional to the fraction of melt remaining. When D is very large ($>> 1$), the melt will be rapidly depleted in that particular element.

An accurate knowledge of how an element distributes between a crystal and coexisting liquid is required for the quantitative application of the fractional crystallization equation to magmatic processes. Trace element distribution coefficients (K_d's) have been measured for a variety of minerals in different igneous rock types (Schnetzler and Philpotts, 1970; Philpotts and Schnetzler, 1970; Nagasawa and Schnetzler, 1971; Sun and Hanson, 1975). Distribution coefficients have been measured most precisely for the REE, Rb, Sr, and Ba which thus become most useful for trace element modelling.

In this study, the distribution coefficients used

in the trace element modelling calculations were selected and/or estimated from both natural and experimental systems of basaltic compositions and lie well within the range of published values. Where partitioning data was not available for certain elements such as Zr in amphibole, K_d's were estimated through construction of Onuma diagrams (Onuma et al., 1968; Jensen, 1973; Philpotts, 1978). These K_d's are given in Table 5 and those for the REE are illustrated on Fig. 47.

A brief discussion of the distribution of REE and other trace elements within individual minerals (Table 5 and Fig. 47) and the qualitative effect of these minerals upon a basaltic melt during differentiation follows.

Olivine: Olivine effectively excludes the REE and most other large radius, multi-charged elements. Therefore, crystallization of olivine from a basaltic melt will enrich the melt in the trace elements for which it has low K_d's. However, olivine has high affinities for the transition metals, especially nickel ($K_d \sim 8$)(Leeman, 1974), which results in its rapid depletion in the magma with olivine separation.

Table 5. Mineral-Melt Distribution Coefficient Data Used in Model Calculations.

	Clino-pyroxene [a]	Ortho-pyroxene [b]	Olivine [c]	Amphibole [d]	Plagio-clase [e]	Apatite [f]	Sphene [g]	Garnet [h]	Biotite [i]
La	0.07	0.01	0.007	0.44	0.20	14.1	30.0	0.18	0.34
Ce	0.20	0.015	0.007	0.72	0.15	16.6	53.3	0.35	0.32
Nd	0.38	0.03	0.007	1.16	0.12	21.0	88.3	0.53	0.29
Sm	0.54	0.04	0.007	1.56	0.09	20.7	102	2.66	0.26
Eu	0.50	0.04	0.007	1.28	0.50	14.5	101	1.50	0.24
Gd	0.62	0.07	0.007	1.84	0.09	21.7	102	10.5	0.28
Dy	0.59	0.11	0.008	1.71	0.06	16.9	80.6	28.6	0.29
Er	0.54	0.17	0.009	1.65	0.05	14.1	58.7	37.0	0.35
Yb	0.43	0.22	0.01	1.52	0.04	9.4	37.4	39.9	0.44
Rb	0.001	0.001	0.01	0.42	0.07				3.0
Sr	0.07	0.007	0.014	0.50	3.0				
Ba	0.001	0.001	0.001	1.4	0.23				12.0
Sc	3.4	1.1	0.25	3.6	---				
Ni	1.5	3.0	8.0	0.80	---				0.50
Co	0.40	1.2	2.4	0.50	---				0.60
Cr	6.0	1.2	0.20	1.5	---				1.2
Zr	0.22	0.11	---	0.44	---				
Nb	0.02	0.01	---	0.04	---				

[a] Cpx: REE melt Kd's modification of Sun and Hanson's (1976) cpx (#61) partition coefficients; Rb and Ba data from Shimizu (1974); Ba from Philpotts and Schnetzler (1970); transition metal data estimated from experimental studies (Lindstrom and Weill, 1974; Lindstrom, 1976; Lindstrom and Weill, 1978); Nb and Zr data from McCallum and Charette (1978).

[b] Opx: REE, Rb, Sr and Ba Kd's modified from data of Philpotts and Schnetzler (1970) and Schnetzler and Philpotts (1970); transition metal data estimated from experimental studies (Lindstrom, 1976; Mysen, 1978; Bird, 1971; McKay and Weill, 1977). Zr and Nb values are intuitive guesses.

[c] Oliv: REE, Rb, Sr, Ba melt Kd's average of two from Schnetzler and Philpotts (1970) and Philpotts and Schnetzler (1970) as reported in Arth and Hanson (1975). Transition metal data estimated from both experimental and natural system studies (Leeman, 1974; Dale and Henderson, 1972; Leeman and Scheidegger, 1977; Huebner et al., 1976); Nb and Zr arbitrarily set at 0.001.

[d] Amph: Mineral-melt Kd's for REE modified from kaersutite phenocryst of Sun and Hanson (1975) for sample #1167; Rb and Sr modified from data of Sun and Hanson (1976); and Philpotts and Schnetzler (1970); Ba, Zr, Nb and transition metal kaersutite-melt Kd's are estimated based on data from this study.

[e] Plag: REE, Rb, Sr and Ba Kd's compiled from various sources (Drake, 1972; Schnetzler and Philpotts, 1970; Philpotts and Schnetzler, 1970; Sun and Hanson, 1976; and Arth and Barker, 1976).

[f] Apatite: REE melt Kd's average of four from Nagasawa (1970) as reported in Arth and Hanson (1975); La determined by extrapolation.

[g] Sphene: REE Kd's from Simmons and Hedge (1978); La determined by extrapolation.

[h] Garnet: REE distribution coefficients from Schnetzler and Philpotts (1970); La determined by extrapolation; Er modified from 43 to 37 as part of this study.

[i] Biotite: Mineral-melt Kd's for REE from Higuschi and Nagasawa (1969); La by extrapolation; Rb, Sr, and Ba Kd's estimated from data of Schnetzler and Philpotts (1970) and Philpotts and Schnetzler (1970); transition metal Kd's are estimated based on data from this study.

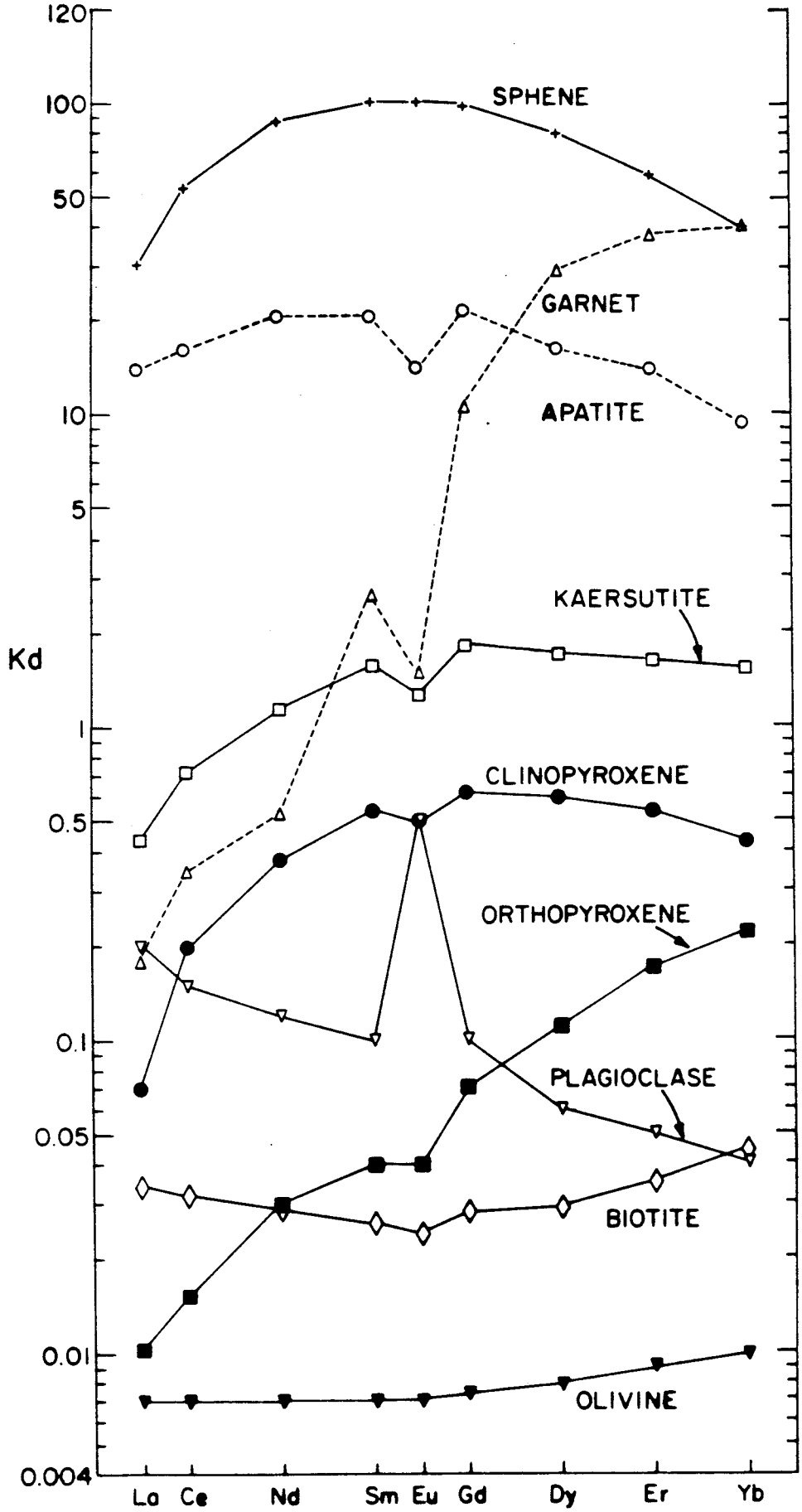

Fig. 47. Mineral-melt K_d's for the rare earth elements listed in Table 5.

Clinopyroxene: The K_d's for high-Ca clinopyroxene are greater for the MREE and HREE than they are for the LREE, resulting in a distinct concave down shape and negative Eu anomaly (Fig. 47). Although the REE partition coefficients for clinopyroxene are much greater than those for olivine, the K_d's are generally less than one for basic magmas. Separation of clinopyroxene from a melt will enrich all the REE in the residual magma; the LREE are more enriched than the MREE and HREE. Clinopyroxene, like olivine, has high K_d's for the transition metals with a particularly high distribution coefficient for Cr ($K_d \sim 6$) (Lindstrom, 1976). Clinopyroxene, like olivine, also discriminates against Rb, Sr, and Ba (Schnetzler and Philpotts, 1970; Philpotts and Schnetzler, 1970; Shimuzu, 1974).

Orthopyroxene: Orthopyroxene has a similar REE distribution pattern to that of clinopyroxene (Fig. 47), but has lower contents of rare earths relative to the same melt. Orthopyroxene, like clinopyroxene, also has very low partition coefficients for Rb, Sr, and Ba (Schnetzler and Philpotts, 1970; Philpotts and Schnetzler, 1970) and also has K_d's greater than unity for the transition metals (Dale and Henderson, 1972).

Kaersutite: This titaniferous calcic amphibole has a similar REE pattern of distribution coefficients to that of clinopyroxene, but with much higher absolute values

(Fig. 47). Kaersutite, like both pyroxenes, discriminates against Eu^{2+} and its REE K_d pattern has a slight negative Eu anomaly. Separation of large amounts of kaersutite will cause a relative depletion of the MREE and HREE and a pronounced enrichment of the LREE in the residual magma. The alkali-bearing A site of amphibole causes kaersutite-melt K_d's for Rb, Sr, and Ba to be higher than those for pyroxene (Schnetzler and Philpotts, 1970; Philpotts and Schnetzler, 1970; Sun and Hanson, 1976). However, the similarity of M sites in both amphibole and pyroxene causes transition metal K_d's to be similar (Table 5). However, while the REE K_d's between clinopyroxene and kaersutite are similar, the data of Sun and Hanson (1976) indicate that when these phases coexist, kaersutite will have the higher REE abundance.

Biotite: Biotite discriminates against all REE in a similar manner (K_d's < 1) and thus does not seriously affect the distribution of REE in the melt. Biotite does, however, have high affinities for transition metals as well as Rb and Ba (Schnetzler and Philpotts, 1970; Philpotts and Schnetzler, 1970; Leeman, 1976).

Plagioclase: Plagioclase has low K_d's for the trivalent REE, but feldspar has a large positive Eu anomaly because it preferentially accepts Eu^{2+} (Fig. 47). Plagioclase K_d's for the REE, other than Eu, are essentially

independent of composition and temperature (Drake and Weil, 1975). The Eu anomaly increases with decreasing temperature (Ab increases) and $\underline{f}O_2$, and is significant in almost all terrestrial igneous rocks (Drake, 1975). Plagioclase has high distribution coefficients for Sr and Ba but effectively excludes Rb from its structure due to its larger ionic size and lower +1 valance (Schnetzler and Philpotts, 1970; Philpotts and Schnetzler, 1970; Drake, 1972; Sun and Hanson, 1976).

Apatite and Sphene: Apatite has high mineral-melt K_d's for the REE (Nagasawa and Schnetzler, 1971) and a concave down distribution pattern (Fig. 47). Fractionation of apatite will deplete the melt more in the MREE than it will for the LREE and HREE. Because apatite is a phosphate mineral, phosphorous abundances in a rock can be significantly increased due to accumulation of this phase.

Sphene has a similar REE partition coefficient pattern to that of apatite (Simmons and Hedge, 1978), but with greater K_d values (Fig. 47). Crystallization of both sphene and apatite, even to the extent of a few tenths of a percent, can strongly influence the REE patterns of the residual magma.

Garnet: Garnet has very low K_d's for the LREE and increasingly larger K_d's for the HREE, with the overall difference in the LREE and HREE varying by two orders of magnitude (Schnetzler and Philpotts, 1970). The presence of garnet will, therefore, have a pronounced effect on the HREE abundance of the melt.

PARENTAL MAGMA

As was stated earlier, the geochemical characteristics of the Cortlandt region amphibole-pyroxenites approximate the composition of the parental magma from which the various Cortlandt plutons could be derived. Further evaluation of the major and trace element characteristics of three amphibole-pyroxenite samples (15, 40, 48) also revealed that the amphibole-pyroxenites are very similar in chemical composition to proposed mantle-derived, primary, alkali basalts. A primary magma is a melt which has undergone little or no crystal fractionation upon separation from its source region and, hence, is still in chemical equilibrium with its source. Recent investigators (Green, 1970; Green et al., 1974; Sun and Hanson, 1975; Frey et al., 1978) have suggested that primary alkali or tholeiitic basalts derived from upper mantle peridotite should have Mg numbers of 0.68-0.75 and Ni abundances of 300-500 ppm. In addition, values for compatible trace elements Sc (15-28 ppm) and Co (27-80 ppm) in a primary, mantle-derived, basaltic magma were estimated by Frey et al., 1978. Examination of the major and trace element chemistries of amphibole-pyroxenite sample 40 (Tables 1 and 3) reveals it to have many of the characteristics of a primary magma. For

example, the amphibole-pyroxenite sample 40 has an Mg number of 0.72 and compatible element values (Ni 196 ppm, Co 68 ppm, Sc 41 ppm) which indicate that this sample has not undergone extensive differentiation nor does it contain significant cumulate minerals. The absence of modal olivine precludes the high Ni, Co and Mg number and the result of olivine accumulation. The presence of chilled dike rocks at Stony Point (samples 43 and 44) with similar major, trace, and phase chemical compositions to this amphibole-pyroxenite sample (40) further supports the conclusion that the chemical composition of this plutonic rock is truly representative of a primary liquid. Sun and Hanson (1975, 1976) used their proposed primary composition to successfully model the fractional crystallization history of the more evolved alkali basaltic samples of Antarctica. Hence, amphibole-pyroxenite sample 40 which has many of the chemical characteristics of a primary magma is proposed to be a parental composition of the Cortlandt basic suite.

The REE data for the amphibole-pyroxenite (40) and for the primary alkali basalts from Ross Island, Antarctica (Sun and Hanson, 1975), Victoria, Australia (Frey et al., 1978) and a proposed alkali basalt parental composition from southwest Finland (Arth et al., 1978) have been

plotted on a chondrite normalized REE diagram (Fig. 48). Sample 40, the proposed parental composition, has a fractionated REE pattern similar to those of other primitive alkali basalts. Its REE are most similar to sample 69-1036, the postulated primary and parental magma of alkali basalts in Victoria, Australia (Frey et al., 1978). The major REE differences among these proposed parent liquids are in the overall abundances of the LREE and the MREE. These rare earth differences could reflect differences in source chemistry and/or degree of partial melting.

Kay and Gast (1973), Sun and Hanson (1975), and Frey et al., (1978) suggest that the fractionated REE patterns of alkali basalts are the result of partial melting of a mantle source in which garnet was a residual phase. They also suggest that source regions for alkali basalts must be enriched in the LREE relative to HREE (La/Yb = 7.5 and 5.3 for Sun and Hanson and Frey et al., respectively). Primary alkalic basalts can be produced from a chondritic (flat) REE source, but only by very small degrees of partial melting (< 2%). Separation of such a small amount of liquid from its source is considered to be difficult (Waff, 1980). However, if the mantle source is fractionated (La/Yb $\gtrsim$ 4), alkali basalts

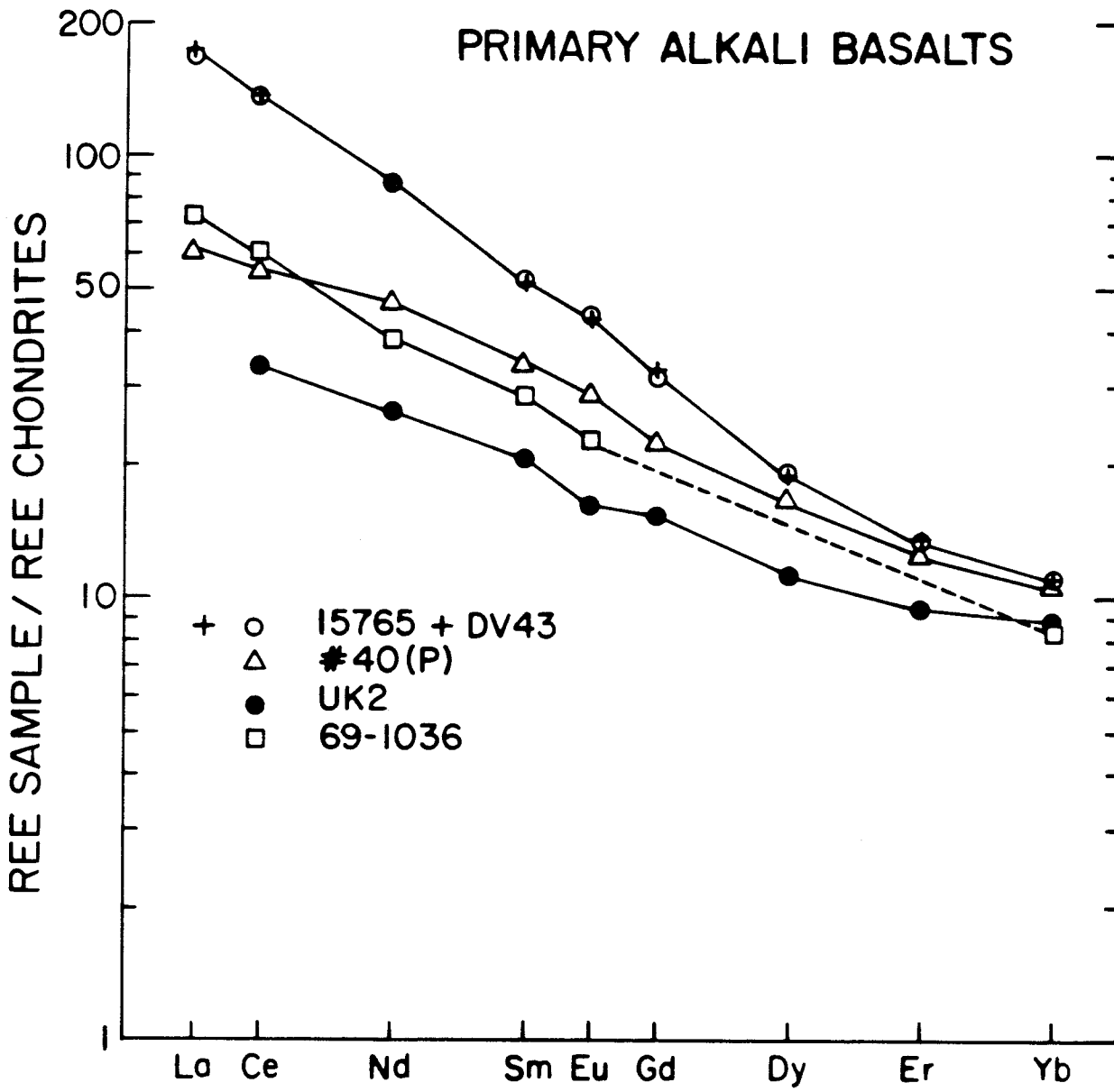

Fig. 48. Chondrite-normalized rare-earth patterns for proposed primary/parental alkali basalts.

can be produced by more reasonable degrees of partial melting ($\sim$ 7 to 15%) and, therefore, can be more easily separated from their residuum.

From its major (Mg number $\approx$ 0.72; TiO_2 $\approx$ 2.14 wt.%; K_2O $\approx$1.04 wt.%) and trace (Ni $\approx$ 196 ppm; Sc $\approx$ 41 ppm; Cr $\approx$ 292 ppm; Rb $\approx$ 16 ppm; Ba $\approx$ 35 ppm) element characteristics and from its low $^{87}Sr/^{86}Sr)_i$ (0.70428), it can be seen that the amphibole-pyroxenite sample (40) may be a primary magma and a possible parental magma. However, sample 40 has experienced slight modification of its chemistry due to crystal fractionation at the emplacement site. As was mentioned earlier, the olivine-pyroxene bearing cortlandtites associated with the amphibole-pyroxenite plutons are cumulus rocks formed by differentiation of the amphibole-pyroxenite composition. However, because olivine and pyroxene have low partition coefficients (K_d's) for the incompatible elements (Rb, Sr, Ba, REE, Zr, Nb), the ratios of these elements in the fractionated melt should be very similar to those of the original magma. It is necessary to closely examine sample 40 both petrographically and chemically for evidence of crystal accumulation since it is a plutonic igneous rock and not part of a chill margin. This examination indicates that the proposed

parental rock (40) contains ∿ 20% cumulate amphibole and clinopyroxene. The high scandium value (41 ppm) of sample 40, when compared to those of other proposed primary basalts (Sc ∿ 25 ppm) also support this crystal accumulation assumption because both clinopyroxene and kaersutite have high (∿ 3.5) K_d's for Sc. The adjustment of the major and trace element chemistries of the amphibole-pyroxenite sample 40 caused by the subtraction of clinopyroxene and amphibole in a 2:1 proportion is shown in Table 6. The subtraction of 20% cumulate minerals in a 2:1 (clinopyroxene: amphibole) ratio was determined on the basis of textural and major element chemistry to be a reasonable proportion for the removal of the cumulate phases. However, to illustrate that the exact ratio of removal of phases is not critical, 20% cumulate crystals in ratios of 1:0, 1:2, 1:1, and 0:1 were extracted to determine the effect on the major and trace element chemistry. Table 6 shows the narrow variation (∿ 10%) that results from removal of phases in various proportions.

The amphibole-pyroxenite composition, minus the 20% cumulate phases, will be referred to as 40P (parental) and will be used in the fractional crystallization models unless otherwise stated. The major and trace element

Table 6. Amphibole-Pyroxenite #40 Removal of 20% Cumulate Phases in Different Proportions.

	#40 W.R.	a	b	c	d	e
REE Normalized						
La	51.4	62.7	59.9	60.7	58.2	61.5
Ce	47.7	57.1	52.8	53.8	50.8	54.8
Nd	43.8	49.9	44.7	46.1	42.3	47.4
Sm	32.8	35.9	31.2	32.4	29.0	34.0
Eu	26.6	29.0	26.5	27.3	25.0	28.6
Gd	22.3	23.7	20.2	21.2	18.5	22.6
Dy	16.2	17.0	15.1	15.7	13.8	16.6
Er	12.2	13.0	11.4	11.9	10.6	12.6
Yb	9.97	10.8	9.60	10.0	8.90	10.6
ppm						
Rb	16.4	20.5	19.3	19.6	18.7	19.9
Sr	379	466	437	445	424	452
Ba	257	321	261	275	235	289
Ni	196	175	195	190	205	185
Co	68	77.7	76.8	76.9	76.0	77.2
Cr	292	95.7	188	158	261	133
Sc	41	24.0	23.3	23.5	23.0	23.6
P	1178	1472	1472	1472	1472	1472
Nb	16.2	20.2	20.1	20.2	20.1	20.2
Zr	108	128	124	125	122	128
Wt.%						
SiO_2	47.3	46.4	48.1	47.6	48.9	47.2
Al_2O_3	12.0	13.9	12.3	12.7	11.5	13.1
"FeO"	10.6	11.5	10.9	11.0	10.5	11.2
MgO	11.3	10.2	10.7	10.6	11.0	10.4
TiO_2	2.21	2.58	1.95	2.11	1.64	2.27
CaO	12.9	11.2	13.6	12.3	13.4	11.9
Na_2O	1.80	2.12	1.80	1.99	1.65	1.96
K_2O	1.07	1.34	1.18	1.22	1.11	1.26

a. Clinopyroxene only (1:0)
b. Clinopyroxene + amphibole (1:2)
c. Clinopyroxene + amphibole (1:1)
d. Amphibole only (0:1)
e. Clinopyroxene + amphibole (2:1)

abundances of 40P are listed in Table 7.

Table 8 compares the major and trace element abundances of amphibole-pyroxenite 40P to the proposed primary alkali basalt compositions of Sun and Hanson (1975) and Frey et al. (1978), as well as the parent composition of Arth et al. (1978). As can be seen from Table 8, most of the major element oxide concentrations proposed for the Cortlandt parental magma compare favorably with the chemical abundances of proposed, primary, alkali basalts from Antarctica, Australia, and Finland. Differences in some elements (TiO_2, CaO, Na_2O, K_2O, Rb, Sr) probably reflect chemical differences in the source regions of these melts and/or degrees of partial melting. The REE pattern of 40P is characterized by a slight concave down curvature in its LREE (Fig. 48). The parental composition (UK-7) for the gabbro-diorite-tonalite-trondhjemite suite of southwest Finland proposed by Arth et al. (1978) also has a slight downward curvature of its LREE (Fig. 48). The peculiar shaped REE pattern in 40P and of the Proterozoic age alkali basalts from Finland cannot be explained simply by crystal accumulation. Instead, it seems to be a characteristic feature imposed by either the source itself or by the partial melting of the source.

Table 7. Amphibole-Pyroxenite #40 Parental Composition.

	#40 Sample	#40 Parental[a]
REE Normalized		
La	51.4	61.5
Ce	47.7	54.8
Nd	43.8	47.4
Sm	32.8	34.0
Eu	26.6	28.6
Gd	22.3	22.6
Dy	16.2	16.6
Er	12.2	12.6
Yb	10.0	10.6
ppm		
Rb	16.4	19.9
Sr	379	452
Ba	257	289
Ni	196	185
Co	68	77.2
Cr	292	133
Sc	41	23.6
P	1178	1472
Nb	16.2	20.2
Zr	108	128
Wt.%		
SiO_2	47.3	47.2
Al_2O_3	12.0	13.1
"FeO"	10.6	11.2
MgO	11.3	10.4
TiO_2	2.21	2.27
CaO	12.9	11.9
Na_2O	1.80	1.96
K_2O	1.07	1.26

[a] *Removed 20% clinopyroxene and amphibole in a 2:1 ratio from Sample #40 whole rock composition.*

Table 8. Proposed Primary Continental Alkali Basalt Compositions.

	#40 Parental[a]	15765[b]	DV43[c]	69-1036[d]	UK-2[e]
SiO_2	47.2	43.7	45.0	48.0	48.9
Al_2O_3	13.1	11.9	13.3	13.9	13.9
"FeO"	11.2	10.7	11.1	10.9	9.40
MgO	10.4	12.9	9.50	11.4	10.9
TiO_2	2.27	3.64	3.07	2.14	1.41
CaO	11.9	10.9	12.5	8.35	10.0
Na_2O	1.96	3.52	2.61	3.23	2.02
K_2O	1.26	1.28	1.03	1.18	0.74
Mg#	0.72	0.74	0.71	0.69	0.70
Rb	19.9	42	30	24	22.6
Sr	452	880	1000	543	297
Ba	289	395	408	350	131
Ni	185	290	300	364	177
Rb/Sr	0.044	0.048	0.030	0.044	0.076
Ba/Sr	0.690	0.449	0.408	0.645	0.441

[a] *This study.*

[b] *Ross Island Antarctica (Sun and Hanson, 1975).*

[c] *Ross Island Antarctica (Sun and Hanson, 1975).*

[d] *Mt. Frazer-West Victoria, Australia (Frey et al., 1978).*

[e] *S. W. Finland (Arth et al., 1978).*

MAJOR AND TRACE ELEMENT MODELLING TECHNIQUES

For the quantitative modelling part of this investigation, the mineral-melt K_d's and trace element fractionation equation were combined with the proposed parental liquid (40P) to test if the spectrum of compositions of the Cortlandt suite could be related by a liquid line of descent from a common parent composition. The mathematical modelling process used not only the trace element data, but also the major element, phase chemical, field, and petrographic data to fully assess the possible parent-daughter relationships. Major elements were modelled using similar procedures incorporated into computerized petrologic mixing programs (Wright and Doherty, 1970; Zielinski and Frey, 1970; Zielinski, 1975). All modelling calculations were performed with the aid of a hand calculator and not only made use of the actual phase chemistry of a sample (Appendixes 2-9) but also carefully evaluated the petrography of the sample to determine the validity of a solution.

PETROGENESIS OF THE CORTLANDTITE AND AMPHIBOLE-PYROXENITE SUITE

Since it is proposed that the amphibole-pyroxenite composition is the possible parental composition of the Cortlandt basic suite, samples of the cortlandtite-amphibole-pyroxenite suite are quantitatively modelled first. As was discussed earlier, major and trace elements, phase chemistry, and Sr isotopes suggest that samples of the cortlandtite and amphibole-pyroxenite suites from the Cortlandt (pluton 4), Stony Point, and Rosetown complexes appear to be related to a common parent magma (similar to 40P) by fractionation involving clinopyroxene, orthopyroxene, olivine, and/or kaersutite. Cortlandtite samples 14 and 41 appear to be cumulates of olivine and pyroxene while the two amphibole-pyroxenites (15, 48) appear to be differentiates of the original alkalic parental magma. The determined relationship of these four samples to the parental composition 40P follows.

Sample 14 from the Cortlandt complex consists of approximately 50% clinopyroxene, 12% orthopyroxene, 23% olivine, and 15% kaersutitic amphibole (Appendix 1). The pyroxene and olivine show cumulate textural relationships (Figs. 19 and 20) while the amphibole is interstitial with a vein-like appearance. The kaersutite

and its peculiar texture represent a portion of the parent magma which eventually solidified as intercumulus material. The REE pattern is characterized by a negative Eu anomaly and by pronounced depletion of the LREE (Fig. 39). This REE pattern and the high compatible element (Cr 767 ppm; Sc 44 ppm; Ni 643 ppm) abundances are consistent with clinopyroxene accumulation. Quantitative modelling of the major and trace element data (Table 9) show that cortlandtite sample 14 can be related to the proposed parental composition by accumulation of approximately 50% clinopyroxene, 16% orthopyroxene, 25% olivine, and 15% trapped (intercumulus) parental liquid.

The mathematical modelling contained in Table 9 was performed in two steps. In the initial step, clinopyroxene, orthopyroxene, and olivine were crystallized from the amphibole-pyroxenite 40P, and then these minerals were accumulated in the proportions 0.59 (clinopyroxene), 0.16 (orthopyroxene), 0.25 (olivine). These proportions are very similar to the modal proportions of cortlandtite sample 14. The major element compositions of this calculated cumulate rock were determined from the phase chemistry of the natural sample (Appendix 5). Partition coefficients and the proportion of each

Table 9. Sample #14 Quantitative Modelling.

	#40 Parental	a	b	#14 Sample
REE Normalized				
La	61.5	2.75	11.6	12.1
Ce	54.8	6.69	13.9	14.0
Nd	47.4	10.9	16.4	17.0
Sm	34.0	11.1	14.5	15.0
Eu	28.6	8.67	11.7	11.9
Gd	22.6	8.56	10.7	10.5
Dy	16.6	6.10	7.68	7.41
Er	12.6	4.38	5.61	5.39
Yb	10.6	3.07	4.19	4.23
ppm				
Rb	19.9	0.06	3.04	3.06
Sr	452	20.8	85.5	89.0
Ba	289	0.0	43.4	43.3
Ni	185	623	557	643
Co	77.2	79.4	79	119
Cr	133	503	448	767
Sc	23.6	53	48.6	44
P	1472	0.0	221	87
Nb	20.2	0.27	3.3	2.4
Zr	128	18.9	35.3	32
Wt.%				
SiO_2	47.2	48.8	48.6	47.2
Al_2O_3	13.1	2.76	4.31	4.13
"FeO"	11.2	10.6	10.7	11.1
MgO	10.4	23.8	21.8	22.2
TiO_2	2.27	0.38	0.66	0.66
CaO	11.9	13.2	13.0	13.7
Na_2O	1.96	0.14	0.41	0.49
K_2O	1.26	0.00	0.19	0.13

[a] *Cumulate (0.59 cpx; 0.16 opx; 0.25 oliv) crystallized from #40 parental composition.*

[b] *Cumulate plus 15% liquid (#40 parental composition).*

phase in the cumulate pile determined the trace element abundances within the calculated rock.

In the second step of the modelling, 15% of the parental liquid was added to the cumulate mineralogy in order to obtain a closer chemical match between the calculated cumulate and the natural sample (14). This step assumes that the volume of melt greatly exceeds the amount of crystalline (cumulus material) and, hence, that the melt has not appreciably changed in chemical composition. The resulting major and trace element chemistry was obtained by mass balance. Because the amount of interstitial liquid is small ($\sim$15%), the phase chemistry and modal proportions of the three cumulate phases (clinopyroxene, orthopyroxene, and olivine) determine the major element chemistry. However, even this small amount of trapped parental liquid causes a significant increase in Al_2O_3, Na_2O, K_2O, and TiO_2. There is a close fit between the calculated and natural rock compositions after the addition of the parental liquid (Table 9). Entrapment of approximately 15% of the parental liquid also causes the incompatible elements Rb, Sr, Ba, P, Zr, Nb, and LREE to be increased to abundances nearly identical to those of sample 14 (Table 9). The very low abundances of the incompatible elements restrict the amount of intercumulus liquid present in cortlandtite sample 14.

A substantial proportion of this intercumulus liquid crystallized as amphibole, explaining the interstitial vein-like texture of this phase in this cortlandtite sample (Figs. 19 and 20).

The successful duplication of the major and trace element abundances of sample 14 by the quantitative modelling scheme would indicate that reasonable approximations have been made for both the mineral-melt distribution coefficients (K_d's) and chemical compositions of the parental magma. However, it should be noted that these values are not independent; rather, they are inversely proportionate. Hence, if the estimates of the trace element abundances of the parental composition (40P) exceed the original amount by 30%, then, in order to successfully duplicate the calculated modelling, the K_d's of each mineral would have to be lowered appropriately. Because of the great care taken in selecting a parental composition and mineral-melt distribution coefficients, the modelling values are believed to be within 10-20% of the actual values. Calculations (not displayed here) with independently varied K_d's, parental composition, cumulate mineralogy, and intercumulus liquid indicate that the estimated error for the quantitative modelling for the REE, Rb, Sr, Ba, Zr, Nb, P and major elements is approximately 15%. With this assigned error, the

amount of trapped liquid within sample 14 can vary between 13-17%. However, the assigned error for Ni, Co, and Cr is considerably larger because of variable oxidation states and the presence of iron oxides and iron sulfides, the K_d's of which are not precisely known.

Cortlandtite from the Stony Point complex (sample 41) contains minerals that are chemically very similar to those of cortlandtite sample 14 from the Cortlandt complex (Appendix 5). From the REE pattern (Fig. 39) of sample 41, which lacks a downward concavity of the LREE and from its higher incompatible element abundances (Table 3), it is apparent that the Stony Point cortlandtite (41) contains significantly more trapped parental liquid (less cumulus minerals) than sample 14, assuming a relationship to the same parental magma at similar stages of differentiation. Incompatible element abundances of sample 41 imply that 40% parental liquid has been trapped within the mafic cumulate (Table 10). Entrapment of 40% parental magma to a cumulate pile consisting of olivine ($\sim$ 80%), clinopyroxene ($\sim$ 5%), and orthopyroxene ($\sim$ 15%) will closely match the major element chemistry of sample 41 (Table 10). Abundances of Rb, Sr, Nb, Ba, and Zr within this cortlandtite are also matched closely

Table 10. Sample #41 Quantitative Modelling.

	#40 Parental	a	b	#41 Sample
REE Normalized				
La	61.5	0.34	24.8	45.2
Ce	54.8	0.98	22.5	35.0
Nd	47.4	1.38	19.8	23.8
Sm	34.0	1.31	14.4	14.8
Eu	28.6	1.05	12.1	11.0
Gd	22.6	1.08	9.69	10.4
Dy	16.6	0.87	7.16	6.50
Er	12.6	0.74	5.48	4.81
Yb	10.6	0.65	4.63	4.06
ppm				
Rb	19.9	0.18	8.07	8.40
Sr	452	7.12	185	201
Ba	289	0.0	116	136
Ni	185	1281	843	1163
Co	77.2	164	129	161
Cr	133	85	104	198
Sc	23.6	12.6	17.0	15.0
P	1472	0.00	589	873
Nb	20.2	0.05	8.1	10.0
Zr	128	3.52	53.3	67
Wt.%				
SiO_2	47.2	41.2	43.7	39.2
Al_2O_3	13.1	0.38	5.47	4.95
"FeO"	11.2	20.0	16.5	15.6
MgO	10.4	36.9	26.3	25.9
TiO_2	2.27	0.02	0.92	0.83
CaO	11.9	1.10	5.42	4.47
Na_2O	1.96	0.06	0.82	0.62
K_2O	1.26	0.00	0.50	0.48

[a] *Cumulate (0.80 olivine; 0.15 cpx; 0.05 opx) crystallized from #40 parental composition.*

[b] *Cumulate plus 40% liquid (#40 parental composition).*

by this model using the amphibole-pyroxenite parental composition (40P). However, reproduction of the REE abundances of this sample is not possible with this calculation scheme. The REE pattern of sample 41 cannot be reproduced from any liquid having REE abundances comparable to those of 40P. Resultant LREE abundances of the calculated model (Table 10) are low, while the HREE abundances are high. In order to match the LREE observed in sample 41, more intercumulus liquid and/or more clinopyroxene must be added to the cumulate pile. However, these manipulations cause the HREE abundances to increase to unreasonably high values. Hence, it would seem that the REE abundances of sample 41 are compatible with a parental liquid that is more fractionated ($La_N \approx 90$; $Yb_N \approx 8$) in REE than the proposed parental composition 40P. This second liquid is still a primitive composition as evidenced by the similarity of olivine composition (Fo_{77}) in samples 14 and 41. This implies that at least two different magmas exist within the Stony Point cortlandtite pluton. The major and trace element chemistries of these melts are similar with the exception of the REE.

The low Rb and K_2O values of sample 41 indicate that interaction with the pelitic country rock cannot be responsible for the LREE enrichment of the parental liquid

or cortlandtite sample 41. The location of sample 41, near the margin of the Stony Point cortlandtite pluton and its field relationships (Ratcliffe, 1968) indicate that this region of the body may represent a distinct intrusion. REE abundances of two dikes (43, 44) at Stony Point are very similar to those needed to produce the REE values of the Stony Point cortlandtite, 41.

Amphibole-pyroxenite (sample 15) from the Cortlandt complex is unusual in that it contains $\sim$ 3 modal percent calcite and has low silica ($\sim$ 40 wt.%) and high CaO (16.6 wt.%) abundances. Its REE pattern (Fig. 39) is fractionated and lacks any concave down curvature in its LREE, indicating that accumulation of ferromagnesian minerals in this sample is minimal. The major and trace element modelling (Table 11) reveals that 15 can be obtained from 40P through crystal fractionation (30%) involving amphibole (60%), clinopyroxene (30%), and biotite (10%). One explanation for the low HREE, low SiO_2, and high CaO values of this amphibole-pyroxenite is the addition of approximately 15% calcareous material to the fractionated parental liquid. The REE abundances for carbonates (Haskin et al., 1966) are such (approximately an order of magnitude lower) that addition of this amount of material will deplete all the REE and especially the HREE (Table 11). Quantitative modelling calculations

Table 11. Sample #15 Quantitative Modelling.

	a	b	c	#15 Sample
REE Normalized				
La	78.4	10.0	68.1	68.1
Ce	64.9	6.80	56.2	58.3
Nd	50.2	4.90	43.4	45.1
Sm	32.8	3.40	28.4	30.1
Eu	29.2	1.90	25.1	23.4
Gd	20.2	3.05	17.6	19.5
Dy	15.3		13.4	13.3
Er	11.8	1.85	10.3	10.3
Yb	10.2	1.50	8.9	8.73
Wt.%		*		
SiO_2	48.6	0.31	41.4	40.0
Al_2O_3	14.3	0.07	12.2	15.0
"FeO"	12.5	0.08	10.6	10.3
MgO	8.60	21.5	10.6	11.2
TiO_2	2.50	0.01	2.13	2.57
CaO	11.8	30.5	14.6	16.6
Na_2O	2.23	0.08	1.91	2.16
K_2O	1.11	0.03	0.95	1.96

[a] *30% fractional crystallization (0.60 amph; 0.30 cpx; 0.10 biotite) of #40 parental composition.*

[b] *Dolomite (REE--Haskin et al., 19[illegible]).*

[c] *Addition of 15% dolomite (b) to a.*

* *Major elements for dolomite; U. S. National Bureau of Standards sample 88, Illinois State Geological Survey Circular 308, 196 P-38.*

contained in Table 11 show that, if carbonate is to be added, the additional carbonate material must be dolomitic ($\sim$ 31 wt.% CaO: $\sim$ 24 wt.% MgO) in order to explain the high MgO (11.2 wt.%) content of sample 15. The high K_2O abundances ($\sim$ 2 wt.%) of this rock may be a consequence of the addition of cumulate biotite ($\sim$ 10%), a phase that is present in this sample. The similarity of amphibole-pyroxenite sample 15 to the calculated model strongly suggests that a carbonate bulk assimilation scheme is a viable explanation for its unusual chemistry. Calcite, not dolomite, is the composition of the carbonate phase in sample 15 suggesting that it may be of igneous origin. The location of sample 15, close to the dolomitic Inwood marble contact (Paige, 1956) (Fig. 2), further supports this assimilation idea.

While the local dolomitic marble was not analyzed for strontium isotopes, it is probable that it, like most marine carbonates of Paleozoic age, had an $^{87}Sr/^{86}Sr$ ratio of approximately 0.708 (Peterman, 1967). Assimilation (15%) of this carbonate material by 40P $(^{87}Sr/^{86}Sr)_i \approx 0.70428$) will cause an increase in the strontium 87/86 ratio. Table 4 shows that amphibole-pyroxenite sample 15 has a much higher initial strontium

value (0.7062) than either the cortlandtite #14 (0.7049) or amphibole-pyroxenite #48 (0.7048) samples. These differences, which are very much greater than the precision of the measurement, support, but do not confirm a carbonate assimilation model for sample 15.

As shown by Bowen (1928), assimilation, because of the heat balance problem, promotes the crystallization of the cumulus mineral phases already precipitating, thus hastening the fractional crystallization process along the same liquid line of descent. While assimilation may enhance the proportion of late differentiates, changes in the liquid composition may not be seriously affected. However, carbonate assimilation by a basic liquid can result in desilication of the melt and crystallization of diopsidic augite (Bowen, 1928). The high alumina (9-11 wt.%) contents of the clinopyroxenes of sample 15 (Appendix 5) could be the result of their crystallization from a melt which assimilated calcareous material. The lack of sufficient silica in the melt could have caused the crystallizing clinopyroxene to incorporate an unusually high amount of alumina in its structure. The consequence of this can be seen in Appendix 5 where the structural formulae of the clinopyroxenes of sample 15 show greater amounts of tetrahedral alumina than do clinopyroxenes of other amphibole-pyroxenite samples.

The amphibole-pyroxenite sample 48 from the Rosetown complex has major and trace element abundances

(Tables 1 and 3) very similar to those of sample 40. The phase chemistries of amphibole and clinopyroxene in samples 48 and 40 are also remarkably similar (Appendix 5). Also, like sample 40, the major and trace elements of sample 48 are consistent with accumulation of approximately 20% clinopyroxene and amphibole in a 2:1 proportion. The overall higher REE abundances ($\sim$20%) of the Rosetown amphibole-pyroxenite 48 (Fig. 32) compared to those of the Stony Point amphibole-pyroxenite 40 are too great to be explained entirely by fractionation. Instead, it would seem that the parent composition of sample 48, while having similar major and trace element chemistry to that of sample 40, had an approximately 20% higher REE content than the parental compositions of sample 40. If there has not been contamination, the difference in $^{87}Sr/^{86}Sr)_i$ (#40-0.70428; #48-0.70479) between these two primary compositions would suggest origin from isotopically distinct source regions.

In summary, it appears that the cortlandtites and the amphibole-pyroxenites of the Cortlandt, Stony Point and Rosetown complexes are related to a primitive alkali basalt magma by crystal accumulation (cortlandtites) and fractional crystallization (amphibole-pyroxenites).

Petrographic and chemical data reveal that olivine, clinopyroxene, and orthopyroxene were the near-liquidus phases of this primary magma when it was intruded at the various emplacement sites. Subsequent differentiation of this parental liquid resulted in the termination of olivine and orthopyroxene precipitation and the onset of amphibole (kaersutite), clinopyroxene, and plagioclase co-crystallization. The co-crystallization of amphibole and clinopyroxene in the amphibole-pyroxenite indicates an increase in the water fugacity of the melt after the cessation of olivine precipitation. This conclusion is based on experimental studies (Green, 1972; Helz, 1973; Allen et al., 1975; Cawthorn and O'Hara, 1976; Stewart et al., 1976) which have shown that in hydrous basaltic melts, amphibole and clinopyroxene can only exist as near-liquidus phases (at pressures between 2 and 20 kb) when $P_{H_2O} > 0.5\ P_T$.

Crustal contamination of the alkali basalt parent of the Cortlandt region cortlandtites and amphibole-pyroxenites seems to have been minimal with the exception of one area in the Cortlandt complex near the carbonate contact. The apparent REE and slight isotopic differences of this mafic parental magma at the Stony Point and Rosetown emplacement sites could be attributable to source heterogeneity and/or crustal contamination.

PETROGENESIS OF THE CLINOPYROXENITE SUITE

Physically separate (as mapped by Ratcliffe, unpublished data) clinopyroxenite bodies occur on both the western and eastern margins of the noritic pluton of the Cortlandt complex (Fig. 2). A representative sample from each of these pyroxenites was analyzed for both major and trace elements (Tables 1 and 3). Sample 11 from the western pluton and sample 31 from the eastern have similar modal mineralogies (Appendix 1) and nearly identical phase chemistries (Appendix 4) suggesting similar modes of origin. Textures suggest that these pyroxenites are cumulates. In addition, they are characterized by a strong downward concavity in their LREE (Fig. 40) and very low incompatible element (Rb, Sr, Ba, Zr, P) abundances. However, while the REE patterns and incompatible element abundances of pyroxenite samples 11 and 31 are similar to those of Cortlandtite sample 14, the ferromagnesian phases show substantially higher iron enrichment (Appendix 4). As a result,in order to successfully model these two clinopyroxenites, the starting parental composition (40P) had to be differentiated by fractional crystallization (20%) (Table 12). The separating minerals, clinopyroxene, orthopyroxene, olivine, and amphibole form the cumulate pile. Modelling

Table 12. Sample #11 Quantitative Modelling.

	a	b	c	#11 Sample
REE Normalized				
La	74.9	5.30	17.8	19.1
Ce	65.4	11.2	21.0	22.8
Nd	55.0	17.3	24.1	26.5
Sm	38.6	17.0	20.9	22.8
Eu	32.4	13.0	16.5	15.6
Gd	25.3	13.0	15.2	16.0
Dy	18.6	9.18	10.9	11.4
Er	14.2	6.64	8.00	8.40
Yb	12.1	4.80	6.11	6.80
ppm				
Rb	24.4	0.56	4.8	4.8
Sr	550	40.8	132	69.3
Ba	351	24.6	83	59.4
Ni	128	326	291	358
Co	79.4	63	65.9	97.6
Cr	71.4	304	262	651
Sc	17.3	45.5	42.9	53
P	1840	0.0	331	232
Nb	24.8	0.42	4.8	<1.8
Zr	153	28.3	50.7	51.2
Wt.%				
SiO_2	46.6	49.0	48.6	49.5
Al_2O_3	15.3	4.05	6.08	4.68
"FeO"	11.4	10.4	10.6	10.8
MgO	7.82	19.8	17.6	18.7
TiO_2	2.66	0.73	1.08	0.76
CaO	11.4	14.8	14.2	14.1
Na_2O	2.35	0.33	0.69	0.18
K_2O	1.44	0.07	0.32	0.16

[a] *20% fractional crystallization (10% 0.60 cpx; 0.20 opx; 0.20 olivine; then 10% 0.60 cpx; 0.20 opx; 0.10 olivine; 0.10 amph.) of #40 parental composition.*

[b] *Cumulate (0.66 cpx; 0.16 opx; 0.13 olivine; 0.05 amph) crystallized from #40 parental composition.*

[c] *Cumulate plus 18% liquid (a).*

calculations (Table 12) show that clinopyroxenite sample 11 can be derived from 40P by fractional crystallization of olivine, pyroxene, and amphibole from the melt, and then accumulation of clinopyroxene (54%), orthopyroxene (13%), olivine (11%), kaersutitic amphibole (4%), while retaining 18% interstitial liquid. This trapped liquid has the chemical composition of the liquid with which the cumulate minerals were last in equilibrium. Elements such as Rb, Sr, Nb, Zr, P, and Ba, which are essentially excluded from the cumulate minerals in sample 11, constrain the amount of calculated trapped intercumulus liquid. The vein-like appearance of kaersutite in clinopyroxenite sample 11 suggests that, like the Cortlandtite sample 14, substantial kaersutite crystallized from the interstitial liquid. However, unlike sample 14, sample 11 contains a small amount ($\sim$ 5%) of kaersutitic amphibole as a cumulate phase. The overall higher REE abundances ($\sim$ 55%) of clinopyroxenite, when compared to those of cortlandtite sample 14, are the results of the crystallization of sample 11 from a more differentiated liquid containing both cumulate amphibole and less cumulus olivine.

This modelling scheme (Table 12) reveals a close fit for most elements with the exception of Sr and Ba. These elements are higher in the modelled rock than

those of the natural sample by a factor of almost 2. This discrepancy indicates that the abundances of these two elements in the parental composition must be considerably lower than those of the proposed parent (differentiated 40P) or that amphibole cannot be a cumulus phase. Because kaersutite is a cumulate mineral and also is needed to explain the overall REE abundances of sample 11, the parental liquid of this clinopyroxenite, while having major and trace element values similar to those of the proposed parental composition, 40P, apparently had lower strontium ($\sim$ 200 ppm) and Ba ($\sim$ 250 ppm) contents. The lower Cr and Co abundances of the calculated model of sample 11 probably reflect the presence of Fe oxides and Fe sulfides in the natural sample. These phases are ignored in this particular modelling calculation.

The similarity of $^{87}Sr/^{86}Sr)_i$ of sample 11 (0.70614) to that of the amphibole-pyroxenite sample 15 (0.70615) is believed to be fortuitous, but does suggest that the parental magma of this clinopyroxenite had a higher initial strontium value than the parental magmas of the cortlandtite (14) and amphibole-pyroxenite (40, 48) samples. It should also be noted that the higher $^{87}Sr/^{86}Sr)_i$ of the norites ($\sim$ 0.70646) would seem to preclude the clinopyroxenites of pluton 3 from being crystallization products of the norite magma.

The major and trace element chemistries of the eastern pyroxenite sample 31 can be produced by crystal accumulation (clinopyroxene 50%; orthopyroxene 37%; olivine 8%; amphibole 5%) from the same parental composition used to model the western pyroxenite sample 11. Compared to sample 11, the lower REE and incompatible element (Rb 1.1 ppm; Sr 50 ppm; P 44 ppm) abundances of sample 31 (Table 3, Fig. 33) place the amount of calculated intercumulus liquid at 6%, substantially less than the 18% of sample 11. The high proportion of cumulate minerals of clinopyroxenites 11 (82%) and 31 (94%) indicate that the process by which interstitial liquid was excluded from these cumulate rocks was efficient.

PETROGENESIS OF THE HORNBLENDITES AND KAERSUTITE GABBROS

Hornblendites and kaersutite gabbros from pluton 1 of the Cortlandt complex formed at moderate pressures from a hydrous basaltic liquid resulting in crystallized amphibole (kaersutite) and plagioclase. Clinopyroxene and olivine are absent. Hornblendite sample 2 appears from its phase chemistry (Appendix 2) to be the least differentiated of the samples. The REE pattern of sample 2 (Fig. 41) is characterized by a strong concave down curvature in the LREE and a negative Eu anomaly consistent with amphibole accumulation. Textural features plus the low SiO_2 content (39.1 wt.%) of this sample further support an amphibole accumulation origin of this rock.

Quantitative modelling of this kaersutite cumulate began with the amphibole pyroxenite parental composition, 40P, from which clinopyroxene (60%), orthopyroxene (20%), olivine (15%), and minor amphibole (5%) were fractionated (20%) (Table 13). Crystallization of olivine, clinopyroxene, and orthopyroxene was then replaced by kaersutite and plagioclase coprecipitation (5%). The lack of any olivine and pyroxene indicates that these minerals were no longer crystallizing from the hornblendite parental liquid; hence, they were excluded from

Table 13. Sample #2 Quantitative Modelling.

	a	b	c	d	#2 Sample
REE Normalized					
La	74.9	77.4	28.5	30.3	29.4
Ce	65.4	66.9	36.7	40.5	39.0
Nd	55.0	55.9	47.0	52.7	51.4
Sm	38.6	38.4	43.0	48.6	46.4
Eu	32.4	32.7	34.2	36.8	34.1
Gd	25.3	24.9	32.7	37.1	33.6
Dy	18.6	18.4	22.4	25.4	22.8
Er	14.2	14.1	16.5	18.8	16.8
Yb	12.1	12.0	13.0	14.7	12.9
ppm					
Rb	24.4	25.3	8.0	8.9	8.4
Sr	550	543	679	543	584
Ba	351	351	368	409	506
Ni	128	131	73	84	16
Co	79.4	82.1	28.7	32.8	85
Cr	71.4	71.2	75	85	41
Sc	17.3	16.0	40.3	46	52
P	1840	1914	0.0	0.0	100
Nb	24.8	25.6	9.0	10.2	11.0
Zr	153	158	48.7	55.6	60.8
Wt.%					
SiO_2	46.6	46.7	43.9	42.9	39.1
Al_2O_3	15.3	15.1	19.6	17.8	17.4
"FeO"	11.4	11.5	9.03	10.3	13.1
MgO	7.82	7.79	8.33	9.50	9.14
TiO_2	2.66	2.65	2.80	3.20	3.55
CaO	11.4	11.4	12.2	11.8	11.0
Na_2O	2.35	2.35	2.42	2.30	1.58
K_2O	1.44	1.46	1.04	1.16	1.22

[a] *See Sample #11 calculated composition a.*

[b] *5% fractional crystallization (0.70 amph; 0.30 plag) from composition a.*

[c] *Cumulate (0.70 amph; 0.30 plag) crystallized from composition b.*

[d] *Cumulate (0.80 amph; 0.20 plag) crystallized from composition b.*

the modelling scheme. Accumulation of kaersutite and plagioclase from this liquid in the ratio of 7:3 or 8:2, respectively, reveals that the REE and most other trace element abundances are closely duplicated (Table 13). The major element chemistry resulting from this calculation (Table 13) has a close resemblance to that of hornblendite sample 2 except for the abundances of SiO_2, TiO_2, and FeO. However, this sample contains approximately 5 modal % opaques (ilmenite and iron-sulfides). Addition of 5% opaques (3% iron-sulfides; 2% ilmenite) to the calculated composition decreases the silica by 5% (42.9 → 40.8%), and increases the FeO (12.7%) and titania (3.9%) abundances resulting in values similar to those of hornblendite sample 2. This 5% addition also improves the modelling fit for the major elements Al_2O_3, MgO, CaO, and Na_2O. The high sulfur content of sample 2 (Table 1) is consistent with substantial iron-sulfide (pyrite, pyhrrotite) accumulation. The close fit of the major and trace element chemistry of this hornblendite to the calculated modelling scheme suggests that this sample lacks differentiated liquid and is an amphibole-plagioclase adcumulate.

The conventional interpretation of adcumulates is that they consist of segregated minerals that grew from an intercumulus liquid which was communicating by diffusion

with a larger reservoir of magma (Wager and Brown, 1968). Growth of the cumulate minerals continued until their grain boundaries met and formed interlocking mosaic texture. For hornblendite sample 2, it would appear that the cumulus amphibole ($\sim$ 75%) and plagioclase ($\sim$ 25%) crystals of this rock removed their essential components from the magma, grew, and, consequently, forced out the inappropriate intercumulus melt during their growth. The low abundances of phosphorus ($\sim$ 100 ppm), whose D is approximately zero for plagioclase, amphibole, and opaques, further supports the idea that this rock is a two-mineral adcumulate, devoid of trapped interstitial liquid.

In an adcumulate, because the cumulus minerals are overgrown by material of the same composition, the original cumulate cores and overgrowth rims should theoretically not be detectable (Wager and Brown, 1968). Amphiboles in this hornblendite (2) are not zoned; however, the plagioclase is weakly reverse zoned (Appendix 2).

McBirney and Noyes (1979) have recently shown that cumulate textures, preferred orientation of crystals, and layering, which are features generally associated with crystal settling can be explained in terms of <u>in</u>

in situ crystallization. These are all features of the Cortlandt complex hornblendites. The process of *in situ* growth can explain the close association of amphibole and plagioclase minerals of very different densities in this cumulus rock. It would be expected that if the hornblendites formed by a crystal settling process instead of by *in situ* growth, density differences would have caused segregation of these two minerals. The exclusion of incompatible elements from hornblendite sample 2 indicates that the rate of growth of the cumulate kaersutite and plagioclase crystals must have been slower than the rate of diffusion of the incompatible components out of the interstitial liquid.

Since sample 2 is composed primarily of kaersutite ($\sim$ 75%) and apparently lacks trapped interstitial melt, kaersutite-melt distribution coefficients can be estimated for elements such as Ba, Zr, and Nb. Using the calculated parental composition of this hornblendite contained in Table 13, and assuming that these trace elements are excluded from plagioclase, K_d's of approximately 1.4 (Ba), 0.4 (Zr), and 0.5 (Nb) are estimated for kaersutite to match these trace element abundances in sample 2. Because Nb has a reported K_d of approximately 0.8 for ilmenite-basalt liquid (McCallum and Charette, 1978), it may also have a high affinity for pyrite and pyhrrotite, minor constituents ($\sim$ 3 volume %) of this rock. Therefore, the estimated partition

coefficient for Nb in kaersutite by this calculation scheme is a maximum.

Another hornblendite sample (1) from pluton 1 has essentially the same modal mineralogy as sample 2 (Appendix 1) but has much higher (factor of 2-5) incompatible element abundances. This difference indicates that hornblendite sample 1 is probably not an adcumulate but contains some ($\sim$40%) trapped interstitial liquid. Zoned plagioclase (Appendix 2) plus the presence of biotite and sphene in sample 1 might be indicative of this intercumulus melt. Hornblendite sample 1 and 2 have very similar REE patterns (Fig. 41). However, the overall abundances in 1 are much higher (LREE by a factor of $\sim$ 2; MREE and HREE by $\sim$ 30%). REE and major elements were also determined on a kaersutite mineral separate from hornblendite sample 1 (Tables 1 and 3). Because kaersutite is the major constituent of sample 1, the REE abundances in the amphibole separate from this sample could constrain the K_d's of the kaersutite REE and parental REE compositions. REE abundances for the kaersutite minerals separate (1 KAER), compared to that of the whole rock, are higher for the HREE, equal for the MREE, and substantially lower for the LREE (Fig. 41). Calculations reveal that an additional 25% differentiation of the sample 2 melt (Table 14) is needed to produce

Table 14. Sample #1 Quantitative Modelling.

	a	b	c	d	#1 Sample
REE Normalized					
La	92.4	98.1	71.1	81.9	74.1
Ce	77.3	80.4	68.3	73.1	80.0
Nd	59.7	60.0	84.6	74.8	81.5
Sm	39.5	38.8	72.2	58.8	62.7
Eu	33.4	32.6	53.2	45.0	42.0
Gd	24.7	24.0	51.4	40.4	42.9
Dy	18.6	18.4	34.9	28.3	29.2
Er	14.4	14.4	25.0	20.8	22.0
Yb	12.6	12.7	19.4	16.7	17.5
ppm					
Rb	31.2	33.4	16.1	23.0	44.2
Sr	453	420	272	331	522
Ba	364	374	677	556	628
Ni	153	164	118	136	38
Co	98	106	48	71	54.8
Cr	75.1	77.3	104	93.5	20.8
Sc	12.3	11.5	37.3	27	51
P	2556	2840	0.0	1136	528
Nb	314	34.1	14.1	22.1	23.5
Zr	195	212	77.2	131	96.5
Wt.%					
SiO_2	47.1	46.9	41.3	43.5	42.8
Al_2O_3	12.9	12.0	16.0	14.4*	17.1
"FeO"	13.0	13.6	14.2	14.0	11.9
MgO	8.19	8.47	10.7	9.80	7.86
TiO_2	2.89	3.00	3.62	3.37	3.59
CaO	11.2	11.4	10.2	10.7	9.60
Na_2O	2.31	2.14	1.59	1.81	1.94
K_2O	1.76	1.82	2.00	1.93	1.86

[a] *30% fractional crystallization (10% 0.7 amph.; 0.3 plag.; then 20% 0.5 plag.; 0.5 amph.) from sample #2 calculated composition a (Table).*

[b] *10% fractional crystallization (0.50 plag.; 0.446 amph.; 0.004 sphene; 0.05 biotite) from composition a.*

[c] *Cumulate (0.9 amph.; 0.05 plag.; 0.046 biotite; 0.004 sphene) crystallized from composition a.*

[d] *Cumulate plus 40% liquid (b).*

* *Starting composition must have ∿ 18.0 wt. Al_2O_3.*

the appropriate REE characteristics of hornblendite sample 1. Modelling (Table 14) indicates that sample 1 must be an amphibole-rich cumulate (90% kaersutite; 5% plagioclase; 4.7% biotite, and 0.3% sphene) in order to explain its HREE abundances. Cumulate phases make up approximately 60% of the rock with the remainder trapped differentiated liquid. Sphene, which is a minor constituent of this sample 1, must be a cumulate ($\sim$ 0.3%) phase of the LREE or values of this hornblendite cannot be reproduced.

Elements that are not reasonably approximated by this mathematical fractionation model contained in Table 14 include Rb, Sr, and Al_2O_3, whose higher values in sample 1 can only be explained by abundances that are much greater than those of the original parental melt, 40P. If the original cumulus pile contained more plagioclase and biotite and hence, less amphibole, this would increase the calculated values of Sr, Rb, and Al_2O_3. However, it will also cause a greater discrepancy for the REE, especially the HREE, making them much too low. As a result of these calculations, the Rb and Al_2O_3 abundances of the parental magma of this hornblendite are estimated at approximately 45 ppm and 18 wt.%, respectively. One possibility for the apparent

modelling discrepancies is that the parental magma of sample 1 was originally similar to the amphibole-pyroxenite parent magma, 40P, but experienced a contamination event which increased its Rb and Al_2O_3. The proximity of sample 1 to the country rock contact (Fig. 2) and the inclusion of several large pelitic and calc-silicate xenoliths within this portion of the hornblendite pluton, represent permissive evidence for such a model.

The higher $^{87}Sr/^{86}Sr)_i$ ratios of samples 1, 2, and 3 (Table 4) from this pluton, compared to those of the amphibole-pyroxenite (40) may be a consequence of pelitic assimilation (high $^{87}Sr/^{86}Sr)_i$ ratio). However, the similarity of $^{87}Sr/^{86}Sr)_i$ in the three samples from this pluton requires that the assimilation and/or isotopic equilibration process with an older crustal component occurred prior to emplacement. It is also possible that the hornblendite melt experienced a second stage of mixing at the emplacement site. This second stage mixing may have resulted from the addition of an aqueous fluid from the pelitic country rock which contained the components Rb, Ba, K_2O and SiO_2 and did not significantly change the initial strontium value of the basic melt. However, this fluid material needs to have a very high Rb/Sr ratio. Such a high ratio could be obtained if Sr, which already has a low abundance ($\sim$100 ppm) in the pelitic material, had an even lower solubility than Rb in an aqueous fluid.

Modelling of the kaersutite gabbro from pluton 1 (sample 4) reveals that it is an amphibole-plagioclase (55:45) cumulate with approximately 40% differentiated interstitial liquid (Table 15). The parent composition used in the calculations (Table 15) is the same as that for hornblendite sample 1, and as in sample 1, the proposed parental melt composition for the gabbro (sample 4) needs to have Al_2O_3 abundances of approximately 18 wt.%. Such high alumina values cannot be produced from the parental composition 40P by any reasonable fractionation scheme because the liquidus phases of this liquid, kaersutite and plagioclase, both have relatively high (14 and 27 wt.%) Al_2O_3 abundances. To obtain such a high Al_2O_3 value, a phase such as pyroxene would have to be a major fractionating phase.

For gabbroic sample 3, the most differentiated of the rocks analyzed from pluton 1, modelling of the major and trace element chemistries proved unsuccessful. The chemical abundances of this quartz, K-feldspar bearing gabbro could not be produced from the parental composition 40P by any fractionation method. Calculation schemes tested varied the types and amount of fractionating phases and K_d's, but failed to properly reproduce

Table 15. Sample #4 Quantitative Modelling.

	a	b	c	d	#4 Sample
REE Normalized					
La	92.4	100.1	30.7	58.5	61.8
Ce	77.3	82.6	35.8	54.5	59.6
Nd	59.7	62.3	41.3	49.7	59.0
Sm	39.5	40.4	35.5	37.5	43.6
Eu	33.4	33.8	31.0	32.1	32.9
Gd	24.7	24.8	26.0	25.5	28.4
Dy	18.6	18.9	18.0	18.4	18.8
Er	14.4	14.7	13.4	13.9	14.3
Yb	12.6	12.9	10.8	11.6	11.0
ppm					
P	2556	2840	0.0	1136	655
Wt.%					
SiO_2		47.1	46.4	46.7	46.8
Al_2O_3		11.8	21.7	17.7*	19.4
"FeO"		13.8	6.60	9.48	8.20
MgO		8.45	6.44	7.24	7.56
TiO_2		3.03	1.83	2.31	2.76
CaO		11.1	12.0	11.6	9.89
Na_2O		2.26	2.66	2.50	2.65
K_2O		1.86	0.94	1.31	1.81

[a] *SEE Sample #1 calculated composition a.*

[b] *10% fractional crystallization (0.5 amph.; 0.5 plag.) from composition a.*

[c] *Cumulate (0.55 amph.; 0.45 plag.) crystallized from composition a.*

[d] *Cumulate plus 40% liquid (b).*

* *Starting composition must have ∿ 18.0 wt.% Al_2O_3.*

the high SiO_2 (57 wt.%), Al_2O_3 (18.4 wt.%), Na_2O (3.35 wt.%), K_2O (3.58 wt.%), Rb (76 ppm), Sr (585 ppm), Ba (1181 ppm) and LREE values of sample 3. The reasonable success obtained in modelling the major and trace element abundances of hornblendites 1 and 2 and gabbroic sample 4 suggests that the late-stage differentiated liquid of pluton 1, represented by sample 3, is chemically anomalous. Since the pelitic country rock (samples 35 and 45) is enriched in the same elements that are anomalously high in sample 3, the addition of pelitic material to gabbroic sample 3 may have occurred. The high $^{87}Sr/^{86}Sr)_i$ of sample 3 (0.70690) is only slightly higher than the strontium initials of sample 1 (0.70668) and 2 (0.70681) from the same pluton and indicates that if interaction took place with the pelitic schist, the magma could not have consumed much strontium ($< 10\%$). Thus, addition to the melt of an aqueous fluid rich in silica and alkalis but low in Sr could increase the abundances of the necessary elements in the melt but still not significantly increase its $^{87}Sr/^{86}Sr)_i$. Further supporting this idea is data from a recent trace element and oxygen isotopic study of a basic plutonic igneous rock suite (Arth et al., 1978). Arth cliamed that, prior to solidification, the magmas from SW Finland underwent addition of water from the metamorphic country

rock. His conclusion, that this process may also have introduced Rb into the crystallized magma, can be applicable to the in alkalis and other elements in the Cortlandt region kaersutite gabbros.

In summary, the basic rocks of pluton 1 of the Cortlandt complex appear to be related to the amphibole-pyroxenite parental composition by differentiation involving kaersutite and plagioclase. The hornblendites, as well as some of the gabbros, contain substantial amounts of cumulus kaersutite and plagioclase and variable amounts of interstitial melt. One hornblendite sample lacks trapped interstitial melt.

The results of quantitative modelling of the differentiation history of several samples from pluton 1, plus Sr isotopic data on these samples, indicate that contamination by older crustal rocks probably took place. This event increased both the $^{87}Sr/^{86}Sr)_i$ and Al_2O_3 values of the original amphibole-pyroxenite parental melt. A second stage mixing event is proposed, one involving an aqueous fluid, which caused an enrichment of Rb, Ba, LREE, K_2O, Na_2O, and SiO_2 contents of the late-stage differentiated gabbroic liquids but did not affect the strontium isotopic systematics to any great extent.

PETROGENESIS OF THE DIORITE SUITE

The strontium isotopic values (Fig. 37), the presence of garnet, and the corundum normative nature of samples from the Cortlandt diorite pluton 2 indicate that these rocks have experienced crustal contamination. Quantitative modelling (Table 16) of one diorite sample (7) from this pluton reveals that it is a kaersutite, plagioclase, and opaque (56:38:6) adcumulate which crystallized from a parental liquid similar in chemical composition to the proposed parental melt (related to 40P by fractional crystallization) of hornblendite sample 2 (pluton 1). These calculations indicate that the diorite parental liquid of the amphibole-rich rock (7) had a REE pattern with a stronger upward concavity than did the parental magma of hornblendite sample 2. Removal of apatite ($\sim$ 1.5%) from the parental melt composition of hornblendite sample 2 produces a liquid with the appropriate REE characteristics. The addition of 6 wt.% opaques (ilmenite (4%) and iron sulfides (2%)) to the plagioclase, kaersutite cumulate pile increases the FeO and TiO_2 values and decreases silica to abundances that coincide with those of diorite sample 7. The estimated modal mineralogy of sample 7 (Appendix 1) is very close to that proposed by this calculation scheme.

Table 16. Sample #7 Quantitative Modelling.

	a	b	#7 Sample
REE Normalized			
La	63.5	20.5	22.9
Ce	52.8	24.3	24.3
Nd	41.3	28.7	28.2
Sm	28.5	25.9	24.5
Eu	26.7	24.2	23.9
Gd	18.2	19.1	18.2
Dy	14.5	14.2	13.8
Er	11.6	10.9	10.9
Yb	10.6	9.18	8.95
ppm			
Rb	25.7	6.0	3.6
Sr	551	782	731
Ba	356	310	
Ni	133	60	31
Co	78.4	22	52
Cr	72.5	61	31
Sc	16.2	32.7	31
P		0.0	262
Nb	26.5	7.4	13
Zr	160	39	43
Wt.%			
SiO_2	46.7	41.2	40.8
Al_2O_3	15.1	20.5	20.6
"FeO"	11.5	11.4	12.7
MgO	7.79	6.66	6.22
TiO_2	2.65	3.62	3.64
CaO	11.4	11.9	10.8
Na_2O	2.35	2.27	1.94
K_2O	1.46	0.61	0.63

[a] *Sample #2 calculated composition b with 1.5% apatite removed.*

[b] *Cumulate (0.56 amph.; 0.38 plag.; 0.04 ilmenite; 0.02 Fe sulfides) crystallized from composition a.*

It should be noted that the relative percentages of minerals fractionated (Tables 13 and 16) correspond closely to the modal abundances observed.

As in hornblendite sample 2, the trace element modelling indicates that an intercumulus liquid component is lacking, making diorite sample 7, like sample 2, a rock that has experienced adcumulate mineral growth. The phase chemistry of these two samples are very similar, with each lacking zonation of amphibole crystals but showing reverse zoning of plagioclase (Appendixes 3 and 2). The similarity of the major, trace, and phase chemistries of hornblendite sample 2 and diorite sample 7 suggests that these two rock types, though from different plutons, crystallized from magmas that were chemically similar.

Diorite sample 9 from pluton 2 has a parallel REE pattern to that of sample 7 but has higher REE abundances and is characterized by a negative, rather than a positive, Eu anomaly (Fig. 42). Quantitative modelling (Table 17) reveals that sample 9 is an amphibole (53%), plagioclase (38%), biotite (4%), and opaque (5%) cumulate which crystallized from a liquid very similar in major ($Al_2O_3 \sim 18$ wt.%) and trace element abundances to the parental melt of diorite sample 7. However, sample 9 differs from sample 7 in that it contains approximately 30% trapped intercumulus liquid.

Table 17. Sample #9 Quantitative Modelling.

	a	b	c	#9 Sample
REE Normalized				
La	77.4	25.0	40.7	38.2
Ce	66.9	30.2	41.2	39.8
Nd	55.9	37.6	43.1	43.9
Sm	38.4	33.5	35.0	38.7
Eu	32.7	28.7	29.9	30.9
Gd	24.9	25.4	25.3	27.3
Dy	18.4	17.3	17.6	19.1
Er	14.1	12.8	13.2	14.4
Yb	12.0	10.1	10.7	10.9
ppm				
Rb	25.3	9.3	14.1	16.1
Sr	543	764	698	720
Ba	351	460	427	458
P	1914	0.0	574	306
Wt.%				
SiO_2	46.7	43.6	44.5	43.9
Al_2O_3	~ 18.0	19.3	18.9	20.6
"FeO"	11.5	11.4	11.5	12.3
MgO	7.79	6.21	6.68	5.58
TiO_2	2.65	3.36	3.15	3.49
CaO	11.4	9.95	10.4	9.88
Na_2O	2.35	2.75	2.63	2.86
K_2O	1.46	1.22	1.29	1.11

[a] *See Sample #2 calculated composition b.*

[b] *Cumulate (0.53 amph.; 0.38 plag.; 0.03 ilmenite; 0.02 Fe-sulfides; 0.04 biotite) crystallized from composition a.*

[c] *Cumulate plus 30% liquid (a).*

From the mineralogy of sample 9, this interstitial liquid apparently crystallized biotite, orthopyroxene, apatite, and quartz in addition to amphibole and plagioclase. The interaction of this interstitial liquid with the cumulus minerals (amphibole and plagioclase) has resulted in the formation of weak normal zoning in kaersutite and plagioclase crystals (Appendix 3). The Rb (16.1 ppm) and Ba (458 ppm) abundances in this sample imply that biotite is a minor cumulate phase. As in diorite sample 7, addition of approximately 5 volume % opaques [ilmenite (3%) and iron sulfides (2%)] is needed to resolve the high FeO (12.3 wt.%) and TiO_2 (3.49 wt.%) values. Although diorite samples 9 and 7 can be reasonably modelled from a similar melt composition, the initial strontium isotopic values of these samples (#7-0.70607; #9-0.70810) are different. The Sr isotopes suggest that the parental magma of sample 9 experienced the addition of material with a much higher $^{87}Sr/^{86}Sr$ ratio such as that possessed by the pelitic country rock (sample 45). Contamination of the parental magma of sample 9 by assimilation of pelitic material would also increase the major (SiO_2, K_2O, Na_2O) and trace element (LREE, Rb, Ba) abundances of the parental melt. Hence, sample 9 may contain much less than the 30% interstitial liquid proposed by the calculation scheme in Table 17.

Quantitative modelling of diorite sample 8, the most differentiated diorite from pluton 2, proved to be impossible by any reasonable fractionation scheme. Starting with the same liquid composition that successfully modelled diorites 7 and 9, removal of plagioclase, amphibole, biotite, apatite, and opaques in differing proportions, plus varying K_d's, failed to replicate the REE and other trace element abundances of diorite sample 8. These calculation schemes were also unsuccessful in obtaining a match for the major elements of sample 8. The presence of trace amounts of almandine garnet in this diorite suggest that this mineral may have been a fractionating phase in the late-stage dioritic magma. However, even the fractionation of a small amount of garnet from many different calculated melt compositions did not improve the overall trace element modelling significantly. In addition, the textural relationships of sample 8 indicate that this rock has undergone accumulation of apatite ($\sim$ 1 volume %), amphibole ($\sim$ 10%), and orthopyroxene ($\sim$ 5%). The high P_2O_5 value (1.51 wt.%) of sample 8, as well as the slight concave down curvature of the LREE (Fig. 42) and negative Eu anomaly support these textural observations. The high Al_2O_3, K_2O, Na_2O, Ba, LREE and Rb abundances of diorite sample 8, plus the presence of garnet and its normative corundum (Table 2), imply that this sample may have experienced

introduction of a pelitic country rock component. Strontium isotopic data supports a pelitic contamination model for rocks of the diorite pluton. Diorite samples 8 (0.70823) and 9 (0.70810) have very high $^{87}Sr/^{86}Sr)_i$ and, with sample 7 (0.70607), define a potential mixing line with a nearby pelitic crustal unit (Fig. 37). An example of how chemical alteration of late-stage differentiated melt by a partial melt from a pelitic schist might happen is shown in Table 18. A sample of the nearby pelitic country rock (45) was analyzed for major and trace elements (Tables 1 and 3). Partial melting of sample 45 under P-T conditions where garnet is a residual phase ($\sim$ 29 volume %), could have resulted in a granodioritic type melt (Evans, 1964) that is enriched in the LREE, Ba, and Rb. The residuum of the pelitic schist after partial melting has the composite mineralogy of emery (Evans, 1964). The major constituents of this emery include almandine garnet, corundum, spinel, staurolite, sillimanite, corderite, magnetite, biotite, muscovite, sapphirine, and quartz. Of these minerals, only garnet and biotite have K_d's of sufficient value to affect REE, Rb, and Ba abundances of a partial melt produced from the pelitic schist. The percentage of biotite in the residuum determines the abundances of Rb and Ba, while the high K_d's for the HREE of garnet (Table 5) determine

Table 18. Partial Melting of Pelitic Schist Sample #45.

	a	b	c
REE Normalized			
La	130	294	243
Ce	108	235	197
Nd	64.4	134	114
Sm	38.7	52.7	49.7
Eu	20.5	34.5	31.0
Gd	24.6	14.7	15.7
Dy	18.4	4.8	5.4
Er	18.0	3.7	4.3
Yb	18.1	3.5	4.0
ppm			
Rb	176	294	265
Sr	104	255	205
Ba	1332	1753	1665

[a] *Sample #45--starting pelitic composition.*

[b] *40% partial melting of a leaving a residue of 20% garnet; 10% quartz, 10% biotite, 20% opaques; 20% Al silicates; and 20% Fe-Mg silicates (e.g., staurolite, cordierite).*

[c] *50% partial melting of a with same residue as b.*

Hybridization of Basic Melt with Pelitic Partial Melt.

	d	e	f
REE Normalized			
La	115	243	153
Ce	92	197	123
Nd	65.3	114	79.8
Sm	40.6	49.7	43.3
Eu	33.5	31.0	32.8
Gd	24.2	15.7	21.7
Dy	18.9	5.45	14.9
Er	14.9	4.27	11.7
Yb	13.3	4.01	10.5
PPM			
Rb	~ 40	265	108
Sr	~ 500	205	412
Ba	~ 600	1665	920

d *Hypothetical basic melt.*

e *50% partial melt of pelitic schist--composition b*

f *Hybrid melt. 70% d plus 30% e*

the extent to which the partial melt is fractionated. A simple calculation that shows the results of homogeneous mixing between an anetectic melt produced from a pelitic schist and a basic melt is shown in Table 18. These calculations show that the addition to a basic magma of partial melt produced by 40-50% partial melting of pelitic material (Evans, 1964) can result in an enrichment of LREE, Rb, and Ba abundances of the former basic liquid. The amount of residual garnet determines the extent of HREE depletion in the hybrid melt. The silica, potassium, and sodium abundances of this hybrid liquid are also significantly increased.

Thompson and Tracy (1979) have shown that the optimum conditions for anatectic melt generation from pelitic schists occur in a pressure range of 4-6 kb and a temperature range of 640-720°C. Pressure and temperature estimates for emplacement for the Cortlandt plutons (Caporuscio and Morse, 1978), plus their intrusion during, at, or near the waning stages of a regional metamorphic event would suggest that the pelitic country rocks were probably under these optimum anatectic conditions.

Diorite sample 42 from Stony Point is characterized by a REE pattern (Fig. 42) that is highly fractionated ($(La/Yb)_N \approx 66$). Sample 42 also has very low HREE abundances and a large positive Eu anomaly. The

rock contains approximately 3.5 modal % almandine garnet and, like diorite sample 8 from pluton 2, is corundum normative ($\sim$ 3.5%). The presence of euhedral garnet concentrated in small cumulate lenses distributed throughout the Stony Point diorite pluton suggests that garnet was a fractionating phase and is responsible for the low HREE abundances of sample 42. The experimental work of Green (1977) reveals that almandine garnet can crystallize from a silica magma at pressures of 5-7 kb. This supports the conclusion that almandine garnet can crystallize from a melt. Temperatures of 1000°C obtained from biotite-garnet pairs (Ferry and Spear, 1978) in sample 42 further support the idea that almandine garnet in these rocks is not exotic. The Stony Point diorite (42) is also enriched in Al_2O_3 (20.9 wt.%), K_2O (2.97 wt. %), and Na_2O (5.20 wt.%), Ba (2641 ppm), Rb (69.4 ppm), and Sr (1639 ppm). This diorite shows a remarkable chemical and mineralogical similarity to the Archean age syenodiorites of northeastern Minnesota studied by Arth and Hanson (1975). However, sample 42 has much lower HREE abundances than the alkalic syenodiorites from Minnesota. Arth and Hanson proposed that these high Al_2O_3, and alkali-rich rocks were produced by partial melting from a near-silica-saturated eclogite

derived from an olivine basalt. Crystallization of garnet at Stony Point is probably responsible for the lower HREE abundances in diorite sample 42. The high Al_2O_3 and Sr and the large positive Eu anomaly suggest that sample 42 may contain cumulate plagioclase ($\sim$ 20%). While partial melting of eclogite may be responsible for the chemical data of diorite sample 42, another possibility is that this rock was contaminated with a partial melt fraction that subsequently enriched its SiO_2, Na_2O, Al_2O_3, LREE, Rb, Ba, and Sr abundances. However, garnet as a fractionating phase is still required in this assimilation model. The low $^{87}Sr/^{86}Sr)_i$ (0.70457) is inconsistent with a model involving the assimilation of high Rb/Sr ratio materials such as pelitic sample 45. Sr isotope values of sample 42 require that the contaminant have a $^{87}Sr/^{86}Sr)_i$ equal to or lower than that of sample 42.

In summary the diorites of the Cortlandt complex (pluton 2) and the diorites of Stony Point are chemically and isotopically distinct. Some of the diorites of pluton 2 are chemically and texturally very similar to the hornblendites of pluton 1 and can be related to 40P through fractionation, adcumulate growth, and crystal accumulation processes. Chemical and isotopic data indicate that progressive contamination (bulk, partial melt, aqueous fluid) may have been operative within this diorite

pluton of the Cortlandt complex. Geochemical characteristics of the diorite at Stony Point suggest that the magma at this emplacement site experienced garnet fractionation and is significantly different from the diorite liquid of pluton 2. Major and trace element data suggest that the Stony Point diorite may either represent a partial melt produced from eclogite or have experienced extensive contamination. If contamination is responsible for unusual geochemistry of the Stony Point diorite, then the assimilation process was such that it did not affect the Sr isotopic systematics.

PETROGENESIS OF THE NORITE SUITE

Trace element modelling indicates that the Cortlandt ultramafic rock types (cortlandtites, clinopyroxenites, hornblendites) (pluton 2) and the less evolved diorites (pluton 1) could be derived from 40P by fractional crystallization processes. The differentiated diorites (pluton 2) and kaersutite gabbros (pluton 1) also appear to be related to 40P, in this case through crustal contamination processes. However, 40P cannot be the parental composition for the norites. The parental magma of the norites must be enriched in SiO_2, Al_2O_3, K_2O, Na_2O, LREE, Rb, Sr, and Ba and have considerably less CaO ($\sim$ 8 wt.%) than 40P. Any reasonable fractionation scheme could not generate the major and trace element abundances of a potential norite parent from 40P. As was discussed in both the kaersutite gabbro and the diorite petrogenesis sections, it is believed that the basic magmas of these plutons have undergone trace element enrichment as a result of crustal contamination. The contamination of a magma by bulk assimilation, partial melt, or aqueous fluid may be sufficient to cause the hybrid magma to appear chemically unique. Hence, it is believed that 40P and the norite parental composition may be genetically related, but with the norite melt having been chemically

modified by assimilation processes. Bulk assimilation of aluminous metasediments has been proposed to be responsible for the production of norite gabbros (Bowen, 1928). The presence of many pelitic zenoliths in the norite pluton, many of which have been changed to emery, indicates that contamination and, therefore, hybridization of a parental alkalic magma such as 40P could have occurred.

In order to quantitatively evaluate the petrogenetic relationships between rocks of pluton 5, norite sample 21 was selected to be geochemically representative of the noritic liquid. From its textural features, norite sample 21 does not appear to contain any cumulate phases. Its fractionated REE pattern (Fig. 43) ($(La/Yb)_n \approx 14.5$) and high Rb (42.8 ppm), Sr (730 ppm), Ba (1165 ppm), and Al_2O_3 (18.4 wt.%) support this observation.

Calculations (Tables 19 and 20) reveal that norite samples 20 and 22 can be derived from a liquid having the composition of sample 21 by 20% fractionation of plagioclase ($\sim$ 60%), clinopyroxene (10%), orthopyroxene (10-20%), and amphibole (10-20%). Generation of norite sample 22 requires more amphibole fractionation and less orthopyroxene than that required for sample 20. The failure of the fractionation modelling scheme to successfully calculate the Rb (40% low) and K_2O (30% low) abundances

Table 19. Sample #20 Quantitative Modelling.

	a	b	#20 Sample
REE Normalized			
La	126	151	152
Ce	96.6	116	112
Nd	63.5	75.4	74.9
Sm	36.9	43.4	42.9
Eu	34.2	38.4	35.0
Gd	21.3	24.8	25.0
Dy	13.7	16.1	15.5
Er	10.0	11.7	12.0
Yb	8.65	10.2	10.5
ppm			
Rb	42.8	52.5	49
Sr	730	646	720
Ba	1165	1369	1469
Ni	54	56	37
Co	30.9	35.9	34
Cr	45.4	45.4	84
Sc	18	18.3	22
P	2226	2782	2357
Nb	15.3	19.1	19
Zr	118	144	136
Wt.%			
SiO_2	53.5	53.4	53.5
Al_2O_3	18.4	18.5	17.3
"FeO"	8.09	8.07	8.54
MgO	4.22	3.71	4.83
TiO_2	1.78	2.14	1.50
CaO	7.13	6.42	6.56
Na_2O	3.61	3.54	3.02
K_2O	2.39	2.92	3.05

[a] *Sample #21 noritic parental composition.*

[b] *20% fractional crystallization (0.60 plag.; 0.10 amph.; 0.20 opx.; 0.10 cpx.) from composition a.*

Table 20. Sample #22 Quantitative Modelling.

	a	b	#22 Sample
REE Normalized			
La	126	150	151
Ce	96.6	114.1	110
Nd	63.5	73.5	74.6
Sm	36.9	42.0	42.4
Eu	34.2	37.3	34.6
Gd	21.3	23.9	24.2
Dy	13.7	15.5	13.1
Er	10.0	11.4	11.3
Yb	8.65	9.9	9.8
ppm			
Rb	42.8	52.3	80
Sr	730	639	697
Ba	1165	1326	1456
P	2226	2782	2575
Wt.%			
SiO_2	53.5	53.5	52.9
Al_2O_3	18.4	18.2	18.8
"FeO"	8.09	8.28	8.31
MgO	4.22	3.97	3.30
TiO_2	1.78	2.14	1.80
CaO	7.13	5.92	6.16
Na_2O	3.61	3.51	3.22
K_2O	2.39	2.78	3.72

[a] *Sample #21 noritic parental composition.*

[b] *20% fractional crystallization (0.60 plag.; 0.20 amph.; 0.10 opx.; 0.10 cpx.;) from composition a.*

of sample 22 suggests that some of the biotite in this norite may be cumulate ($\sim$ 10%). Phase chemistry (Appendix 6), mineralogy, and major and trace elements indicate that the quartz-norite sample 23 is the most differentiated of all the norite samples. Modelling (Table 21) reveals that this sample can be derived from a melt having the calculated composition of sample 20 through the removal of 30% crystalline phases (70% plagioclase; 20% orthopyroxene; 5% clinopyroxene; and 5% amphibole). The high ($\sim$ 30%) calculated Ba value (Table 21) suggests that biotite and K feldspar are also fractionating ($\sim$ 15%) phases. The negative Eu value of sample 23 can be produced by the calculated model if the plagioclase K_d for Eu is increased by a factor of three (0.5 to 1.5). The increased K_d for Eu, with decreasing temperature and increasing sodium content, is in agreement with measured partition coefficients in volcanic rocks (Philpotts and Schnetzler, 1970; Schnetzler and Philpotts, 1970) and experimental systems (Drake and Weill, 1975).

While the norite samples 20, 22, and 23 seem to be related to sample 21 by crystal fractionation involving plagioclase, pyroxene, and amphibole, norite samples 18 and 19, on the basis of their more primitive phase chemistry (Appendix 6) and lower trace element abundances (Table 3),

Table 21. Sample #23 Quantitative Modelling.

	a	b	#23 Sample
REE Normalized			
La	151	203	214
Ce	115	157	170
Nd	75.4	102	104
Sm	43.4	58.2	57.3
Eu	38.4	46.8	33.6
Gd	24.8	33.0	31.5
Dy	16.1	21.6	20.4
Er	11.7	15.7	15.9
Yb	10.2	13.7	14.2
ppm			
Rb	52.5	75.0	117
Sr	646	433	659
Ba	1369	1801	1261
Ni	56	62	69
Co	35.9	46.3	26.7
Cr	45.4	52	16
Sc	18.3	21.3	16
P	2782	3974	2313
Nb	19.1	27.3	36
Zr	144	202	380
Wt.%			
SiO_2	53.4	52.7	54.5
Al_2O_3	18.5	18.0	17.6
"FeO"	8.07	8.22	8.14
MgO	3.71	2.29	3.21
TiO_2	2.14	2.99	1.69
CaO	6.42	5.82	5.57
Na_2O	3.54	3.17	3.18
K_2O	2.92	3.97	3.69

[a] *Sample #20 calculated composition b.*

[b] *30% fractional crystallization (0.70 plag.; 0.20 opx.; 0.05 cpx.; 0.05 amph.) from composition a.*

seem to have originated from a less differentiated melt than that of sample 21. These less evolved compositions, however, could not be used as starting parent compositions for modelling fractionation due to their low incompatible element (Rb, Nb, and Zr)abundances, and textural features which suggest that these two noritic samples 18 and 19 are cumulate rocks lacking appreciable differentiated liquid. A parental melt composition for samples 18 and 19 was estimated by the re-addition of pyroxene (20%), plagioclase (45%), and amphibole (35%) to that of sample 21 (Table 22). The mineral proportions for this calculation scheme were estimated from the modal mineralogies of samples 18 and 19. Because apatite shows cumulate textural relationships in these two samples, some apatite (1.8%) was also re-added in order to create a less-differentiated parental composition (Table 22). From this resultant less-differentiated composition, the major and trace element chemistries of samples 18 and 19 were modelled. These calculations (Table 22) indicate that kaersutite-bearing norite sample 18 is an adcumulate consisting of 50% amphibole, 20% plagioclase, 8.8% clinopyroxene, 13.5% orthopyroxene, 1.7% apatite, and 6% opaques (4% ilmenite, 2% iron sulfides). These mineral proportions are nearly

Table 22. Sample #18 Quantitative Modelling.

	a	b	c	#18 Sample
REE Normalized				
La	115	119	60.6	75.0
Ce	88.3	89.8	62.1	72.6
Nd	58.2	56.9	56.8	63.7
Sm	34.0	32.3	38.9	41.1
Eu	32.3	31.3	32.4	30.0
Gd	19.7	18.3	25.1	24.8
Dy	12.6	11.9	14.5	14.2
Er	9.10	8.70	9.96	10.2
Yb	7.90	7.70	7.70	7.90
ppm				
Rb		∿ 25	5.6	5.2
Sr	783	768	658	718
Ba		∿500	373	304
Ni	60	75	62	98
Co	33	45	18.9	76
Cr	70	70	101	183
Sc	16.5	17	38	31
P	2003	2123	3116	3273
Nb	13.8	12.4	0.33	13
Zr	106	98	31.2	62
Wt.%				
SiO_2	53.6		41.3	42.4
Al_2O_3	18.3		14.1	14.3
"FeO"	8.19		14.5	14.6
MgO	4.46		9.31	10.3
TiO_2	1.61		2.99	2.99
CaO	7.28		11.2	9.98
Na_2O	3.58		1.55	1.34
K_2O	2.18		0.90	0.63

[a] *Add 10% cumulate (0.60 plag.; 0.30 opx.; 0.10 cpx.) to #21 noritic parental composition.*

[b] *Add 10% cumulate (0.70 amph.; 0.282 plag.; 0.018 apatite) to composition a.*

[c] *Cumulate (0.50 amph.; 0.20 plag.; 0.088 cpx.; 0.135 opx.; 0.017 apatite; 0.04 Fe sulfides; 0.02 ilmenite) crystallized from composition b.*

identical to those of sample 18 and textural features are also consistent with a cumulate origin for this rock. The small percentage of cumulate apatite is responsible for the unexpectedly high LREE abundances in this sample which lacks interstitial liquid. The presence of large euhedral apatite crystals enclosed within euhedral orthopyroxene grains indicates that apatite is, indeed, a cumulate mineral in this rock. The low Rb (5.2 ppm) and Ba (304 ppm) abundances of this kaersutite-norite 18 suggest that the parental magma from which the amphibole and plagioclase crystallized must have contained approximately 25 ppm Rb and 500 ppm Ba.

Modelling of norite sample 19 indicates that this rock, like sample 18, appears to be an adcumulate consisting of plagioclase (45%), orthopyroxene (25%), clinopyroxene (3%), amphibole (20%), apatite (2.4%), and opaques (5%) (Table 23). Sample 19 was modelled from the same melt composition as that of the kaersutite-norite 18 because of similar mineral chemistries (Appendix 6), suggesting that both these rocks crystallized from the same magma with similar chemical abundances. The quantitative modelling (Table 23) of norite sample 19, from this proposed parental composition, successfully replicates most of the major and trace element characteristics of this rock. Again, as in sample 18, apatite

Table 23. Sample #19 Quantitative Modelling.

	a	b	#19 Sample
REE Normalized			
La	119.4	62.2	79.4
Ce	89.8	55.6	65.1
Nd	56.9	46.0	48.9
Sm	32.3	28.3	27.9
Eu	31.3	26.7	26.1
Gd	18.3	17.7	16.2
Dy	11.9	9.80	9.20
Er	8.70	6.51	6.60
Yb	7.70	4.73	5.50
ppm			
Rb	∿ 25	4.0	2.8
Sr	768	1135	914
Ba	∿500	288	249
Ni	75	71	27
Co	45	13.8	37
Cr	70	54.3	73
Sc	17	18.6	19
P	2123	4400	4102
Nb	12.4	1.3	15
Zr	98	9.3	33
Wt.%			
SiO_2		44.9	46.0
Al_2O_3		17.2	17.2
"FeO"		11.5	12.9
MgO		7.66	7.33
TiO_2		3.32	
CaO		10.4	9.48
Na_2O		2.15	1.92
K_2O		0.59	0.33

[a] *See sample #18 calculation b.*

[b] *Cumulate (0.45 plag.; 0.03 cpx.; 0.246 opx.; 0.20 amph.; 0.024 apatite; 0.05 Fe sulfides) crystallized from composition a.*

a cumulus phase, is responsible for increasing the overall REE abundances, especially the LREE. However, in norite sample 19 plagioclase is the predominant cumulate phase rather than amphibole as in sample 18. The observed textures and the modal mineralogy of sample 19 are consistent with the calculated phase abundances and the cumulate model calculated. As a consequence of the large modal percentage ($\sim$45%) of plagioclase in sample 19, the HREE abundances are approximately 50% lower than those of norite sample 18. This large proportion of plagioclase also accounts for the positive Eu anomaly of sample 19 (Fig. 43), as well as the high Sr content (914 ppm). The very low Rb (2.8 ppm) and Ba (249 ppm) contents of this norite indicate that the Rb and Ba values of the parental liquid for sample 19 were very similar to those proposed for sample (Rb $\approx$ 25 ppm; Ba $\approx$ 500 ppm).

In summary, the more differentiated norites of pluton 5 apparently are related to one another through fractionation of plagioclase (65%), orthopyroxene, clinopyroxene, and amphibole. Norite samples from the central portion of this body have textural and chemical characteristics that are consistent with an adcumulate origin. The similarity of $^{87}Sr/^{86}Sr)_i$ (Table 4) for both early (sample 19) and later (samples 22, 23) formed

norites within this pluton suggests that crustal contamination,mixing, and homogenization occurred prior to emplacement if the norite parent magma is genetically related to the alkalic basalt parent 40P. This assimilation event is probably responsible for the high Al_2O_3 ($\sim$18 wt.%), and alkali (Rb, K, Ba) concentrations, as well as the high $^{87}Sr/^{86}Sr)_i$ of the norites of pluton 5. Finally, Rb, Ba, and K data for the norites indicate that mixing of an aqueous fluid (containing Rb, Br, and K) with the differentiated noritic magma may have occurred prior to solidification of the norite body.

PETROGENESIS OF THE GRANODIORITE SUITE

Granodiorite plutons are closely associated, both temporally and spatially, with the mafic rocks of the Cortlandt and Rosetown complexes (Figs. 1 and 4). Initially, it was thought that the granodiorites might be related to the Cortlandt region basic rocks by fractional crystallization processes. However, trace element abundances of three granodiorites (samples 24, 34, 51) indicate that these silica-rich compositions cannot be related to any of the more basic rocks of the complex solely by fractional crystallization. To illustrate, granodiorite sample 51 from the Rosetown complex has much lower REE (Fig. 49) Nb (1.4 ppm), Zr (92 ppm), and P (0.03 wt.%) abundances than diorite sample 49 (Nb 53 ppm; Zr 199 ppm; P_2O_5 0.69 wt.%) and amphibole-pyroxenite sample 48 (Nb 23 ppm; Zr 138 ppm; P_2O_5 0.44 wt.%) from the same complex. The trace elements (REE, Nb, Zr, P) should be concentrated in the more silicic liquid if fractional crystallization was operative between these samples at this locality. The major and trace element chemistry of a single sample from the Peekskill granodiorite, sample 34, and a granodiorite dike that crosscuts the norite pluton, sample 24, are reported in Tables 1 and 3. The REE patterns (Fig. 44)

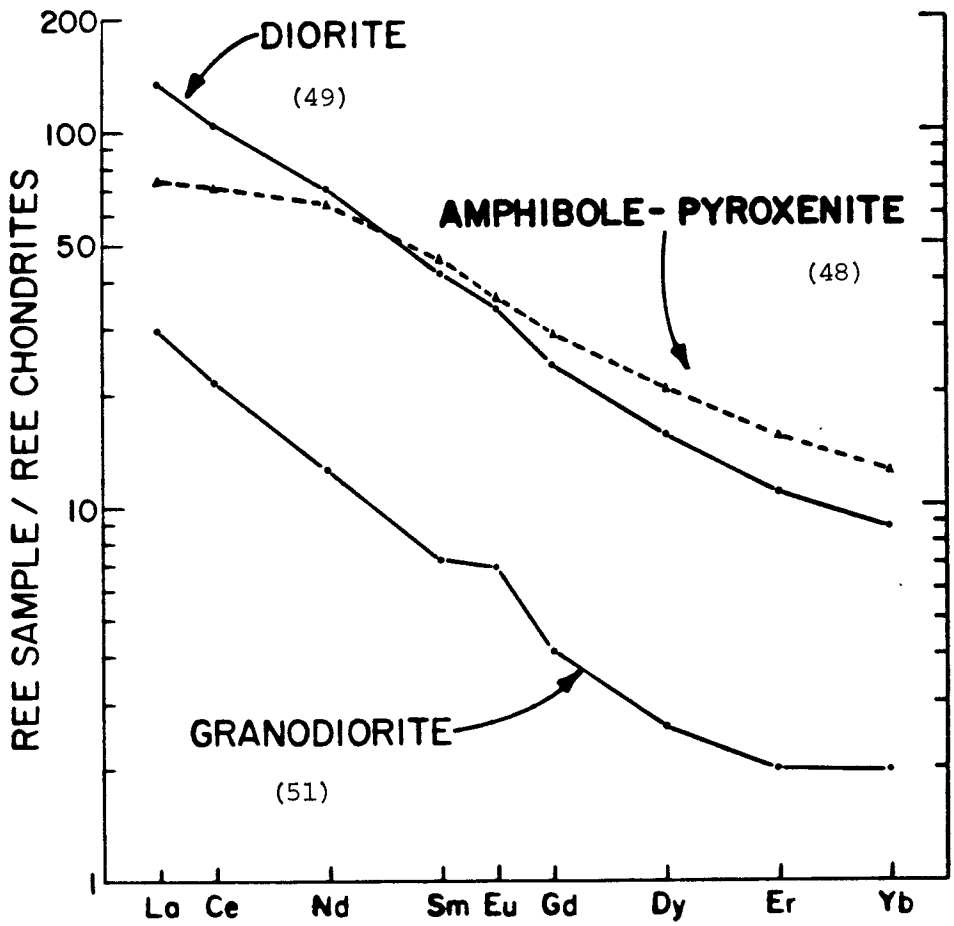

Fig. 49. Chondrite-normalized rare-earth patterns for Rosetown granodiorite (51), diorite (49) and amphibole-pyroxenite (48).

of these two granodiorite samples are remarkably similar to those of the Rosetown granodiorite (51). These REE patterns indicate that the granodiorites are not related by fractional crystallization to any basic rocks of the Cortlandt region. The similarity of phase chemistry (Appendix 7) and major (Table 1) and trace (Table 3) element abundances of these granodiorite samples suggests that these widely separated rocks were produced by the same petrogenetic process.

The low REE and incompatible trace element abundances of these granodiorite samples are unusual. In general, granodioritic or granitic rocks have much higher REE abundances (La $\approx$ 100x chondrites and Yb $\approx$ 10-20) than those of granodiorite samples 51, 24, and 34. Table 24 shows the comparison of several of the major (SiO_2, Al_2O_3, Na_2O, K_2O) and trace element (Zr, Nb, La) abundances of the Rosetown granodiorite with the average composition of 33 East Greenland granites (Wright et al., 1973). The East Greenland granitic rocks have been selected for comparison because they have trace element values that are typical of most granodiorite-granite suites and also because Zr and Nb data have been reported for these rocks. From Table 24 it can be seen that the La abundance of the average of East Greenland granites is greater by an order of magnitude than that of the Rosetown granodiorite ($\approx$ 400x

Table 24. Comparison of selected major and trace element abundances of Rosetown granodiorite and an average East Greenland granite.

	Rosetown Granodiorite	Average East Greenland Granite*
Wt.%		
SiO_2	71.7	71.8
Al_2O_3	15.5	14.5
Na_2O	5.24	3.68
K_2O	3.29	5.08
ppm		
Rb	47.4	190
Sr	605	150
Ba	1184	830
La	9.35	120
Zr	92	360
Nb	1.4	27

*Average of 33. Wright et al. (1973) as reported in Atherton and Tarney (1979).

chondrites vs ≈ 30x). Zr abundances in the Rosetown granodiorite are lower by approximately a factor of four, and Nb is lower by more than an order of magnitude than those of the average East Greenland granite. In addition to lower Zr and Nb abundances, the Rosetown granodiorite is characterized by a higher Zr/Nb ratio. The Rosetown diorite has a Zr/Nb ratio of 66 while the Zr/Nb ratio of the average East Greenland granites is ≈ 13. Comparison of the Zr/Nb ratios of all the Cortlandt region samples is illustrated on Fig. 50. The three granodiorites (24, 34, 51) have extremely high Zr/Nb ratios compared to the other rocks of this study (Fig. 50) reflecting their low Nb abundances. With the exception of one pyroxenite sample (31), all the rocks of the Cortlandt region plot near and above the chondritic line on the La/Ce vs Zr/Nb plot; most samples, including both cumulate and differentiated rocks, have Zr/Nb ratios between 2 and 14. Most rock types have rather restricted Zr/Nb ratios that vary from approximately 6 (alkali basalts) to 16 (crustal sediments). Appreciably higher (∿37) Zr/Nb ratios are found in ocean ridge basalts (Erlank and Kable, 1976). Due to the incompatible nature of both Zr and Nb, partial melting of crustal rocks to produce a granitic composition will result in a melt with a

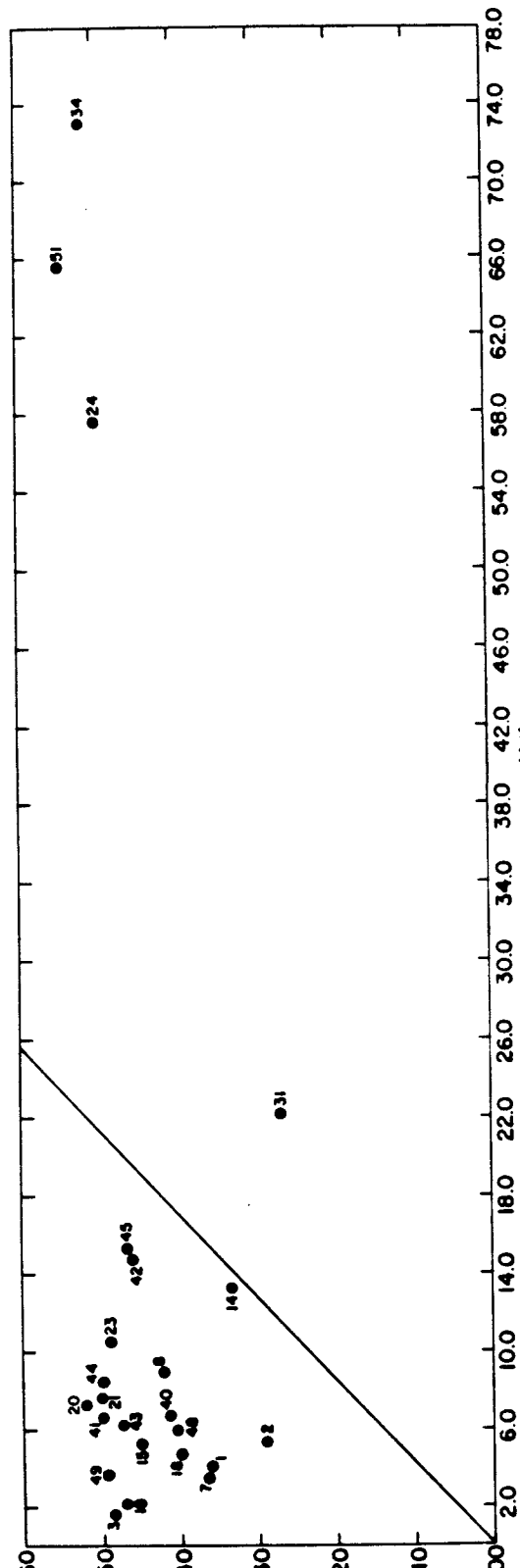

Fig. 50. La/Ce vs Zr/Nb plot of Cortlandt, Stony Point, and Rosetown samples. Chondritic abundances are represented by solid line.

Zr/Nb ratio very similar to that of the parent ($\sim$6 to 16). Ocean ridge basalts are not considered likely parents for granodiorite because of their extremely low potassium abundances. Crystal fractionation cannot appreciably change this Zr/Nb ratio because of the incompatibility of both Zr and Nb in most melts. Thus, it would seem that the high Zr/Nb values of the three granodiorite samples (24, 34, 51) cannot be the result of partial melting or differentiation processes.

In order to explain the origin of the Cortlandt region granodiorites, a successful model should explain the overall low incompatible element (REE, Zr, Nb) abundances of the granodiorites and also the unusually high Zr/Nb ratios (58-73). Several models were tested in order to reproduce the geochemical characteristics of the Cortlandt area granodiorites. These include: (1) partial melt of crustal rocks including basalts; (2) a granitic cumulate; (3) a residue from an aqueous fluid derived from silicate melts or rock; and (4) liquid immiscibility.

Arth and Hanson (1972) and Barker et al. (1976) have proposed that tonalites, trondhjemites, and granodiorites with slightly enriched REE patterns (Ce/Yb $\approx$ 10) and low HREE abundances could be generated from a parental basaltic source by partial melting having

garnet as a residual phase. While partial melting of eclogite may produce a liquid with a granitic composition and REE, Rb, and Sr abundances similar to those of the three Cortlandt region granodiorites, this model can explain neither the low Zr and Nb abundances of samples 24, 34, and 51 nor their high Zr/Nb ratios. Since most basalt compositions have Zr/Nb ratios of approximately 10 and Zr and Nb abundances of approximately 100 ppm and 12 ppm, respectively (Atherton and Tarney, 1979; Frey et al., 1978; Erlank and Kable, 1976), partial melting of this basic material will produce a liquid of granodiorite composition with Zr and Nb abundances much higher than those of the three granodiorites, and with a Zr/Nb ratio similar to that of the starting composition. Thus, the high Zr/Nb ratios of the three granodiorites, in addition to the low concentrations of these elements in these three samples, eliminate an origin by partial melting of eclogite.

Origin of these granodiorites through crystal accumulation from a typical granitic liquid was eliminated as a viable model for two reasons. First, the chilled granodiorite dike (sample 24) has major and trace element chemistry similar to the two plutonic granodiorites (samples 51 and 34); and second, the low HREE abundances of these three granodiorites suggests that

these samples would contain approximately 80% cumulate crystals. To effectively separate feldspar and quartz from a silica-rich melt, filter pressing is necessary due to the small density differences of the crystals and melt. There is no textural evidence in the coarse-grained granodiorites of any occurrence of filter pressing.

The distribution coefficient data of Flynn and Burnham (1978) and Wendlandt and Harrison (1978) for water-rich fluids originating either from a silicate melt or crustal rocks indicate that an aqueous fluid could have subparallel and significantly lower REE abundances than the parent. Productions of such liquids occur at pressures of 4-5 kb and at temperatures of 800-1000°C. Higher temperatures and pressures cause the aqueous fluid, because of higher K_d's, to be more enriched in REE than the parent. While an aqueous fluid could produce a composition with the major and REE abundances of the Cortlandt region granodiorites, the Zr-Nb data and the size of the granodioritic bodies indicate that these rocks did not originate by such a process. In order to explain the high Zr/Nb ratios of the three granodiorite samples, an aqueous fluid originating from a silicate melt or crustal rocks would have to preferentially incorporate Zr over Nb. The lack of

Zr and Nb partitioning data between fluid and silicate melt rock prevents adequate assessment of the Zr and Nb data. However, one study of an aqueous-rich pegmatite (Mikuszewski et al., 1976) reveals that Nb ($K_d \approx 10$) is preferentially enriched in the pegmatite. This suggests the possibility that Nb is more strongly partitioned into the H_2O-rich fluid than Zr. Hence, the aqueous fluid may have a lower Zr/Nb ratio rather than a higher ratio. The large size of the Peekskill ($\sim$6.5 sq. km) and the Rosetown ($\sim$1.5 sq. km) granodiorite plutons seems to make production from an aqueous fluid unlikely.

Recent studies of both lunar and terrestrial igneous rocks have shown that immiscibility is a petrogenetic process (Roedder and Weiblen, 1970, 1971, 1972; De, 1974; Philpotts, 1971, 1972, 1976, 1977; Eby, 1979; Cawthorn et al., 1979). Furthermore, there has been experimental confirmation of silicate liquid immiscibility in Skaergaard melts (McBirney and Nakamura, 1974; McBirney, 1975). Immiscibility in silicate melts has been shown to produce a basic iron-rich liquid and a high silica-rich liquid (Rutherford et al., 1974; Watson, 1976; Naslund, 1976; Ryerson and Hess, 1978). Recent two-liquid partition experiments for basaltic starting compositions indicate that the high-iron liquid is enriched

in high field strength cations (REE, P, Ba, Sr, Cr, Zr, and Mg) compared to the coexisting SiO_2-rich liquid (Watson, 1976; Ryerson and Hess, 1978; Dickinson et al., 1980; Danckwerth and Ryerson, 1980). The three Cortlandt region granodiorites (24, 34, 51) are characterized by low abundances of the high field strength cations. To test for a possible immiscibility relationship, granodiorite 51 was compared to diorite sample 49. These rock types were selected because their gradational contact in the field suggests a possible genetic relationship. Table 25 shows the two-liquid partition coefficient data ($D_{B/A}$) of Watson (1976) and Ryerson and Hess (1978) and the distribution of these same elements between the Rosetown diorite 49 and granodiorite 51. The two-liquid partition coefficient is defined:

$$D_{B/A} = \frac{\text{concentration in Basic (Fe-rich liquid)}}{\text{concentration in Acidic (SiO_2-rich liquid)}}$$

The distribution of elements between the Rosetown diorite and granodiorite are in excellent agreement with the experimental two-liquid partitioning model, especially for the REE, P, and Zr. While there is no experimental two-liquid partition data available for Nb, Watson (1976) has data for Ta, an element that is similar in size and charge to Nb. Watson's $D_{B/A}$ for Ta is

Table 25. Summary of Two-Liquid Partitioning Data ($D_{\underline{B}asic/\underline{A}cidic}$).

	a	b	c	d
Element				
K	0.45	0.21	0.67	0.79
Fe	2.18	4.02	8.20	8.6
Si	0.75	0.61	0.74	0.73
Mn	2.93	5.0	7	14
Ba	1.50	~1	0.81	
Sr	1.54	~1	1.99	
Mg	2.15	6.0	9.9	17.3
Cr	3.76		6.6	
Zr	2.36		2.2	
P	10.84	24.0	22	
V			12.3	
Ti	3.08	3.90	12.4	10.5
Rb		~ 1	0.97	
La	3.91	~10	4.5	3.5
Ce			4.9	4.2
Nd			5.6	4.7
Sm	4.42	~10	5.8	4.7
Eu			4.9	4.0
Gd			5.8	4.7
Dy		~10	6.0	5.1
Er			5.4	4.9
Yb		~10	4.4	4.5
Lu	4.18			

[a] *Experimental data of Watson (1976).*

[b] *Experimental data of Ryerson and Hess (1978).*

[c] $D_{B/A}$ *samples 49/51.*

[d] $D_{B/A}$ *samples 50/51.*

approximately 4.3 higher by approximately a factor of 2 than his value for Zr ($\sim$ 2.4). Hence, if Nb is distributed similarly to Ta during immiscibility, Nb will have a much greater affinity for basic (iron-rich) liquid than Zr. Because of these partitioning value differences between Zr and Nb, immiscibility can change the Zr/Nb ratios of the two end-member liquids. The silica-rich liquid should have low Zr and Nb abundances and a high Zr/Nb ratio. The Rosetown granodiorite and the other two granodiorite samples are characterized by low Zr (92 ppm) and Nb (1.4 ppm) abundances plus high Zr/Nb ratios (58-73). The Rosetown diorite, compared to the granodiorite, has high Zr (199 ppm) and Nb (53 ppm) abundances and a low Zr/Nb ratio (3.75). Zr and Nb data for both the granodiorite and diorite are consistent with an immiscibility model.

Immiscibility can also account for the REE distribution differences between these two Rosetown rock types. Two-liquid partitioning data (Table 25) shows that immiscibility of a basic parent produces two liquids with different overall REE abundances. The REE patterns of the two end-member liquids are subparallel, but the silica-rich liquid has REE abundances much lower than those of the iron-rich liquid. The actual REE abundance of either liquid depends upon the two-liquid partition

coefficient and the fraction of each melt formed. The silica-rich liquid, when it is an infinitesimal fraction of the parent, has REE abundances approximately $1/D_{(B/A)}$ those of the melt prior to melt separation. Larger fractions of silica-rich melt cause the REE abundances to approach those of the total melt. Two-liquid partitioning data for Sr (Table 25) suggests that when the parent melt has a significant Eu^{2+} component, the granitic melt has a positive Eu anomaly relative to the basic end-member liquid. Figure 51 from Hanson (1980) shows the calculated normalized REE patterns for immiscible alkaline liquids with a $D_{(B/A)}$ of 5 for all the trivalent REE and with Eu equal to 3.5. The parent melt in this calculation is split in a proportion of 3:1 (basic:acidic). From Fig. 51 it can be seen that the REE distributions produced by this immiscibility calculation are remarkably similar to those of the Rosetown diorite sample 49 and granodiorite sample 51.

Major element compositions of the Rosetown diorite and granodiorite have been plotted on the pseudoternary phase diagram (Fig. 52) SiO_2-Na_2O + K_2O + Al_2O_3-TiO_2 + Fe_2O_3 + FeO + MnO + MgO + CaO + P_2O_5 (Greig, 1972; Weiblen and Roedder, 1973; McBirney, 1975). This Greig diagram (Roedder, 1978) is well suited to the plotting

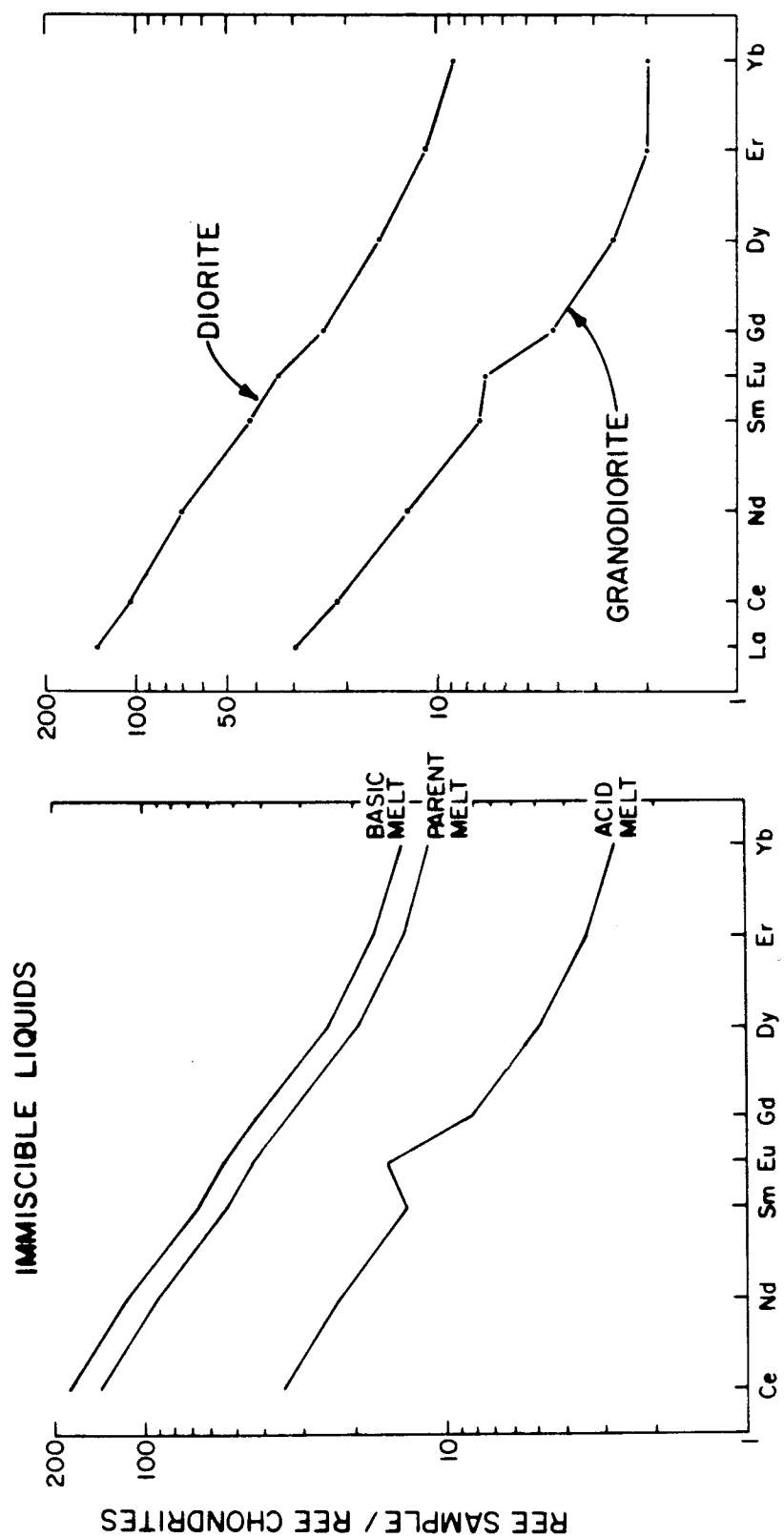

Fig. 51. Calculated chondrite-normalized rare-earth patterns for immiscible alkaline liquids compared with the chondrite-normalized Rosetown granodiorite and diorite rare-earth patterns. Calculated diagram from Hanson (1980). $D_{B/A}$ is 5 for all 3+ REE and 3.5 for Eu. 25% of the parent is acidic melt; 75% basic melt.

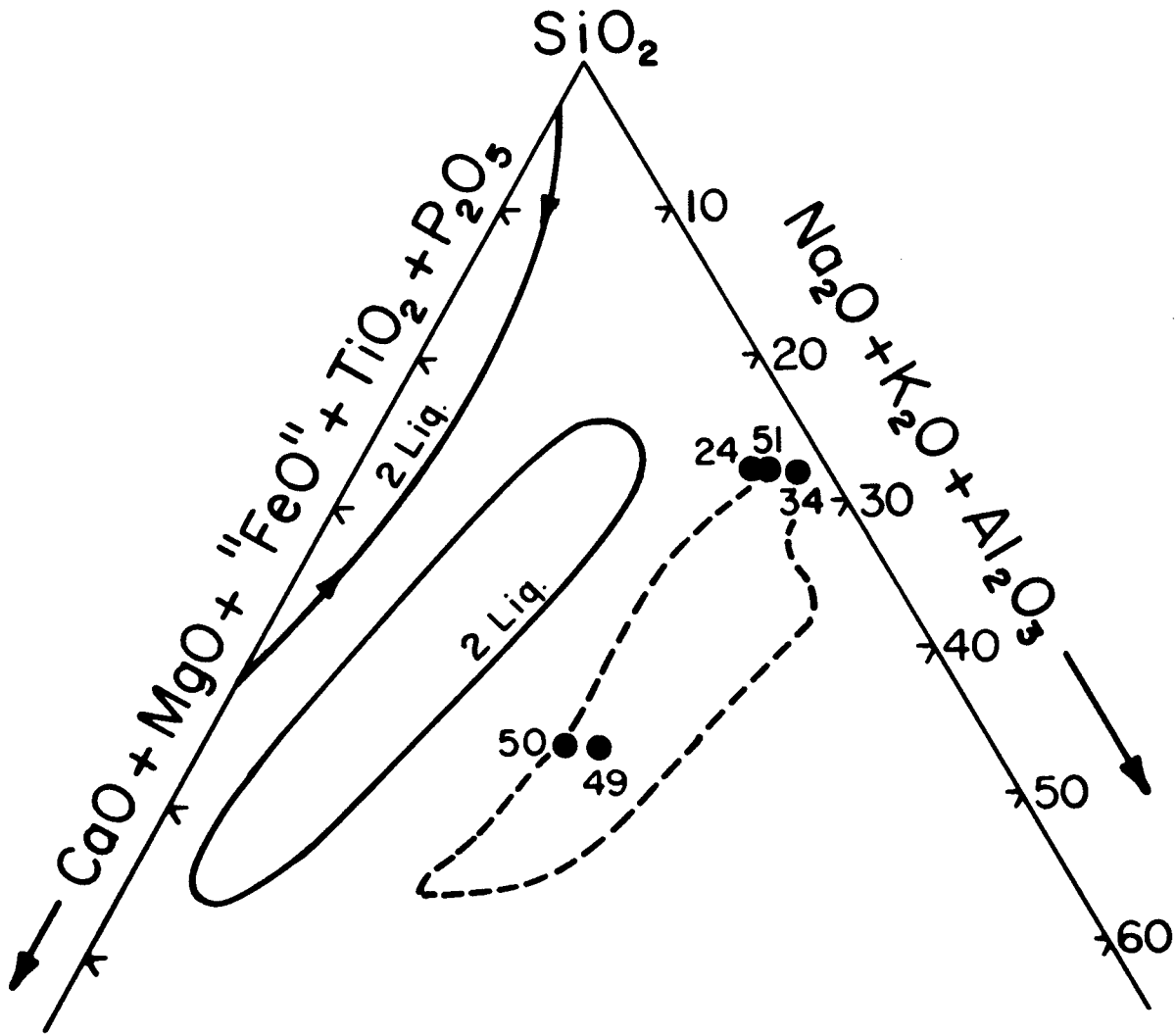

Fig. 52. Greig diagram showing field for immiscible terrestrial volcanic (broken line) and possible Cortlandt region immiscible end members.

of rocks exhibiting immiscibility. It groups together those elements that tend to be associated during magma splitting. Diorite sample 49 and granodiorite sample 51 plot within the immiscibility field of terrestrial volcanic samples that have demonstrable immiscibility (Roedder, 1978). This lends further support to the two-liquid hypothesis but does not confirm it. Phase chemical, isotopic, and textural data of the diorite and granodiorite are compatible with immiscibility. Bowen (1928) demonstrated that, in immiscible systems, any crystalline phase that is common between the two end-member liquids should have the same chemical composition. Phase chemistries of plagioclase and biotite in the granodiorite (An_{5-28}; Fe# 0.57-0.61) and diorite (An_{15-30}; Fe# 0.61-0.64) overlap. A similarity of isotopic values for these two samples would also strengthen an immiscibility model of origin. Unfortunately, Sr isotopic data has been collected only for granodiorite sample 51. However, the $^{87}Sr/^{86}Sr)_i$ of sample 51 (0.70505) is very similar to that of the Rosetown amphibole-pyroxenite sample 48 (0.70479) indicating that the diorite (49) might also be similar.

The presence of ocelli in the diorite and/or granodiorite would lend further support to the immiscibility hypothesis. However, as indicated by Roedder

(1978), if the process is truly effective and large scale, the best field evidence for immiscibility, ocelli, is probably eliminated. Any large mass of magma undergoing immiscibility under plutonic conditions will generally have sufficient time for the two conjugate liquids to cleanly separate from each other.

Basic inclusions ranging from less than 1 mm to several centimeters occur near the granodiorite-diorite contact (Fig. 53). These inclusions have been interpreted as diorite cognate xenoliths incorporated by the intruding granodiorite magma (Ratcliffe, unpublished data). This may be a correct interpretation. However, these fine-grained diorite inclusions may also represent basic ocelli trapped in the silica-rich liquid. Many of the smaller diorite inclusions are spherical; thus, they could be immiscible globules. However, many of the larger inclusions have distorted angular shapes consistent with a xenolithic model. A textural feature of these larger inclusions is the presence of inward pointing cusps around their margins (Fig. 53). Such textural features have been noted in immiscible globules (Cawthorn _et al._, 1979; Hess, personal communication) that have formed from liquids which contained significant amounts of crystals. In these cases, the points (peaks) of the cusps point towards the silica-rich liquid. This

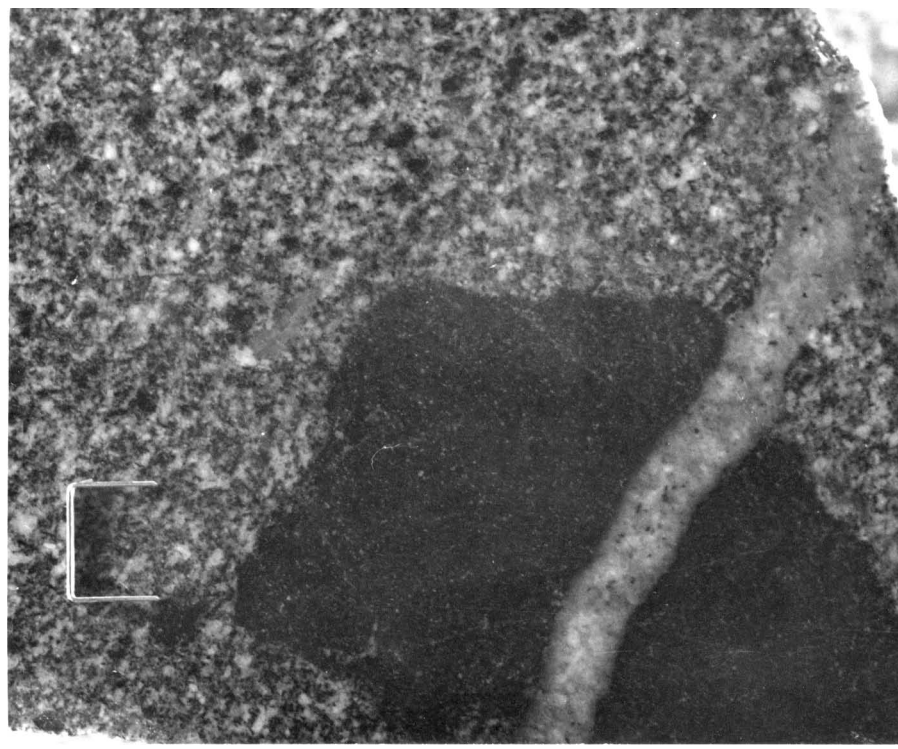

Fig. 53. Photograph of diorite (dark area) in clusions in granodiorite. Large inclusion and granodiorite sample are both crosscut by granitic dike. Scale in lower left corner is 1.1 cm in length.

is also true of the Rosetown diorite inclusion (Fig. 53).

One large angular diorite inclusion (sample 50) was separated from the granodiorite and analyzed for major and REE abundances (Tables 1 and 3). This diorite inclusion has REE abundances similar to those of sample 49, but sample 50 is less fractionated. Sample 50 might then represent the composition of the basic (iron-rich) immiscible liquid immediately after separation but before it underwent fractionation to form diorite sample 49.

The distribution of major and trace elements between diorite sample 49 and granodiorite sample 50 (Table 25) are consistent with a relationship through silicate liquid immiscibility. However, a xenolith origin for the basic inclusions is not eliminated.

It should be noted that both alkalis (Roedder, 1978; Vissor and Koster Van Gross, 1979) and increased pressure (Watson and Naslund, 1977) enhance silicate liquid immiscibility. At Rosetown, the probable parent was an alkali basalt similar in composition to the amphibole-pyroxenite 40P. The presence of both end-member liquids at Rosetown suggests that the immiscibility event happened very near to the original depth of the emplacement site. Large differences in specific gravities between the basic- and silica-rich magma

would tend to cause these two melt fractions to be widely separated. The lack of a basic conjugate liquid associated with the Peekskill granodiorite may be the result of such density differences. The end-member basic melt at this locality, because of its higher specific gravity, could not rise to the same elevation as the silica-rich fraction (Peekskill granodiorite).

In summary, the three Cortlandt region granodiorite samples are characterized by low incompatible trace element abundances and unusually high Zr/Nb ratios. To explain the geochemistry of the granodiorites, models such as partial melting of eclogite, crystal accumulation and aqueous fluids were examined. These three models were able to explain some, but not all, of the trace element data, most especially the Zr/Nb ratios of these samples. A fourth model, silicate liquid immiscibility was able to explain all the chemical characteristics of the granodiorite samples. At Rosetown, the granodiorite and diorite rock types are believed to be related to such an immiscibility process. Phase chemistry, textural features, and Sr isotopes of the Rosetown diorite and granodiorite are consistent with an immiscibility hypothesis.

PETROGENESIS OF THE SALT HILL EMERY AND QUARTZ-FELDSPATHIC ROCKS

Emery from the Salt Hill emery mine, located within the eastern clinopyroxenite pluton six of the Cortlandt complex, is characterized by low silica (29.2 wt.%), low alkalis (Na_2 ≈ 1.11 wt.%; K_2O ≈ 1.13 wt.%), high alumina (30.4 wt.%), and high ferric iron (18.6 wt.%) (Table 1, sample 37). As a consequence, the emery is quartz (4.6%), corundum (2.02%), and hematite (8.1%) normative (Table 2). This emery is a product of the reactions between an original pelitic schist country rock inclusion and the parent magma of the cumulate clinopyroxenite. Because the major and REE element abundances of most pelitic material is very similar (Haskin et al., 1968; Nance and Taylor, 1976), the REE abundances of sample 45 (Table 3), a nearby pelitic schist, are believed to reasonably approximate those of the pristine pelitic xenolith. Comparison of the REE patterns (Fig. 46) of sample 45 to those of the Salt Hill emery (sample 37) eliminate the possibility that the emery was formed through a partial melting process. Partial melting of a pelitic parent, similar to sample 45, would have caused a strong depletion of the LREE in the residual emery. This is not observed in sample 37 (Fig. 46). Instead, the REE patterns of both the schist and emery are parallel in the LREE and

MREE. However, the HREE are depleted in the emery relative to the pelitic schist. Lowering of the HREE abundances of the emery is unexpected since the emery contains a substantial amount ($\sim$ 20%) of almandine garnet, a phase that, if present during emery formation, would be expected to retain the HREE. Thus, it would seem that the process that caused the formation of emery from pelitic country rock was able to remove SiO_2, Na_2O, K_2O, and HREE, while leaving alumina, iron, titania, and LREE and MREE. Since a partial melting process is excluded, the best explanation for the production of the Salt Hill emery would be a metasomatic process involving H_2O-rich fluids. Such an aqueous solution, originating either from the pelitic schist or surrounding magma, passed through the xenolith, transporting Si, K, Na, and HREE away from the pelitic schist.

Since the many quartz-feldspathic veins and dikes present at Salt Hill (Fig. 29) might represent products of this metasomatic process, one of these dikes (sample 36) was analyzed for major and trace elements (Tables 1 and 3). This quartz-feldspathic dike consists essentially of silica (90.5%) with minor amounts of quartz. feldspar, almandine garnet, and chlorite. The REE pattern (Fig. 46) for this sample 36 is quite unusual in that it is concave upward in its LREE and MREE

abundances, and then flattens in the HREE abundances. If the quartz-feldspathic dike (36) represents aqueous fluid produced from the pelitic schist at a temperature between 800 and 1000°C, and a pressure of approximately 4 kb, the aqueous fluid experimental data (Wendlandt and Harrison, 1978; Flynn and Burnham, 1978) indicates that the REE concentrations of the H_2O-rich fluid should be much lower than that of the parent rock. Hence, using the experimental data of Wendlandt and Harrison (1978) and Flynn and Burnham (1978), REE abundances for an aqueous fluid eminating from a pelitic schist such as sample 45 were estimated to be subparallel to the pelite and contain approximately 10% of the REE abundances of the parent pelitic schist. The REE abundances of sample 36 can be modelled (Table 26) from this calculated aqueous fluid if garnet crystallized from the H_2O-rich solution and was a cumulate phase. Sample 36 does contain approximately 5 modal % almandine garnet. Since the mineral-fluid partition coefficients of garnet are much higher than those of garnet-silicate melt (Cullers et al., 1973; Flynn and Burnham, 1978), the K_d's of garnet used to model sample 36 were increased by a factor of 2.5 over those listed in Table 5. Calculations (Table 26) reveal that accumulation of ∿ 5% garnet and 98% aqueous fluid results in a composition that has a concave upward,

Table 26. Sample #36 Quantitative Modelling.

	a	b	c	#36 Sample
REE Normalized				
La	16.0	0.45	15.6	15.5
Ce	9.4	0.88	9.34	8.54
Nd	5.8	1.32	5.89	5.29
Sm	3.8	6.65	4.87	5.21
Eu	4.2	3.75	4.87	5.40
Gd	2.4	26.2	5.42	6.98
Dy	1.9	71.5	8.60	8.68
Er	1.5	92.5	8.36	8.22
Yb	1.4	100	8.33	7.98

[a] *Estimated REE compositions of an aqueous fluid from pelitic sample #45.*

[b] *Estimated mineral-fluid Kd's for garnet used in modelling calculations.*

[c] *5% cumulate garnet crystallized from composition a plus 95% of a.*

[d] *Sample #36 present REE values.*

dipper-shaped, REE pattern very similar to that of sample 36. Since it appears that the quartz-feldspathic dike (36) may indeed be the product of an aqueous fluid produced from the pelitic xenolith, the process that produced this fluid-rock may also be responsible for the formation of the emery. Re-circulation of this aqueous fluid through the xenolith after it has precipitated garnet, could be responsible for the depleted HREE abundances of the Salt Hill emery compared to those of the original pelitic schist.

TECTONIC SETTING

This investigation has primarily emphasized the chemical and petrogenetic affinities of the Cortlandt alkalic suite, but the nature of the tectonic environment at the time of emplacement of the Cortlandt plutons presents a problem. In general, alkali basalts and related rock types (kimberlites, carbonatites and highly potassic rocks) are associated with the initiation of continental rifts, two examples being the East African rift system and the Rhine graben. This relationship of mantle derived alkalic magmas to extensional tectonic features, contrasts with Ratcliffe's (1968, unpublished data) conclusion that the Cortlandt suite was generated and extruded late in the Taconic cycle of southeastern New York. Plate convergence during the Taconic indicates a compressional tectonic framework along the margin of the North American continent. The prevalent interpretation (R. Stanley and N. Ratcliffe, personal communication) is that the Taconic orogeny represents the convergence of the North American craton with an island arc overlying an eastward dipping subduction zone. The volcanic arc apparently developed 200 kilometers to the east of the present location of the Cortlandt plutons. Geochemical data of the Cortlandt

suite reveals that with the possible exception of the Stony Point diorite (eclogite parent), all the Cortlandt magmas were not partial melts of an oceanic crustal slab. Rather a better source for the primary alkali basalt would have been an undepleted mantle peridotite. This alkalic parental magma was emplaced into the crust where it underwent differentiation, crustal contamination, and liquid immiscibility.

A modern convergent tectonic setting where alkali basalts are being extruded is in the Lake Van region of Turkey, which lies in the convergence zone of the Anatolian-Iranian mass (Eurasian plate) and the Arabian plate. At this locality contemporaneous calc-alkaline and alkaline volcanism co-exist (Innocenti et al., 1976 and 1980). These calc-alkaline rocks are believed to be derived from magmas generated during the subduction process, while the alkaline volcanics are believed to be mantle derived (Innocenti et al., 1976, 1980). These alkaline volcanics, which are located above a former Benioff zone, are related to tensional tectonic stresses that affected the Lake Van region immediately after continental collision (Innocenti et al., 1976). The waning of calc-alkaline magmatism and the onset of alkaline volcanism in the Lake Van area, marks the end

of oceanic crustal subduction and the introduction of new mantle related magmatic-tectonic processes.

Although the Lake Van and Cortlandt geotectonic settings are not identical, both are characterized by alkaline magmatism, basaltic compositions rarely found associated with convergent plate areas. Emplacement of these mantle-derived alkali melts at these two localities may be a consequence of unusual tectonic conditions that initiated partial melting of the mantle and/or provided the necessary conduits to the surface.

SUMMARY

The parental magma of the Cortlandt region plutons is similar in major and trace element composition to several primary alkali basalts (1)*. These basic liquids and the Cortlandt parental magma seem to be partial melts of mantle peridotite having garnet as a residual phase (2). The Cortlandt alkali basalt parent, which is similar in chemical composition to the present-day amphibole-pyroxenite, underwent fractionation in two steps. The first minerals fractionated were olivine, clinopyroxene, orthopyroxene (3). These were later followed by kaersutite, plagioclase, and biotite (5) which formed gabbroic (6) and dioritic liquids (8). The different rock types found within the various plutons of the three complexes are the end products of these differentiation events. The presence of many diverse rock types in such close proximity is indicative of the complexity of the magmatic plumbing system during the time of emplacement.

Many of the rock types in these plutons were successfully modelled from the parental composition, showing the extent of the differentiation and crystal

*The proposed evolution of the Cortlandt, Stony Point, and Rosetown complexes is summarized in Fig. 54. Numbers in parentheses in this section of the text refer only to corresponding numbers in Fig. 54.

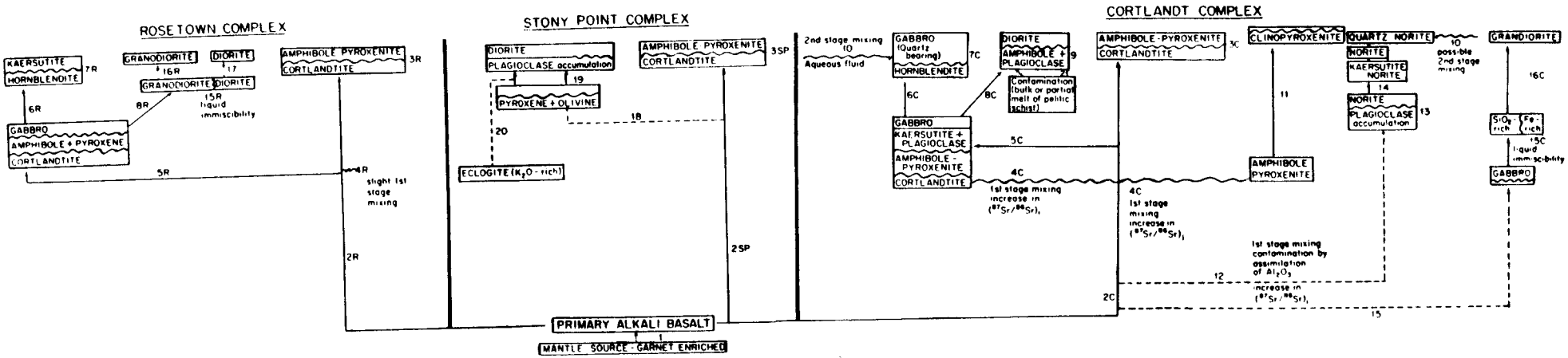

Fig. 54. Summary of the possible evolution of the Cortlandt region. The vertical dimensions crudely represent depth, the horizontal crudely represent the geographical location of the various intrusive types. Duplicate numbers correspond to similar events and are identified according to complex (R = Rosetown; SP = Stony Point; C = Cortlandt).

accumulation processes. These calculated models suggest that many of the cortlandtite (3), clinopyroxenite (11) hornblendite (7), and diorite (9) samples contain small amounts of trapped interstitial liquid and that a few samples may be two-phase adcumulates lacking intercumulus melt (7, 9, 14). The quantitative modelling calculations suggest also that many of the differentiated rocks have major and trace element abundances too high to be explained by any fractionation scheme. Hence, this enrichment of the major (SiO_2, K_2O, Na_2O) and trace (Rb, Ba, LREE) elements of the differentiating magma is the result of mixing with an aqueous fluid, which originated from the pelitic country rock (10).

Strontium isotopes indicate that this proposed country rock component contained only small amounts of Sr since the $^{87}Sr/^{86}Sr)_i$ of these plutons, with the exception of pluton 2, are very similar. Sr isotopic data, however, do indicate that the norite, diorite, and gabbroic magmas of the Cortlandt complex apparently underwent crustal contamination before emplacement, probably at an intermediate level (4). This first stage mixing event is believed to be responsible for higher $^{87}Sr/^{86}Sr)_i$ ratios of these bodies compared to the parental amphibole-pyroxenite. However, because of the

success in relating the earlier formed rocks of the diorite and gabbro plutons to the parental composition, it is believed that this first stage mixing event, while changing the isotopic systematics, did not appreciably change the major and trace element chemistries of these magmas before emplacement. Yet, the inability to directly relate the norites to the parental composition suggests that the parental magma of the norites had its chemistry significantly altered by this first-stage mixing event (12). Bulk assimilation and/or partial melts from aluminous-rich crustal rocks modified not only the Sr isotopes of the norite liquids but also the original major (SiO_2, Al_2O_3, Na_2O, K_2O, CaO) and trace (REE, Rb, Sr, Ba) element compositions of the norites, thereby creating a hybrid magma (13). Cumulate and differentiated compositions within the norite pluton were determined by quantitative modelling of a norite composition (14).

The trace element abundances of the granodiorite plutons of the Cortlandt region suggest that these silica-rich plutons formed as a result of liquid immiscibility from a basic alkali magma (15). The granodiorite plutons are related to the same source and have unusual trace element characteristics (16). At Rosetown, the basic end member liquid (17) of the immiscibility process was also

emplaced.

At Stony Point, the diorite is either related to the parental liquid by fractional crystallization of pyroxene and olivine at depth (18, 19) or by a partial melt of eclogite (20).

Albee, A. L., and Ray, L., 1970. Correction factors for electron probe microanalysis of silicates, oxides, carbonates, phosphates, and sulfates. Anal. Chem., 42, 1408-1414.

Allen, J. C., Boettcher, A. L., and Marlard, 1975. Amphiboles in andesite and basalt: I, Stability as function of P-T-fO_2. Amer. Mineral., 60, 1069-1085.

Arth, J. G., Barker, F., Peterman, Z. E., and Friedman, I., 1978. Geochemistry of the Gabbro-Diorite-Tonalite-Trondhjemitic suite of southwest Finland and its implications for the origin of tonalitic and trondhjemitic magmas. Jour. Petrol. 19, 289-316.

_____, and Barker, F., 1976. Rare-earth partitioning between hornblende and dacitic liquid and implications for the genesis of trondhjemitic-tonalitic magmas. Geology, 4, 534-536.

_____, and Hanson, G. N., 1972. Quartz diorites derived by partial melting of eclogite or amphibolite at mantle depths. Contrib. Mineral. Petrol., 37, 161-174.

_____, and Hanson, G. N., 1975. Geochemistry and origin of the early Precambrian crust of Northeastern Minnesota. Geochim. Cosmochim. Acta, 39, 325-362.

Atherton, M. P., and Tarney, J., 1979. Origin of granite batholiths: Geochemical Evidence. Univ. of Liverpool and Univ. of Birmingham. 148 pp.

Ayuso, R. A., Bence, A. E., and Taylor, S. R., 1976. Upper Jurassic tholeiitic basalts from DSDP Leg 11. J. Geophys. Res., 81, 4305-4325.

Balk, R., 1927. Die primäre struktur des Noritmassivs von Peekskill am Hudson Nördlish New York. Neues Jahrb. Min., Berlageband, 57, 249-303.

_____, 1937. Structural behavior of igneous rocks. Geol. Soc. Amer., Mem. 5, 177 pp.

Barker, F., 1964. Reaction between mafic magmas and pelitic schist, Cortlandt, N. Y. Am. J. Sci., 262, 614-634.

_____, Arth, J. G., Peterman, Z. E., and Friedman, I., 1976. The 1.7 to 1.8 G.y.-old trondhjemites of southeastern Colorado and northern New Mexico: Geochemistry and depths of genesis. Geol. Soc. Amer. Bull., 87, 189-198.

Bence, A. E., and Albee, A. L., 1968. Empirical correction factors for the electron microanalysis of silicates and oxides. J. Geol., 76, 382-403.

Bird, M. L., 1971. Distribution of trace elements in olivines and pyroxenes--an experimental study. Ph.D. thesis, Univ. of Missouri, Rolla, 249 pp.

Bowen, N. L., 1922. The behavior of inclusions in igneous magmas. J. Geol., 30, 513-570.

_____, 1928. The Evolution of the Igneous Rocks. Princeton University Press, N. J., 332 pp.

Bryan, W. B., Finger, L. W. and Chayes, F., 1969. Estimating proportions in petrographic mixing equations by least-squares approximatien. Science, 163, 926-927.

Butler, J. W., 1936. Origin of the emery deposits near Peekskill, N. Y. Am. Mineral., 21, 537-574.

Caporuscio, F. A., and Morse, S. A., 1978. Occurrence of sapphirine plus quartz at Peekskill, N. Y. Am. J. Sci., 278, 1334-1342.

Cawthorn, R. G., and O'Hara, M. J., 1976. Amphibole fractionation in calc-alkaline magma genesis. Am. J. Sci., 276, 309-329.

Cawthorn, R. G., and Brown, P. A., 1976. Proposed phase re - lations to explain corundum-normative magmas and garnets in silica-rich igneous rocks. J. Geol., 84, 467-476.

_____, Strong, D. F., and Brown, P. G., 1976. Origin of corundum-normative intrusive and extrusive magmas. Nature, 259, 102-104.

_____, McIver, J. R., McCarthy, T. S., Wyatt, B. A., Ferguson, J., and Barnes, S. J., 1979. Possible liquid immiscibility textures in high-magnesia basalts from the Ventersdorp Supergroup, South Africa. J. Geol., 87, 105-113.

Cullers, R. L., Medaris, L. G., and Haskin, L. A., 1973. Experimental studies of the distribution of rare earth or trace elements among silicate minerals and liquids and water. Geochim. Cosmochim. Acta, 37, 1499-1512.

Dale, I. M., and Henderson, P., 1972. The partition of transition elements in phenocryst-bearing basalts and the implications about melt structure. 24th Inter. Geol. Cong. Proc., 10, 105-111.

Dallmeyer, R. D., 1970. $^{40}Ar/^{39}Ar$ release spectra of biotite and hornblende from the Cortlandt and Rosetown plutons, N. Y., and their regional implications. J. Geol., 83, 629-643.

Dana, J. D., 1881. Origin of the rocks of the Cortlandt series. Am. J. Sci., 22, 103-112.

Danckwerth, P. A., and Ryerson, F. J., 1980. REE partitioning between coexisting silicate liquids. EOS, 61, 398.

De, A., 1974. Silicate liquid immiscibility in the Deccan traps and its petrogenetic significance. Geol. Soc. Amer. Bull., 85, 471-474.

Dickinson, J. E., Hess, P. C., and Rutherford, M. J., 1980. REE partitioning between zircon, whitlockite, and two liquids. EOS, 61, 397.

Drake, M. J., 1972. The distribution of major and trace elements between plagioclase feldspar and magmatic silicate liquid: An experimental study. Ph.D. thesis, Eugene, Univ. Oregon, 190 pp.

_____, 1975. The oxidation state of europium as an indicator of oxygen fugacity. Geochim. Cosmochim. Acta, 39, 55-64.

_____, and Weill, D. F., 1975. Partition of Sr, Ba, Ca, Y, Eu^{2+}, Eu^{3+}, and other REE between plagioclase, feldspar, and magmatic liquid: An experimental study. Geochim. Cosmochim. Acta, 39, 689-712.

Eby, G. N., 1979. Mount Johnson, Quebec--An example of silicate-liquid immiscibility? Geology, 7, 491-494.

Erlank, A. J., and Kable, E. J. D., 1976. The significance of incompatible elements in mid-Atlantic Ridge basalts from 45°N with particular reference to Zr/Nb. Contrib. Mineral. Petrol., 54, 281-291.

Evans, B. W., 1964. Fractionation of elements in the pelitic hornfelses of the Cashel-Lough Wheelann intrusion, Connemora, Eire. Geochim. Cosmochim. Acta, 28, 127-156.

Ferry, J. M., and Spear, F. S., 1978. Experimental calibration of the partitioning of Fe and Mg between biotite and garnet. Contrib. Mineral. Petrol., 66, 113-117.

Flanagan, F. J., 1972. Values for international geochemical reference samples. Geochim. Cosmochim. Acta, 37, 1189-1200.

Flynn, R. T., and Burnham, C. W., 1978. An experimental determination of rare earth partition coefficients between a chloride containing vapor phase and silicate melts. Geochim. Cosmochim. Acta, 42, 682-701.

Frey, F. A., Green, D. H., and Roy, S. D., 1978. Integrated models of basalt petrogenesis: A study of quartz tholeiites to olivine nelilitites from South Eastern Australia utilizing geochemical and experimental petrological data. J. Petrol., 19, 463-513.

Friedman, G. M., 1952. Sapphirine occurrence of Cortlandt, N. Y., Am. Mineral., 37, 244-249.

_____, 1954. The spinel-silica reaction succession: A study of incompatible mineral phases. J. Geol., 62, 366-374.

_____, 1956. The origjn of spinel-emery deposits with particular reference to those of the Cortlandt Complex, N. Y.,

Green, D. H., 1970. The origin of basaltic and nephelinitic magmas. Trans. Leicester Lit. Phil. Soc., 64, 28-54.

_____, Edgar, A. D., Beasley, P., Kiss, E., and Ware, N. G., 1974. Upper mantle source for some hawaiites, muglarites, and fenmorlites. Contr. Mineral. Petrol., 48, 33-43.

Green, T. H., Ringwood, A. E., 1968. Origin of garnet phenocrysts in calc-alkaline rocks. Contrib. Mineral. Petrol., 18, 163-174.

_____, 1972. Crystallization of calc-alkaline andesite under controlled high-pressure hydrous conditions. Contrib. Mineral. Petrol., 34, 150-166.

Green, T. H., 1977. Garnet in silic liquids and its possible use as a P-T indicator. Contrib. Mineral. Petrol., 65, 59-67.

Greenland, L. P., 1970. An equation for trace element distribution during magmatic crystallization. Am. Mineral., 55, 455-465.

Greig, J. W., 1927. Immiscibility in silicate melts. Am. J. Sci., 13, 1-44, 133-154.

Gribble, C. D., and O'Hara, M. J., 1967. Interaction of basic magma with pelitic materials. Natute (London), 214, 1198-1201.

Griffen, W. L., and Murthy, V. R., 1969. Distribution of K, Rb, Sr, and Ba in some minerals relevant to basalt genesis. Geochim. Cosmochim. Acta, 33, 1389-1414.

Grover, J. E., and Orville, P. M., 1969. The partitioning of cations between co-existing single- and multi-site phases with application to the assemblages: Orthopyroxene-clinopyroxene and clinopyroxene-olivine. Geochim. Cosmochim. Acta, 33, 205-226.

Guitzeck, M. W., Kridelbaugh, S. J., and Weill, D. F., 1974. The distribution of Sr and REE between diopside and silicate liquid. Geophys. Res. Lett., 1, 273-275.

Hanson, G. N., 1980. Geochemical constraints on the evolution of the early continental crust. Phil. Trans. Royal Soc. (in press).

_____, 1978. The application of trace elements to the petrogenesis of igneous rocks of granitic composition. Earth Planet. Sci. Lett., 38, 26-43.

_____, 1977. Geochemical evolution of the suboceanic mantle. J. Geol. Soc., 134, 235-253.

_____, 1976. Rare earth element analysis by isotope dilution. Natl. Bur. Stand. Spec. Publ., 422, 937-949.

_____, Goldich, S. S., Arth, J. G., and Yardley, D. H., 1971. Age of the early Precambrian rocks of the Sagnaga Lake-Northern Light Lake Area, Ontario-Minn., Can. J. Earth Sci., 8, 1110-1124.

Haskin, L. A., Frey, F. A., Schmitt, R. A., and Smith, R. H., 1966. Meteoritic, solar, and terrestrial rare earth distributions. Phys. Chem. Earth., 7, 167-321.

_____, Haskin, M. A., and Frey, F. A., 1968. Relative and absolute terrestrial abundances of the rare earths. In: Origin and Distribution of the Elements, ed. L. H. Ahrens, Oxford: Pergamon. pp. 889-912.

Helz, R. T., 1973. Phase relations of basalts in their melting range at P_{H_2O} = 5 kb as a function of oxygen fugacity. Part 1. Mafic phases. J. Petrol., 14, 249-302.

Higuchi, H. and Nagasawa, H. (1969). Partition of trace elements between rock-forming minerals and the host volcanic rocks. Earth Planet. Sci. Lett., 7, 281-287.

Huebner, J. S., Lipin, B. R., and Wiggins, L. B., 1976. Partitioning of chromium between silicate melts. Proc. Seventh Lunar Sci. Conf., 1195-1220.

Innocenti, F., Mazzuoli, R., Pasquare, G., Radicati di Brozolo, F., and Villari, L., 1976. Evolution of the volcanism in the area of interaction between the Arabian, Anotolian, and Iranian plates (Lake Van, Eastern Turkey). J. Volcan. Geotherm. Res., 1, 103-112.

_____, Mazzuoli, R., Pasquare, G., Servi, G., and Villari, L., 1980. Geology of the volcanic area north of Lake Van (Turkey). Geol. Rudsh., 69, 292-323.

Irving, A. J., 1978. A review of experimental studies of crystal-liquid trace element partitioning. Geochim. Cosmochim. Acta, 42, 743-770.

Irvine, T. N., 1975. The silica immiscibility effect in magmas. Carnegie Inst. Wash. Year Book, 74, 484-492.

_____, and Baragar, W. R. A., 1971. A guide to the chemical classification of common volcanic rocks. Can. J. Earth Sci., 8, 523-548.

Jackson, E. D., 1971. The origin of ultramafic rocks by cumulus processes. Fortschr. Mineral., 48, 128-174.

Jensen, B. B., 1973. Patterns of trace element partitioning. Geochim. Cosmochim. Acta, 37, 2227-2242.

Kay, R. W., and Gast, P. W., 1973. The rare earth content and origin of alkali-rich basalts. J. Geol., 81, 653-683.

Kemp, J. F., 1888. On the Rosetown extension of the Cortlandt series. Am. J. Sci., 36, 247-253.

Leeman, W. P., 1974. Petrology of basaltic lavas from the Snake River Plain, Idaho (Pt. 1), and Experimental determination of partitioning of divalent cations between olivine and basaltic

liquid (Pt. 2). Ph.D. thesis, Eugene, Univ. Oregon, 337 pp.

_____, 1976. Petrogenesis of McKinney (Snake River) olivine tholeiite in light of rare-earth element and Cr/Ni distributions. Geol. Soc. Am. Bull., 87, 1582-1586.

_____, and Scheidegger, K. F., 1977. Olivine/liquid distribution coefficients and a test for crystal-liquid equilibrium. Geol. Soc. Am. Bull., 35, 247-257.

Lindstrom, D. J., 1976. Experimental study of the partitioning of the transition metals between clinopyroxene and coexisting silicate liquid. Ph.D. thesis, Univ. of Oregon, Eugene.

_____, and Weill, D. F., 1978. Partitioning of transition metals between diopside and coexisting silicate liquids. I. Nickel, cobalt, manganese. Geochim. Cosmochim. Acta, 42, 817-832.

Long, L. E., and Kulp, J. L., 1962. Isotopic age study of the metamorphic history of the Manhattan and Reading prongs. Geol. Soc. Am. Bull., 73, 969-996.

McBirney, A. R., 1975. Differentiation of the Skaergaard Intrusion. Nature, 253, 691-694.

_____, and Nakamura, Y., 1974. Immiscibility in late-stage magmas of the Skaergaard Intrusion. Carnegie Inst. Wash. Year Book, 73, 348-352.

_____, and Noyes, R. M., 1979. Crystallization and layering of the Skaergaard Intrusion. J. Petrol., 20, 487-554.

McCallum, I. S., and Charette, M. P., 1978. Zr and Nb partition coefficients: Implications for the genesis of mare basalts, KREEP, and sea floor basalts. Geochim. Cosmochim. Acta, 42, 859-869.

McCarthy, T. S., and Hasty, R. A., 1976. Trace element distribution patterns and their relationships to the crystallization of granitic melts. Geochim. Cosmochim. Acta, 40, 1351-1358.

McKay, G. A., and Weill, D. F., 1977. KREEP petrogenesis revisited. Proc. Eighth Lunar Sci. Conf. 2339-2355.

Mysen, B., 1976. Partitioning of samarium and nickel between olivine, orthopyroxene, and liquid; preliminary data at 20kbar and 1025°C. Ibid., 31, 1-7.

Masuda, A., Nakamura, N., and Tanaka, T., 1973. Fine structures of mutually normalized rare-earth patterns of chondrites. Geochim. Cosmochim. Acta, 37, 239-248.

Mazzullo, L. J., and Bence, A. E., 1976. Abyssal tholeiites from DSDP Leg 34: The Nazca Plate. J. Geophys. Res., 81, 4327-4351.

Mikuszewski, J., Kanasiewicz, J., and Jeczmyk, M., 1976. Beryllium, tin, lithium, niobium, and elements of rare earths in pegmatites and other crystalline rocks of the Gary Sowee (Mts.) the Sudetes. Geol. Inst. Warsaw, In: The Current Metallogenic Problems of Central Europe, pp. 289-303.

Mose, D. G., Ratcliffe, N. M., Odom, A. L., and Hayes, J., 1976. Rb-Sr geochronology and tectonic setting of the Peekskill pluton, southeastern N. Y. Geol. Soc. Am. Bull., 87, 361-365.

Nagasawa, H., 1970. Rare earth concentrations in zircons and apatites and their host dacites and granites. Earth Planet. Sci. Lett., 9, 359-364.

_____, and Schnetzler, C. C., 1971. Partitioning of rare-earth, alkali and alkaline earth elements between phenocryst and acidic igneous magma. Geochim. Cosmochim. Acta, 35, 953-968.

Nance, W. B., and Taylor, S. R., 1976. Rare earth element patterns and crustal evolution. I. Australian post-Archean sedimentary rocks. Geochim. Cosmochim. Acta, 40, 1539-1551.

Naslund, H. R., 1976. Liquid immiscibility in the system $KAlSi_3O_8$-$NaAlSi_3O_8$-FeO-Fe_2O_3-SiO_2 and its application to natural magmas. Carnegie Inst. Wash. Year Book, 75, 592-597.

Neumann, H., Mead, J. and Vitaliano, C. J., 1954. Trace element variations during fractional crystallization as calculated from the distribution law. Geochim. Cosmochim. Acta, 40, 1539-1531.??

Nicholls, I. A., 1974. A direct fusion method of preparing silicate glasses for energy dispersive electron microprobe analysis. Chem. Geol., 14, 141-157.

Nockolds, S. R., 1941. The Garabal Hill-Glen Fyne igneous complex. Quart. J. Geol. Soc. London, 96, 451-511.

O'Hara, M. J., 1968. The bearing of phase equilibria studies in synthetic and natural systems on the origin and evolution of basic and ultrabasic rocks. Earth Sci. Rev., 4, 69-133.

Onuma, N., Higuchi, H., Walsita, H., and Nagasawa, H., 1968. Trace element partitioning between two pyroxenes and the host lava. Earth Planet. Sci. Lett., 5, 47-51.

Paige, S., 1956. Cambro-Ordovecian Age of the Inwood limestone and Manhattan Schist near Peekskill, N. Y. Geol. Soc. Amer. Bull, 67, 391-394.

Papike, J. J., Cameron, K. L., and Baldwin, K., 1974. Amphiboles and pyroxenes: Characterization of OTHER than quadrilateral components and estimates of ferric iron from microprobe data. Geol. Soc. Amer. Abstr. Progr., 6, 1053-1054.

Peterman, Z. E., Carmichael, I. S. E., Coleman, R. G., and Snavely, P. D., 1967. $^{87}Sr/^{86}Sr$ ratios in some eugeosynclinal sedimentary rocks and their bearing on the origin of granitic rocks in Orogenic Belts. Earth Planet. Sci. Lett., 2, 433-439.

Philpotts, A. R., 1971. Immiscibility between feldspathic and gabbroic magmas. Nature Phys. Sci., 229, 107-109.

_____, 1972. Density, surface tension and viscosity of the immiscible phase in a basic alkaline magma. Lithos, 5, 1-18.

_____, 1976. Silicate liquid immiscibility, its probable extent and petrogenetic significance. Amer. J. Sci., 276, 1147-1177.

_____, 1977. Archean variolites--quenched immiscible liquids: A discussion. Can. J. Earth. Sci., 14, 139-144.

_____ and Schnetzler, C. C., 1970. Phenocryst-matrix partition coefficients for K, Rb, Sr, and Ba with applications to anorthosite and basalt genesis. Geochim. Cosmochim. Acta, 34, 307-322.

Philpotts, J. A., 1978. The law of constant rejection. Geochim. Cosmochim. Acta, 42, 909-920.

Presnall, D. C., Dixon, J. R., O'Donnell, T. H. and Dixon, S. A., 1979. Generation of mid-ocean ridge tholeiites. J. Petrol., 20, 3-35.

Ratcliffe, N. M., 1968. Contact relations of the Cortlandt Complex at Stony Point, N. Y., and their regional implications. Geol. Soc. Amer. Bull., 79, 777-786.

_____, 1971. The Ramapu fault system in New York and adjacent northern New Jersey: A case of tectonic heredity. Geol. Soc. Amer. Bull., 82, 125-142.

Rayleigh, J. W. S., 1896. Theoretical considerations respecting the separation of gases by diffusion and similar processes. Philos. Mag., 42, 77-107.

Roedder, E., 1978. Silicate liquid immiscibility in magmas and in the system K_2O-FeO-Al_2O_3-SiO_2: An example of serendipity. Geochim. Cosmochim. Acta, 42, 1597-1617.

_____ and Weiblen, P. W., 1971. Petrology of silicate melt inclusions. Apollo 11 and Apollo 12 and terrestrial equivalent. Proc. Second Lunar Sci. Conf., Geochim. Cosmochim. Acta, Suppl. 2, 1, 507-528.

_____ and Weiblen, P. W., 1972. Petrographic features and petrologic significance of melt inclusions in Apollo 14 and 15 rocks. Proc. Third Lunar Sci. Conf., Geochim. Cosmochim. Acta, Suppl. 3, 1, 251-279.

Rogers, G. S., 1911. Geology of the Cortlandt series and its emery deposits. N. Y. Acad. Sci., 21, 11-86.

Rutherford, M. J., Hess, P. C., and Daniel, G. H., 1974. Experimental liquid line of descent and liquid immiscibility for basalt 70017. Proc. Fifth Lunar Sci. Conf., Geochim. Cosmochim. Acta, Suppl. 5, 1, 569-583.

Ryerson, F. J., and Hess, P. C., 1978. Implications of liquid-liquid distribution coefficients to mineral-lqiuid partitioning, Geochim. Cosmochim. Acta, 42, 921-932.

Saunders, A. D., and Tarney, J., 1979. The geochemistry of basalts from a back-arc spreading center in the East Scotia Sea. Geochim. Cosmochim. Acta, 43, 555-572.

Schnetzler, C. C., and Philpotts, J. A., 1970. Partition coefficients of rare-earth elements between igneous matrix material and rock-forming mineral phenocrysts, II. Geochim. Cosmochim. Acta, 34, 331-340.

Schultz, K. J., Smith, I. E. M., and Blanchard, D. P., 1979. The nature of Archean alkalic rocks from the southern portion of the Superior Province. EOS, 60, 410.

Shand, J. S., 1942. Phase petrology in the Cortlandt Complex, New York. Geol. Soc. Amer. Bull., 53, 409-428.

Shimizu, N., 1974. An experimental study of the partitioning of K, Rb, Cs, Sr, and Ba, between clinopyroxene and liquid at high pressures. Ibid., 38, 1789-1798.

Simmons, E. C., and Hedge, C. E., 1978. Minor-element geochemistry and Sr-isotope of tertiary stocks, Colorado mineral belt. Contrib. Mineral. Petrol., 67, 379-396.

Steenland, N. C., and Woollard, G. P., 1952. Gravity and magnetic investigation of the structure of the Cortlandt Complex, New York. Geol. Soc. Amer. Bull., 63, 1075-1104.

Stewart, D. C., Allen, J. C., and Boettcher, A. L., 1976. Genesis of andesitic magma by amphibole fractionation: Petrographic and experimental evidence (abst.). EOS, 57, 344.

Sun, S. S., and Hanson, G. N., 1975. Origin of Ross Island basanitoids and limitations upon the heterogeneity of mantle sources for alkali basalts and nephelinites. Contrib. Mineral. Petrol., 52, 77-106.

_____ and Hanson, G. N., 1976. Rare earth element evidence for differentiation of McMurdo Volcanics, Ross Island Antarctica. Contrib. Mineral. Petrol., 54, 139-155.

Thompson, A. B., and Tracy, R. J., 1979. Model systems for anatexis of pelitic rocks. II. Facies series melting and reactions in the system $CaO-KAlO_2-NaAlO_2-Al_2O_3-SiO_2-H_2O$. Contrib. Mineral. Petrol., 70, 429-438.

Tilley, C. E. and Harwood, 1931. The dolerite-chalk contact at Scawt Hill. Mineral. Mag., 22, 439-468.

_____and Muir, I. D., 1962. The Hibridean Plateau magma type, Edinburgh. Geol. Soc. Trans., 19, 208-215.

Visser, W., and Koster Van Gross, A. F., 1979. Liquid immiscibility in $K_2O-FeO-Al_2O_3-SiO_2$. Amer. J. Sci., 279, 1160-1175.

Vocke, R., 1980. Ph.D. thesis, S.U.N.Y. at Stony Brook.

Waff, H. S., 1980. Effects of the gravitational field on liquid distribution in partial melts within the upper mantle. J. Geophys. Res., 85, 1815-1825.

Walawender, M. J., 1976. Petrology and emplacement of the Los Pinos pluton, Southern California. Can. J. Earth Sci., 13, 1288-1300.

_____, Hoppler, H., and Smith, T. E., 1979. Trace element evidence for contamination in a gabbronorite-quartz diorite sequence in the Peninsular Ranges batholith. J. Geol., 87, 87-97.

_____, and Smith, T. E., 1980. Geochemical and petrologic evolution of the basic plutons of the Peninsular Ranges batholith, Southern California. J. Geol., 88, 233-247.

Wager, L. R., and Brown, G. M., 1968. Layered Igneous Rocks. Oliver and Boyd, Edinburgh, 588 pp.

Watson, E. B., 1976. Two-liquid partition coefficients: Experimental data and geochemical implications. Contrib. Mineral. Petrol., 56, 119-134.

_____, and Naslund, H. R., 1977. The effect of pressure on liquid immiscibility in the system K_2O-FeO-Al_2O_3-SiO_2-CO_2. Carnegie Inst. Wash. Year Book, 76, 410-414.

Weiblen, P. W., and Roedder, E., 1973. Petrology of melt inclusions in Apollo samples 15598 and 62295, and of clasts in 67915 and several lunar soils. Proc. Fourth Lunar Sci. Conf., Geochim. Cosmochim. Acta, Suppl. 4, 1, 681-703.

Wendlandt, R. F., and Harrison, W. J., 1979. Rare earth element partitioning between immiscible carbonate and silicate liquids and CO_2 vapor: Results and implications for the formation of light rare earth-enriched rock. Contrib. Mineral. Petrol., 69, 409-419.

Williams, G. H., 1884. On the paramorphism of pyroxenes to hornblende in rocks. Am. J. Sci., 28, 259

_____, 1886. The peridotites of the Cortlandt series on the Hudson River near Peekskill. Am. J. Sci., 31, 26-31.

_____, 1888. The norites of the Cortlandt series on the Hudson River near Peekskill. Am. J. Sci., 33, 135-191.

Willis, J. P., Ahrens, L. H., Danchin, R. V., Erlank, A. J., Gurney, J. J., Hofnays, P. K., McCarthy, T. S., and Orren, M. J., 1971. Some inter-element relationships between lunar rocks and fines, and stony meteorites. Proc. Second Lunar Sci. Conf., 1, 2, 1123-1138.

Wright, A. E., Tarney, J., Palmer, K. F., Moorlock, B. S. P., and Skinner, A. C., 1973. The geology of the angmagssalik nea, East Greenland, and possible relationships with the Lewisian of Scotland. In: The Precambrian of Scotland and related rocks of Greenland, edited by R. G. Park and J. Tarney. Univ. of Keele, pp. 157-177.

Wright, T. L., and Doherty, P. C., 1970. A linear programming and least squares computer method for solving petrologic mixing problems. Geol. Soc. Amer. Bull., 91, 1995-2008.

Yoder, H. S., and Tilley, C. E., 1962. Origin of basalt magmas: An experimental study of material and synthetic rock systems. J. Petrol., 3, 344-532.

Zielinski, R. A., 1975. Trace element evaluation of a suite of rocks from Reunion Island, Indian Ocean. Geochim. Cosmochim. Acta, 39, 713-734.

_____, and Frey, F. A., 1970. Gough Island: Evaluation of a fractional crystallization model. Contrib. Mineral. Petrol., 29, 242-254.

APPENDIX 1

ROCK TYPES AND PETROGRAPHIC DESCRIPTIONS OF SAMPLES

Sample #	Rock Type	Description
1	Hornblendite	Coarse-grained, black colored, rock consisting of approximately 60% kaersutite, 30% plagioclase, 10% biotite, and sphene. Euhedral kaersutite and plagioclase crystals have cumulate textural relationships. Both kaersutite and biotite exhibit well-developed rutile and ilmenite lamellae.
2	Hornblendite	Medium-grained, black colored rock comprised almost entirely of kaersutite (80%) and plagioclase. Biotite is a relatively minor constituent. Euhedral kaersutite and plagioclase crystals have cumulate textural relationships.
3	Kaersutite Gabbro (Amphibole-norite)	Medium-grained, grey to black colored rock whose major mineral constituents are subhedral plagioclase ($\sim$ 60%) crystals and brown-green biotite (35%). Subhedral amphibole grains ($\sim$ 1%) coexist with rounded (0.5-2.0mm) euhedral orthopyroxene grains. Quartz and K-feldspar are common interstitial phases. Apatite and zircon are minor accessory phases.
4	Kaersutite Gabbro	Medium-grained, black colored rock containing approximately equal amounts of kaersutite and plagioclase. Euhedral kaersutite crystals contain exsolution lamellae of ilmenite and

APPENDIX 1 (continued)

Sample #	Rock Type	Description
		also plagioclase, biotite, and apatite. Red-brown biotite and opaques are relatively minor (~ 5%).
5	Hornblendite	Medium-grained, black colored rock having mineral abundances and grain sizes very similar to those of sample 2.
6	Norite	Medium to coarse-grained grey colored rock located within the margins of pluton 1. Probably a dike or sill-like extension of the younger norite. Plagioclase (~ 60%), orthopyroxene (20%), clinopyroxene (10%), biotite (5%), and K-feldspar (~ 5%). Plagioclase displays an antiperthitic texture, while coexisting K-feldspars are perthitic.
7	Diorite	Medium to coarse-grained grey-black colored rock composed of approximately equal amounts of euhedral kaersutite and plagioclase. The brown to yellow colored kaersutite commonly contains oriented ilmenite lamellae. Amphibole and plagioclase display cumulate textural relationships. Biotite is a minor constituent (~1%) and usually accompanies amphibole.
8	Diorite	Medium-grained, grey colored rock consisting esentially of plagioclase (~ 60%) and biotite (~ 25%). The yellow-brown mica exists as

APPENDIX 1 (continued)

Sample #	Rock Type	Description
		large (3-6mm) plates that frequently enclose crystals of apatite, ilmenite, and plagioclase. Amphibole and orthopyroxene occur as small (o.5-2.5mm) subhedral crystals and together comprise less than 10% of the rock. Almandine garnet grains are infrequently present.
9	Diorite	Medium-grained, grey colored rock consisting of equal proportions of euhedral kaersutite and plagioclase crystals with accessory amounts of orthopyroxene, biotite, and opaques. Orthopyroxene grains are generally enclosed by dark green-brown fibrous amphibole. Kaersutite generally has euhedral outlines and exhibit ilmenite exsolution.
10	Diorite	Medium-grained, grey colored rock with euhedral kaersutite crystals comprising approximately 50% of the rock which coexist with an equal amount of similar sized euhedral to subhedral plagioclase grains. Rounded orthopyroxene grains occasionally altered to fibrous brown amphibole along fracture is a minor constituent ($\sim$3%) as is red-brown biotite ($\sim$3%).
11	Clinopyroxene	Coarse-grained, black colored rock composed of approximately 60% clinopyroxene, 20% orthopyroxene, 15% olivine, and 5% kaersutite. Clinopyroxene and orthopyroxene grains display hypidiomorphic outlines and a very variable grain size (0.5mm-1cm). Large euhedral ortho-

APPENDIX 1 (continued)

Sample #	Rock Type	Description
		pyroxene crystals are often deformed. Olivine occurs as colorless, round,anhedral grains (1-5mm) that are commonly cut by a network of fractures. Serpentinization of olivine is minor.
12	Clinopyroxene	Medium to coarse-grained, black colored rock consisting of approximately 65% clinopyroxene, 35% orthopyroxene. Olivine and kaersutite are rare. Sample 12 exhibits similar cumulate textural features to those of sample 11.
14	Cortlandtite	Medium-grained, black colored rock comprised of approximately 60% clinopyroxene, 10% orthopyroxene, 25% olivine, and 5% kaersutite. Olivine grains are often crosscut by numerous fractures which are often filled by serpentine or magnetite. Kaersutite has vein-like interstitial texture.
15	Amphibole-pyroxenite	Medium-grained, breenish black colored rock consisting of approximately 75% kaersutite and 25% clinopyroxene. Calcite ($\sim$ 3%) and biotite are interstitial phases. Kaersutite has both poikilitic and prismatic habits.
16	Cortlandtite	Medium-grained, black colored rock with same textures and modal mineralogy as sample 14.
17	Cortlandtite	Similar to Cortlandtite samples 14 and 16.

APPENDIX 1 (continued)

Sample #	Rock Type	Description
18	Kaersutite-norite	Medium to coarse-grained, dark brown colored rock containing approximately 45% kaersutite in addition to plagioclase (20%), orthopyroxene (20%), and clinopyroxene (5%). Frequently large (0.2-1.0cm) poikilitic kaersutites enclose plagioclase, amphibole, pyroxene, apatite, and opaque grains. Biotite grains are rare but apatite is abundant (~ 1.5%) and frequently occurs as inclusions within orthopyroxene. Ilmenite, iron-sulfide, and magnetite comprise approximately 6% of this sample.
19	Norite	Medium-grained, grey to brown colored rock containing plagioclase (~50%), orthopyroxene (~25%), kaersutite (~15%), clinopyroxene (~5%), and opaques (~5%). Euhedral apatite crystals comprise approximately 2.5% of this sample. Biotite is a minor interstitial phase.
20	Quartz-norite	Medium-grained, light grey colored rock containing plagioclase (~50%), orthopyroxene (~20%), clinopyroxene (~5%), quartz (~10%), and K-feldspar (~15%). Opaques are minor constituents (~1%).
21	Norite	Medium-grained, dark grey to light greyish-brown colored rock characterized by pink coloration of plagioclase and black pyroxene crystals. Plagioclase (~60%), orthopyroxene (~20%), clinopyroxene (10%), and biotite (~10%). Large and small plagioclase laths show excellent

APPENDIX 1 (continued)

Sample #	Rock Type	Description
		parallel alignment with each other and co-existing pyroxene and biotite grains. Plagioclase twin lamellae are often strained.
22	Quartz-norite	This sample has a similar textural and modal mineralogy to that of sample 21. However, quartz (~2%) and K-feldspar (~5%) are present. The K-feldspar is perthitic and quartz grains are usually enclosed within biotite plates. Biotite is found as small (.25-.5mm) plates and in fan-shaped aggregates. Both pyroxenes are frequently rimmed by a fine-grained assemblage of amphibole and biotite. Ilmenite, magnetite, and apatite are the predominant accessory phases.
23	Quartz-norite	Medium-grained, dark grey colored rock consisting of plagioclase (~50%), K-feldspar (~15%), orthopyroxene (15%), clinopyroxene (~5%), amphibole (~10%), biotite (~5%), and minor amounts of quartz (~3%). Plagioclase grains are well oriented and display ocsillatory zoning, and myrmekitic texture when it is contiguous with the interstitial K-feldspar. Amphibole sometimes has a poikilitic habit.
24	Granodiorite	Fine-grained, white to light grey colored rock collected from a one meter wide dike. It consists of plagioclase (~50%), quartz (~30%) and K-feldspar (~15%). Plagioclase phenocrysts comprise approximately 5% of this dike rock. Biotite, muscovite, epidote, and chlorite are minor constituents. Biotite occurs as single

APPENDIX 1 (continued)

Sample #	Rock Type	Description
		grains randomly distributed throughout the groundmass, and in multi-aggregates that sometimes attain 1mm size dimensions.
25	Norite	This sample has textures and modal mineralogy similar to norite sample 21.
26	Norite	Same as above.
27	Kaersutite-Norite	Medium grained, brownish-black colored rock with similar modal mineralogy and texture to that of sample 18. However, sample 27 contains approximately 10% red-brown biotite, while sample 18 lacks this phase.
28	Norite	Medium-grained, dark grey colored rock collected from a 2 meter wide dike crosscutting the sample 27 outcrop. Primary mineral constituents are plagioclase ($\sim$50%), amphibole ($\sim$35%) and biotite ($\sim$15%). This sample contains two different types of amphibole. The first is a transparent to green, fibrous variety that completely replaced euhedral to subhedral pyroxene crystals. The second variety is green to brown in color and is found rimming the fibrous variety.
29	Norite	This sample has textures and modal mineralogy similar to sample 21.

APPENDIX 1 (continued)

Sample #	Rock Type	Description
30	Norite	Same as above.
31	Clinopyroxenite	Medium to coarse-grained, black colored rock with an allotriomorphic granular texture. Clinopyroxene (~50%) and orthopyroxene (~50%) grains from 3-8mm in size, form an interlocking mosaic pattern. Olivine is rare. Minor amounts (~1%) of interstitial kaersutite and plagioclase are found between pyroxene grain boundaries.
32	Clinopyroxenite	Medium to coarse-grained, black colored rock with a similar texture to that of sample 31. Contains substantial olivine (~25-35%), however, and only minor amounts of orthopyroxene (~1%). Olivine grains are large (4-9mm) and usually highly fractured. Minor amounts of green-grown serpentine are often found along these cracks. Kaersutite (~5%), biotite (~3%), and opaques are interstitial phases. Rare spinel grains, generally enclosed in pyroxene, are found in this sample.
33	Clinopyroxenite	Almost identical in texture and modal mineralogy to sample 32.
34	Granodioirte	Medium-grained, white colored rock composed of plagioclase (~50%), quartz (~30%), and K-feldspar (~15%). This granular textured sample is composed of euhedral to subhedral plagioclase laths (0.5-2.0mm) with anhedral

APPENDIX 1 (continued)

Sample #	Rock Type	Description
		Quartz (∿ 1mm) and K-feldspar (.25-1.0mm grains). K-feldspars are perthitic and frequently exhibit grid twinning. Biotite, muscovite, and chlorite plates are interstitial and randomly distributed throughout the rock along with rare epidote grains.
35	Pelitic Schist	Medium to coarse-grained, strongly foliated rock consisting predominantly of muscovite, biotite, and almandine garnet.
36	Quartz-feldspathic Dike	Fine to medium-grained, white to light-grey colored rock consisting of quartz (~ 85%), plagioclase (∿ 10%), almandine garnet (~ 5%). Minor amounts of muscovite and chlorite are dispersed interstitally throughout the rock. Garnets occur as small (~ 0.1mm), rounded, slightly pink, crystals and are often found in a chain-like fashion between larger anhedral quartz grains.
37	Emery	Fine-to medium-grained, dense, dark black colored rock consisting of various proportions of sillimanite, spinel (pleonaste), corundum, cordierite, garnet, staurolite, white mica, sapphirine, quartz, plagioclase, biotite, and magnetite. Sapphirine occurs as large, blue-green, tabular crystals that are strongly pleochroic. Cordierite contains numerous yellow pleochroic halos.

APPENDIX 1 (continued)

Sample #	Rock Type	Description
40	Amphibole-pyroxenite	Medium to coarse-grained, black to green colored rock comprised of kaersutite (~50%), and clinopyroxene (~30%) with subordinate amounts of plagioclase (~10%), biotite, apatite, and opaques. Kaersutite has both prismatic and poikilitic habits.
41	Cortlandtite	Medium-grained, black colored rock consisting of approximately 40% olivine, 30% clinopyroxene, 15% orthopyroxene, and 15% kaersutite. Kaersutite poikilitically encloses olivine and pyroxene grains. As in the other cortlandtite samples, olivine grains are colorless and usually crosscut by numerous fractures which sometimes contain serpentine. A small amount of sodic phlogopite (<1%) is found within the serpentine network.
42	Diorite	Coarse-grained, grey colored rock composed of plagioclase (~70%), and biotite (~30%). Euhedral plagioclase crystals are quite large (0.4-1.0cm) and often are partially sericitized. Anhedral plates (1-7mm) of green-brown biotite are evenly distributed throughout the sample and often have opaque (magnetite and ilmenite) minerals near their margins. Zircon, epidote, and apatite are minor additional phases. Euhedral (0.5-5mm) almandine garnets constitute approximately 2% of the sample.

APPENDIX 1 (continued)

Sample #	Rock Type	Description
43	Lamprophyre	Fine-grained, dark grey colored, allotriomorphic-granular dike with grain sizes less than 0.1mm. Biotite (~30%), kaersutite (~20%), plagioclase (~45%), and opaques are the principal constituents of this sample. Apatite, epidote, and sphene are minor accessory phases.
44	Lamprophyre	Medium-grained, black-green colored dike with extremely variable grain sizes. The sample is comprised of kaersutite (~40%), biotite (~30%), plagioclase (~20%), clinopyroxene (~5%), and opaques (~3%). Apatite, quartz, and calcite are accessory. Large (0.5-1.5mm) euhedral kaersutite grains display ilmenite lamellae.
45	Pelitic Schist	Fine-grained, black, graphitic quartz muscovite schist.
48	Amphibole-pyroxenite	Very similar in modal mineralogy and texture to sample 40.
49	Diorite	Medium-grained, grey colored rock consisting of equal amounts of felsic and mafic minerals. Kaersutite (~30%), biotite (~20%), plagioclase (~40%), K-feldspar (~5%), and quartz (~5%). Euhedral kaersutite crystals are frequently partially replaced with red-brown biotite. Sphene and apatite are common accessories. Ilmenite, magnetite, and iron-sulfides are minor constituents that are randomly distributed throughout the rock.

APPENDIX 1 (continued)

Sample #	Rock Type	Description
50	Diorite	Fine-grained, dark grey colored rock with a similar modal mineralogy to that of sample 49. However, sample 50 contains approximately 1% epidote.
51	Granodiorite	Similar modal mineralogy and texture to granodiorite sample 34.

Appendix 2 Selected Amphibole Analyses from Hornblendites-Kaersutite Gabbros of the Cortlandt Complex (Pluton 1).

Sample #	1		1	1	2		2
	Core	Rim		Mineral Separate	Core	Rim	
SiO_2	41.4	43.8	43.8	40.6	41.3	40.9	41.0
Al_2O_3	15.3	12.3	12.8	14.3	14.1	14.5	14.2
FeO	13.9	14.2	14.4	14.9	12.7	12.4	12.5
MgO	11.2	11.6	11.6	11.1	11.6	11.5	11.8
MnO	0.20	0.18	0.27	0.26	0.07	0.02	0.07
TiO_2	1.89	1.20	1.08	3.94	4.22	4.14	4.36
Cr_2O_3	0.00	0.03	0.03	0.04	0.00	0.00	0.00
CaO	12.0	11.4	11.9	10.9	11.0	11.4	11.2
Na_2O	1.48	1.42	1.62	1.40	2.01	1.91	2.14
K_2O	1.30	1.09	0.76	1.72	1.56	1.65	1.51
Σ	98.5	97.2	98.3	99.3	98.6	98.5	98.7
FeO	11.4	12.0	12.1	11.5	11.5	11.9	11.4
Fe_2O_3	2.85	2.41	2.57	3.77	1.30	0.60	1.21
	Structural formulae on the basis of 23 oxygens						
Si	6.053	6.469	6.405	5.938	6.044	6.010	5.997
Al^{IV}	1.947	1.531	1.595	2.062	1.956	1.990	2.003
Σ tet	8.000	8.000	8.000	8.000	8.000	8.000	8.000
Al^{VI}	0.689	0.619	0.610	0.401	0.481	0.518	0.447
Fe^{2+}	1.391	1.486	1.479	1.409	1.409	1.460	1.397
Fe^{3+}	0.314	0.268	0.283	0.414	0.143	0.066	0.133
Mg	2.432	2.544	2.534	2.423	2.534	2.516	2.572
Mn	0.025	0.022	0.033	0.322	0.009	0.002	0.009
Ti	0.208	0.133	0.119	0.433	0.464	0.457	0.480
Cr	0.000	0.004	0.003	0.005	0.000	0.000	0.000
Σ oct(M1-3)	5.059	5.076	5.061	5.117	5.040	5.019	5.038
X oct	0.059	0.076	0.061	0.117	0.040	0.019	0.038
Ca	1.874	1.805	1.869	1.713	1.730	1.801	1.749
Na(M4)	0.067	0.119	0.071	0.170	0.230	0.180	0.213
Σ(M4)	2.000	2.000	2.000	2.000	2.000	2.000	2.000
Na	0.352	0.288	0.388	0.227	0.341	0.364	0.394
K	0.243	0.206	0.142	0.321	0.291	0.309	0.282
Σ(A)	0.595	0.494	0.530	0.548	0.632	0.673	0.676
Ca	32.9	30.9	31.8	30.9	30.5	31.2	30.6
Mg	42.7	43.6	43.1	43.7	44.7	43.5	45.0
Fe	24.4	25.5	25.1	25.4	24.8	25.3	24.4
QUAD	2.6	23.4	20.3	0.0	2.2	0.5	0.0
OTHERS	97.4	76.4	79.7	100	97.8	99.5	100

Appendix 2(cont.) Selected Amphibole Analyses from Hornblendites-Kaersutite Gabbros of the Cortlandt Complex (Pluton 1).

Sample #	5	5		4	4		3	3
	Core	Rim		Core	Rim			
SiO_2	41.4	40.9	41.3	42.4	43.6	42.1	41.5	41.0
Al_2O_3	13.5	14.8	14.3	14.3	12.6	13.6	12.4	13.2
FeO	14.0	14.7	15.3	12.0	12.0	11.6	19.9	20.0
MgO	11.4	10.6	10.3	11.7	12.1	11.8	7.91	7.81
MnO	0.11	0.04	0.07	0.06	0.05	0.06	0.20	0.15
TiO_2	5.40	2.71	3.24	3.32	3.29	3.44	2.55	2.25
Cr_2O_3	0.00	0.00	0.00	0.00	0.02	0.02	0.01	0.01
CaO	10.9	11.0	11.2	11.6	11.5	11.2	10.9	11.3
Na_2O	1.47	1.65	1.87	1.39	1.49	1.48	1.27	0.83
K_2O	1.23	1.36	1.47	1.62	1.51	1.48	1.96	2.00
Σ	99.3	97.8	99.1	98.3	98.2	96.8	98.6	98.6
FeO	11.5	12.1	13.6	11.4	11.6	10.8	17.8	17.4
Fe_2O_3	2.69	2.88	1.90	0.61	0.47	0.88	2.30	2.87
Structural formulae on the basis of 23 oxygens								
Si	6.016	6.054	6.066	6.183	6.367	6.226	6.263	6.185
Al^{IV}	1.984	1.946	1.934	1.817	1.633	1.774	1.737	1.815
Σ tet	8.000	8.000	8.000	8.000	8.000	8.000	8.000	8.000
Al^{IV}	0.321	0.636	0.548	0.645	0.533	0.590	0.468	0.533
Fe^{2+}	1.401	1.499	1.671	1.398	1.415	1.342	2.249	2.191
Fe^{3+}	0.294	0.320	0.210	0.067	0.052	0.099	0.261	0.325
Mg	2.463	2.329	2.263	2.537	2.645	2.605	1.780	1.755
Mn	0.014	0.005	0.009	0.007	0.006	0.007	0.026	0.019
Ti	0.590	0.301	0.358	0.365	0.361	0.383	0.289	0.255
Cr	0.000	0.000	0.000	0.000	0.002	0.002	0.001	0.001
Σ oct(M1-3)	5.083	5.090	5.059	5.019	5.014	5.028	5.074	5.079
X oct	0.083	0.090	0.059	0.019	0.014	0.028	0.074	0.079
Ca	1.690	1.738	1.766	1.821	1.795	1.779	1.765	1.830
Na(M4)	0.227	0.172	0.175	0.160	0.191	0.193	0.161	0.091
Σ(M4)	2.000	2.000	2.000	2.000	2.000	2.000	2.000	2.000
Na	0.187	0.301	0.358	0.234	0.231	0.232	0.211	0.152
K	0.228	0.257	0.276	0.302	0.281	0.279	0.377	0.385
Σ(A)	0.415	0.558	0.634	0.536	0.512	0.511	0.588	0.537
Ca	30.4	31.2	31.0	31.6	30.6	31.1	30.5	31.7
Mg	44.4	41.9	39.7	44.1	45.2	45.5	30.7	30.4
Fe	25.2	26.9	29.3	24.3	24.2	23.4	38.8	37.9
QUAD	0.8	2.7	3.3	9.2	18.3	11.3	13.2	9.2
OTHERS	99.2	97.3	96.7	90.8	81.7	88.7	86.8	90.8

Appendix 2(cont.) Selected Pyroxene Analyses from Hornblendites Kaersutite Gabbros (Pluton 1).

Sample #	3		3
	Core	Rim	
SiO_2	49.9	49.6	49.4
Al_2O_3	1.61	1.66	1.51
FeO	33.2	32.5	32.6
MgO	14.3	14.2	14.3
MnO	0.76	0.82	0.75
TiO_2	0.15	0.07	0.06
Cr_2O_3	0.00	0.00	0.00
CaO	0.82	1.01	1.24
Na_2O	0.00	0.00	0.00
Σ	100.8	99.9	99.9
FeO	32.5	31.8	31.4
Fe_2O_3	0.82	0.74	1.40
Structural formulae on the basis of 6 oxygens			
Si	1.947	1.949	1.943
Al^{IV}	0.053	0.051	0.057
Σ tet	2.000	2.000	2.000
Al^{VI}	0.021	0.025	0.012
Fe^{3+}	0.024	0.022	0.041
Cr	0.000	0.000	0.000
Ti	0.004	0.002	0.002
Mg	0.833	0.835	0.836
Fe^{2+}	1.058	1.046	1.031
Mn	0.025	0.027	0.025
Ca	0.034	0.043	0.052
Na	0.000	0.000	0.000
Σ oct	1.999	2.000	1.999
Ca	1.78	2.21	2.72
Mg	43.3	43.4	43.6
Fe	55.0	54.4	53.7
QUAD	94.7	94.9	94.2
OTHER	5.3	5.1	5.8

Appendix 2(cont.)

Selected Biotite Analyses from Hornblendite-Kaersutite Gabbro of the Cortlandt Complex (Pluton 1).

Sample #	1	1	1	2	2	5	5	4	4	3	3
SiO_2	38.0	37.6	37.4	36.6	36.5	37.1	36.5	39.1	38.0	35.6	35.4
Al_2O_3	16.7	17.2	16.8	16.4	16.5	17.0	17.5	16.0	15.2	15.4	14.8
FeO	14.3	14.9	14.0	11.9	12.5	13.8	13.7	12.6	13.2	19.9	22.1
MgO	15.3	14.9	15.5	16.1	15.4	15.1	15.1	15.8	15.5	10.3	8.96
MnO	0.13	0.12	0.08	0.00	0.00	0.00	0.00	0.00	0.00	0.09	0.13
TiO_2	1.70	1.61	1.60	5.19	5.11	2.79	2.59	3.83	4.26	4.42	5.78
Cr_2O_3	0.02	0.00	0.00	0.00	0.00	0.00	0.01	0.02	0.00	0.01	0.01
CaO	0.06	0.05	0.05	0.02	0.00	0.00	0.17	0.06	0.01	0.04	0.01
Na_2O	0.17	0.19	0.22	0.06	0.08	0.09	0.15	0.00	0.00	0.01	0.02
K_2O	7.32	9.12	8.45	9.07	9.37	9.40	8.88	6.63	9.14	9.87	9.84
Σ	93.6	95.8	94.1	95.3	95.4	95.3	94.6	94.0	95.3	95.6	97.1

Appendix 2(cont.) Selected Feldspar Analyses from Hornblendites-Kaersutite Gabbros (Pluton 1).

Sample #	1		1		1	2		2		2
	Core	Rim	Core	Rim		Core	Rim	Core	Rim	
SiO_2	57.0	59.5	59.8	59.7	55.1	50.3	48.7	50.7	49.4	48.7
Al_2O_3	27.4	26.0	25.5	25.5	28.4	31.6	33.2	32.2	33.2	33.0
FeO	0.05	0.06	0.04	0.06	0.05	0.00	0.23	0.20	0.23	0.22
CaO	9.39	7.46	7.08	7.07	11.0	15.0	16.0	14.9	16.0	16.0
Na_2O	6.14	7.34	7.44	7.13	5.26	2.80	2.31	3.16	2.47	2.18
K_2O	0.04	0.05	0.07	0.03	0.03	0.12	0.09	0.09	0.04	0.06
Σ	100.0	100.4	100.0	99.4	99.9	99.8	100.6	101.3	101.3	100.3
Si	2.552	2.641	2.664	2.668	2.485	2.297	2.218	2.284	2.232	2.222
Al	1.450	1.362	1.339	1.342	1.511	1.699	1.780	1.709	1.765	1.778
Fe	0.002	0.002	0.001	0.002	0.002	0.000	0.009	0.008	0.009	0.008
Ca	0.451	0.355	0.338	0.339	0.532	0.731	0.781	0.720	0.772	0.783
Na	0.533	0.632	0.642	0.618	0.460	0.248	0.204	0.276	0.216	0.193
K	0.002	0.003	0.004	0.002	0.002	0.007	0.005	0.005	0.002	0.003
Σ	4.991	4.995	4.989	4.971	4.991	4.981	4.997	5.002	4.995	4.987
Or	0.2	0.3	0.4	0.2	0.2	0.7	0.5	0.5	0.2	0.3
Ab	54.1	63.8	65.2	64.4	46.3	25.2	20.6	27.6	21.8	19.7
An	45.7	35.9	34.4	35.4	53.5	74.1	78.9	71.9	78.0	80.0

Appendix 2(cont.) Selected Feldspar Analyses from Hornblendites-Kaersutite Gabbros (Pluton 1).

Sample #	5		5		5	4		4	3	3
	Core	Rim	Core	Rim		Core	Rim			
SiO_2	51.6	49.2	49.4	49.8	50.5	54.8	55.0	51.4	58.6	58.8
Al_2O_3	32.2	33.8	33.4	33.0	33.0	29.8	29.6	30.8	26.0	26.2
FeO	0.08	0.14	0.13	0.15	0.15	0.07	0.08	0.74	0.13	0.07
CaO	14.4	16.3	16.0	15.3	15.3	11.5	11.5	12.6	8.01	8.02
Na_2O	3.23	2.26	2.38	2.68	2.68	4.85	5.02	4.21	6.95	6.94
K_2O	0.04	0.03	0.03	0.03	0.03	0.08	0.09	0.10	0.31	0.19
Σ	101.6	101.7	101.4	101.0	101.4	101.1	101.4	99.8	99.9	100.2
Si	2.308	2.212	2.227	2.249	2.265	2.444	2.449	2.342	2.622	2.621
Al	1.699	1.789	1.776	1.758	1.743	1.566	1.554	1.657	1.371	1.377
Fe	0.003	0.005	0.005	0.006	0.006	0.003	0.003	0.028	0.005	0.003
Ca	0.692	0.787	0.773	0.741	0.723	0.549	0.549	0.614	0.384	0.383
Na	0.280	0.197	0.208	0.235	0.256	0.419	0.433	0.372	0.603	0.600
K	0.002	0.002	0.002	0.002	0.001	0.005	0.005	0.006	0.018	0.011
Σ	4.984	4.993	4.990	4.990	4.993	4.985	4.993	5.019	5.003	4.996
Or	0.2	0.2	0.2	0.2	0.1	0.5	0.5	0.6	1.8	1.1
Ab	28.7	20.0	21.2	24.0	26.1	43.1	43.9	37.5	60.0	60.4
An	71.1	79.8	78.6	75.8	73.8	56.4	55.6	61.9	38.2	38.5

Appendix 3

Selected Amphibole Analyses from Diorites of the Cortlandt, Stony Point, and Rosetown Complexes.

Sample #	7	7		10	10		9	9	
	Core	Rim		Core	Rim		Core	Rim	
SiO_2	41.0	40.9	40.7	41.9	41.6	40.8	40.7	41.9	41.8
Al_2O_3	14.8	15.1	14.8	14.7	14.7	14.5	14.2	13.9	12.1
FeO	14.4	14.4	14.0	13.3	14.2	14.4	15.5	15.5	14.6
MgO	11.6	11.2	11.6	12.2	11.3	11.0	10.7	11.2	11.3
MnO	0.19	0.20	0.20	0.15	0.19	0.14	0.18	0.19	0.14
TiO_2	2.90	2.84	2.96	1.95	2.61	3.18	3.18	2.55	5.73
Cr_2O_3	0.04	0.06	0.05	0.03	0.09	0.02	0.07	0.06	0.07
CaO	10.4	11.6	11.2	11.2	11.1	11.2	10.2	10.8	10.6
Na_2O	2.42	2.25	2.40	1.65	1.89	1.95	1.58	1.54	1.43
K_2O	0.86	0.91	0.90	1.39	1.29	1.39	1.54	1.34	1.44
Σ	98.6	99.5	98.8	98.4	99.0	98.5	97.7	98.9	99.2
FeO	10.3	12.1	11.2	10.0	11.5	12.1	11.4	11.5	12.2
Fe_2O_3	4.64	2.53	3.01	3.69	2.98	2.55	4.60	4.46	2.68
	Structural formulae on the basis of 23 oxygens								
Si	5.971	5.960	5.954	6.096	6.066	6.001	6.010	6.109	6.102
Al^{IV}	2.029	2.040	2.046	1.904	1.934	1.999	1.990	1.891	1.898
Σ tet	8.000	8.000	8.000	8.000	8.000	8.000	8.000	8.000	8.000
Al^{VI}	0.511	0.548	0.509	0.613	0.598	0.511	0.486	0.498	0.181
Fe^{2+}	1.251	1.470	1.376	1.219	1.402	1.490	1.403	1.402	1.493
Fe^{3+}	0.509	0.277	0.331	0.404	0.327	0.282	0.512	0.489	0.295
Mg	2.527	2.441	2.522	2.643	2.446	2.425	2.360	2.438	2.460
Mn	0.024	0.025	0.025	0.018	0.024	0.018	0.022	0.024	0.017
Ti	0.317	0.311	0.325	0.214	0.286	0.352	0.353	0.280	0.629
Cr	0.005	0.007	0.006	0.004	0.010	0.002	0.008	0.007	0.008
Σ oct(M1-3)	5.144	5.079	5.094	5.115	5.093	5.080	5.144	5.138	5.083
X oct	0.144	0.079	0.094	0.115	0.093	0.080	0.144	0.138	0.083
Ca	1.618	1.813	1.757	1.752	1.734	1.761	1.622	1.687	1.657
Na(M4)	0.238	0.108	0.149	0.133	0.173	0.159	0.234	0.175	0.260
Σ(M4)	2.000	2.000	2.000	2.000	2.000	2.000	2.000	2.000	2.000
Na	0.446	0.527	0.531	0.333	0.362	0.398	0.220	0.261	0.146
K	0.160	0.169	0.168	0.258	0.240	0.261	0.290	0.250	0.268
Σ(A)	0.606	0.696	0.699	0.591	0.602	0.659	0.510	0.511	0.414
Ca	30.0	31.7	31.1	31.2	31.1	31.0	30.1	30.5	29.5
Mg	46.8	42.6	44.6	47.1	43.8	42.7	43.8	44.1	43.8
Fe	23.2	25.7	24.3	21.7	25.1	26.3	26.1	25.4	26.6
QUAD	0.0	0.0	0.0	4.8	3.3	0.0	0.5	5.4	5.1
OTHERS	100	100	100	95.2	96.7	100	99.5	94.6	94.9

Appendix 3(cont.) Selected Amphibole Analyses from Diorites of the Cortlandt, Stony Point, and Rosetown Complexes.

Sample #	7	7		10	10		9	9	
	Core	Rim		Core	Rim		Core	Rim	
SiO_2	41.0	40.9	40.7	41.9	41.6	40.8	40.7	41.9	41.8
Al_2O_3	14.8	15.1	14.8	14.7	14.7	14.5	14.2	13.9	12.1
FeO	14.4	14.4	14.0	13.3	14.2	14.4	15.5	15.5	14.6
MgO	11.6	11.2	11.6	12.2	11.3	11.0	10.7	11.2	11.3
MnO	0.19	0.20	0.20	0.15	0.19	0.14	0.18	0.19	0.14
TiO_2	2.90	2.84	2.96	1.95	2.61	3.18	3.18	2.55	5.73
Cr_2O_3	0.04	0.06	0.05	0.03	0.09	0.02	0.07	0.06	0.07
CaO	10.4	11.6	11.2	11.2	11.1	11.2	10.2	10.8	10.6
Na_2O	2.42	2.25	2.40	1.65	1.89	1.95	1.58	1.54	1.43
K_2O	0.86	0.91	0.90	1.39	1.29	1.39	1.54	1.34	1.44
Σ	98.6	99.5	98.8	98.4	99.0	98.5	97.7	98.9	99.2
FeO	10.3	12.1	11.2	10.0	11.5	12.1	11.4	11.5	12.2
Fe_2O_3	4.64	2.53	3.01	3.69	2.98	2.55	4.60	4.46	2.68
	Structural formulae on the basis of 23 oxygens								
Si	5.971	5.960	5.954	6.096	6.066	6.001	6.010	6.109	6.102
Al^{IV}	2.029	2.040	2.046	1.904	1.934	1.999	1.990	1.891	1.898
Σ tet	8.000	8.000	8.000	8.000	8.000	8.000	8.000	8.000	8.000
Al^{VI}	0.511	0.548	0.509	0.613	0.598	0.511	0.486	0.498	0.181
Fe^{2+}	1.251	1.470	1.376	1.219	1.402	1.490	1.403	1.402	1.493
Fe^{3+}	0.509	0.277	0.331	0.404	0.327	0.282	0.512	0.489	0.295
Mg	2.527	2.441	2.522	2.643	2.446	2.425	2.360	2.438	2.460
Mn	0.024	0.025	0.025	0.018	0.024	0.018	0.022	0.024	0.017
Ti	0.317	0.311	0.325	0.214	0.286	0.352	0.353	0.280	0.629
Cr	0.005	0.007	0.006	0.004	0.010	0.002	0.008	0.007	0.008
Σ oct(M1-3)	5.144	5.079	5.094	5.115	5.093	5.080	5.144	5.138	5.083
X oct	0.144	0.079	0.094	0.115	0.093	0.080	0.144	0.138	0.083
Ca	1.618	1.813	1.757	1.752	1.734	1.761	1.622	1.687	1.657
Na(M4)	0.238	0.108	0.149	0.133	0.173	0.159	0.234	0.175	0.260
Σ(M4)	2.000	2.000	2.000	2.000	2.000	2.000	2.000	2.000	2.000
Na	0.446	0.527	0.531	0.333	0.362	0.398	0.220	0.261	0.146
K	0.160	0.169	0.168	0.258	0.240	0.261	0.290	0.250	0.268
Σ(A)	0.606	0.696	0.699	0.591	0.602	0.659	0.510	0.511	0.414
Ca	30.0	31.7	31.1	31.2	31.1	31.0	30.1	30.5	29.5
Mg	46.8	42.6	44.6	47.1	43.8	42.7	43.8	44.1	43.8
Fe	23.2	25.7	24.3	21.7	25.1	26.3	26.1	25.4	26.6
QUAD	0.0	0.0	0.0	4.8	3.3	0.0	0.5	5.4	5.1
OTHERS	100	100	100	95.2	96.7	100	99.5	94.6	94.9

Appendix 3(cont.)

Selected Amphibole Analyses from Diorites of the Cortlandt, Stony Point, and Rosetown Complexes.

Sample #	8	8	8	49		49	50	50
				Core	Rim			
SiO_2	46.1	43.9	43.4	41.0	41.6	39.9	47.7	44.0
Al_2O_3	12.1	14.6	13.8	12.2	10.7	11.6	6.13	8.66
FeO	17.2	17.2	17.1	18.3	22.2	17.0	17.0	18.8
MgO	13.5	10.9	11.5	8.97	6.99	9.08	11.7	9.99
MnO	0.40	0.34	0.33	0.23	0.36	0.22	0.44	0.54
TiO_2	0.41	0.70	1.10	3.36	2.68	4.75	0.71	1.01
Cr_2O_3	0.05	0.08	0.06	0.00	0.02	0.04	0.49	0.03
CaO	6.66	8.99	8.80	10.8	11.3	11.3	11.4	11.9
Na_2O	0.69	1.18	1.16	2.37	1.94	2.18	1.09	1.50
K_2O	0.18	0.30	0.46	1.08	1.25	1.12	0.75	1.07
Σ	97.3	98.3	97.7	98.3	99.0	97.2	97.5	97.5
FeO	13.8	12.7	11.9	16.6	20.9	16.8	14.8	16.2
Fe_2O_3	3.77	4.98	5.83	1.93	1.42	0.26	2.47	2.82
	Structural formulae on the basis of 23 oxygens							
Si	6.694	6.369	6.328	6.172	6.348	6.094	7.096	6.666
Al^{IV}	1.306	1.631	1.672	1.828	1.652	1.906	0.904	1.334
Σ tet	8.000	8.000	8.000	8.000	8.000	8.000	8.000	8.000
Al^{VI}	0.765	0.871	0.699	0.336	0.269	0.189	0.170	0.212
Fe^{2+}	1.676	1.544	1.448	2.086	2.668	2.142	1.839	2.059
Fe^{3+}	0.412	0.543	0.640	0.218	0.163	0.030	0.276	0.322
Mg	2.915	2.353	2.506	2.012	1.589	2.068	2.601	2.255
Mn	0.049	0.042	0.041	0.029	0.046	0.028	0.055	0.069
Ti	0.045	0.076	0.121	0.380	0.308	0.546	0.079	0.115
Cr	0.006	0.009	0.007	0.000	0.002	0.005	0.058	0.004
Σ oct(M1-3)	5.868	5.438	5.462	5.061	5.045	5.008	5.078	5.036
X oct	0.868	0.438	0.462	0.061	0.045	0.008	0.078	0.036
Ca	1.035	1.397	1.375	1.745	1.846	1.854	1.814	1.925
Na(M4)	0.097	0.165	0.163	0.194	0.109	0.138	0.108	0.039
Σ(M4)	2.000	2.000	2.000	2.000	2.000	2.000	2.000	2.000
Na	0.097	0.167	0.165	0.498	0.465	0.508	0.206	0.401
K	0.033	0.056	0.086	0.207	0.243	0.218	0.142	0.207
Σ(A)	0.130	0.223	0.251	0.705	0.708	0.726	0.348	0.608
Ca	18.4	26.4	25.8	29.9	30.3	30.6	29.0	30.8
Mg	51.8	44.4	47.0	34.4	26.0	34.1	41.6	36.2
Fe	29.8	29.2	27.2	35.7	43.7	35.3	29.4	33.0
QUAD	34.7	18.4	16.4	8.6	17.4	4.7	54.8	33.3
OTHERS	65.3	81.6	83.6	91.4	82.6	95.3	45.2	66.7

Appendix 3(cont.) Selected Pyroxene Analyses from Diorites of the Cortlandt, Stony Point and Rosetown Complexes.

Sample #	10	10	9	8
SiO_2	51.2	50.7	51.2	50.6
Al_2O_3	3.93	4.68	4.09	6.94
FeO	22.9	22.5	24.8	21.0
MgO	21.8	22.0	20.3	18.6
MnO	0.46	0.43	0.62	0.71
TiO_2	0.15	0.15	0.16	0.19
Cr_2O_3	0.11	0.01	0.09	0.06
CaO	0.59	1.12	1.29	0.39
Na_2O	0.00	0.00	0.00	0.39
Σ	101.2	101.5	102.5	98.9
FeO	21.2	19.7	22.9	21.0
Fe_2O_3	1.89	3.04	2.06	0.0
Structural formulae on the basis of 6 oxygens				
Si	1.883	1.853	1.877	1.890
Al^{IV}	0.117	0.147	0.123	0.110
Σ tet	2.000	2.000	2.000	2.000
Al^{VI}	0.053	0.055	0.054	0.196
Fe^{3+}	0.052	0.084	0.057	0.000
Cr	0.003	0.000	0.003	0.002
Ti	0.004	0.004	0.004	0.005
Mg	1.196	1.196	1.108	1.038
Fe^{2+}	0.653	0.604	0.704	0.656
Mn	0.014	0.013	0.019	0.022
Ca	0.023	0.044	0.051	0.016
Na	0.000	0.000	0.000	0.028
Σ oct	1.999	2.000	2.000	1.963
Ca	1.2	2.4	2.7	0.9
Mg	63.9	64.9	59.5	60.7
Fe	34.9	32.7	37.8	38.4
QUAD	88.3	85.3	87.7	79.7
OTHERS	11.7	14.7	12.3	20.3

Appendix 3(cont.)

Selected Biotite Analyses from Diorites of the Cortlandt, Stony Point, and Rosetown Complexes.

Sample #	7	7	10	10	9		9	8	8	42	42	49	49	50	50
					Core	Rim									
SiO_2	36.2	36.3	37.2	37.2	37.4	37.0	36.8	36.6	38.2	34.7	34.3	35.6	35.2	37.3	37.0
Al_2O_3	17.6	18.5	16.5	16.7	16.2	16.4	15.8	18.7	18.5	16.8	16.5	14.2	14.6	15.3	14.6
FeO	12.7	10.8	12.1	13.7	13.2	13.0	13.2	14.8	13.2	24.2	24.7	23.6	24.8	18.3	20.7
MgO	15.8	17.3	16.6	15.2	16.0	16.3	15.7	14.5	15.4	6.21	6.31	8.00	7.89	13.0	10.1
MnO	0.00	0.00	0.00	0.00	0.01	0.01	0.01	0.00	0.00	0.18	0.16	0.18	0.21	0.23	0.25
TiO_2	3.94	2.78	4.05	3.66	3.88	3.51	3.56	1.73	1.52	3.74	3.70	4.11	4.20	1.37	3.62
Cr_2O_3	0.07	0.07	0.08	0.08	0.09	0.05	0.08	0.04	0.07	0.02	0.05	0.02	0.01	0.26	0.01
CaO	0.01	0.15	0.03	0.13	0.02	0.06	0.03	0.04	0.01	0.01	0.01	0.06	0.13	0.11	0.11
Na_2O	0.09	0.18	0.12	0.04	0.00	0.00	0.00	0.19	0.16	0.00	0.00	0.00	0.00	0.00	0.00
K_2O	7.46	7.18	9.33	8.77	9.47	9.38	9.49	8.28	8.92	9.60	9.06	8.93	8.53	9.30	9.36
Σ	93.9	93.3	96.0	95.5	96.2	95.8	94.7	94.9	95.9	95.5	94.8	94.7	95.6	95.1	95.8

Appendix 3(cont.) Selected Feldspar Analyses from Diorites of the Cortlandt, Stony Point and Rosetown Complexes.

Sample #	7		7	7	10		10		9		9	
	Core	Rim			Core	Rim	Core	Rim	Core	Rim	Core	Rim
SiO_2	50.9	49.3	52.0	48.7	54.0	52.9	51.6	51.7	53.3	54.4	54.5	53.0
Al_2O_3	31.3	32.1	31.0	32.5	30.0	30.5	31.4	31.9	30.2	29.6	29.4	30.1
FeO	0.22	0.24	0.19	0.29	0.25	0.23	0.33	0.31	0.23	0.24	0.23	0.33
CaO	14.1	15.2	13.7	16.0	11.8	12.7	14.0	14.0	12.3	11.9	11.4	12.3
Na_2O	3.58	3.14	3.97	2.58	5.04	4.24	3.47	3.79	4.76	5.06	4.93	4.66
K_2O	0.04	0.03	0.04	0.03	0.10	0.06	0.09	0.06	0.11	0.07	0.13	0.08
Σ	100.2	100.0	100.9	100.0	101.3	100.6	101.0	101.8	100.8	101.2	100.6	100.4
Si	2.313	2.257	2.341	2.230	2.415	2.381	2.326	2.314	2.395	2.429	2.446	2.393
Al	1.678	1.729	1.648	1.753	1.583	1.619	1.669	1.683	1.600	1.562	1.555	1.600
Fe	0.008	0.009	0.007	0.011	0.009	0.009	0.012	0.012	0.009	0.009	0.009	0.012
Ca	0.688	0.743	0.664	0.784	0.565	0.613	0.677	0.670	0.592	0.568	0.549	0.595
Na	0.315	0.279	0.347	0.229	0,437	0.370	0.303	0.329	0.415	0.438	0.429	0.408
K	0.002	0.002	0.002	0.002	0.006	0.003	0.005	0.003	0.006	0.004	0.007	0.005
Σ	5.006	5.019	5.009	5.009	5.014	4.996	4.993	5.011	5.016	5.011	4.995	5.013
Or	0.2	0.2	0.2	0.2	0.6	0.3	0.5	0.3	0.6	0.4	0.7	0.5
Ab	31.3	27.2	34.3	22.6	43.4	37.5	30.8	32.8	41.0	43.4	43.6	40.5
An	68.5	72.6	65.5	77.2	56.0	62.2	68.7	66.9	58.4	56.2	55.7	59.0

Appendix 3(cont.) Selected Feldspar Analyses from Diorites of the Cortlandt, Stony Point and Rosetown Complexes.

Sample #	8		8	42	42	42	49		49	50	50	50
	Core	Rim					Core	Rim				
SiO_2	50.3	55.5	50.1	63.0	61.9	62.2	64.1	65.05	60.2	62.0	62.8	63.9
Al_2O_3	32.5	28.8	32.5	23.1	24.3	23.9	23.5	22.2	24.2	24.9	24.1	19.2
FeO	0.18	0.15	0.14	0.01	0.11	0.12	0.04	0.16	0.06	0.04	0.04	0.02
CaO	14.6	10.3	14.6	3.40	5.09	4.55	4.33	3.30	6.16	5.31	4.71	0.09
Na_2O	3.27	5.62	3.42	8.76	8.80	9.15	9.41	9.91	7.97	8.88	8.94	0.58
K_2O	0.03	0.04	0.09	0.20	0.18	0.17	0.18	0.14	0.15	0.16	0.33	14.7
Σ	100.9	100.4	100.9	98.5	100.3	100.0	101.6	100.8	98.8	101.2	100.9	98.5
Si	2.272	2.487	2.267	2.813	2.737	2.755	2.791	2.847	2.710	2.719	2.759	2.974
Al	1.731	1.520	1.734	1.217	1.266	1.247	1.208	1.147	1.286	1.286	1.246	1.056
Fe	0.007	0.006	0.005	0.000	0.004	0.004	0.001	0.006	0.002	0.001	0.001	0.001
Ca	0.707	0.495	0.707	0.163	0.241	0.216	0.202	0.155	0.297	0.250	0.222	0.004
Na	0.287	0.488	0.300	0.758	0.755	0.786	0.795	0.841	0.695	0.756	0.761	0.052
K	0.002	0.002	0.005	0.011	0.010	0.010	0.010	0.008	0.009	0.009	0.018	0.872
Σ	5.006	4.998	5.019	4.963	5.013	5.019	5.007	5.004	4.999	5.021	5.008	4.960
Or	0.2	0.2	0.5	1.2	1.0	1.0	1.0	0.8	0.9	0.9	1.8	94.0
Ab	28.8	49.6	29.6	81.3	75.0	77.7	78.9	83.8	69.4	74.5	76.0	5.6
An	71.0	50.2	69.9	17.5	24.0	21.3	20.1	15.4	29.7	24.6	22.2	0.4

Appendix 3(cont.) Selected Garnet Analyses from Stony Point Diorite.

Sample #	42		42		42
	Core	Rim	Core	Rim	
SiO_2	37.6	37.4	37.4	37.7	37.9
Al_2O_3	20.7	20.9	21.2	21.0	20.9
FeO	32.5	33.3	33.0	33.2	32.2
MgO	3.44	2.74	3.21	3.38	3.77
MnO	2.24	2.92	2.74	2.41	2.11
TiO_2	0.07	0.09	0.07	0.06	0.07
Cr_2O_3	0.04	0.05	0.03	0.08	0.08
CaO	3.82	3.50	3.03	3.30	3.51
Na_2O	0.00	0.00	0.00	0.00	0.00
K_2O	0.00	0.00	0.00	0.00	0.00
Σ	100.5	100.9	100.7	101.1	100.6
Structural formulae on the basis of 12 oxygens					
Si	3.000	2.989	2.987	2.995	3.010
Al	0.000	0.011	0.013	0.005	0.000
Σ tet	3.000	3.000	3.000	3.000	3.010
Al	1.952	1.959	1.979	1.960	1.956
Cr	0.003	0.003	0.002	0.005	0.005
Ti	0.004	0.006	0.004	0.004	0.004
Σ oct	1.959	1.968	1.985	1.969	1.965
Mg	0.410	0.326	0.381	0.401	0.446
Fe	2.173	2.227	2.202	2.205	2.142
Mn	0.152	0.198	0.185	0.162	0.142
Ca	0.326	0.300	0.259	0.280	0.299
Σ VIII	3.061	3.051	3.127	3.048	3.029

Appendix 4 Selected Pyroxene Analyses from Clinopyroxenites of the Cortlandt Complex (Plutons 3 and 6).

Sample #	11		11	11		11	12	12	12	12	12
	Core	Rim		Core	Rim						
SiO_2	52.5	52.6	52.9	50.8	50.7	52.0	53.7	52.2	53.7	49.1	51.4
Al_2O_3	3.07	3.06	2.37	3.44	4.55	3.66	2.44	2.19	1.96	4.52	4.93
FeO	14.5	15.0	14.8	7.53	6.51	7.65	16.1	20.3	18.8	8.54	6.71
MgO	27.2	27.5	28.1	15.9	14.6	16.2	26.4	24.0	25.5	14.4	14.2
MnO	0.13	0.20	0.15	0.08	0.05	0.09	0.18	0.32	0.26	0.12	0.06
TiO_2	0.17	0.15	0.09	0.58	0.82	0.71	0.19	0.15	0.15	0.96	0.94
Cr_2O_3	0.00	0.00	0.00	0.02	0.05	0.17	0.08	0.07	0.02	0.14	0.18
CaO	1.28	0.74	0.51	20.0	21.4	20.4	1.33	0.64	0.44	21.6	22.7
Na_2O	0.00	0.00	0.00	0.24	0.37	0.24	0.00	0.00	0.00	0.43	0.48
Σ	98.9	99.3	98.9	98.6	99.0	101.2	100.4	99.9	100.9	99.8	101.5
FeO	12.6	12.9	12.5	6.06	6.10	6.54	15.4	18.6	18.1	4.11	5.73
Fe_2O_3	2.15	2.40	2.62	1.64	0.46	1.23	0.76	1.84	0.81	4.92	1.08
Si	1.901	1.898	1.911	1.894	1.884	1.891	1.932	1.922	1.943	1.819	1.868
Al^{IV}	0.099	0.102	0.089	0.106	0.116	0.109	0.068	0.078	0.057	0.181	0.132
Σ tet	2.000	2.000	2.000	2.000	2.000	2.000	2.000	2.000	2.000	2.000	2.000
Al^{VI}	0.032	0.028	0.012	0.045	0.083	0.048	0.035	0.017	0.026	0.017	0.079
Fe^{3+}	0.059	0.065	0.071	0.046	0.013	0.034	0.021	0.051	0.022	0.137	0.030
Cr	0.000	0.000	0.000	0.001	0.001	0.005	0.002	0.002	0.001	0.004	0.005
Ti	0.005	0.004	0.002	0.016	0.023	0.019	0.005	0.004	0.004	0.027	0.026
Mg	1.470	1.479	1.512	0.884	0.808	0.879	1.418	1.317	1.376	0.795	0.767
Fe^{2+}	0.381	0.389	0.377	0.189	0.190	0.199	0.463	0.574	0.546	0.128	0.174
Mn	0.004	0.006	0.005	0.003	0.002	0.003	0.005	0.010	0.008	0.004	0.002
Ca	0.050	0.029	0.020	0.800	0.854	0.796	0.051	0.025	0.017	0.858	0.883
Na	0.000	0.000	0.000	0.017	0.027	0.017	0.000	0.000	0.000	0.031	0.034
Σ oct	2.001	2.000	1.999	2.001	2.001	2.000	2.000	2.000	2.000	2.001	2.000
Ca	2.6	1.5	1.0	42.7	46.1	42.5	2.6	1.3	0.9	48.2	48.4
Mg	77.3	78.0	79.2	47.2	43.6	46.9	73.4	68.7	70.9	44.6	42.0
Fe	20.0	20.5	19.8	10.1	10.2	10.6	24.0	30.0	28.2	7.2	9.6
QUAD	90.1	89.8	91.1	89.2	88.0	89.1	93.2	92.2	94.3	81.5	86.0
OTHER	9.9	10.2	8.9	10.8	12.0	10.9	6.8	7.8	5.7	18.5	14.0

Appendix 4(cont.)

Selected Pyroxene Analyses from Clinopyroxenites of the Cortlandt Complex (Plutons 3 and 6).

Sample #	31		31	31		31	32	32	32		32	33	33	33		33
	Core	Rim		Core	Rim				Core	Rim				Core	Rim	
SiO_2	52.6	51.5	52.8	50.8	49.1	49.2	53.6	54.0	51.5	51.1	50.6	51.4	52.5	51.3	49.9	49.2
Al_2O_3	3.83	4.11	3.78	3.92	5.98	6.09	3.22	2.39	3.99	4.40	5.10	3.66	3.24	3.16	5.19	5.34
FeO	14.9	15.0	15.2	7.63	7.18	8.28	12.8	13.0	5.59	5.33	6.84	12.5	12.9	5.19	5.34	5.21
MgO	26.3	25.9	26.0	14.4	13.7	14.8	28.9	29.1	14.8	15.2	15.4	28.7	29.2	16.2	14.5	14.5
MnO	0.25	0.24	0.28	0.21	0.16	0.19	0.24	0.25	0.17	0.13	0.16	0.21	0.22	0.13	0.12	0.13
TiO_2	0.15	0.23	0.64	0.95	1.38	1.22	0.24	0.25	0.64	0.75	0.88	0.30	0.26	0.53	0.95	0.97
Cr_2O_3	0.08	0.11	0.08	0.11	0.15	0.15	0.34	0.22	0.72	0.49	0.53	0.36	0.33	1.05	0.77	0.73
CaO	0.56	1.38	1.45	20.5	21.0	18.3	0.82	0.51	22.2	22.6	20.4	0.91	0.65	21.2	22.3	22.8
Na_2O	0.00	0.00	0.00	0.50	0.62	0.61	0.00	0.00	0.54	0.47	0.47	0.00	0.00	0.46	0.56	0.39
Σ	98.6	98.5	100.2	99.0	99.2	98.9	100.1	99.7	100.1	100.4	100.4	98.2	99.3	99.1	99.7	99.3
FeO	14.9	13.6	15.2	7.05	5.61	7.08	11.5	12.1	4.56	3.51	5.43	9.18	9.89	3.66	3.42	2.64
Fe_2O_3	0.00	1.60	0.00	0.64	1.74	1.33	1.36	0.94	1.15	2.02	1.57	3.72	3.35	1.70	2.13	2.86
Si	1.915	1.882	1.902	1.895	1.826	1.833	1.903	1.927	1.889	1.866	1.853	1.858	1.875	1.894	1.840	1.820
Al^{IV}	0.085	0.118	0.098	0.105	0.174	0.167	0.097	0.073	0.111	0.134	0.147	0.142	0.125	0.106	0.160	0.180
Σ tet	2.000	2.000	2.000	2.000	2.000	2.000	2.000	2.000	2.000	2.000	2.000	2.000	2.000	2.000	2.000	2.000
Al^{VI}	0.079	0.059	0.063	0.067	0.088	0.101	0.038	0.028	0.062	0.056	0.073	0.014	0.012	0.032	0.066	0.053
Fe^{3+}	0.000	0.044	0.000	0.018	0.049	0.037	0.036	0.025	0.032	0.056	0.043	0.101	0.090	0.047	0.059	0.080
Cr	0.002	0.003	0.002	0.003	0.004	0.004	0.010	0.006	0.021	0.014	0.015	0.010	0.009	0.031	0.022	0.021
Ti	0.004	0.006	0.017	0.027	0.039	0.034	0.006	0.007	0.018	0.021	0.024	0.008	0.007	0.015	0.026	0.027
Mg	1.430	1.412	1.396	0.802	0.758	0.823	1.529	1.546	0.812	0.826	0.841	1.547	1.555	0.889	0.795	0.800
Fe^{2+}	0.453	0.415	0.457	0.220	0.175	0.221	0.342	0.361	0.140	0.107	0.166	0.277	0.296	0.113	0.106	0.082
Mn	0.008	0.007	0.009	0.007	0.005	0.006	0.007	0.008	0.005	0.004	0.005	0.006	0.007	0.004	0.004	0.004
Ca	0.022	0.054	0.056	0.820	0.837	0.729	0.031	0.019	0.873	0.883	0.798	0.035	0.025	0.837	0.882	0.906
Na	0.000	0.000	0.000	0.036	0.045	0.044	0.000	0.000	0.038	0.033	0.033	0.000	0.000	0.033	0.040	0.028
Σ oct	1.998	2.000	2.000	2.000	2.000	1.999	1.999	2.000	2.001	2.000	1.998	1.998	2.001	2.001	2.000	2.001
Ca	1.1	2.9	2.9	44.5	47.3	41.1	1.6	1.0	47.8	48.6	44.2	1.9	1.3	45.5	49.5	50.7
Mg	75.1	75.1	73.1	43.6	42.8	46.4	80.4	80.3	44.5	45.5	46.6	83.2	82.9	48.3	44.6	44.7
Fe	23.8	22.0	24.0	11.9	9.9	12.4	18.0	18.7	7.7	5.9	9.2	14.9	15.8	6.2	5.9	4.6
QUAD	91.4	88.2	90.2	88.5	82.0	82.3	90.3	92.7	86.8	85.4	84.4	85.8	87.5	87.6	82.6	81.9
OTHER	8.6	11.8	9.8	11.5	18.0	17.7	9.7	7.3	13.2	14.6	15.6	14.2	12.5	12.4	17.4	18.1

Appendix 4 (cont.)

Selected Amphibole Analyses from Clinopyroxenites of the Cortlandt Complex (Plutons 3 and 6).

Sample #	11	11	12	12	31	32	32	33	33
SiO_2	42.4	41.6	42.9	43.4	41.7	41.6	41.8	41.5	41.1
Al_2O_3	11.9	13.2	12.8	12.8	13.7	13.2	13.1	13.6	13.8
FeO	11.3	10.1	10.7	10.6	11.0	7.71	7.98	7.79	8.14
MgO	13.2	14.1	13.4	13.6	13.3	15.4	14.9	15.3	14.8
MnO	0.00	0.00	0.00	0.01	0.10	0.07	0.09	0.03	0.09
TiO_2	3.14	3.25	3.49	3.43	2.20	2.97	3.11	3.04	3.42
Cr_2O_3	0.06	0.08	0.09	0.13	0.21	0.90	1.02	0.91	1.03
CaO	11.4	9.74	11.6	11.9	11.2	11.8	11.8	11.7	11.8
Na_2O	1.66	2.19	1.59	1.70	2.00	2.33	2.08	2.50	2.15
K_2O	1.52	1.08	1.34	1.11	0.00	1.53	1.61	0.61	1.23
Σ	96.6	95.3	98.0	98.7	95.4	97.6	97.4	96.9	97.5
FeO	9.94	5.92	9.50	9.58	7.33	6.49	6.97	5.87	6.60
Fe_2O_3	1.48	4.64	1.29	1.10	4.03	1.36	1.12	2.14	1.71
			Structural formulae on the basis of 23 oxygens						
Si	6.283	6.130	6.239	6.267	6.158	6.052	6.0930	6.041	5.979
Al^{IV}	1.717	1.870	1.761	1.733	1.842	1.948	1.9070	1.959	2.021
Σ tet	8.000	8.000	8.000	8.000	8.000	8.000	8.000	8.000	8.000
Al^{VI}	0.367	0.424	0.439	0.440	0.545	0.326	0.350	0.369	0.345
Fe^{2+}	1.232	0.730	1.155	1.156	0.905	0.790	0.851	0.714	0.804
Fe^{3+}	0.165	0.516	0.141	0.120	0.447	0.149	0.123	0.234	0.187
Mg	2.925	3.106	2.913	2.930	2.924	3.341	3.241	3.309	3.213
Mn	0.000	0.000	0.000	0.001	0.013	0.009	0.011	0.004	0.011
Ti	0.350	0.361	0.382	0.372	0.244	0.325	0.341	0.333	0.374
Cr	0.007	0.009	0.010	0.015	0.025	0.104	0.118	0.105	0.119
Σ oct	5.046	5.146	5.040	5.034	5.103	5.044	5.035	5.068	5.053
X oct	0.046	0.146	0.040	0.034	0.103	0.044	0.035	0.068	0.053
Ca	1.809	1.539	1.815	1.833	1.780	1.847	1.837	1.818	1.840
Na(M4)	0.145	0.315	0.145	0.133	0.117	0.109	0.128	0.114	0.107
Σ(M4)	2.000	2.000	2.000	2.000	2.000	2.000	2.000	2.000	2.000
Na	0.333	0.312	0.304	0.343	0.455	0.546	0.461	0.589	0.500
K	0.288	0.203	0.249	0.204	0.000	0.284	0.300	0.113	0.228
Σ(A)	0.621	0.515	0.553	0.547	0.455	0.830	0.761	0.702	0.728
Ca	30.3	28.6	30.9	31.0	31.7	30.9	31.0	31.1	31.4
Mg	49.0	57.8	49.5	49.5	52.1	55.9	54.7	56.7	54.9
Fe	20.7	13.6	19.6	19.5	16.1	13.2	14.3	12.2	13.7
QUAD	14.2	6.5	11.9	13.3	7.9	2.6	4.7	2.0	0.0
OTHER	85.8	93.5	88.1	86.7	92.1	97.4	95.3	98.0	100.0

Appendix 4(cont.) Selected Olivine Analyses from Clinopyroxenites of the Cortlandt Complex (Plutons 3 and 6).

Sample #	11	11	32	32	33	33
SiO_2	38.4	38.0	39.0	38.9	38.7	38.6
Al_2O_3	0.00	0.00			0.04	
FeO	23.7	23.5	19.8	19.9	19.4	19.5
MgO	38.9	39.2	41.2	41.0	41.9	41.8
MnO	0.16	0.17			0.16	
Cr_2O_3	0.00	0.00			0.07	
CaO	0.02	0.00	0.01	0.02	0.00	0.01
Na_2O	0.00	0.00			0.00	
Σ	101.1	101.0	99.9	99.8	100.4	99.8
Si	0.992	0.986	1.000	1.001	0.991	0.991
Al	0.000	0.000			0.001	
Fe	0.512	0.510	0.425	0.428	0.416	0.419
Mg	1.499	1.515	1.575	1.570	1.596	1.598
Mn	0.004	0.004			0.003	
Cr	0.000	0.000			0.001	
Ca	0.001	0.000	0.000	0.001	0.000	0.000
Na	0.000	0.000			0.000	
Σ	3.008	3.014	3.000	2.999	3.008	3.009
Fo	74.5	74.8	78.8	78.6	79.3	79.2
Fa	25.5	25.2	21.2	21.4	20.7	20.8

Appendix 4(cont.) Spinel Analysis from Clinopyroxenite Sample #32.

Sample #	32
SiO_2	1.29
Al_2O_3	4.34
FeO	70.0
MgO	1.57
MnO	0.48
TiO_2	2.39
Cr_2O_3	16.3
CaO	0.32
Na_2O	0.00
K_2O	0.00
Σ	96.7

Selected Biotite Analyses from Clinopyroxenites of the Cortlandt Complex (Plutons 3 and 6).

Sample #	32	32	32
SiO_2	37.9	37.0	37.5
Al_2O_3	15.8	15.7	15.9
FeO	6.37	7.11	6.72
MgO	20.6	19.3	19.8
MnO	0.03	0.00	0.02
TiO_2	3.76	4.58	4.07
Cr_2O_3	0.66	0.72	0.69
CaO	0.02	0.00	0.00
Na_2O	0.38	0.45	0.40
K_2O	9.56	9.22	9.35
Σ	95.2	94.0	94.4

Appendix 4(cont) Selected Feldspar Analyses from Clinopyroxenites of the Cortlandt Complex (Plutons 3 and 6).

Sample #	12	12	31
SiO_2	54.3	49.4	44.9
Al_2O_3	29.9	32.6	34.0
FeO	0.00	0.19	0.18
CaO	11.8	15.4	18.2
Na_2O	4.71	2.91	0.74
K_2O	0.13	0.04	0.00
Σ	100.8	100.4	98.0
Si	2.430	2.246	2.109
Al	1.576	1.748	1.882
Fe	0.000	0.007	0.007
Ca	0.567	0.749	0.917
Na	0.409	0.257	0.067
K	0.007	0.002	0.000
Σ	4.990	5.009	4.983
Or	0.7	0.2	0.0
Ab	41.6	25.5	6.8
An	57.7	74.3	93.2

Appendix 5 Selected Amphibole Analyses from Cortlandtites and Amphibole-Pyroxenites of the Cortlandt, Stony Point and Rosetown Complexes.

Sample #	14	14	14	16	16	16	17	17
SiO_2	42.1	42.2	42.4	45.4	41.2	43.1	43.3	42.2
Al_2O_3	13.6	13.5	13.8	10.7	13.2	12.2	13.3	13.0
FeO	8.85	9.19	8.72	8.06	10.0	9.29	7.27	7.47
MgO	15.3	15.1	14.8	17.0	14.4	15.6	15.8	15.8
MnO	0.06	0.05	0.03	0.00	0.00	0.00	0.00	0.00
TiO_2	2.26	2.57	2.71	0.98	2.97	1.95	2.45	2.99
Cr_2O_3	0.26	0.28	0.24	0.04	0.13	0.07	0.54	0.39
CaO	11.6	11.5	12.1	11.9	11.0	11.8	12.0	12.0
Na_2O	1.98	2.07	2.07	1.91	2.29	2.08	2.49	1.91
K_2O	1.38	1.20	1.28	0.33	1.03	0.85	0.07	1.41
Σ	97.3	97.7	98.1	96.4	96.2	96.8	97.2	97.1
FeO	5.92	6.51	7.55	4.15	7.12	6.18	5.74	5.95
Fe_2O_3	3.26	2.98	1.30	4.35	3.23	3.45	1.70	1.69
	Structural formulae on the basis of 23 oxygens							
Si	6.102	6.105	6.135	6.533	6.070	6.265	6.227	6.129
Al^{IV}	1.898	1.895	1.865	1.467	1.930	1.735	1.773	1.871
Σ tet	8.000	8.000	8.000	8.000	8.000	8.000	8.000	8.000
Al^{VI}	0.430	0.415	0.477	0.356	0.368	0.355	0.475	0.354
Fe^{2+}	0.718	0.787	0.913	0.499	0.877	0.752	0.691	0.723
Fe^{3+}	0.356	0.325	0.141	0.471	0.350	0.378	0.184	0.185
Mg	3.306	3.247	3.183	3.637	3.153	3.370	3.376	3.419
Mn	0.007	0.006	0.004	0.000	0.000	0.000	0.000	0.000
Ti	0.247	0.280	0.295	0.106	0.329	0.213	0.265	0.327
Cr	0.030	0.032	0.027	0.005	0.015	0.008	0.061	0.045
Σ oct	5.094	5.092	5.040	5.074	5.102	5.076	5.053	5.053
X oct	0.094	0.092	0.040	0.074	0.102	0.076	0.053	0.053
Ca	1.799	1.799	1.867	1.841	1.739	1.834	1.855	1.865
Na(M4)	0.107	0.119	0.093	0.085	0.159	0.090	0.092	0.082
Σ(M4)	2.000	2.000	2.000	2.000	2.000	2.000	2.000	2.000
Na	0.450	0.461	0.487	0.448	0.495	0.497	0.602	0.456
K	0.248	0.221	0.236	0.061	0.194	0.158	0.013	0.261
Σ(A)	0.698	0.682	0.723	0.509	0.689	0.655	0.615	0.717
Ca	30.9	30.7	31.3	30.8	30.1	30.8	31.3	31.1
Mg	56.8	55.8	53.4	60.9	54.7	56.6	57.0	56.9
Fe	12.3	13.5	15.3	8.3	15.2	12.6	11.7	12.0
QUAD	5.1	5.3	6.7	26.7	3.5	13.3	11.4	6.4
OTHER	94.9	94.7	93.3	73.3	96.5	86.7	88.6	93.6

Appendix 5(cont.) Selected Amphibole Analyses from Cortlandtites and Amphibole-Pyroxenites of the Cortlandt, Stony Point and Rosetown Complexes.

Sample #	41		41	15		15	40		40	48
	Core	Rim		Core	Rim		Core	Rim		
SiO_2	41.5	40.8	41.9	39.8	38.4	40.3	39.8	39.7	39.8	40.1
Al_2O_3	13.7	13.9	13.4	16.5	17.8	16.2	13.0	14.2	14.6	11.9
FeO	9.52	9.29	8.95	10.6	10.7	9.82	11.3	12.6	12.8	11.6
MgO	14.4	14.7	15.3	12.8	11.9	13.0	12.5	11.6	11.6	12.5
MnO	0.13	0.09	0.08	0.09	0.10	0.11	0.14	0.13	0.17	0.08
TiO_2	3.39	3.49	1.97	2.24	2.63	2.01	6.23	4.04	4.53	4.64
Cr_2O_3	0.10	0.03	0.09	0.05	0.06	0.06	0.05	0.04	0.04	0.02
CaO	11.0	10.9	10.6	11.5	12.0	11.9	11.0	10.8	10.6	11.1
Na_2O	3.01	2.99	3.12	1.89	1.79	1.88	2.52	2.64	2.63	2.27
K_2O	1.05	0.98	1.06	2.44	2.33	2.47	1.01	1.00	1.01	1.15
Σ	97.8	97.1	96.5	97.9	97.6	97.8	97.6	96.7	97.7	95.3
FeO	7.66	6.82	5.89	8.81	9.70	9.01	10.4	10.9	10.7	10.7
Fe_2O_3	2.06	2.74	3.40	1.93	1.08	0.90	1.00	1.92	2.35	0.92
Structural formulae on the basis of 23 oxygens										
Si	6.033	5.966	6.134	5.843	5.682	5.916	5.889	5.925	5.875	6.077
Al^{IV}	1.967	2.034	1.866	2.157	2.318	2.084	2.111	2.075	2.125	1.923
Σ	8.000	8.000	8.000	8.000	8.000	8.000	8.000	8.000	8.000	8.000
Al^{VI}	0.382	0.358	0.437	0.695	0.781	0.727	0.152	0.428	0.418	0.207
Fe^{2+}	0.933	0.833	0.720	1.082	1.200	1.107	1.288	1.355	1.321	1.360
Fe^{3+}	0.226	0.302	0.375	0.214	0.120	0.099	0.112	0.215	0.261	0.105
Mg	3.125	3.194	3.337	2.806	2.621	2.852	2.764	2.588	2.545	2.817
Mn	0.016	0.011	0.010	0.011	0.013	0.014	0.017	0.016	0.021	0.010
Ti	0.371	0.383	0.217	0.247	0.293	0.222	0.693	0.454	0.503	0.529
Cr	0.011	0.004	0.010	0.006	0.007	0.007	0.006	0.005	0.005	0.002
Σ oct	5.064	5.085	5.106	5.061	5.035	5.028	5.032	5.061	5.074	5.030
X oct	0.064	0.085	0.106	0.061	0.035	0.028	0.032	0.061	0.074	0.030
Ca	1.717	1.702	1.658	1.816	1.902	1.876	1.740	1.721	1.672	1.801
Na(M4)	0.219	0.213	0.236	0.123	0.063	0.096	0.228	0.218	0.254	0.169
Σ(M4)	2.000	2.000	2.000	2.000	2.000	2.000	2.000	2.000	2.000	2.000
Na	0.630	0.634	0.649	0.415	0.451	0.439	0.494	0.547	0.499	0.498
K	0.195	0.183	0.198	0.457	0.440	0.463	0.191	0.191	0.190	0.222
Σ(A)	0.825	0.817	0.847	0.872	0.891	0.902	0.685	0.738	0.689	0.720
Ca	29.7	29.7	29.0	31.8	33.2	32.1	30.0	30.4	30.2	30.1
Mg	54.1	55.7	58.4	49.2	45.8	48.9	47.7	45.7	46.0	47.1
Fe	16.2	14.6	12.6	19.0	21.0	19.0	22.2	23.9	23.8	22.8
QUAD	1.7	0.0	6.7	0.0	0.0	0.0	0.0	0.0	0.0	3.8
OTHER	98.3	100	93.3	100	100	100	100	100	100	96.2

Appendix 5(cont.) Selected Pyroxene Analyses from Cortlandtites and Amphibole-Pyroxenites of the Cortlandt, Stony Point and Rosetown Complexes.

Sample #	14	14	14		14	16	16	16		16	16	17	17		17
			Core	Rim				Core	Rim				Core	Rim	
SiO_2	53.9	53.8	52.6	51.6	50.8	53.0	54.6	51.3	50.9	53.3	50.9	53.5	52.3	51.6	52.8
Al_2O_3	2.42	2.70	1.99	4.03	4.71	2.71	1.09	3.91	4.07	0.85	4.53	2.16	3.24	3.84	2.70
FeO	13.8	14.3	4.91	5.18	6.57	14.0	14.0	6.29	7.18	3.91	6.66	12.0	5.19	5.87	5.55
MgO	28.9	27.9	15.0	15.4	15.2	27.6	29.2	15.8	15.4	16.9	15.5	30.9	16.8	16.4	17.3
MnO	0.25	0.18	0.11	0.13	0.11	0.17	0.21	0.03	0.06	0.00	0.04	0.14	0.07	0.00	0.05
TiO_2	0.09	0.14	0.23	0.61	0.90	0.25	0.07	0.77	0.60	0.10	0.89	0.22	0.57	0.65	0.51
Cr_2O_3	0.09	0.14	0.23	0.21	0.27	0.07	0.00	0.11	0.13	0.00	0.15	0.10	0.23	0.25	0.22
CaO	0.56	1.00	23.6	22.2	21.2	1.54	0.36	20.0	20.8	23.9	20.4	0.71	21.3	20.9	21.0
Na_2O	0.00	0.00	0.23	0.24	0.34	0.00	0.00	0.43	0.46	0.01	0.39	0.00	0.29	0.36	0.29
Σ	100.0	100.2	99.0	99.6	100.0	99.4	99.4	98.7	99.7	98.9	99.5	99.8	100.0	99.9	100.5
FeO	12.1	13.1	4.91	5.11	5.64	12.3	12.7	6.21	5.12	3.16	6.07	9.49	4.43	4.47	4.52
Fe_2O_3	1.89	1.31	0.00	0.08	1.03	1.90	1.34	0.09	2.29	0.83	0.65	2.84	0.84	1.56	1.14
Si	1.920	1.920	1.955	1.900	1.867	1.909	1.957	1.906	1.878	1.968	1.879	1.895	1.910	1.887	1.920
Al^{IV}	0.080	0.080	0.045	0.100	0.133	0.091	0.043	0.094	0.122	0.032	0.121	0.090	0.090	0.113	0.080
Σ tet	2.000	2.000	2.000	2.000	2.000	2.000	2.000	2.000	2.000	2.000	2.000	1.985	2.000	2.000	2.000
Al^{VI}	0.022	0.034	0.042	0.075	0.071	0.024	0.003	0.077	0.055	0.005	0.077	0.000	0.049	0.053	0.035
Fe^{3+}	0.051	0.035	0.000	0.002	0.029	0.051	0.036	0.002	0.064	0.023	0.018	0.076	0.023	0.043	0.031
Cr	0.003	0.004	0.007	0.006	0.008	0.002	0.000	0.003	0.004	0.000	0.004	0.003	0.007	0.007	0.006
Ti	0.002	0.004	0.006	0.017	0.025	0.007	0.002	0.022	0.017	0.003	0.025	0.006	0.016	0.018	0.014
Mg	1.533	1.488	0.832	0.845	0.832	1.482	1.557	0.876	0.846	0.928	0.852	1.634	0.915	0.897	0.936
Fe^{2+}	0.361	0.393	0.152	0.158	0.173	0.370	0.382	0.193	0.158	0.098	0.187	0.281	0.135	0.137	0.137
Mn	0.008	0.005	0.003	0.004	0.003	0.005	0.006	0.001	0.002	0.000	0.001	0.004	0.002	0.000	0.002
Ca	0.021	0.038	0.940	0.876	0.834	0.059	0.014	0.795	0.823	0.944	0.807	0.027	0.832	0.820	0.818
Na	0.000	0.000	0.017	0.017	0.024	0.000	0.000	0.031	0.033	0.001	0.028	0.000	0.021	0.026	0.020
Σ oct	2.001	2.001	1.999	2.000	1.999	2.000	2.000	2.000	2.002	2.002	1.999	2.031	2.000	2.001	1.999
Ca	1.1	2.0	48.8	46.6	45.3	3.1	0.7	42.7	45.1	47.9	43.7	1.4	44.2	44.2	43.2
Mg	80.1	77.5	43.2	45.0	45.2	77.5	79.7	47.0	46.3	47.1	46.1	84.1	48.6	48.4	49.5
Fe	18.8	20.5	8.0	8.4	9.4	19.4	19.6	10.3	8.6	5.0	10.2	14.5	7.2	7.4	7.3
QUAD	92.0	92.0	94.5	90.0	86.7	90.9	95.7	89.6	86.1	96.8	87.6	91.0	90.5	87.9	91.3
OTHER	8.0	8.0	5.5	10.0	13.3	9.1	4.3	10.4	13.9	3.2	12.4	9.0	9.5	12.1	8.7

Appendix 5(cont.) Selected Pyroxene Analyses from Cortlandtites and Amphibole-Pyroxenites of the Cortlandt, Stony Point and Rosetown Complexes.

Sample #	41		41	41	41	15	15	15	15	40	40	40	48
	Core	Rim											
SiO_2	52.0	52.5	54.4	51.4	51.6	45.8	45.2	46.0	47.4	51.0	51.9	48.6	49.1
Al_2O_3	4.09	3.57	1.16	4.32	3.69	11.2	11.1	10.4	9.22	4.32	1.93	6.43	3.98
FeO	13.4	13.6	13.9	6.02	6.10	7.38	7.96	7.79	7.61	7.08	9.19	7.73	8.87
MgO	27.6	27.9	28.9	15.1	15.7	9.94	9.89	10.1	10.6	15.8	14.1	14.4	12.6
MnO	0.24	0.26	0.31	0.18	0.18	0.05	0.10	0.07	0.05	0.17	0.31	0.17	0.16
TiO_2	0.30	0.22	0.00	0.61	0.30	1.90	1.96	2.00	1.91	0.74	0.20	1.23	0.90
Cr_2O_3	0.03	0.02	0.02	0.46	0.34	0.05	0.07	0.06	0.06	0.17	0.09	0.10	0.00
CaO	1.22	1.26	0.94	21.0	20.4	22.3	21.7	22.1	21.3	19.7	21.0	19.9	20.5
Na_2O	0.00	0.00	0.00	1.25	1.25	1.40	1.33	1.54	1.44	0.52	0.54	0.58	0.59
Σ	98.8	99.4	99.6	100.3	99.6	100.0	99.3	100.0	99.6	99.6	99.3	99.1	96.7
FeO	11.4	11.4	12.3	2.18	1.87	3.60	4.08	3.22	5.49	5.58	7.42	5.24	7.94
Fe_2O_3	2.18	2.52	1.80	4.26	4.70	4.21	4.31	5.08	2.36	1.67	1.97	2.76	1.03
Si	1.875	1.884	1.948	1.870	1.887	1.694	1.687	1.701	1.763	1.879	1.942	1.806	1.891
Al^{IV}	0.125	0.116	0.049	0.130	0.113	0.306	0.313	0.299	0.237	0.121	0.058	0.194	0.109
Σ tet	2.000	2.000	1.997	2.000	2.000	2.000	2.000	2.000	2.000	2.000	2.000	2.000	2.000
Al^{VI}	0.049	0.035	0.000	0.055	0.046	0.182	0.176	0.155	0.167	0.066	0.027	0.087	0.071
Fe^{3+}	0.059	0.068	0.048	0.117	0.129	0.117	0.121	0.141	0.066	0.046	0.055	0.077	0.030
Cr	0.001	0.001	0.001	0.013	0.010	0.001	0.002	0.002	0.002	0.005	0.003	0.003	0.000
Ti	0.008	0.006	0.000	0.017	0.008	0.053	0.055	0.056	0.053	0.020	0.006	0.034	0.026
Mg	1.483	1.493	1.542	0.820	0.854	0.548	0.551	0.557	0.589	0.869	0.786	0.797	0.721
Fe^{2+}	0.345	0.341	0.369	0.067	0.057	0.111	0.127	0.100	0.171	0.172	0.123	0.163	0.256
Mn	0.007	0.008	0.009	0.006	0.006	0.002	0.003	0.002	0.002	0.005	0.010	0.005	0.005
Ca	0.047	0.048	0.036	0.817	0.801	0.885	0.868	0.877	0.847	0.779	0.842	0.791	0.846
Na	0.000	0.000	0.000	0.088	0.089	0.100	0.096	0.111	0.104	0.037	0.039	0.042	0.044
Σ oct	1.999	2.000	2.005	2.000	2.000	1.999	1.999	2.001	2.001	1.999	2.001	1.999	1.999
Ca	2.5	2.6	1.8	48.0	46.8	57.3	56.2	57.2	52.7	42.8	45.3	45.2	46.4
Mg	79.1	79.3	79.2	48.1	49.9	35.5	35.6	36.3	36.7	47.8	42.2	45.5	39.6
Fe	18.4	18.1	19.0	3.9	3.3	7.2	8.2	6.5	10.6	9.4	12.5	9.3	14.0
QUAD	87.5	88.4	95.1		80.7	64.7	64.6	64.6	71.2	86.2	90.9	79.8	87.3
OTHER	12.5	11.6	4.9		19.3	35.3	35.4	35.4	28.8	13.8	9.1	20.2	12.7

Appendix 5(cont.) Selected Olivine Analyses from Cortlandtites of the Cortlandt and Stony Point Complexes.

Sample #	14	14		16	16	16	17	17	17	41	41	41
	Core	Rim		Core	Rim							
SiO_2	39.5	38.8	38.8	38.6	38.7	39.0	39.3	39.4	39.7	38.4	38.5	38.1
Al_2O_3												
FeO	21.9	21.6	21.5	22.5	21.3	20.9	18.9	18.7	18.8	22.0	23.0	22.0
MgO	40.6	40.5	40.2	39.9	40.9	41.0	42.2	42.6	42.3	40.0	38.8	39.7
MnO												
Cr_2O_3												
CaO	0.02	0.03	0.00	0.00	0.04	0.04	0.01	0.04	0.02	0.02	0.02	0.02
Na_2O												
Σ	102.0	101.0	100.5	101.0	101.0	101.0	100.4	100.8	100.8	100.4	100.3	99.9
Si	1.000	0.994	0.997	0.993	0.991	0.996	0.999	0.998	1.004	0.992	0.999	0.991
Al												
Fe	0.465	0.464	0.464	0.484	0.456	0.447	0.402	0.396	0.397	0.474	0.499	0.479
Mg	1.534	1.548	1.542	1.531	1.562	1.560	1.600	1.607	1.594	1.542	1.502	1.539
Mn												
Cr												
Ca	0.001	0.001	0.000	0.000	0.001	0.001	0.000	0.001	0.001	0.001	0.001	0.001
Na												
Σ	3.000	3.006	3.003	3.007	3.009	3.004	3.001	3.002	2.996	3.008	3.001	3.009
Fo	76.7	77.0	76.9	76.0	77.4	77.7	79.9	80.2	80.0	76.5	75.0	76.3
Fa	23.3	23.0	23.1	24.0	22.6	22.3	20.1	19.8	20.0	23.5	25.0	23.7

Appendix 5(cont.) Selected Mica Analyses from Cortlandtites and Amphibole-Pyroxenites.

Sample #	41	41	15	15	40	40	48
	Phlogopite		Biotite		Biotite		Biotite
SiO_2	38.8	39.0	37.9	37.0	36.9	36.4	36.1
Al_2O_3	16.8	16.7	18.0	17.6	15.3	15.2	13.9
FeO	5.92	5.84	9.01	9.27	13.4	15.1	15.8
MgO	22.9	23.3	19.3	18.8	15.5	14.2	13.6
MnO	0.00	0.00	0.02	0.00	0.09	0.07	0.03
TiO_2	0.15	0.23	2.21	2.23	3.32	3.73	5.36
Cr_2O_3	0.00	0.01	0.05	0.03	0.04	0.10	0.00
CaO	0.01	0.01	0.11	0.02	0.03	0.02	0.09
Na_2O	2.33	2.65	0.03	0.21	0.16	0.08	0.00
K_2O	6.65	5.57	6.61	9.42	9.25	9.40	9.47
Σ	93.6	93.3	93.2	94.6	93.9	94.3	94.3

Appendix 5(cont.) Selected Feldspar Analyses from Amphibole-Pyroxenites.

Sample #	40	40	40	48	48	48
SiO_2	55.8	59.1	55.1	53.8	57.7	54.2
Al_2O_3	28.6	25.9	27.9	28.7	25.3	28.0
FeO	0.06	0.28	0.13	0.20	0.18	0.15
CaO	10.2	7.18	10.4	11.0	7.42	10.9
Na_2O	5.98	7.55	5.92	4.79	6.68	5.12
K_2O	0.07	0.07	0.06	0.33	0.51	0.33
Σ	100.7	100.1	99.6	98.8	97.8	98.8
Si	2.494	2.638	2.496	2.459	2.638	2.478
Al	1.507	1.362	1.490	1.545	1.362	1.510
Fe	0.002	0.010	0.005	0.008	0.007	0.006
Ca	0.489	0.343	0.506	0.537	0.363	0.536
Na	0.518	0.653	0.520	0.424	0.592	0.454
K	0.004	0.004	0.003	0.019	0.030	0.019
Σ	5.014	5.010	5.020	4.991	4.992	5.003
Or	0.4	0.4	0.3	1.9	3.1	1.9
Ab	51.2	65.3	50.5	43.3	60.1	45.0
An	48.4	34.3	49.2	54.8	36.8	53.1

Appendix 6 Selected Amphibole Analyses from Norites of the Cortlandt Complex (Pluton 5).

Sample #	19	19	18		18	22	22
			Core	Rim			
SiO_2	39.4	39.8	40.7	40.3	39.8	44.2	43.1
Al_2O_3	14.2	14.7	12.9	13.4	13.2	11.8	11.3
FeO	14.2	13.7	13.8	13.7	14.2	18.0	17.1
MgO	10.2	10.7	11.4	11.0	11.0	9.71	8.23
MnO	0.15	0.12	0.13	0.15	0.12	0.47	0.38
TiO_2	3.71	3.17	5.18	5.07	5.62	0.64	1.17
Cr_2O_3	0.12	0.13	0.14	0.11	0.08	0.01	0.01
CaO	11.4	11.5	10.9	11.4	11.5	11.1	11.3
Na_2O	1.57	1.28	2.20	2.07	2.11	1.09	1.05
K_2O	1.84	2.26	1.46	1.44	1.69	1.12	1.46
Σ	96.8	97.3	98.8	98.6	99.3	98.2	95.0
FeO	13.3	12.3	12.5	13.1	13.7	14.5	17.0
Fe_2O_3	1.02	1.53	1.40	0.66	0.53	3.88	0.13
Si	5.953	5.955	5.996	5.969	5.892	6.546	6.660
Al^{IV}	2.047	2.045	2.004	2.031	2.108	1.454	1.340
Σ tet	8.000	8.000	8.000	8.000	8.000	8.000	8.000
Al^{VI}	0.482	0.549	0.242	0.298	0.194	0.607	0.714
Fe^{2+}	1.679	1.542	1.546	1.618	1.693	1.797	2.194
Fe^{3+}	0.116	0.172	0.155	0.073	0.059	0.432	0.015
Mg	2.301	2.398	2.494	2.437	2.422	2.142	1.895
Mn	0.019	0.015	0.016	0.019	0.015	0.059	0.050
Ti	0.422	0.357	0.574	0.564	0.625	0.071	0.136
Cr	0.014	0.015	0.016	0.013	0.009	0.001	0.001
Σ oct	5.033	5.048	5.043	5.022	5.017	5.109	5.005
X oct	0.033	0.048	0.043	0.022	0.017	0.109	0.005
Ca	1.855	1.846	1.725	1.806	1.819	1.764	1.864
Na(M4)	0.112	0.106	0.232	0.172	0.164	0.127	0.131
Σ(M4)	2.000	2.000	2.000	2.000	2.000	2.000	2.000
Na	0.348	0.266	0.397	0.421	0.441	0.186	0.184
K	0.355	0.432	0.275	0.272	0.319	0.212	0.288
Σ(A)	0.703	0.698	0.672	0.693	0.760	0.398	0.472
Ca	31.8	31.9	29.9	30.8	30.7	30.9	31.3
Mg	39.4	41.4	43.3	41.6	40.8	37.6	31.8
Fe	28.8	26.7	26.8	27.6	28.5	31.5	36.9
QUAD	0.0	0.0	0.0	0.0	0.0	27.3	33.0
OTHER	100	100	100	100	100	72.7	67.0

Appendix 6(cont.)

Selected Amphibole Analyses from Norites of the Cortlandt Complex (Pluton 5).

Sample #	27		27	28	28	28	28	23	23
	Core	Rim							
SiO_2	40.9	40.1	39.5	52.1	53.0	43.3	44.9	42.1	41.8
Al_2O_3	13.6	14.3	13.8	3.05	2.96	13.2	11.5	10.0	10.2
FeO	14.1	13.9	14.5	19.8	19.8	16.1	15.5	19.3	19.0
MgO	11.2	10.8	10.9	17.3	17.1	10.6	11.5	9.60	9.47
MnO	0.17	0.19	0.19	0.88	0.82	0.25	0.26	0.21	0.23
TiO_2	4.17	3.87	4.54	0.11	0.11	0.65	0.35	1.92	2.06
Cr_2O_3	0.11	0.10	0.15	0.00	0.02	0.00	0.03	0.09	0.08
CaO	11.1	11.3	10.8	2.63	3.09	11.1	10.9	11.2	10.7
Na_2O	2.15	1.89	2.20	0.19	0.23	0.46	1.60	1.48	1.44
K_2O	1.46	1.83	1.36	0.04	0.04	0.00	0.17	1.85	1.96
Σ	99.0	98.3	98.0	96.2	97.2	97.2	96.7	97.8	97.0
FeO	12.6	12.8	12.3	19.0	19.4	10.6	11.6	16.6	16.2
Fe_2O_3	1.68	1.23	2.45	0.95	0.47	6.20	4.35	2.99	3.10
Si	6.011	5.954	5.880	7.667	7.719	6.430	6.623	6.399	6.393
Al^{IV}	1.989	2.046	2.120	0.333	0.281	1.570	1.377	1.601	1.607
Σ tet	8.000	8.000	8.000	8.000	8.000	8,000	8.000	8.000	8.000
Al^{VI}	0.370	0.462	0.305	0.196	0.227	0.732	0.621	0.197	0.236
Fe^{2+}	1.553	1.593	1.525	2.336	2.364	1.310	1.433	2.109	2.074
Fe^{3+}	0.186	0.138	0.274	0.105	0.051	0.692	0.483	0.342	0.356
Mg	2.449	2.378	2.424	3.800	3.711	2.336	2.518	2.175	2.158
Mn	0.021	0.024	0.024	0.110	0.101	0.031	0.033	0.027	0.030
Ti	0.461	0.432	0.508	0.012	0.012	0.072	0.039	0.220	0.237
Cr	0.013	0.012	0.018	0.000	0.002	0.000	0.003	0.011	0.010
Σ oct	5.053	5.039	5.078	6.559	6.468	5.173	5.130	5.081	5.101
X oct	0.053	0.039	0.078	1.559	1.468	0.173	0.130	0.081	0.101
Ca	1.753	1.801	1.730	0.414	0.483	1.760	1.722	1.829	1.760
Na(M4)	0.194	0.160	0.192	0.027	0.049	0.067	0.148	0.090	0.139
Σ(M4)	2.000	2.000	2.000	2.000	2.000	2.000	2.000	2.000	2.000
Na	0.419	0.384	0.443	0.027	0.016	0.065	0.310	0.346	0.288
K	0.274	0.347	0.258	0.008	0.007	0.000	0.032	0.359	0.382
Σ(A)	0.693	0.731	0.701	0.035	0.023	0.065	0.342	0.705	0.670
Ca	30.5	31.2	30.5	6.3	7.4	32.6	30.4	29.9	29.4
Mg	42.5	41.2	42.7	58.0	56.6	43.2	44.4	35.6	36.0
Fe	27.0	27.6	26.9	35.7	36.0	24.2	25.2	34.5	34.6
QUAD	0.6	0.0	0.0	83.4	85.9	21.5	31.2	20.0	19.6
OTHER	99.4	100	100	16.6	14.1	78.5	68.8	80.0	80.4

Appendix 6(cont.)

Selected Pyroxene Analyses from Norites of the Cortlandt Complex (Pluton 5).

Sample #	19		19	19	19	20		20	20	21	21	21	21	21
	Core	Rim				Core	Rim							
SiO_2	51.6	51.0	51.0	49.6	49.7	50.0	50.4	50.1	49.7	51.6	51.6	50.9	51.8	51.4
Al_2O_3	2.31	3.02	2.48	4.21	3.89	1.40	1.43	1.57	2.89	1.66	1.69	2.67	3.05	3.29
FeO	23.6	23.0	23.5	11.6	12.0	25.2	24.9	24.7	11.2	25.9	26.1	16.8	13.2	14.4
MgO	21.1	20.5	21.0	12.6	12.8	19.2	19.0	19.1	11.6	18.2	18.3	13.1	11.9	12.3
MnO	0.56	0.56	0.54	0.36	0.37	0.51	0.47	0.37	0.18	0.63	0.58	0.48	0.33	0.33
TiO_2	0.41	0.35	0.31	0.71	0.62	0.15	0.07	0.12	0.38	0.17	0.20	0.49	0.55	0.45
Cr_2O_3	0.11	0.12	0.10	0.09	0.10	0.00	0.00	0.00	0.00	0.02	0.02	0.03	0.04	0.05
CaO	1.25	1.91	1.39	18.8	19.6	0.88	1.17	0.97	19.6	1.88	1.29	14.3	19.2	17.2
Na_2O	0.00	0.00	0.00	0.48	0.45	0.00	0.00	0.00	0.34	0.00	0.00	0.27	0.48	0.43
Σ	101.0	100.5	100.3	98.5	99.6	97.4	97.4	96.9	95.9	100.0	99.8	99.1	100.5	99.9
FeO	22.3	21.6	21.6	10.9	9.48	24.2	24.6	24.4	11.2	25.9	26.1	16.8	13.2	14.0
Fe_2O_3	1.45	1.58	2.07	0.79	2.75	1.21	0.35	0.34	0.00	0.00	0.00	0.00	0.00	0.00
Si	1.916	1.900	1.906	1.890	1.872	1.946	1.960	1.955	1.946	1.963	1.965	1.946	1.945	1.940
Al^{IV}	0.084	0.100	0.094	0.110	0.128	0.054	0.040	0.045	0.054	0.037	0.035	0.054	0.055	0.060
Σ tet	2.000	2.000	2.000	2.000	2.000	2.000	2.000	2.000	2.000	2.000	2.000	2.000	2.000	2.000
Al^{VI}	0.017	0.033	0.015	0.079	0.045	0.010	0.026	0.028	0.080	0.038	0.041	0.066	0.080	0.086
Fe^{3+}	0.040	0.044	0.058	0.023	0.078	0.035	0.010	0.010	0.000	0.000	0.000	0.000	0.000	0.000
Cr	0.003	0.004	0.003	0.003	0.003	0.000	0.000	0.000	0.000	0.001	0.001	0.001	0.001	0.001
Ti	0.011	0.010	0.009	0.020	0.018	0.004	0.002	0.004	0.011	0.005	0.006	0.014	0.016	0.013
Mg	1.168	1.141	1.166	0.712	0.721	1.111	1.099	1.111	0.674	1.030	1.041	0.748	0.664	0.695
Fe^{2+}	0.692	0.674	0.676	0.347	0.298	0.786	0.799	0.795	0.368	0.824	0.833	0.539	0.414	0.455
Mn	0.018	0.018	0.017	0.012	0.012	0.017	0.015	0.012	0.006	0.020	0.019	0.016	0.010	0.011
Ca	0.050	0.076	0.056	0.769	0.793	0.037	0.049	0.041	0.824	0.077	0.053	0.585	0.770	0.697
Na	0.000	0.000	0.000	0.035	0.033	0.000	0.000	0.000	0.026	0.000	0.000	0.020	0.035	0.031
Σ oct	1.999	2.000	2.000	2.000	2.001	2.000	2.000	2.001	1.989	1.995	1.994	1.989	1.989	1.989
Ca	2.6	4.0	2.9	42.0	43.8	1.9	2.5	2.1	44.2	4.0	2.7	31.2	41.7	37.8
Mg	61.2	60.3	61.5	39.0	39.8	57.5	56.5	57.0	36.1	53.3	54.0	40.0	35.9	37.6
Fe	36.2	35.7	35.6	19.0	16.4	40.6	41.0	40.9	19.7	42.7	43.2	28.8	22.4	24.6
QUAD	91.6	90.0	90.6	87.5	85.7	94.6	96.0	95.5	90.9	95.7	95.3	91.9	90.4	89.9
OTHER	8.4	10.0	9.4	12.5	14.3	5.4	4.0	4.5	9.1	4.3	4.7	8.1	9.6	10.1

Appendix 6(cont.)

Selected Pyroxene Analyses from Norites of the Cortlandt Complex (Pluton 5).

Sample #	27		27	27	27	23	23	23	23	23	23	25	25	25	25
	Core	Rim													
SiO_2	49.8	48.9	49.5	51.6	49.3	50.1	50.7	49.8	50.8	49.8	50.6	50.6	51.0	51.6	50.7
Al_2O_3	3.99	4.27	4.35	1.68	4.39	1.55	0.85	1.67	3.11	3.33	2.37	1.90	1.56	2.60	2.75
FeO	22.5	22.3	22.4	8.31	9.07	29.8	32.8	31.6	12.3	17.5	20.5	26.4	26.0	12.1	12.3
MgO	22.1	21.4	21.5	13.9	12.6	15.8	14.7	14.6	12.2	11.9	11.8	19.5	19.8	13.0	13.0
MnO	0.48	0.52	0.48	0.17	0.24	0.61	0.87	0.73	0.26	0.49	0.53	0.59	0.68	0.34	0.35
TiO_2	0.31	0.30	0.19	0.12	0.53	0.28	0.16	0.39	0.78	0.56	1.40	0.68	0.17	0.36	0.41
Cr_2O_3	0.10	0.11	0.05	0.02	0.03	0.10	0.09	0.09	0.07	0.10	0.09	0.06	0.04	0.07	0.10
CaO	0.91	0.95	0.66	22.7	20.8	1.66	1.00	1.82	19.3	14.5	13.6	1.27	0.95	20.3	20.0
Na_2O	0.00	0.00	0.00	0.29	0.51	0.00	0.00	0.00	0.42	0.37	0.19	0.00	0.00	0.33	0.39
Σ	100.2	98.8	99.1	98.9	97.5	100.0	101.2	100.7	99.2	98.5	101.2	101.0	100.3	100.7	100.0
FeO	18.8	18.8	19.8	6.44	7.81	29.2	32.3	30.8	12.3	17.5	20.5	25.0	24.2	11.0	10.1
Fe_2O_3	4.11	3.86	0.71	2.08	1.40	0.71	0.50	0.86	0.00	0.00	0.0	1.55	2.06	1.31	2.52
Si	1.845	1.840	1.856	1.940	1.884	1.944	1.967	1.936	1.929	1.927	1.925	1.906	1.928	1.925	1.905
Al^{IV}	0.155	0.160	0.144	0.060	0.116	0.056	0.033	0.064	0.071	0.073	0.075	0.084	0.069	0.075	0.095
Σ tet	2.000	2.000	2.000	2.000	2.000	2.000	2.000	2.000	2.000	2.000	2.000	1.990	1.997	2.000	2.000
Al^{IV}	0.020	0.030	0.048	0.015	0.082	0.015	0.006	0.013	0.068	0.079	0.031	0.000	0.000	0.040	0.026
Fe^{3+}	0.115	0.109	0.084	0.059	0.040	0.021	0.015	0.025	0.000	0.000	0.000	0.044	0.059	0.037	0.071
Cr	0.003	0.003	0.001	0.001	0.001	0.003	0.003	0.003	0.002	0.003	0.003	0.002	0.001	0.002	0.003
Ti	0.009	0.008	0.005	0.003	0.015	0.008	0.005	0.011	0.002	0.016	0.040	0.019	0.005	0.010	0.012
Mg	1.219	1.201	1.199	0.780	0.716	0.916	0.852	0.847	0.689	0.686	0.672	1.096	1.117	0.722	0.728
Fe^{2+}	0.583	0.593	0.620	0.202	0.249	0.947	1.049	1.001	0.389	0.565	0.654	0.787	0.764	0.342	0.316
Mn	0.015	0.017	0.015	0.005	0.008	0.020	0.029	0.024	0.008	0.016	0.017	0.019	0.022	0.011	0.011
Ca	0.036	0.038	0.027	0.914	0.851	0.069	0.042	0.076	0.784	0.600	0.556	0.051	0.038	0.813	0.805
Na	0.000	0.000	0.000	0.021	0.038	0.000	0.000	0.000	0.031	0.028	0.014	0.000	0.000	0.024	0.028
Σ oct	2.000	1.999	1.999	2.000	2.001	1.999	2.001	2.000	1.993	1.993	1.987	2.018	2.006	2.001	2.000
Ca	2.0	2.1	1.4	48.2	46.8	3.6	2.1	3.9	42.1	32.4	29.6	2.6	2.0	43.3	43.5
Mg	66.3	65.6	65.0	41.1	39.4	47.4	43.9	44.1	37.0	37.1	35.7	56.7	58.2	38.5	39.4
Fe	31.7	32.3	33.6	10.7	13.7	49.0	54.0	52.0	20.9	30.5	34.7	40.7	39.8	18.2	17.1
QUAD	84.5	84.0	85.6	92.3	86.2	94.4	96.7	93.6	90.8	90.2	92.5	91.6	93.0	91.1	88.8
OTHER	15.5	16.0	14.4	7.7	13.8	5.6	3.3	6.4	9.2	9.8	7.5	8.4	7.0	8.9	11.2

Appendix 6(cont.)

Selected Pyroxene Analyses from Norites of the Cortlandt Complex (Pluton 5).

Sample #	26	26	26		26	29		29	29	29	29	30	30	30	30	30
			Core	Rim		Core	Rim									
SiO_2	51.4	51.2	51.0	51.3	51.3	49.8	49.5	51.3	49.4	48.6	49.5	51.9	51.1	50.8	49.7	51.0
Al_2O_3	1.91	1.74	3.08	2.94	2.73	2.00	2.32	1.87	3.63	3.22	3.37	1.96	1.76	3.33	3.29	3.32
FeO	26.4	26.7	12.0	13.7	11.6	26.2	27.1	26.8	13.0	15.3	12.0	24.8	24.4	11.53	11.9	10.0
MgO	19.3	19.3	12.1	13.0	12.5	19.1	18.9	19.5	12.2	13.0	12.3	20.5	20.9	13.6	13.4	14.2
MnO	0.62	0.68	0.34	0.37	0.32	0.68	0.68	0.67	0.33	0.40	0.35	0.50	0.53	0.29	0.31	0.22
TiO_2	0.19	0.13	0.52	0.61	0.04	0.17	0.18	0.17	0.62	1.01	0.41	0.41	0.40	0.97	0.87	0.94
Cr_2O_3	0.03	0.00	0.02	0.04	20.8	0.06	0.12	0.08	0.08	0.12	0.07	0.03	0.02	0.03	0.50	0.00
CaO	1.42	1.13	20.5	18.6	0.62	1.80	0.87	1.20	20.2	17.7	20.5	1.91	1.61	19.6	19.2	20.0
Na_2O	0.00	0.00	0.55	0.44	0.00	0.00	0.00	0.00	0.41	0.33	0.39	0.00	0.00	0.48	0.50	0.44
Σ	101.2	100.9	100.2	101.1	100.1	99.8	99.7	101.5	100.0	99.7	98.9	102.0	100.6	100.6	99.2	100.2
FeO	24.9	24.8	10.7	12.5	9.50	23.8	24.2	24.6	9.71	11.9	9.23	22.9	22.6	9.76	9.04	8.65
Fe_2O_3	1.67	2.16	1.44	1.40	2.30	2.73	3.15	2.40	3.66	3.75	3.05	2.10	1.94	1.96	3.17	1.50
Si	1.928	1.927	1.916	1.914	1.920	1.899	1.892	1.919	1.864	1.849	1.882	1.916	1.912	1.889	1.868	1.896
Al^{IV}	0.072	0.073	0.084	0.086	0.080	0.090	0.104	0.081	0.136	0.144	0.118	0.084	0.078	0.111	0.132	0.104
Σ tet	2.000	2.000	2.000	2.000	2.000	1.989	1.996	2.000	2.000	1.993	2.000	2.000	2.000	2.000	2.000	2.000
Al^{VI}	0.013	0.004	0.053	0.043	0.041	0.000	0.000	0.001	0.025	0.000	0.033	0.002	0.000	0.035	0.014	0.041
Fe^{3+}	0.047	0.061	0.041	0.039	0.065	0.078	0.091	0.068	0.104	0.107	0.087	0.058	0.055	0.055	0.090	0.042
Cr	0.001	0.000	0.001	0.001	0.001	0.002	0.004	0.002	0.002	0.004	0.002	0.001	0.001	0.001	0.015	0.000
Ti	0.005	0.004	0.015	0.017	0.009	0.005	0.005	0.005	0.018	0.029	0.012	0.011	0.011	0.027	0.025	0.026
Mg	1.076	1.084	0.680	0.725	0.698	1.083	1.076	1.085	0.687	0.738	0.696	1.130	1.165	0.752	0.751	0.788
Fe^{2+}	0.781	0.780	0.335	0.389	0.186	0.759	0.774	0.769	0.306	0.379	0.294	0.706	0.708	0.304	0.284	0.269
Mn	0.020	0.022	0.011	0.012	0.010	0.022	0.022	0.021	0.011	0.013	0.011	0.016	0.017	0.009	0.010	0.007
Ca	0.057	0.046	0.825	0.742	0.833	0.074	0.036	0.048	0.818	0.720	0.836	0.076	0.065	0.782	0.775	0.795
Na	0.000	0.000	0.040	0.032	0.045	0.000	0.000	0.000	0.030	0.024	0.029	0.000	0.000	0.035	0.036	0.032
Σ oct	2.000	2.001	2.001	2.000	1.998	2.023	2.008	1.999	2.001	2.014	2.000	2.000	2.022	2.000	2.000	2.000
Ca	3.0	2.4	44.9	40.0	45.5	3.8	1.9	2.5	45.2	39.2	45.8	4.0	3.3	42.6	42.8	42.9
Mg	56.2	56.8	36.9	39.0	38.2	56.6	57.1	57.0	37.9	40.2	38.1	59.1	60.1	40.9	41.5	42.6
Fe	40.8	40.9	18.2	21.0	16.3	39.6	41.0	40.4	16.9	20.6	16.1	36.9	36.6	16.5	15.7	14.5
QUAD	92.8	92.7	89.1	89.9	88.4	91.0	89.6	91.9	85.1	85.6	86.5	91.6	92.2	88.2	85.6	89.0
OTHER	7.2	7.3	10.9	10.1	11.6	9.0	10.4	8.1	14.9	14.4	13.5	8.4	7.8	11.8	14.4	11.0

Appendix 6(cont.)

Selected Pyroxene Analyses from Norites of the Cortlandt Complex (Pluton 5).

Sample #	6	6	6 Core	6 Rim	6	18	18	18	18	22	22	22	22
SiO_2	51.3	51.6	49.1	50.2	51.1	51.4	51.1	49.7	49.6	49.6	50.1	50.7	50.6
Al_2O_3	1.67	1.78	3.62	3.16	3.56	2.67	3.67	4.78	5.16	1.18	1.35	2.42	3.42
FeO	24.7	24.3	11.7	12.8	11.1	22.0	21.6	10.8	11.4	29.5	30.2	17.2	11.6
MgO	20.0	20.3	13.6	12.9	13.5	22.6	22.7	13.3	13.0	15.6	15.6	12.1	11.0
MnO	0.39	0.34	0.16	0.19	0.14	0.45	0.47	0.25	0.28	0.94	1.07	0.52	0.29
TiO_2	0.18	0.20	2.58	0.69	0.80	0.31	0.28	0.89	1.06	0.13	0.52	0.53	0.46
Cr_2O_3	0.00	0.03	0.04	0.00	0.05	0.06	0.07	0.09	0.12	0.04	0.04	0.01	0.04
CaO	1.65	1.67	18.3	17.7	18.9	1.38	0.88	20.5	20.1	1.59	1.95	17.1	21.6
Na_2O	0.00	0.01	0.52	0.57	0.55	0.00	0.00	0.51	0.51	0.00	0.00	0.36	0.51
Σ	99.8	100.3	99.7	98.3	99.7	100.9	100.8	100.8	101.3	98.6	100.8	100.9	99.6
FeO	23.4	23.1	10.7	12.0	10.9	19.4	19.3	7.59	8.72	28.6	29.3	15.5	11.0
Fe_2O_3	1.42	1.35	1.16	0.88	0.13	2.92	2.55	3.51	2.93	1.06	1.03	1.82	0.64
Si	1.938	1.936	1.849	1.917	1.916	1.892	1.877	1.839	1.834	1.952	1.935	1.918	1.920
Al^{IV}	0.062	0.064	0.151	0.083	0.084	0.108	0.123	0.161	0.166	0.048	0.062	0.082	0.080
Σ tet	2.000	2.000	2.000	2.000	2.000	2.000	2.000	2.000	2.000	2.000	1.997	2.000	2.000
Al^{IV}	0.012	0.015	0.009	0.060	0.073	0.008	0.035	0.048	0.059	0.007	0.000	0.026	0.072
Fe^{3+}	0.040	0.038	0.033	0.025	0.004	0.081	0.070	0.098	0.081	0.031	0.030	0.052	0.018
Cr	0.000	0.001	0.001	0.000	0.001	0.002	0.002	0.003	0.004	0.001	0.001	0.000	0.001
Ti	0.005	0.006	0.073	0.020	0.023	0.009	0.008	0.025	0.029	0.004	0.015	0.015	0.013
Mg	1.124	1.137	0.765	0.737	0.753	1.237	1.242	0.733	0.716	0.917	0.896	0.680	0.621
Fe^{2+}	0.739	0.725	0.337	0.385	0.343	0.596	0.593	0.235	0.269	0.940	0.948	0.492	0.348
Mn	0.012	0.011	0.005	0.006	0.004	0.014	0.015	0.008	0.009	0.031	0.035	0.017	0.009
Ca	0.067	0.067	0.739	0.725	0.759	0.054	0.035	0.814	0.797	0.067	0.081	0.692	0.879
Na	0.000	0.001	0.038	0.042	0.040	0.000	0.000	0.037	0.037	0.000	0.000	0.026	0.037
Σ oct	1.999	2.001	2.000	2.000	2.000	2.001	2.000	2.001	2.001	1.998	2.006	2.000	1.998
Ca	3.5	3.5	40.1	39.3	40.9	2.9	1.9	45.7	44.7	3.5	4.2	37.1	47.6
Mg	58.2	58.9	41.6	39.9	40.6	65.5	66.4	41.1	40.2	47.7	46.6	36.5	33.6
Fe	38.3	37.6	18.3	20.8	18.5	31.6	31.7	13.2	15.1	48.8	49.2	26.4	18.8
QUAD	93.8	93.6	84.9	89.5	89.9	89.2	87.7	82.7	82.7	95.2	93.9	90.7	89.5
OTHER	6.2	6.4	15.1	10.5	10.1	10.8	12.3	17.3	17.3	4.8	6.1	9.3	10.5

Appendix 6(cont.) Selected Biotite Analyses from Norites of the Cortlandt Complex (Pluton 5).

Sample #	6	6	22	22	27	27	28	28	23	23	25	25
SiO_2	36.3	36.4	34.3	34.2	35.4	34.8	37.0	36.5	36.5	36.4	35.6	36.5
Al_2O_3	15.1	14.9	15.5	15.2	15.8	15.9	16.8	16.9	13.9	14.2	14.7	14.9
FeO	16.8	16.8	18.3	20.7	15.0	15.3	15.3	15.9	21.0	21.0	16.2	17.0
MgO	12.4	12.6	12.2	10.0	13.4	13.2	14.6	14.5	10.3	10.5	13.2	13.0
MnO	0.00	0.00	0.14	0.20	0.09	0.05	0.06	0.07	0.08	0.06	0.03	0.07
TiO_2	5.84	6.46	3.68	4.55	6.47	6.34	1.44	1.46	4.56	4.67	5.34	5.63
Cr_2O_3	0.04	0.07	0.02	0.01	0.04	0.11	0.01	0.04	0.08	0.13	0.08	0.12
CaO	0.00	0.00	0.02	0.02	0.02	0.02	0.01	0.04	0.00	0.03	0.02	0.05
Na_2O	0.00	0.00	0.00	0.00	0.02	0.05	0.12	0.07	0.00	0.00	0.00	0.00
K_2O	9.46	9.70	9.34	9.43	9.13	9.38	8.60	8.27	10.1	10.2	9.30	9.58
Σ	95.9	97.0	93.5	94.3	95.4	95.1	94.0	93.8	96.5	97.3	94.4	97.0

Appendix 6(cont.) Selected Biotite Analyses from Norites of the Cortlandt Complex (Pluton 5).

Sample #	19	19	19	21	21	26	26	29	29	30	30
SiO_2	35.3	36.0	36.1	38.2	37.2	36.4	36.4	35.2	35.7	36.3	36.0
Al_2O_3	15.2	16.7	16.1	13.4	13.5	14.6	13.2	15.0	14.9	15.2	15.0
FeO	17.3	10.4	11.6	17.1	17.1	17.0	16.9	15.6	16.7	17.6	17.9
MgO	11.5	16.6	15.5	12.5	12.3	12.8	12.8	13.5	13.0	12.9	12.7
MnO	0.08	0.01	0.01	0.08	0.09	0.10	0.06	0.05	0.07	0.05	0.07
TiO_2	6.38	5.06	5.72	5.49	5.23	5.67	5.42	5.67	5.82	5.76	5.87
Cr_2O_3	0.09	0.13	0.10	0.03	0.00	0.07	0.05	0.14	0.10	0.02	0.04
CaO	0.04	0.00	0.01	0.00	0.03	0.03	0.01	0.02	0.03	0.01	0.01
Na_2O	0.00	0.00	0.00	0.00	0.00	0.00	0.00	0.00	0.00	0.00	0.00
K_2O	9.07	9.33	9.51	9.06	8.95	10.0	9.99	9.71	9.65	10.4	10.4
Σ	95.1	94.3	94.8	95.9	94.4	96.7	94.8	95.0	95.9	98.2	98.0

Appendix 6(cont.)

Selected Feldspar Analyses from Norites of the Cortlandt Complex (Pluton 5).

Sample #	26		26	29		29	30		30	6	6	6	6	6
	Core	Rim		Core	Rim		Core	Rim						
SiO_2	56.1	57.3	57.5	52.4	53.4	54.2	54.6	56.4	57.3	60.1	59.8	59.0	59.5	62.4
Al_2O_3	27.6	27.2	26.7	30.0	29.4	29.1	28.9	28.7	26.9	25.6	25.6	25.8	24.6	20.6
FeO	0.08	0.14	0.13	0.33	0.43	0.39	0.08	0.09	0.09	0.12	0.11	0.11	0.22	0.08
CaO	9.09	8.46	8.01	12.8	11.8	11.5	11.2	9.40	8.21	7.08	7.08	7.34	6.59	1.88
Na_2O	6.01	6.01	6.41	4.13	4.62	4.96	5.17	6.01	6.72	6.95	5.90	7.12	5.00	2.23
K_2O	0.41	0.71	0.63	0.35	0.36	0.32	0.33	0.39	0.35	0.85	2.92	0.46	4.19	11.7
Σ	99.3	99.8	99.4	100.0	100.0	100.5	100.3	101.0	99.5	100.7	101.4	99.9	100.2	98.8
Si	2.536	2.574	2.591	2.382	2.419	2.443	2.460	2.511	2.578	2.663	2.655	2.640	2.684	2.888
Al	1.473	1.439	1.420	1.605	1.573	1.545	1.535	1.504	1.427	1.340	1.341	1.361	1.311	1.122
Fe	0.003	0.005	0.005	0.013	0.016	0.015	0.003	0.003	0.003	0.004	0.004	0.004	0.008	0.003
Ca	0.440	0.407	0.387	0.624	0.574	0.555	0.540	0.448	0.396	0.336	0.337	0.352	0.318	0.093
Na	0.527	0.523	0.560	0.364	0.406	0.433	0.452	0.518	0.587	0.597	0.508	0.617	0.437	0.200
K	0.024	0.041	0.036	0.020	0.021	0.018	0.019	0.022	0.020	0.048	0.166	0.026	0.241	0.690
Σ	5.003	4.989	4.998	5.008	5.008	5.010	5.008	5.007	5.011	4.990	5.011	5.001	5.000	4.997
Or	2.4	4.2	3.6	2.0	2.1	1.8	1.9	2.2	2.0	4.9	16.4	2.6	24.2	70.2
Ab	53.2	53.9	57.0	36.1	40.6	43.0	44.7	52.5	58.5	60.9	50.3	62.0	43.9	20.3
An	44.4	41.9	39.4	61.9	57.3	55.2	53.4	45.3	39.5	34.2	33.3	35.4	31.9	9.5

Appendix 6(cont.) Selected Feldspar Analyses from Norites of the Cortlandt Complex (Pluton 5).

Sample #	28		23	23	23	25	25
	Core	Rim					
SiO_2	55.1	55.6	57.7	58.5	64.2	55.8	55.4
Al_2O_3	28.5	28.3	26.6	25.8	18.6	28.5	29.9
FeO	0.06	0.13	0.19	0.27	0.20	0.02	0.06
CaO	9.66	9.79	8.72	7.93	0.22	9.93	10.7
Na_2O	5.51	5.55	6.22	7.31	1.49	5.94	5.55
K_2O	0.03	0.03	0.59	0.28	14.7	0.24	0.15
Σ	98.8	99.4	100.1	100.1	99.4	100.4	101.7
Si	2.500	2.508	2.588	2.619	2.975	2.501	2.453
Al	1.523	1.508	1.407	1.364	1.019	1.504	1.560
Fe	0.002	0.005	0.007	0.010	0.008	0.001	0.002
Ca	0.470	0.474	0.419	0.380	0.011	0.477	0.509
Na	0.485	0.486	0.541	0.635	0.134	0.516	0.477
K	0.002	0.002	0.034	0.016	0.871	0.014	0.008
Σ	4.982	4.982	4.996	5.024	5.018	5.012	5.010
Or	0.2	0.2	3.4	1.5	85.7	1.4	0.8
Ab	50.7	50.5	54.4	61.6	13.2	51.2	48.0
An	49.1	49.3	42.2	36.9	1.1	47.4	51.2

Appendix 6(cont.) Selected Feldspar Analyses from Norites of the Cortlandt Complex (Pluton 5).

Sample #	19		19		19	20		20	20	20	21		21
	Core	Rim	Core	Rim		Core	Rim				Core	Rim	
SiO_2	52.3	53.3	51.9	51.8	50.7	49.4	57.7	53.3	57.3	63.6	59.8	59.5	56.4
Al_2O_3	29.9	29.7	30.3	30.2	31.4	31.2	26.3	29.4	26.7	19.2	25.7	25.4	27.4
FeO	0.32	0.37	0.32	0.29	0.37	0.00	0.00	0.00	0.00	0.00	0.07	0.16	0.12
CaO	12.2	11.9	12.3	12.3	14.1	14.4	8.73	12.0	8.82	0.73	8.00	7.98	10.2
Na_2O	4.32	4.57	4.14	4.23	3.39	2.83	6.42	4.48	6.13	0.54	6.79	6.70	5.42
K_2O	0.52	0.64	0.50	0.44	0.36	0.07	0.52	0.16	0.53	14.8	0.71	0.64	0.46
Σ	99.5	100.5	99.5	99.2	100.3	97.9	99.6	99.3	99.5	98.8	101.0	100.3	100.0
Si	2.386	2.410	2.371	2.373	2.307	2.297	2.596	2.425	2.583	2.959	2.647	2.652	2.539
Al	1.607	1.581	1.631	1.627	1.685	1.708	1.394	1.575	1.417	1.053	1.341	1.334	1.451
Fe	0.012	0.014	0.012	0.011	0.014	0.000	0.000	0.000	0.000	0.000	0.003	0.006	0.005
Ca	0.598	0.576	0.601	0.602	0.686	0.715	0.421	0.584	0.426	0.036	0.380	0.381	0.491
Na	0.382	0.400	0.367	0.375	0.299	0.255	0.560	0.395	0.535	0.049	0.583	0.579	0.473
K	0.030	0.037	0.029	0.026	0.021	0.004	0.030	0.009	0.030	0.882	0.040	0.036	0.026
Σ	5.017	5.018	5.011	5.014	5.011	4.979	5.002	4.989	4.991	4.979	4.994	4.989	4.985
Or	3.0	3.6	2.9	2.6	2.1	0.4	3.0	0.9	3.0	91.2	4.0	3.6	2.6
Ab	37.8	39.5	36.8	37.4	29.7	26.2	55.4	40.0	54.0	5.1	58.1	58.1	47.8
An	59.2	56.9	60.3	60.0	68.2	73.4	41.6	59.1	43.0	3.7	37.9	38.3	49.6

Appendix 6(cont.)

Selected Feldspar Analyses from Norites of the Cortlandt Complex (Pluton 5).

Sample #	18		18	22		22	27		27		27
	Core	Rim		Core	Rim		Core	Rim	Core	Rim	
SiO_2	50.6	49.5	49.5	53.1	57.9	57.5	50.1	49.4	49.8	49.8	49.2
Al_2O_3	30.9	32.0	32.3	28.4	26.0	25.4	31.8	31.9	31.6	31.2	32.0
FeO	0.03	0.35	0.31	0.12	0.11	0.00	0.19	0.24	0.15	0.19	0.70
CaO	14.3	15.2	15.4	12.0	8.27	8.06	13.5	13.7	13.9	13.4	14.0
Na_2O	3.47	2.91	2.95	4.95	7.07	6.76	3.40	3.36	3.34	3.65	2.97
K_2O	0.20	0.14	0.13	0.12	0.16	0.17	0.12	0.09	0.10	0.09	0.08
Σ	99.7	100.1	100.6	98.6	99.5	97.8	99.1	98.8	99.0	98.3	98.9
Si	2.317	2.262	2.252	2.438	2.605	2.626	2.297	2.279	2.292	2.304	2.268
Al	1.669	1.724	1.733	1.537	1.382	1.366	1.719	1.735	1.714	1.701	1.740
Fe	0.001	0.013	0.012	0.005	0.004	0.000	0.007	0.009	0.006	0.007	0.027
Ca	0.702	0.743	0.751	0.590	0.399	0.395	0.666	0.678	0.687	0.666	0.691
Na	0.308	0.258	0.260	0.441	0.617	0.599	0.302	0.300	0.298	0.328	0.266
K	0.012	0.008	0.008	0.007	0.009	0.010	0.007	0.005	0.006	0.005	0.005
Σ	5.009	5.009	5.015	5.017	5.017	4.995	4.998	5.007	5.003	5.012	4.997
Or	1.2	0.8	0.8	0.7	0.9	1.0	0.7	0.5	0.6	0.5	0.5
Ab	30.1	25.6	25.5	42.5	60.2	59.7	31.0	30.5	30.1	32.8	27.7
An	68.7	73.6	73.7	56.8	38.9	39.3	68.3	69.0	69.3	66.7	71.8

Appendix 7 Selected Feldspar Analyses from Granodiorites.

Sample #	24*		24*	51	51	51	51	34		34	34
	Core	Rim						Core	Rim		
SiO_2	60.9	62.1	64.9	66.1	65.5	62.9	63.8	64.7	66.0	65.0	64.4
Al_2O_3	23.9	23.0	21.6	20.7	20.5	18.4	19.0	21.6	20.85	21.7	21.8
FeO	0.00	0.00	0.00	0.00	0.00	0.00	0.00	0.00	0.00	0.00	0.00
CaO	5.47	4.52	2.47	1.28	1.04	0.05	0.08	2.59	1.48	2.77	2.46
Na_2O	8.51	8.96	10.0	10.7	10.7	2.10	5.12	9.93	10.8	9.99	10.0
K_2O	0.08	0.16	0.07	0.14	0.11	14.0	9.27	0.09	0.06	0.12	0.15
Σ	98.9	98.8	99.1	98.9	97.8	97.4	97.2	98.9	99.2	99.6	99.9
Si	2.733	2.783	2.876	2.928	2.931	2.971	2.964	2.875	2.917	2.872	2.866
Al	1.266	1.216	1.132	1.080	1.081	1.026	1.041	1.130	1.087	1.129	1.143
Fe	0.000	0.000	0.000	0.000	0.000	0.000	0.000	0.000	0.000	0.000	0.000
Ca	0.263	0.217	0.117	0.061	0.050	0.003	0.004	0.123	0.070	0.131	0.117
Na	0.740	0.778	0.861	0.921	0.926	0.192	0.462	0.855	0.927	0.856	0.864
K	0.005	0.009	0.004	0.008	0.006	0.842	0.550	0.005	0.003	0.007	0.009
Σ	5.007	5.003	4.990	4.997	4.995	5.033	5.021	4.989	5.005	4.995	4.999
Or	0.5	0.9	0.4	0.8	0.6	81.2	54.1	0.5	0.3	0.7	0.9
Ab	73.4	77.5	86.7	93.0	94.3	18.5	45.5	87.0	92.7	86.1	87.3
An	26.1	21.6	11.9	6.2	5.1	0.3	0.4	12.5	7.0	13.2	11.8

*Phenocryst.

Appendix 7(cont.) Selected Mica Analyses from Granodiorites.

Sample #	24	51	51	51	34	34	34
	Biotite	Biotite	Biotite	Muscovite	Muscovite	Biotite	Biotite
SiO_2	35.9	35.6	35.8	44.0	45.8	36.7	35.1
Al_2O_3	16.2	14.4	15.2	35.9	29.5	16.2	15.7
FeO	18.9	21.2	22.5	1.50	4.65	19.2	22.1
MgO	10.2	9.00	8.13	0.00	1.13	8.22	7.15
MnO	0.37	0.26	0.21	0.00	0.01	0.73	0.94
TiO_2	1.85	2.57	2.86	0.00	0.67	1.95	2.52
Cr_2O_3	0.00	0.01	0.00	0.00	0.00	0.00	0.00
CaO	0.01	0.08	0.01	0.00	0.00	0.03	0.01
Na_2O	0.00	0.00	0.00	0.06	0.06	0.00	0.00
K_2O	9.45	8.96	9.25	9.64	9.72	8.01	8.98
Σ	92.9	92.1	93.9	91.1	91.6	91.0	92.5

Appendix 8 Selected Amphibole Analyses from Stony Point Dike Rocks.

Sample #	43	43	44		44
			Core	Rim	
SiO_2	43.7	42.8	41.2	40.6	40.4
Al_2O_3	9.93	11.0	12.2	12.1	12.5
FeO	13.8	14.8	11.4	12.1	13.4
MgO	11.7	10.6	12.8	11.7	10.7
MnO	0.08	0.09	0.01	0.02	0.00
TiO_2	0.89	1.45	1.76	1.49	1.66
Cr_2O_3	0.03	0.01	0.00	0.00	0.00
CaO	11.4	11.2	9.88	11.3	11.6
Na_2O	1.30	1.39	1.41	1.30	1.65
K_2O	0.49	1.06	1.66	1.07	1.32
Σ	93.3	94.3	92.4	91.7	93.2
FeO	12.0	13.5	7.69	10.2	13.0
Fe_2O_3	2.08	1.39	4.14	2.13	0.54
Si	6.702	6.567	6.322	6.336	6.292
Al^{IV}	1.298	1.433	1.678	1.664	1.708
Σ tet	8.000	8.000	8.000	8.000	8.000
Al^{VI}	0.499	0.560	0.531	0.568	0.584
Fe^{2+}	1.537	1.734	0.986	1.333	1.689
Fe^{3+}	0.240	0.161	0.478	0.251	0.063
Mg	2.665	2.411	2.936	2.719	2.488
Mn	0.010	0.012	0.001	0.003	0.000
Ti	0.103	0.167	0.203	0.175	0.195
Cr	0.004	0.001	0.000	0.000	0.000
Σ oct(M1-3)	5.058	5.046	5.135	5.049	5.019
X oct	0.058	0.046	0.135	0.049	0.019
Ca	1.875	1.832	1.624	1.895	1.937
Na(M4)	0.067	0.122	0.241	0.056	0.044
Σ (M4)	2.000	2.000	2.000	2.000	2.000
Na	0.320	0.291	0.179	0.338	0.455
K	0.096	0.207	0.325	0.213	0.262
Σ (A)	0.416	0.498	0.504	0.551	0.717
Ca	30.9	30.7	29.3	31.9	31.7
Mg	43.9	40.3	52.9	45.7	40.7
Fe	25.3	29.0	17.8	22.4	27.6
QUAD	35.1	28.4	16.1	16.8	14.6
OTHER	64.9	71.6	83.9	83.2	85.4

Appendix 8(cont.) Selected Biotite Analyses from Stony Point Dike Rocks.

Sample #	43	43	44	44
SiO_2	37.1	36.6	37.1	36.7
Al_2O_3	14.8	14.6	14.1	14.2
FeO	15.4	15.2	14.0	14.4
MgO	14.2	14.1	15.0	14.9
MnO	0.00	0.00	0.00	0.00
TiO_2	2.79	2.87	2.60	2.62
Cr_2O_3	0.00	0.00	0.00	0.00
CaO	0.04	0.00	0.00	0.00
Na_2O	0.00	0.00	0.00	0.00
K_2O	8.27	8.39	9.00	9.16
Σ	92.5	91.7	91.8	92.0

Appendix 8(cont.) Selected Feldspar Analyses from Stony Point Dike Rocks.

Sample #	43	43	44	44	44
SiO_2	60.7	60.3	62.0	61.7	63.4
Al_2O_3	23.6	25.0	23.7	23.9	22.6
FeO	0.00	0.01	0.00	0.00	0.00
CaO	5.67	6.78	5.08	5.43	3.85
Na_2O	8.15	7.52	8.69	8.61	9.15
K_2O	0.02	0.04	0.07	0.05	0.03
Σ	98.2	99.6	99.5	99.7	99.0
Si	2.740	2.690	2.760	2.743	2.822
Al	1.258	1.313	1.241	1.255	1.185
Fe	0.000	0.000	0.000	0.000	0.000
Ca	0.274	0.324	0.242	0.259	0.184
Na	0.713	0.650	0.750	0.743	0.790
K	0.001	0.002	0.004	0.003	0.002
Σ	4.988	4.980	4.996	5.002	4.982
Or	0.1	0.2	0.4	0.3	0.2
Ab	72.2	66.6	75.3	73.9	80.9
An	27.7	33.2	24.3	25.8	18.9

Appendix 9 Selected Garnet Analyses from Salt Hill Emery (#37) and Quartz Feldspathic Dike (#36).

Sample #	36		36		36	37		37	37
	Core	Rim	Core	Rim		Core	Rim		
SiO_2	38.8	38.5	38.9	38.6	38.8	39.1	38.9	38.4	39.0
Al_2O_3	22.0	21.6	21.8	21.8	22.1	21.6	21.7	21.2	21.7
FeO	26.3	28.2	26.5	26.4	25.0	26.5	27.2	30.4	27.1
MgO	9.52	8.31	9.44	9.56	9.68	9.04	9.15	6.86	9.41
MnO	1.94	2.12	1.78	1.86	2.02	0.99	0.95	0.98	0.95
TiO_2	0.03	0.06	0.05	0.08	0.11	0.07	0.08	0.11	0.13
Cr_2O_3	0.00	0.03	0.00	0.00	0.00	0.00	0.03	0.04	0.03
CaO	1.95	1.79	1.89	1.76	1.98	2.68	1.89	1.89	2.08
Na_2O	0.00	0.00	0.00	0.00	0.00	0.00	0.00	0.00	0.00
K_2O	0.00	0.00	0.00	0.00	0.00	0.00	0.00	0.00	0.00
Σ	100.5	100.7	100.3	100.0	99.7	100.0	99.9	99.9	100.3
	Structural formulae on the basis of 12 oxygens								
Si	2.976	2.980	2.990	2.979	2.985	3.010	3.002	3.009	2.994
Al	0.024	0.020	0.010	0.021	0.015	0.000	0.000	0.000	0.006
Σ tet	3.000	3.000	3.000	3.000	3.000	3.010	3.002	3.009	3.000
Al	1.963	1.953	1.962	1.956	1.989	1.961	1.973	1.963	1.956
Cr	0.000	0.002	0.000	0.000	0.000	0.000	0.002	0.003	0.002
Ti	0.002	0.003	0.003	0.004	0.006	0.004	0.004	0.006	0.008
Σ oct	1.965	1.958	1.965	1.960	1.995	1.965	1.979	1.972	1.966
Mg	1.088	0.957	1.081	1.098	1.109	1.037	1.052	0.802	1.078
Fe	1.690	1.827	1.704	1.702	1.609	1.707	1.754	1.996	1.741
Mn	0.126	0.139	0.116	0.121	0.132	0.065	0.062	0.065	0.062
Ca	0.160	0.148	0.156	0.146	0.163	0.221	0.156	0.159	0.171
Σ VIII	3.064	3.071	3.057	3.067	3.013	3.030	3.024	3.022	3.052

Appendix 9(cont.) Spinel Analyses from Salt Hill Emery Sample #37.

SiO_2	0.36	0.10	0.04
Al_2O_3	62.3	64.2	63.9
FeO	16.6	17.6	17.5
MgO	16.4	15.1	16.2
MnO	0.74	0.85	0.82
TiO_2	0.03	0.00	0.00
Cr_2O_3	0.08	0.06	0.06
CaO	0.02	0.00	0.00
Na_2O	0.00	0.00	0.00
K_2O	0.00	0.00	0.00
Σ	96.5	98.0	98.5

Appendix 9(cont.) Selected Feldspar Analyses from Salt Hill Emery (#37) and Quartz-Feldspathic Dike (#36).

	36	36	36	37
SiO_2	48.4	56.8	60.8	50.2
Al_2O_3	33.4	27.6	25.4	32.3
FeO	0.04	0.00	0.04	0.00
CaO	16.1	9.18	6.90	14.1
Na_2O	2.20	6.32	7.89	3.31
K_2O	0.00	0.01	0.01	0.01
Σ	100.1	99.9	101	99.8
Si	2.210	2.547	2.679	2.283
Al	1.797	1.460	1.319	1.734
Fe	0.002	0.000	0.001	0.000
Ca	0.787	0.441	0.326	0.686
Na	0.195	0.549	0.674	0.292
K	0.000	0.001	0.001	0.001
Σ	4.989	4.998	4.999	4.996
Or	0.0	0.1	0.1	0.1
Ab	19.9	55.4	67.3	29.8
An	80.1	44.5	32.6	70.1